INFORMATION TO USERS

This manuscript has been reproduced from the microfilm master. UMI films the text directly from the original or copy submitted. Thus, some thesis and dissertation copies are in typewriter face, while others may be from any type of computer printer.

The quality of this reproduction is dependent upon the quality of the copy submitted. Broken or indistinct print, colored or poor quality illustrations and photographs, print bleedthrough, substandard margins, and improper alignment can adversely affect reproduction.

In the unlikely event that the author did not send UMI a complete manuscript and there are missing pages, these will be noted. Also, if unauthorized copyright material had to be removed, a note will indicate the deletion.

Oversize materials (e.g., maps, drawings, charts) are reproduced by sectioning the original, beginning at the upper left-hand corner and continuing from left to right in equal sections with small overlaps. Each original is also photographed in one exposure and is included in reduced form at the back of the book.

Photographs included in the original manuscript have been reproduced xerographically in this copy. Higher quality 6" x 9" black and white photographic prints are available for any photographs or illustrations appearing in this copy for an additional charge. Contact UMI directly to order.

UMI

A Bell & Howell Information Company
300 North Zeeb Road, Ann Arbor MI 48106-1346 USA
313/761-4700 800/521-0600

Deprotonated Aza-Crown Ligands as Simple and Effective Alternatives to

C_5Me_5 in Group 3, 4, and Lanthanide Chemistry.

by

Lawrence Lee
B.Sc., University of Victoria, 1992

A Dissertation Submitted in Partial Fulfillment of the
Requirements for the Degree of

DOCTOR OF PHILOSOPHY

We accept this dissertation as conforming
to the required standard

Dr. D.J. Berg, Supervisor (Department of Chemistry)

Dr. P. Wan, Departmental Member (Department of Chemistry)

Dr. K.R. Dixon, Departmental Member (Department of Chemistry)

Dr. E. Ishiguro, Outside Member (Department of Biochemistry)

Dr. J. Takats, External Examiner (Department of Chemistry, University of Alberta)

Supervisor: Dr. David J. Berg

ABSTRACT

The ability of a deprotonated aza-crown ether to allow isolation of soluble lanthanide and yttrium complexes has been investigated. A convenient route to these complexes has been demonstrated by the protonolysis reactions of $Ln[(N(SiMe_3)_2]_3$ with 4,13-diaza-18-crown-6. NMR spectroscopy and X-ray crystallography revealed a C_{2v} structure consisting of a basket shaped geometry. The successful protonolysis route has been extended to the preparation of stable alkyls, dialkyls, and alkyl cations of yttrium and zirconium stabilized by deprotonated aza-crown macrocycles.

A yttrium alkyl complex containing deprotonated diaza-18-crown-6 has been prepared by the protonolysis route. The thermal stability and reactivity of this complex were investigated. This alkyl reacts with terminal alkynes to produce a complex equilibrium between the colourless monomeric and dimeric alkynides and a purple *Z*-butatrienediyl (ie. $RC{=}C{=}C{=}CR^{2-}$) coupling product. NMR studies demonstrate that electron poor alkynes favour coupling and that the carbon-carbon double bond forming process is readily reversible at room temperature.

The flexibility of the deprotonated diaza-crown ligand is apparent from the isolation of both *cis* and *trans*-zirconium dibenzyl complexes from the protonolysis of tetrabenzyl zirconium with 4,13-diaza-18-crown-6. The structure of both isomers were investigated by NMR spectroscopy and X-ray crystallography. Both the *cis* and *trans*-isomers cleanly converted to the stable cation either by protonolysis with $[n\text{-}Bu_3NH]^+[BPh_4]^-$ or by alkyl abstraction with $B(C_6F_5)_3$. The reactivity of the alkyl cation derived from the reaction with

$B(C_6F_5)_3$ was investigated. The reaction of this cation with *t*-BuNC gave a vinylamide complex following a 1,2-proton rearrangement of an initially formed iminoacyl.

Two members of the still rare yttrium dialkyl class of compounds were isolated using monoanionic, deprotonated aza-crown ethers as supporting ligation. The dialkyl complexes were synthesized by protonolysis of $Y(CH_2SiMe_3)_3(THF)_2$ with either aza-18-crown-6 or aza-15-crown-5. NMR and X-ray analyses of the yttrium dialkyl supported by aza-18-crown-6 indicates a *trans*-dialkyl geometry while NMR analysis of the aza-15-crown-5 analog indicates a *cis*-dialkyl geometry. Reaction of the *trans*-dialkyl complex with CO afforded a *trans*-dienolate complex formed by the migration of $SiMe_3$. Alkyl abstraction from the *trans*-dialkyl complex using $B(C_6F_5)_3$ allowed generation of the first yttrium alkyl cation.

Dr. D.J. Berg, Supervisor (Department of Chemistry)

Dr. P. Wan, Departmental Member (Department of Chemistry)

Dr. K.R. Dixon, Departmental Member (Department of Chemistry)

Dr. E. Ishiguro, Outside Member (Department of Biochemistry)

Dr. J. Takats, External Examiner (Department of Chemistry, University of Alberta)

TABLE OF CONTENTS

CHAPTER 2

COORDINATION CHEMISTRY OF DEPROTONATED 4,13-DIAZA-18-CROWN-6 (DAC) WITH GROUP 3 AND LANTHANIDE METALS ---- 27

CHAPTER 4

ORGANOZIRCONIUM COMPLEXES CONTAINING 4,13-DIAZA-18-CROWN-6 (DAC) ---------- 99

LIST OF TABLES

LIST OF TABLES IN APPENDIX

LIST OF FIGURES

LIST OF SCHEMES

LIST OF ABBREVIATIONS

Me	methyl
Et	ethyl
i-Pr	*iso*-propyl
t-Bu	*tert*-butyl
Ph	phenyl
DME	dimethoxyethane
TMEDA	tetramethylethylenediamine
OEt_2	diethyl ether
THF	tetrahydrofuran
DAC	deprotonated diaza-18-crown-6
MAC	deprotonated aza-18-crown-6
15-AC-5	deprotonated aza-15-crown-5
C_5H_5 (Cp)	cyclopentadienyl
C_5Me_5 (Cp*)	pentamethylcyclopentadienyl
OEP	octaethylporphyrin dianion
TPP	tetraphenylporphyrin dianion
acac	2,4-pentanedionate
MAO	methylaluminoxane
$\upsilon_{1/2}$	width at half height
GC	gas chromatography
MS	mass spectroscopy
NMR	nuclear magnetic resonance
R_t	relative retention time
VT	variable temperature
ppm	parts per million
s	singlet
d	doublet
t	triplet
m	multiplet
br	broad
δ	chemical shift
Å	angstrom
Hz	hertz (frequency)
cm^{-1}	reciprocal centimeter

Acknowledgements

I must first extend my gratitude and thanks to my supervisor Professor David J. Berg. He deserves much of the credit to the work presented in this thesis. His patience and guidance are greatly appreciated. I would like to acknowledge the members of the group, Patrick Shao, Laurel Clouston, and Katherine Burrage who also contributed to this project and provided the much needed friendship, counseling, and support throughout this stressful graduate career.

I would like to thank Dr. Dave Berry for his early guidance into inorganic and organometallic chemistry.

I would like to extend my gratitude to the technical support staff. First, Mrs. Chris Greenwood has been very kind and patient to have trained me on the NMR spectrometers. Bob Dean and Terry Wiley have been very helpful in fixing electronic equipment. Roy Bennett and Dick Robinson have been very helpful in fixing mechanical equipment. Sean Adams has been kind to fix all broken glassware. Finally a very special thanks to the secretaries, Susanne, Carol, and Sandra for keeping all my files in order allowing me to finally graduate.

Dedication

To

Mom and Dad

you have worked hard to support me throughout my entire life

To

My little neices

Zeina, Lisette, Nooran, and Janessa

hard work will eventually pay off

CHAPTER 1

INTRODUCTION

1.1 General properties of the lanthanides.

The lanthanide series consists of the fourteen elements which follow lanthanum (Z = 57) in the Periodic Table; they begin with cerium (58) and end with lutetium (71). Including yttrium and lanthanum, these elements are collectively referred to as the rare earths. This name is not very appropriate because it incorrectly creates the impression that the elements are rare. However even the scarcest, thulium, is more abundant than arsenic, cadmium, mercury, and selenium[1]. The lanthanides, yttrium and lanthanum were collectively known by this term because they occur as mixed oxides with the more abundant alkaline earths and their similarities in chemical and physical properties made it difficult to isolate the elements from one another using the known separation techniques available during this time[2].

The sequential filling of the 4f valence orbitals imparts unique properties to the lanthanides which distinguish them from the transition metals. In particular, the poor radial extension of the 4f orbitals beyond the filled 5s and 5p shells results in virtually negligible covalent overlap and essentially ionic bonding. Strong evidence for ionic bonding is provided by spectroscopic and magnetic studies, since for a given lanthanide ion these properties do not vary substantially with the nature of the attached ligand. For example, in transition metals complexes the absorption bands due to forbidden d-d transitions are broadened due to vibronic coupling, while similarly forbidden f-f transitions for the lanthanides are exceedingly sharp because there is no ligand field influence[3].

The lanthanide contraction is observed as the ionic (atomic) radius decreases on increasing atomic number across the series. This effect has been attributed to poor

screening of the nuclear charge by 4f electrons such that the 4f electron added to each subsequent element feels an increased effective nuclear charge resulting in contraction of the ion. The important result of this contraction is a series of trivalent ions having different chemistry and structure based on size (from the early La^{3+} = 1.17 Å to the late Lu^{3+} = 1.00 Å)[3]. As an example, the structure of the anhydrous salts MCl_3 for La-Gd consists of a nine coordinate UCl_3 type lattice, while the smaller Tb-Lu ions adopt a six-coordinate $AlCl_3$ type octahedron[1]. By virtue of the charge to size ratio, the highly electropositive lanthanide ions are electrophilic forming strong bonds with O and N donors and striving to attain the maximum coordination number permissible by intramolecular nonbonding ligand-ligand repulsions. Common coordination numbers are seven, eight, and nine, however, three coordinate monomeric complexes can be prepared and isolated by using sterically bulky ligands, such as bis(trimethylsilyl)amido, $-N(SiMe_3)_2$[4]. For less crowded ligands, the presence of strong donor solvents, such as THF or pyridine, may prevent the formation of polymeric materials by occupying all available coordination sites[5].

While the chemistry of the lanthanides is mainly dominated by the +3 oxidation state, corresponding to ionization of the $6s^25d^1$ electrons, the divalent oxidation state is also available for samarium, europium, and ytterbium. These +2 ions are relatively strong reducing agents ($M^{+2} \rightarrow M^{+3} + e^-$), in the order Sm ($\xi^\circ$ = +1.55 V) >Yb (ξ° = +1.15 V) >Eu (ξ° = +0.43 V)[6]. Conversely, cerium possesses a stable +4 oxidation state and is well known in organic chemistry as an excellent one electron oxidizing agent ($Ce^{+4} + e^- \rightarrow Ce^{3+}$, ξ°= +1.74 V)[7]. The stability of the +2 and +4 oxidation states were originally correlated

with the attainment of empty f^0 (Ce^{+4}), half-filled f^7 (Eu^{+2}), or filled f^{14} (Yb^{+2}) configurations. More recently, Johnson[8] proposed a comprehensive explanation for the stability of these alternate oxidation states by utilizing a full Born Haber treatment, ie, enthalpy of sublimation and ionization (first, second, and third). This provides a better explanation for the stability of Sm^{+2} (f^6) and the less stable Pr^{+4} (f^1) and Tb^{+4} (f^{13}) ions.

The trivalent ions of lanthanum and yttrium are comparable in size to early and late lanthanides, respectively. Although they are technically members of group 3, they display very similar chemistry to the lanthanides[3]. However since they are diamagnetic, their complexes give sharp resonances in the NMR spectrum making characterization much easier. In addition, $YCl_3 \bullet 6H_2O$ is much cheaper than diamagnetic $LuCl_3 \bullet 6H_2O$ (currently the latter is ca. 60 times the price of the former)[9]. As one additional motivation for studying yttrium complexes, ^{89}Y is NMR active (100% natural abundance, I=1/2) so J_{YH} and J_{YC} coupling constants and ^{89}Y chemical shifts provide excellent diagnostic features to assist in elucidating molecular structure[10].

1.2 Historical development of the organo-f-element chemistry

1.2.1 Cyclopentadienyl ligands and derivatives.

During the discovery of the rare earth elements, the organometallic chemistry of the main group and transition metals were evolving as an area of interest. In 1827, Zeise reported the first organometallic complex, $K[Pt(C_2H_4)Cl_3]$. It was not until 1849 when Frankland published the first metal-carbon σ-bonded complex, ethyl zinc iodide, that activity in this area commenced[11]. Surprisingly, the organometallic chemistry of the

lanthanides began some 100 years after that of the transition metals. Early reports in the mid-1930s by several groups were unreliable because they provided no supporting structural evidence for the complexes. Very little effort was directed towards studying the organometallic chemistry of these "unusual" elements. The reasons for the slow development of organolanthanide chemistry are both conceptual and practical[11]. Until quite recently, the perception existed that these elements, whose chemistry was characterized by ionic bonding and a severely limited range of oxidation states, must display predictable and limited reaction chemistry, much like that of the alkaline earth metals[11]. Early synthetic efforts to prepare organolanthanide complexes were frustrated by the ionic nature of these metals, which reduces the significance of ligand to metal orbital interactions, allowing ligand redistribution and fluxional processes to occur. In addition, the oxophilicity of the lanthanides make preparation of organometallic derivatives difficult because the complexes are extremely air and moisture sensitive[12]. While this difficulty has been largely overcome by modern Schlenk and glove box techniques[13], a further difficulty is the fact that, in their most stable trivalent oxidation state, all lanthanide ions except lutetium are paramagnetic. This leads to broad linewidths and loss of coupling information which reduce the utility of NMR as a tool for structural characterization[3,14]. Hence, structural characterization is heavily dependent on X-ray crystallography which requires the growth and isolation of single crystals. Often the single crystal might possess static or thermal disorder which reduces the precision of the structural analysis[15]. Many lanthanide complexes have different solid state and solution structures. While the solid state may represent the most stable geometry, various

intriguing species existing in solution, possibly in equilibrium, may remain undetected. A number of practical problems still exist which make organolanthanide chemistry challenging. Chromatographic methods cannot be used to separate product mixtures; instead sublimation or crystallization are the major purification methods. Sublimation often requires heating while under vacuum and this may thermally decompose the compound. Crystallization requires judicious choice of solvent to selectively precipitate one product of a mixture. Organolanthanide complexes can tolerate only a limited range of solvents, such as hydrocarbons, aromatics, and ethers, which do not possess acidic hydrogens*. Another deterrent is the fact that insoluble polymeric complexes are frequently formed, even in the presence of strong donor solvents, when the ancillary ligands do not provide sufficient coordinative saturation of the metal centre[10, 11, 12].

In 1954 Wilkinson and Birmingham introduced the bulky anionic cyclopentadienyl (C_5H_5) ligand which would overcome the formation of coordination polymers by sterically saturating the metal centre. While initially investigating the chemistry of C_5H_5 with various transition metals, the shift towards the rare earths resulted in the first well characterized organometallic complexes of the type $Ln(C_5H_5)_3$ (Ln= La, Y or lanthanides). The classical method of preparation is shown in equation 1.

$$LnCl_3 + 3\,NaC_5H_5 \rightarrow Ln(C_5H_5)_3 + 3\,NaCl \qquad (1)$$

---

* Generally speaking, most solvents possessing hydrogens with pKa values of less than 35 are unsuitable.

The reaction is done in THF and salt elimination provides the driving force[16]. Renewed interest in this area began in 1963 when Dubeck and coworkers published the synthesis of $Ln(C_5H_5)_2Cl$[17]. The reported preparative routes into the monohalide derivative were metathesis, ligand redistribution, or protonolysis. These routes are outlined in equation (2), (3), and (4), respectively.

$$LnCl_3 + 2\,NaC_5H_5 \rightarrow Ln(C_5H_5)_2Cl + 2\,NaCl \quad (2)$$

Ln = Sm, Gd, Dy, Ho, Er, Yb, and Lu

$$LnCl_3 + 2\,Ln(C_5H_5)_3 \rightarrow 3\,Ln(C_5H_5)_2Cl \quad (3)$$

Ln = Sm, Gd, Dy, Ho, Er, Yb, and Lu

$$Ln(C_5H_5)_3 + HCl \rightarrow Ln(C_5H_5)_2Cl + HCp \quad (4)$$

Ln = Yb

Although all these complexes were reported to be monomeric in THF, they adopt a dimeric structure with bridging chlorides in benzene. For the larger metals, lanthanum, cerium, neodymium, and praseodymium, all three synthetic methods failed to produce the monohalide. Instead, insoluble polymeric materials were obtained. The monohalide derivative would be very useful as a precursor for substitution chemistry; however, metathetical reactions to form σ-bonded alkyl complexes (eq 5) were not carried out until the mid 1970's[18].

$$Ln(C_5H_5)_2Cl + LiR \rightarrow Ln(C_5H_5)_2R + LiCl \quad (5)$$

Ln = Sm, Gd, Dy, Ho, Er, Yb, and Lu; R= alkyl (eg. CH_2SiMe_3)

As a consequence of the ionic nature of the lanthanides, it was expected that interaction of these organometallic complexes with CO or H_2 would give no reaction. However, Evans reported in 1981 that reaction of one equivalent of CO with a lanthanide alkyl complex resulted in insertion of CO to form an acyl complex (eq 6). However, unlike transition metal acyls, the lanthanide acyls were found to behave as oxycarbenes such that further reaction with CO afforded a bimetallic enedionediolate complex (eq 7)[19].

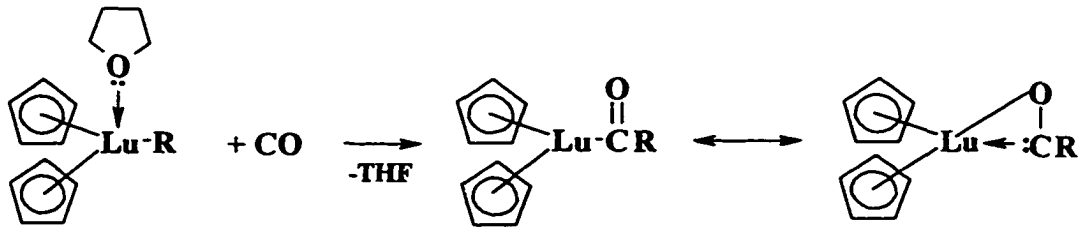

(6)

R = ^{t}Bu

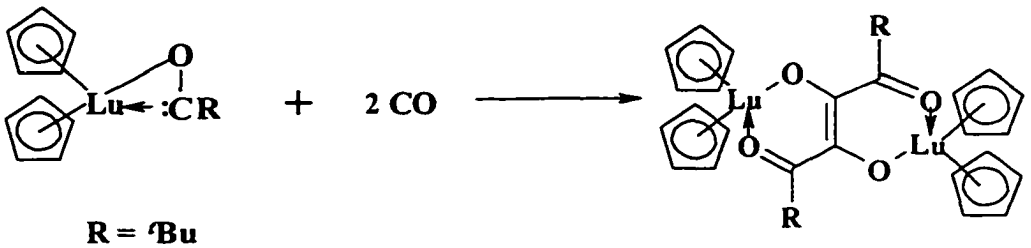

(7)

R = ^{t}Bu

A year later, Evans reported the successful hydrogenation of a Ln-alkyl bond, producing a bridging hydride complex. The reaction was done in the absence of coordinating solvents because they were found to inhibit the reaction by preventing H_2 from attacking the M-C bond. Due to the absence of a two electron redox couple, eg. M^{+}/M^{+3}, commonly observed for late transition metals, oxidative-addition and reductive-elimination can not occur. Instead, a "four-centre" or "sigma-bond metathesis" transition state is proposed (eq 8)[20] which requires no change in metal oxidation state.

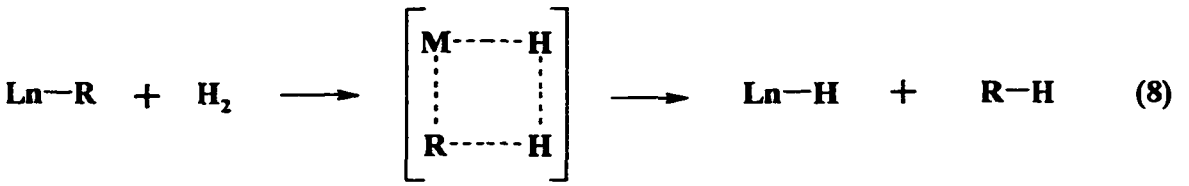

(8)

R = alkyl

Although the discovery of C_5H_5 as a ligand was serendipidous, it made a revolutionary impact on the organometallic chemistry of the rare earths. By the mid- 1970's, the introduction of the pentamethylcyclopentadienyl derivative, C_5Me_5, would reinforce the domination of cyclopentadienyl type ligands in this area of chemistry for the next two decades[21]. The advantages of C_5Me_5 as an ancillary ligand for organolanthanide chemistry were quickly recognized. The increased bulk of C_5Me_5 allows isolation of soluble monomeric complexes of greater crystallinity, making X-ray investigations easier. Besides steric effects, the electronic properties of the ligand are affected by the presence of the methyl substituents, resulting in increased electron donation to the metal. The introduction of C_5Me_5 was obviously a key advancement in the organometallic chemistry of the rare earths and the potential for unique chemistry would soon to be revealed by the pioneering work of Ballard[22], Watson[23], Evans[24], Marks[25], Bercaw[21a, 21b], Teuben[26], and Andersen[27]. However, it was Ballard[22] who first discovered and briefly reported in 1978, the ability of $[(C_5H_5)_2ErMe]_2$ and $[(C_5Me_4Et)_2Y(n\text{-}Bu)]$ to polymerize ethylene. The longer lifetime of the latter catalyst was attributed to the electronic stabilization from the alkyl groups of the cyclopentadienyl ligand. The results of Ballard[22] and Evans[20] inspired Watson's work with $[(C_5Me_5)_2LuMe]_2$ and $[(C_5Me_5)_2LuH]_2$ which established the ability of lanthanide alkyl or hydride complexes to catalyze the oligomerization of olefins.

Watson observed two fundamental processes involved in olefin polymerization: chain propagation by insertion into M-C or M-H bond and chain termination by β-hydrogen or β-alkyl elimination (Scheme 1)[23]. While the latter decomposition pathway is not observed for late transition metals, both pathways are competitive for group 3 and the lanthanides. The observation of β-alkyl elimination can be rationalized on the basis of thermodynamic factors. For the late transition metals, the M-H bond dissociation enthalpy is much greater than that of the M-C bond by about 20 kcal/mol. However, this difference decreases on moving to the left in the Periodic Table (for metals in the same row) to about 5 kcal/mol for early transition metals (d^0) and lanthanides. A large difference between M-H and M-C bond (Δ[D(M-H) – D(M-C)]) favours β-hydrogen elimination, while a smaller difference implies that comparable energy is gained by either of the two decomposition routes so that both pathways are possible[28].

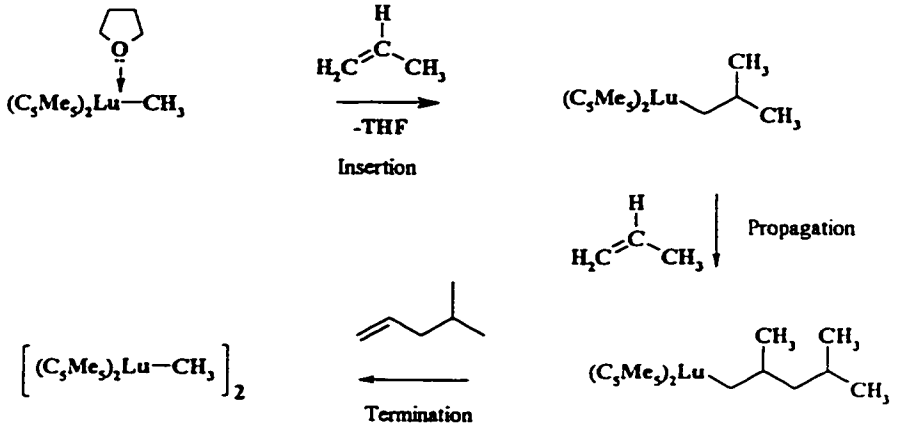

Scheme 1 Olefin polymerization using a lanthanide alkyl complex

Watson's later work demonstrated the ability of alkyl and hydride complexes to activate C-H bonds, including intra- and inter-molecular sp^2 bonds (eq 9) and the sp^3 bond in $SiMe_4$ (eq 10)[29].

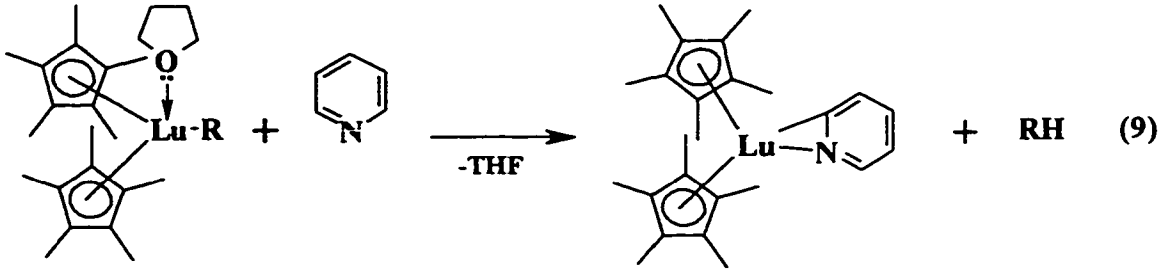

1 R = CH_3
2 R = H

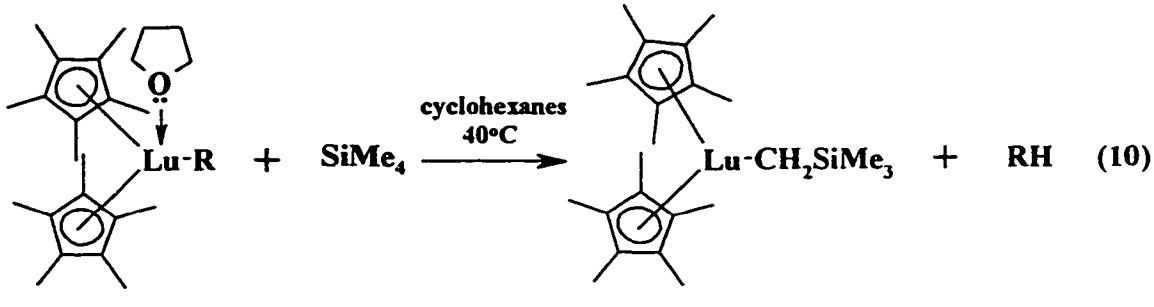

1 R = CH_3
2 R = H

These discoveries clearly showed that the organometallic chemistry of the rare earths was more extensive than originally believed and motivated others to explore this area. In 1987, Teuben reported a series of interesting reactions of unsaturated substrates with $(C_5Me_5)_2YCH(SiMe_3)_2$[26]. Not surprisingly, he observed facile insertion of CO_2 and *t*-BuNC into the Y-alkyl bond. Interestingly, protonolysis of the alkyl complex with stoichiometric quantities of *terminal* acetylenes, HC≡CR, afforded the acetylide complex $(C_5Me_5)_2YC{\equiv}CR$, however, addition of excess acetylene catalytically and regioselectively dimerized the alkyne to produce 3-en-1-ynes[30]. Bulky R groups including *t*-butyl or isopropyl resulted in regioselective head-to-tail dimerization affording $H_2C{=}C(R)\text{-}C{\equiv}C(R)$. For R groups consisting of phenyl or $SiMe_3$, the head to head dimer, $RHC{=}C(H)\text{-}C{\equiv}CR$, exclusively formed. Furthermore, the complexes $(C_5Me_5)_2LnCH(SiMe_3)_2$ for the larger lanthanides, lanthanum and cerium, were found to be efficient catalysts for the cyclodimerization of *internal* alkynes MeC≡CR, for R = Me, Et, *n*-Pr. The proposed catalytic cycle is shown in Figure 1[31].

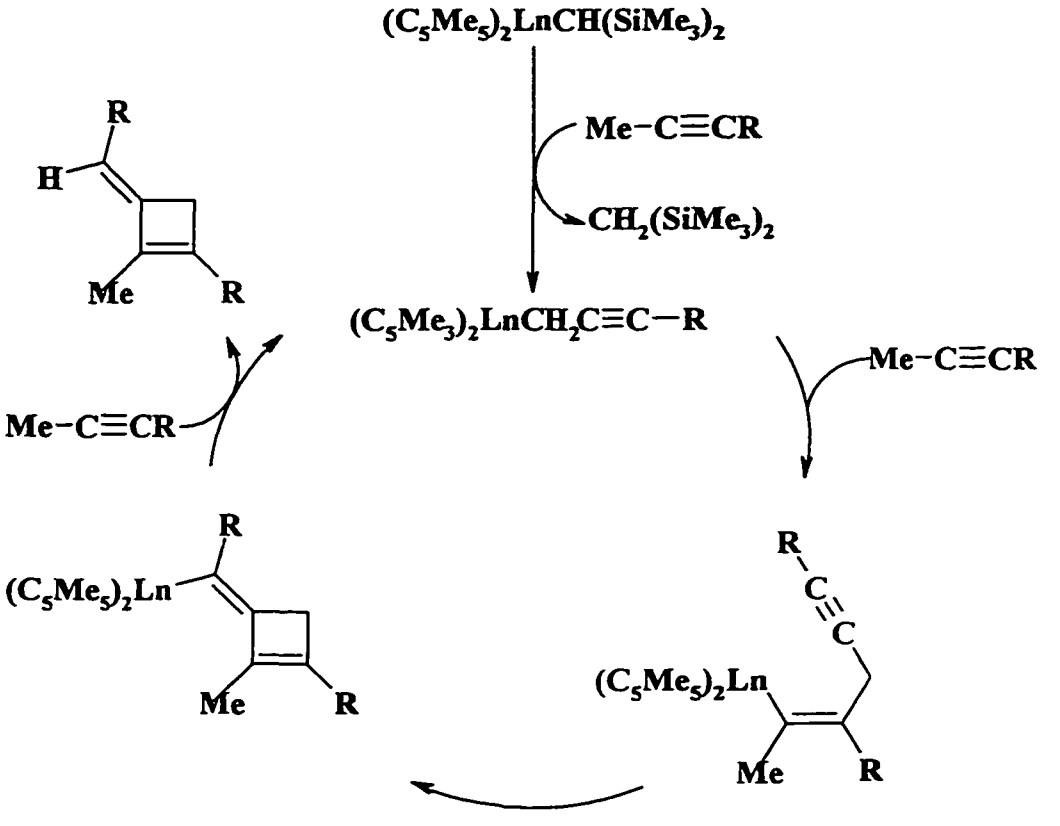

Figure 1 Proposed catalytic cycle for the cyclodimerization of alkynes by $(C_5Me_5)_2LnCH(SiMe_3)_2$[31]

1.2.2 Homoleptic compounds

While the organometallic chemistry of cyclopentadienyl and its derivatives was attracting interest, several other chemists focused their synthetic efforts on preparing homoleptic σ-bonded alkyl or aryl complexes. Hart reported the syntheses of triphenylyttrium and the anionic lithium tetraphenyllanthanate, $Li[LaPh_4]$ in 1970, but the products were not conclusively identified in the absence of X-ray analysis[32]. Later work

revealed that these are in fact polymeric materials[33]. Lappert successfully isolated the first homoleptic complex containing M-C σ-bonds, using the bulky anionic trimethylsilylmethyl and neopentyl alkyls. In 1973, he published the synthesis of $Ln(CH_2EMe_3)_3(THF)_2$ (eq 11)[34].

$$LnCl_3 + 3\,LiCH_2EMe_3 \rightarrow Ln(CH_2EMe_3)_3(THF)_2 + 3\,LiCl \quad (11)$$

Ln = Y; E = C, Si and Ln = Tb, Er, Yb; E = Si

The reaction was reported to work in a 1:1:1 mixture of THF:diethyl ether:hexanes and the presence of THF was necessary to assist the formation of the neutral monomeric tris(alkyl) complex by occupying two apical coordination sites in a trigonal bipyramidal structure. Neither the trimethylsilylmethyl nor the neopentyl ligands were bulky enough to isolate as base-free complexes. In fact, the complexes, $Ln(CH_2SiMe_3)_3(THF)_2$, are thermally sensitive and on prolonged standing at room temperature, they decompose by elimination of THF and TMS to give the postulated pyrophoric polymer $1/n\{[Ln(CH(SiMe_3)(CH_2SiMe_3)\}_n]$, although this has never been confirmed by structural analysis (Fig.2)[35].

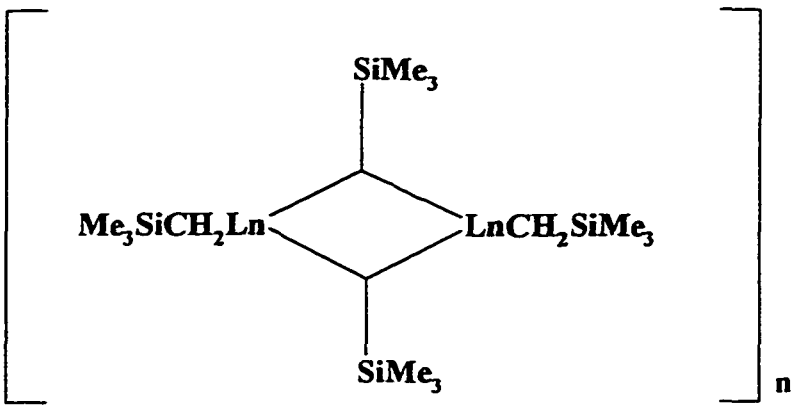

Ln = Lu, Er, and Tm

Figure 2 Proposed decomposition product of $Ln(CH_2SiMe_3)_3(THF)_2$[35]

The first base-free complex was reported in 1974 by Lappert who claimed to have isolated $Y[CH(SiMe_3)_2]_3$ from the reaction of anhydrous yttrium trichloride with a stoichiometric quantity of the disilylated methyl lithium alkyl reagent, $LiCH(SiMe_3)_2$[36]. In a later publication Lappert and coworkers showed that similar reactions involving the metal trichlorides of ytterbium and erbium resulted in retention of LiCl in the complexes, giving the anionic "ate" complexes, $[Li(THF)_4][Ln\{CH(SiMe_3)_2\}_3Cl]$ which was confirmed by X-ray analysis for Ln = Yb[37]. Although coordinative unsaturation around the metal sphere resulted in LiCl retention for erbium and ytterbium, it is surprising that a neutral homoleptic alkyl was isolated for yttrium; since all three metals have similar ionic radii.

Schumann studied in detail the ligation of methyl groups on rare earth metals. The synthesis of $[LnMe_6]^{3-}$ for all rare earth elements (excluding Pm and Eu) and the X-ray crystal structure for holium and erbium complexes were published in 1984[38]. His work is consistent with the electrophilic and ionic nature of the lanthanides which require both steric saturation and charge balance. The presence of three equivalents of lithium tetramethylethylene diamine (TMEDA) or lithium dimethoxyethane (DME) assist the electronic and steric saturation of the $[LnMe_6]^{3-}$ core. The synthesis of these complexes in TMEDA are shown in equation 12 and the molecular structure is shown in Figure 3[39].

$$LnCl_3 + 6\,MeLi + 3\,TMEDA \xrightarrow{Et_2O} [Li(TMEDA)]_3[LnMe_6] + 3\,LiCl \quad (12)$$

Ln = Y, La-Nd, Sm-Lu

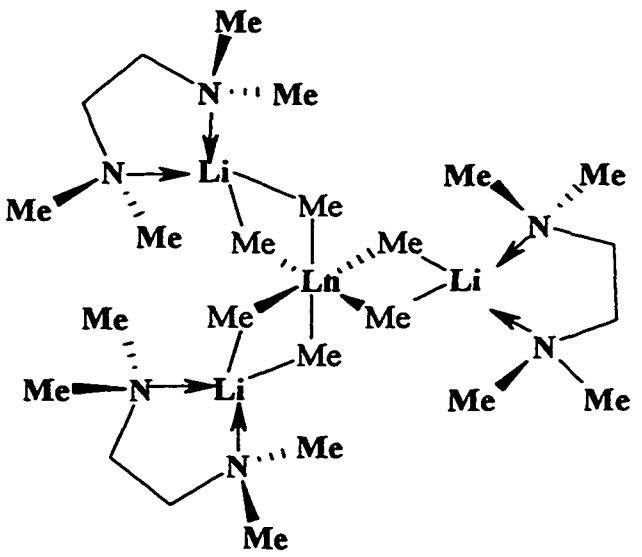

Figure 3 Molecular structure of $\{[Li_3(TMEDA)_3][LnMe_6]\}$[39]

Even for the bulkier neopentyl and trimethylsilylmethyl ligands, reaction of four equivalents of the alkyllithium reagent with one equivalent of the metal trichoride in diethyl ether resulted in the formation of an anionic "ate" complex. Alternatively, the anionic complexes can be accessed in a reaction of the tris(alkyl), $Ln[(CH_2SiMe_3)_3(THF)_2]$ with the corresponding alkyl lithium reagent in a ratio of one to one. In 1988 Lappert introduced a very useful synthetic strategy that would hinder formation of "ate" complexes. Apparently "ate" complexes occur only in strong donor solvents, hence the absence of such solvents is necessary to prevent "ate" formation. Instead of using the slightly THF soluble, metal trichlorides, the bulky, monomeric lanthanide tris(2,4,6-tri-*t*-butylphenoxide) was used as an alternative starting precursor that is soluble in nonpolar solvents[40]. A stoichoimetric reaction of bulky bis(trimethylsilyl)methyl lithium with the

tris(phenoxide) in pentane or hexane resulted in the clean elimination of insoluble lithium phenoxide and formation of the hexane soluble base-free tris(alkyl) product (eq 13).

$$[Ln(OAr)_3] + 3\,Li[CH(SiMe_3)_2] \rightarrow Ln[CH(SiMe_3)_2]_3 + 3\,LiOAr \quad (13)$$

Ln = Y, La, Sm, Lu: OAr = 2,4,6- tri-t-butyl phenoxide

The synthetic utility of these homoleptic complexes was first suggested by Lappert. He reported that based on differences in pKa, protonolysis of the alkyl groups could lead to other novel organometallic complexes. In a test reaction, the lanthanide tris(alkyl) with either three equivalent of the silylamine, $HN(SiMe_3)_2$ or phenol, HOAr (OAr = 2,6-di-*t*-butyl-phenoxide) gave the known complexes, $Ln[N(SiMe_3)_2]_3$ or $Ln(OAr)_3$[41].

1.2.3 Porphyrins

Numerous lanthanide porphyrin coordination compounds were reported in the mid 1980's, such as $Ln(OEP)_2$[42] and [Ln(TPP)(acac)][43] for all lanthanides, but the ability of these ligands to stabilize lanthanide alkyl complexes was not realized until the early 90's[44]. The work with porphyrins was a significant departure from C_5Me_5 ligation in organolanthanide chemistry. It was demonstrated that the smaller lanthanides, yttrium and lutetium fit best into the cavity of the porphyrin macrocycle[44]. The most convenient preparation of these complexes is by protonolysis of the tris(alkyl) precursor with one

equivalent of the diprotic octaethylporphyrin to afford (OEP)LnR and two equivalents of RH[44d]. Alternatively, a chloride derivative can be prepared by treating the octaethylporphrin dianion with one equivalent of the metal trichloride. Subsequent metathesis with an alkyl lithium reagent precipitates LiCl and affords the soluble alkyl complex[44a,b,c]. The latter route is a general entry into various alkyl complexes; however, salt complexation or solvate formation frequently occurs. To avoid this problem, the OEP mono-phenoxide derivative can be isolated by protonolysis of the lanthanide tris(phenoxide) precursor by $OEPH_2$, since the latter has a lower pKa than HOAr (eq 14)[44d].

$$\mathbf{M(OAr)_3 + OEPH_2 \rightarrow (OEP)M(OAr) + 2HOAr} \quad \textbf{(14)}$$

M = Lu, Y; OAr = 2,6, di-t-butyl-phenoxide

The crystal structure of $(OEP)LuCH(SiMe_3)_2$ shows that the metal, with a five coordinate square pyramidal geometry, sits above the plane of the porphyrin ring (Fig 4)[10,33].

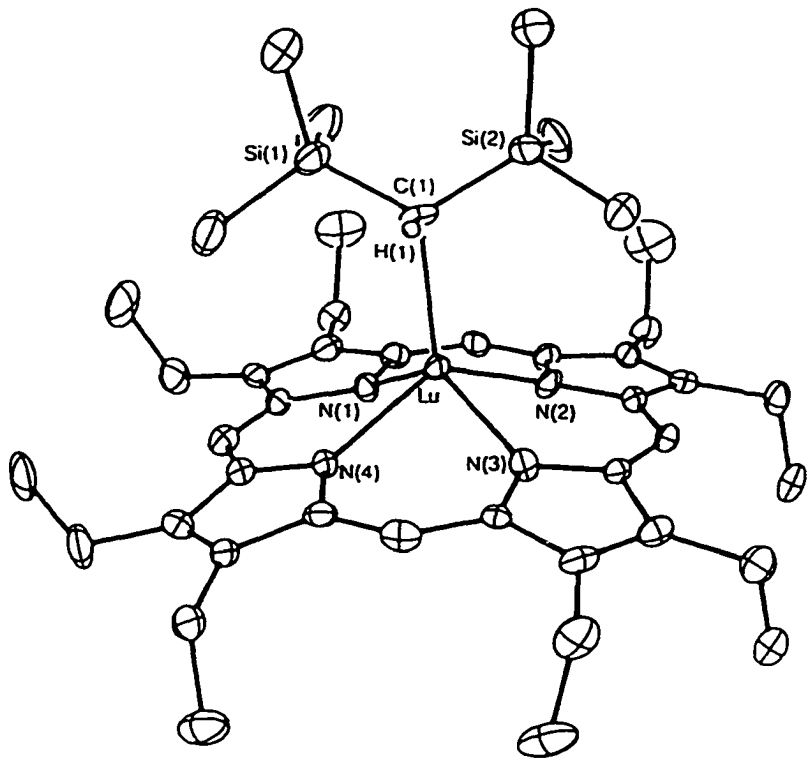

Figure 4 ORTEP drawing of Lu(OEP)[CH(SiMe$_3$)$_2$][10]

The reactivity of (OEP)M[CH(SiMe$_3$)$_2$], for M = Y, Lu, has been studied in detail by several groups[44]. For example the reaction of the terminal acetylene, butyne, afforded the bridging acetylide[44e]. Also, when one equivalent of H_2O was added to the alkyl complex, a dimeric hydroxo complex, [{Ln(μ-OH)(OEP)}$_2$] was isolated[45]. However, in contrast to the facile hydrogenolysis of (C$_5$Me$_5$)$_2$M[CH(SiMe$_3$)$_2$] (M = Y, La, Nd, and Ce), the analogous OEP complex does not react with hydrogen, even when pressurized to 20 bar[10]. The decreased hydrogenolysis reactivity is best explained on the basis of differing electronic properties. Schavarien has proposed that the electronegative, hard nitrogen donors on the porphyrin render the metal centre more electropositive in comparison to the

hydride. Unlike the carbanion, $^{-}CH(SiMe_3)_2$ in which the alkyl complex is stabilized by delocalization of the negative charge through the β-silicon atoms, the less stable hydride complex cannot form unless the negative charge is dispersed. This can be accomplished by formation of bridging hydrides to two metal centres as observed for $[(C_5Me_5)_2Y(\mu\text{-}H)]_2$ and $[(C_5Me_5)Y(OAr)(\mu\text{-}H)]_2$, (OAr = O-2,6-$C_6H_3$-$t$-$Bu_2$). The hydride of the latter complex was formed by hydrogenation of the corresponding alkyl by applying high pressures of 10 bar. This suggests that replacement of C_5Me_5 with OAr decreases hydrogenation reactivity[10].

In light of the difficulty of preparing the hydrides and the inability of the alkyl complexes of the porphyrins to polymerize olefins, the reaction chemistry of these complexes were abandoned to pursue research into fine tuning the environment around the metal centre. Much recent work has focused on designing new ligands with the goal of better understanding the possibilities and constraints on the insertion chemistry of unsaturated organic molecules, with lanthanide hydrides and alkyls.

1.2.4 Alkoxides and amides

While the tris(phenoxides) have attracted attention as precursors to homoleptic lanthanides alkyls, attempts to prepare lanthanide alkyl complexes supported with alkoxides or aryloxides in the absence of C_5Me_5 were frustrated by formation of complicated mixtures of products due to alkoxide exchange or ligand redistribution reactions. Recently, Schavarien introduced the sterically hindered chelating biphenol (I) and binapthol (II). Monomeric complexes were formed by protonolysis of the homoleptic

lanthanum alkyl, $La[CH(SiMe_3)_2]_3$. The unique feature of lanthanide complexes derived from (I) and (II) is their intrinsic molecular chirality which results in two diasterotopic $SiMe_3$ signals being observed in both the ^1H and ^{13}C NMR. Complexes of this type may have potential as asymmetric catalysts[46].

A number of other alternatives to cyclopentadienyl type ligands have surfaced in the 1990's. The tridentate amido phosphine $[N\{SiMe_2CH_2PMe_2)_2]^-$ (III) anion is a rare example of a ligand containing both "soft" phosphorus donors and hard nitrogen donors[47]. The tridentate tris(pyrazolylborate) anion $HB[3\text{-}t\text{-}Bu\text{-}5\text{-}Me\text{-}pz]_3^-$ (IV) is the only example of a ligand that has allowed isolation of novel divalent lanthanide alkyl complexes[48]. The bulky silylated benzamidinate, $[RC(N(SiMe_3)_2]^-$ (V), which has the steric equivalence of C_5H_5[49] and the bulky silanol, $HOSi\text{-}t\text{-}BuAr_2$, Ar = $o\text{-}C_6H_4(CH_2NMe_2)^-$ (VI), which contains a chelating siloxide, have also been explored[50].

The most common ligand design themes involve a sterically bulky chelating ligand incorporating at least one or more oxygen or nitrogen donors. Ideally, the ligand should be simple, leading to symmetrical complexes and easy NMR interpretation. For practical reasons, it is best if the ligand and its derivatives are easy to prepare in high yields. Additionally, it is best if the ligand is soluble in at least one aprotic organic solvent, preferably a hydrocarbon, however, more polar solvents such as diethyl ether or tetrahydrofuran can be tolerated. The challenge is to design new ligands which are capable of satifying the steric requirements of the organolanthanide centre and provide a unique electronic environment different from C_5Me_5 and allow access to new reactivity patterns.

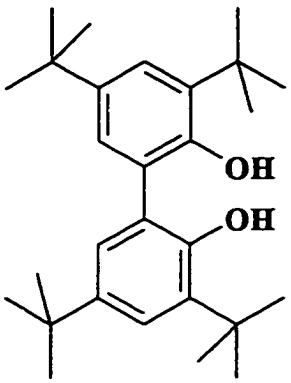

I

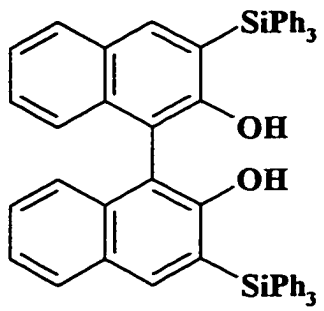

II

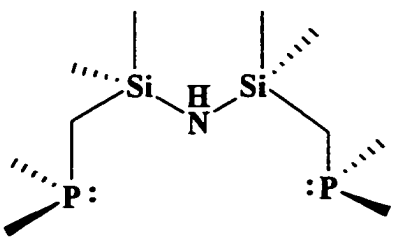

III

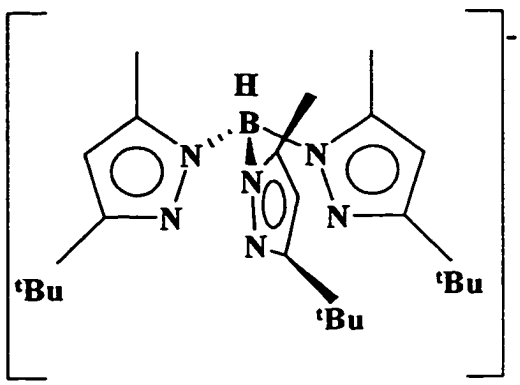

IV

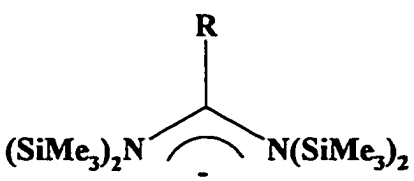

R= H, OMe, CF_3

V

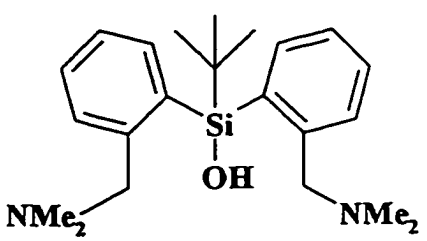

VI

1.3 Scope of this work

It is the goal of this research project to further explore the organometallic chemistry of yttrium, zirconium, and the lanthanides using deprotonated aza-crown ethers as stabilizing ligands. The organometallic chemistry of zirconium is also studied in this thesis because cationic zirconium complexes are isoelectronic (neglecting f electrons) with the monomeric complexes of the lanthanides and group 3[51]. Furthermore, these cationic zirconium complexes exhibit a wealth of impressive stoichiometric and catalytic reactivity and in fact, they are proposed to be the active catalyst in olefin polymerization[51, 52]. In this project, aza-crown macrocycles consisting of oxygen and amido functionalities are utilized as ancillary ligands. Specifically, deprotonated 4,13-diaza-18-crown-6 (DAC) (**1**), deprotonated aza-18-crown-6 (MAC) (**2**), and deprotonated aza-15-crown-5 (15-AC-5) (**3**) are discussed.

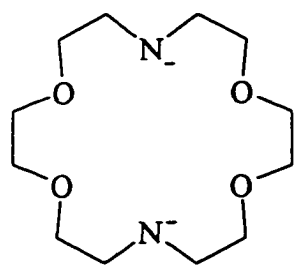

1

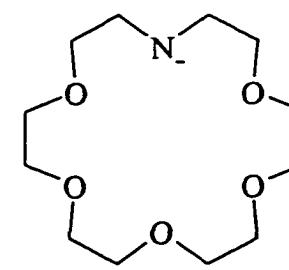

2

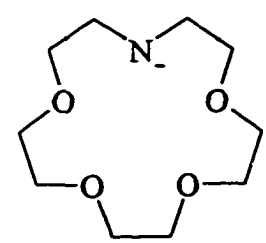

3

In chapter 2, the coordination chemistry of deprotonated 4,13-diaza-18-crown-6 (DAC) with yttrium and the lanthanide metals is investigated. The search for a general entry into the organometallic σ-alkyls of these metals is discussed using silylamides and alkoxides as precursors. An alternative route via divalent lanthanide complexes is also examined. Chapter 3 discusses organoyttrium complexes stabilized by DAC ligation. Synthesis, characterization, thermal decomposition and reactivity studies are included. The synthesis, characterization, and reactivity of organozirconium DAC-supported dialkyl complexes and their cations are presented in Chapter 4. In Chapter 5, the synthesis, characterization, and reactivity studies of yttrium dialkyl complexes supported by the deprotonated aza-crown macrocycles, MAC and 15-AC-5 will be addressed. Also included in this chapter is the preparation and characterization of a novel cationic yttrium alkyl complex. Chapter 6 concludes this thesis with a discussion of general routes to organometallic complexes of yttrium, zirconium, and the lanthanides containing aza-crown ethers, and includes suggestions for future studies. Finally, Chapter 7 provides full experimental detail pertaining to the synthesis and characterization of the ligands and their metal complexes discussed throughout this work.

CHAPTER 2

COORDINATION CHEMISTRY OF DEPROTONATED 4,13-DIAZA-18-CROWN-6 (DAC) WITH THE GROUP 3 AND LANTHANIDE METALS

2.1 Introduction

The synthesis of crown ether macrocycles and their ability to form stable complexes with alkali and alkaline earths metals were significant discoveries pioneered by Pedersen in 1967[53]. This work was followed by the preparation of analogous macrocycles consisting of nitrogen and sulfur donors (either as separate or additional donors)[54]. It became known that a preferential cation complexation resulted when the cavity size and the ionic radius were perfectly matched. All donors in the macrocycle participate in the coordination giving the most stable complexes. Host-guest (ligand to metal) complexation of one to one is common, but variable stoichiometries (1:2, 2:3, 3:4 and 2:1) have also been observed for which the ratio of cavity size and ionic radius are far from unity. The stability and stoichiometry of these macrocyclic complexes are also a function of solvent and other anions that may compete with the macrocyclic donors for coordination sites. Several key applications became well established that attracted attention to the chemistry of host-guest complexation. Some of these processes include isotope separation, selective ion transport through artificial and natural membranes, and models for understanding the mechanism of metalloenzyme action. Details regarding the stability constants and other properties of host-guest complexation are found elsewhere[55].

The macrocyclic coordination chemistry of lanthanides was not investigated until at least 10 years after the published report by Pedersen[56]. This is somewhat surprising considering the fact that the estimated cavity sizes of 15-crown-5 (0.86 – 0.92 Å) and 18-crown-6 (1.34 –1.43 Å) macrocycles relative to the trivalent lanthanide ionic radius (La : 1.03Å to Lu: 0.86Å) are very compatible and strong 1:1 complexes are expected to

form[54a]. However, dissociation of lanthanide-crown ether complexes in aqueous solutions resulting from the large hydration energies of Ln^{3+} ions (Table 1)[56] deterred work in this area until it was discovered that complexes with variable stoichiometry could be isolated in non-aqueous solvents such as acetonitrile, acetone, or acetonitrile-methanol mixture. This work was followed by an extensive investigation of the coordination chemistry of crown ethers and their nitrogen substituted analogs with the lanthanides[57].

Table 1 Hydration energies $-\Delta G_f^\circ$ (kcal/mol) of trivalent lanthanide ions[56]

La	665 ± 5	Pm	669 ± 21	Tb	657 ± 13	Tm	665 ± 17
Ce	672 ± 8	Sm	661 ± 13	Dy	669 ± 17	Yb	644 ± 13
Pr	677 ± 8	Eu	573 ± 13	Ho	686 ± 13	Lu	-
Nd	673 ± 5	Gd	657 ± 13	Er	673 ± 8		

Exploration of the organometallic chemistry of lanthanides using crown ethers or nitrogen substituted macrocycles as ancillary ligand had not been attempted prior to this work. Perhaps these ligands appeared unattractive because the non-directional electrostatic nature of the bonding in lanthanides could form insoluble oligomeric material in the presence of excessive donors of the flexible macrocycle. The only examples of deprotonated aza-crowns in organometallic chemistry are the aluminum alkyl complexes prepared by Robinson[58] and Gokel and Richey[59]. Their results suggested that monomeric macrocyclic complexes could be isolated consisting of a flexible donor array capable of saturating one hemisphere of the metal coordination sphere, while allowing the other

hemisphere free to participate in chemical reactivity. This coordination mode was expected to prevent formation of polymeric products and provide an attractive alternative to bis(pentamethylcyclopentadienyl) ligation. Since 4,13-diaza-18-crown-6 (H_2DAC) is relatively easy to prepare on large scale in good yields, the goal of this work was to obtain a facile route into the organometallic chemistry of yttrium and the lanthanides, so that the synthesis and reactivity of these complexes could be compared to the well-established bis(pentamethylcylcopentadienyl) and porphyrin systems.

2.2 Ligand synthesis

4,13-diaza-18-crown-6 (H_2DAC) can be purchased from Aldrich at a current price of $130 Can. per gram (Aldrich 1997)[9]. Fortunately, the starting materials are relatively inexpensive and the synthesis is fairly simple (Scheme 2). Kulstad and Malmsted[60] initially reported the preparation from 1,2-bis(2-iodoethoxyethane) (**6**) and 1,8-diamino-3,6-dioxaoctane (**5**). Gokel and coworkers[61], later improved the methodology using 1,2-bis(2-iodoethoxyethane) (**6**) and benzylamine to afford dibenzyl protected DAC (7). Subsequent workup followed by recrystallization and hydrogenation of the benzyl protecting group affords crude H_2DAC. After recrystallization from hexane an overall yield of 60% is obtained compared to 30% by the original Kulstad and Malmsted route (Scheme 2).

Scheme 2 Synthesis of 4,13-diaza-18-crown-6 (H_2DAC)

(Kulstad and Mulmsted route)[60]

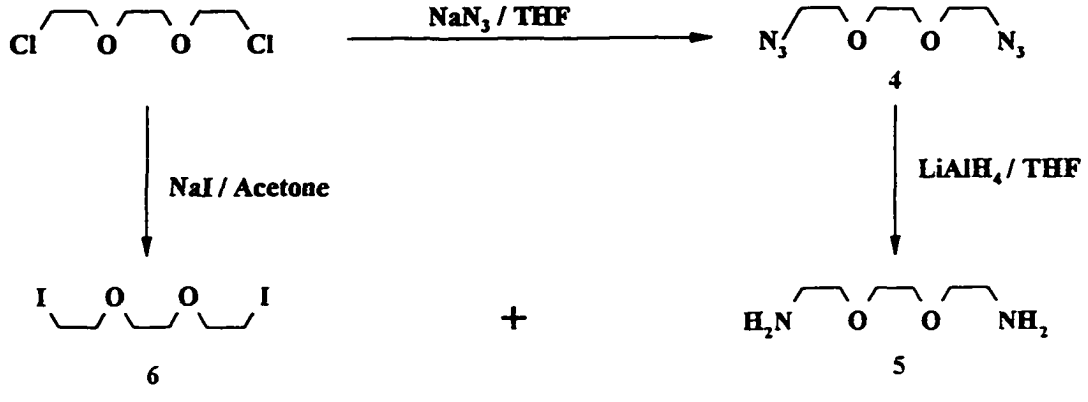

(Gokel route)[61]

2.3 General routes to organolanthanide complexes

2.3.1 Synthesis of octaethylporphyrin (OEP) alkyl complexes by salt elimination [44a,b,c]

A common entry into preparing organometallic complexes of group 3 and the lanthanides is by σ-bond metathesis. In nonpolar hydrocarbon solvents these reactions often proceed with clean elimination of LiCl. One example is the organoscandium chemistry using octaethylporphyrin (OEP) macrocycle as ancillary ligation. Arnold published a wide range of alkyl complexes of scandium which are accessible by alkylation of the hydrocarbon soluble precursor (OEP)ScCl (**VIII**). Complex VIII was prepared by deprotonation of H_2OEP with 2 equivalents of $LiN(SiMe_3)_2$ to afford OEP dilithium dianion, $(THF)_4Li_2OEP$ (**VII**), followed by metathesis with $ScCl_3 \bullet 3THF$ (Scheme 3).

In more polar solvents such as THF, these metathesis reactions can follow a different course and the final product may retain LiCl in the coordination environment around metal. Alternatively, lithium phenoxides have a lower tendency than LiCl to be retained in the final product, thus lanthanide phenoxide precursors are widely preferred over the halide analog[62]. In fact Schavarien gained access to yttrium and lanthanide alkyl complexes of OEP by alkylation of $Ln(OEP)(OC_6H_3\text{-}2,6\text{-}t\text{-}Bu_2)$[44d].

Scheme 3 General route into organoscandium chemistry using OEP ligation[44c]

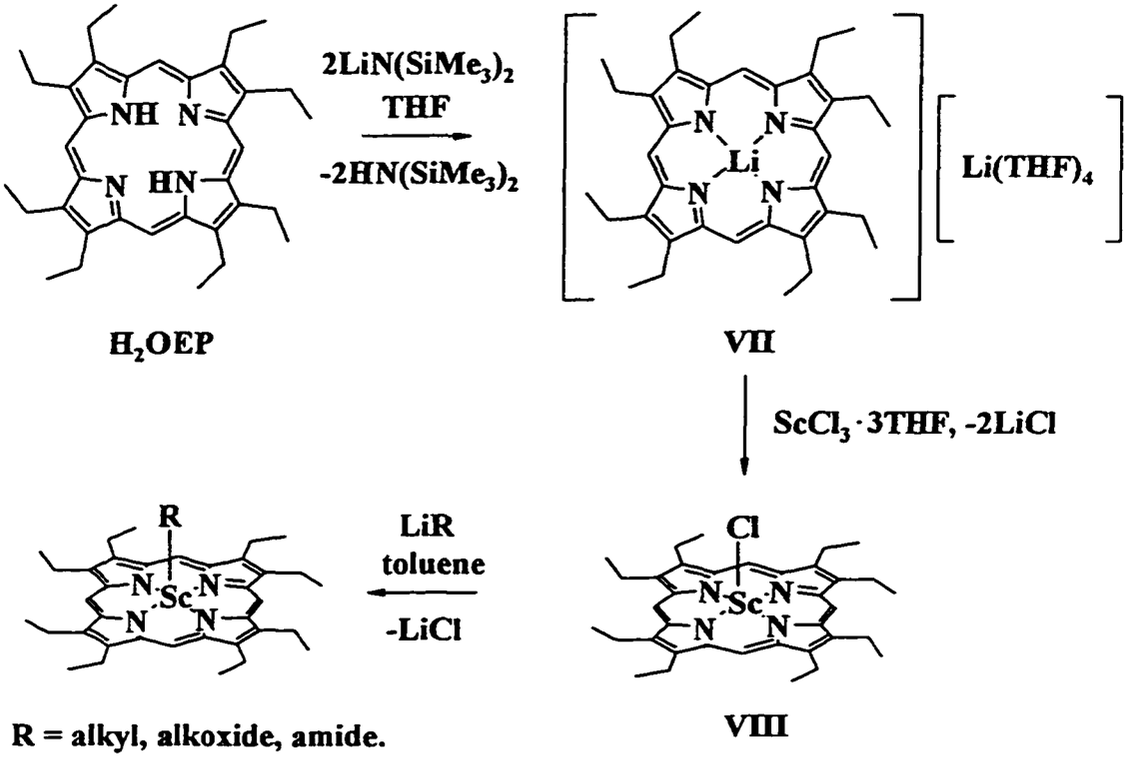

2.3.2 Attempted salt elimination of deprotonated 4,13-diaza-18-crown-6 ligation

Dilithiation of H_2DAC with 2 equivalents of *n*-BuLi, MeLi, $LiN(SiMe_3)_2$, or $LiCH_2SiMe_3$ in toluene cleanly affords soluble Li_2DAC. However, on addition of a solution of Li_2DAC to a suspension of anhydrous YCl_3 in THF, a white precipitate persisted while the reaction mixture was stirred over 24 h at room temperature. Filtration of the precipitate followed by evaporation of the solution resulted in a minute quantity of a toluene soluble transparent residue for which ^1H NMR showed no resonances belonging

to DAC. Presumably, the white product contained LiCl and $[Y(DAC)Cl]_x$ which remained insoluble in THF, precluding characterization by NMR. The insolubility of the product suggests that $[Y(DAC)Cl]_x$ is polymeric in nature. A dimeric structure with bridging chlorides is also possible, however, THF is known to cleave such halide bridges by coordinating to the unsaturated metal centre resulting in a soluble monomeric complex. The preparation of a potentially more soluble phenoxide derivative Y(DAC)(OAr) was attempted by reacting $Y(OC_6H_3\text{-}2,6\text{-}t\text{-}Bu_2)_3$[41] with Li_2DAC. Unfortunately an insoluble white precipitate was also isolated in this case and the toluene soluble residue had a similar ^1H NMR spectrum to that obtained in the YCl_3 reaction. Perhaps the failure of these metathesis reactions is a consequence of the large stability constants of alkali metals in crown ethers[55], such that lithium is retained into the macrocycle in preference to the lanthanide. After these initial attempts, alternative strategies for preparing organometallic complexes of lanthanides and yttrium were investigated which do not involve methathesis.

2.4 Synthesis and characterization of trivalent lanthanide and yttrium complexes of deprotonated 4,13-diaza-18-crown-6 [DAC]

2.4.1 Synthesis of $Ln(DAC)[N(SiMe_3)_2]$

The protonolysis reaction of H_2DAC with one equivalent of the trivalent tris{bis(trimethylsilylamido)} lanthanide complex, $Ln[N(SiMe_3)_2]_3$[4] cleanly affords $Ln(DAC)[N(SiMe_3)_2]$ (eq 15). The silazane by-product (bp 125 °C, 760 mm Hg) was removed under vacuum.

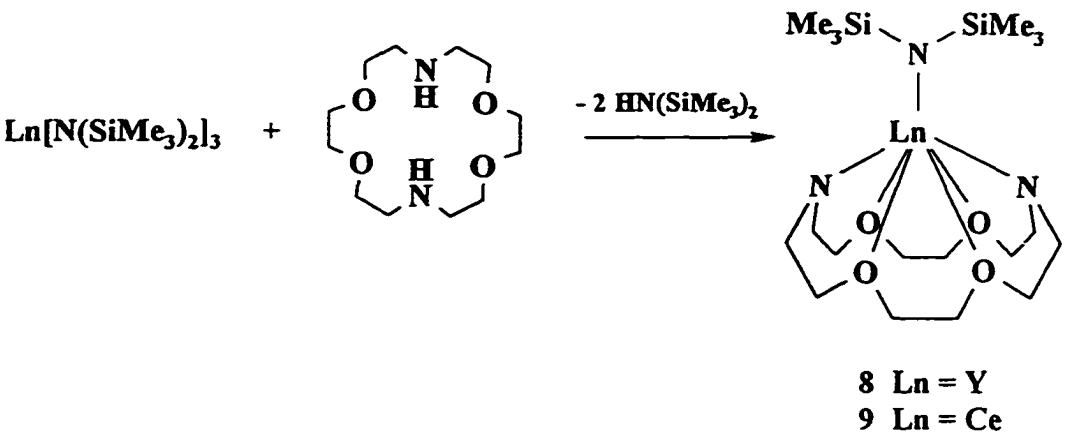

(15)

8 Ln = Y
9 Ln = Ce

Complexes **8** and **9** were recrystallized from a mixture of toluene-hexanes. The crystalline products are moderately soluble in hexanes and very soluble in ether, THF, and toluene. NMR spectral data of both complexes provide strong evidence for a monomeric structure with C_{2v} symmetry as shown for **8**. ^{1}H NMR spectral data for both complexes show six DAC multiplets in addition to one singlet due to the $SiMe_3$ resonance, while three unique DAC resonances are observed in the ^{13}C NMR spectrum of **8**. The NMR data for **8** and **9** are summarized in Table 2.

Table 2 NMR data[a] for Ln(DAC)[N(SiMe$_3$)$_2$] complexes

	Y(DAC)[N(SiMe$_3$)$_2$] **8**				Ce(DAC)[N(SiMe$_3$)$_2$] **9**			
^{1}H NMR	δ^b	mult	Int.	Assign[c]	δ^b	mult	Int.	$\upsilon_{1/2}$[d]
DAC[e]	3.65	m	4H	C_oH	26.0	s	4H	32
	3.55	m	8H	C_oH	19.7	s	4H	28
				C_bH	6.3	s	4H	35
	3.27	m	4H	C_aH	-3.0	s	4H	26
	3.19	m	4H	C_aH	-9.2	s	4H	24
	3.02	m	4H	C_bH	-17.7	s	4H	22
N(SiMe$_3$)$_2$	0.38	s	18H	SiMe_3	1.4	s	18H	16
^{13}C NMR[f]			δ^b					
DAC	55.6 C_a		66.8 C_b	73.3 C_c				
N(SiMe$_3$)$_2$	5.3							

[a]Spectra recorded at 250 MHz (^{1}H) or 62.9MHz (^{13}C) in d_6-benzene or d_8-toluene at 296 K. [b]δ expressed in ppm. [c]Assignment letters refer to the carbon atoms of the unique $NC_aH_2C_bH_2OC_cH_2$ portion of the DAC ligand (the remaining carbons are related to these by the molecular symmetry). [d]$\upsilon_{1/2}$ measured in Hz. [e]No assignment was possible for the DAC protons of this paramagnetic complex. [f]^{13}C spectrum was not observable due to paramagnetic line broadening.

Assignment of the NMR signals were made on the basis of ^{1}H-^{13}C COSY (Fig. 5) experiment for diamagnetic **8**.

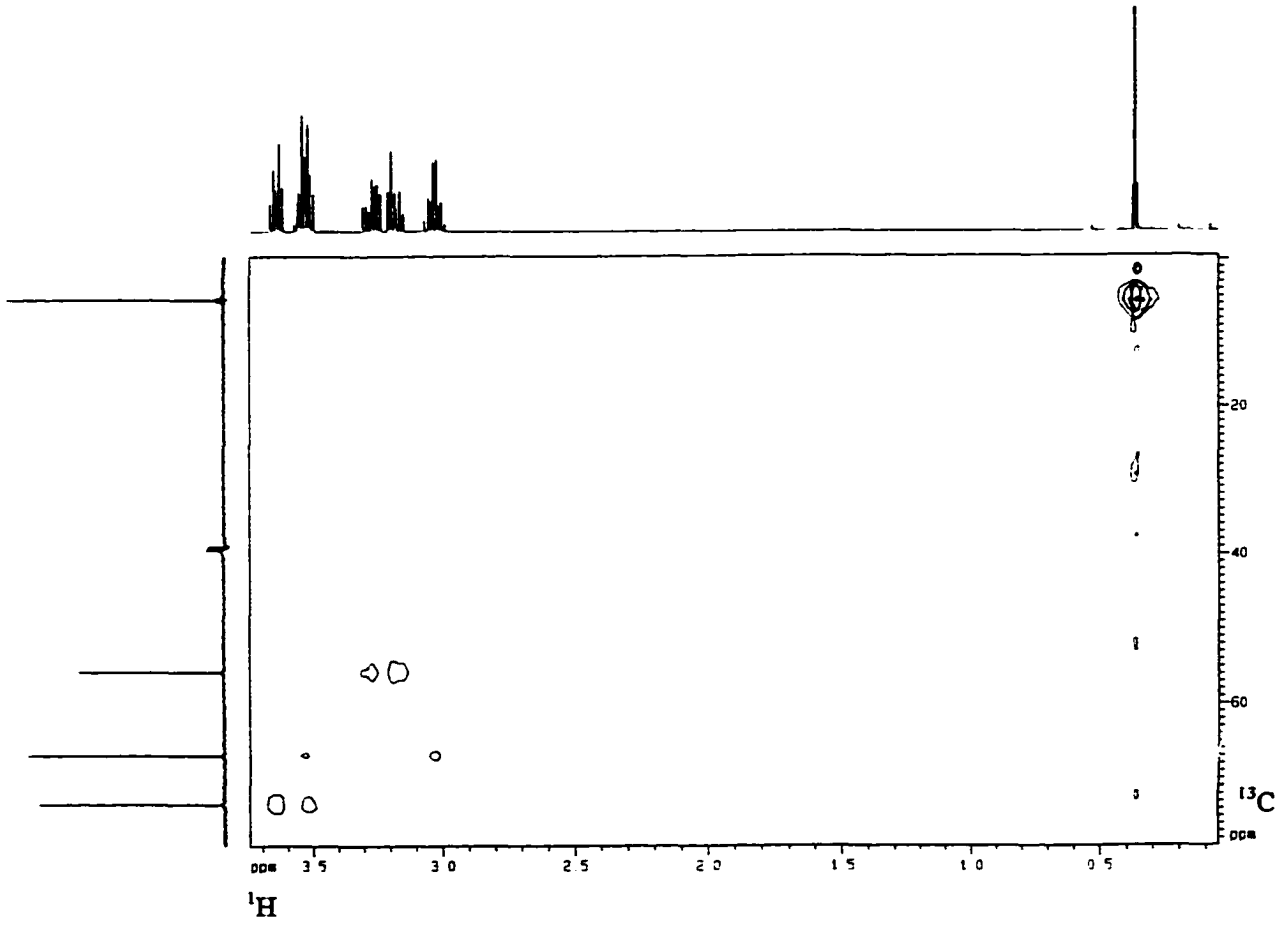

Figure 5 ^{1}H-^{13}C COSY of Y(DAC)[N(SiMe$_3$)$_2$] 8

In the ^{1}H NMR, the DAC resonance at about 3.5 ppm consists of two overlapping multiplets. This is clearly illustrated in the COSY spectrum which shows correlation of two ^{1}H DAC resonances with each ^{13}C signal. Only one quarter of the molecule, consisting of a $NC_aH_2C_bH_2OC_cH_2$ portion, is unique due to the molecular C_{2v} symmetry.

Hence, the unique exo and endo protons on each carbon account for the observation of six DAC multiplets in the ^{1}H NMR and no attempt was made to distinguish these protons unambiguously. One disadvantage of complex **9** is the intrinsic paramagnetism of the cerium which precludes observation of ^{13}C NMR. Fortunately, the ^{1}H NMR spectra of cerium complexes are observable with only slightly broadened linewidths ($\nu_{1/2}$ = 32 Hz) and isotropic paramagnetic shifts that range from +30 to –30 ppm[3]. In view of the differences in sizes between the larger (lighter) and the smaller (heavier) lanthanides, it would be of interest to determine any structural dissimilarity. X-ray diffraction analysis of **8** and **9** were conducted to address this issue and to confirm the monomeric structure of these complexes.

2.4.2 X-ray structural analysis of Y(DAC)[N(SiMe$_3$)$_2$] **8**

An ORTEP drawing of **8** is given in Figure 6. Full crystallographic data are collected in Appendix Tables I-III and selected bond distances and angles are given in Table 3. The structure of **8** is monomeric as suggested by NMR and mass spectroscopy (m/z = 508 M^+); the nearest intermolecular contacts are > 3.5 Å. The bonding geometry around Y may be regarded as consisting of primary trigonal planar coordination of the three amido N (sum of the N-Y-N angles around Y is 359.7°) with secondary coordination of the four ether O above and below the YN_3 plane. The four ether O and the silylamide N form a distorted square pyramid about the Y atom. The DAC N-Y distances are equal within experimental error at 2.29(2) Å

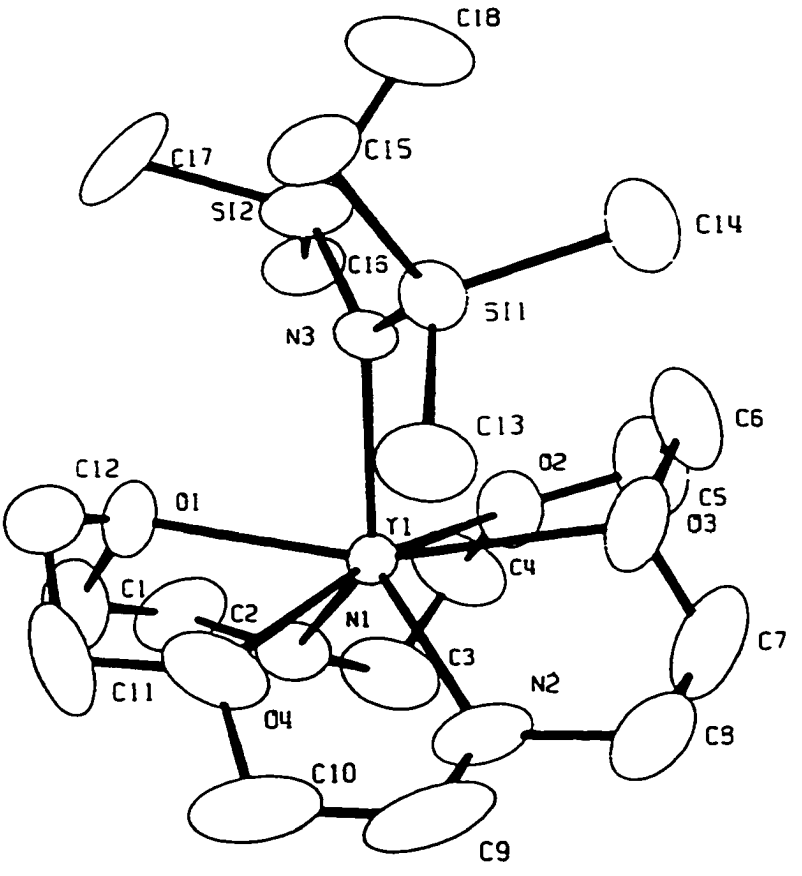

Figure 6 ORTEP drawing of Y(DAC)[(N(SiMe$_3$)$_2$] 8

and marginally shorter than the Y-N(3) (silylamide) distance (2.338(11) Å). The observed Y-N distances fall within the 2.24-2.40 Å range predicted from several other lanthanide silylamides[63] after correction for differences in metal ionic radii[64]. The Y-O distances span a considerable range from 2.457(12) to 2.590(12) Å. The wide range is probably a reflection of packing effects in the solid state. As expected, the silylamide N is planar (sum of angles at N(3) = 360°).

Table 3 Selected bond distances (Å) and angles (deg)[a] for Y(DAC)[N(SiMe$_3$)$_2$] 8

		Distances	
Y(1)-O(1)	2.467(11)	Y(1)-N(1)	2.283(12)
Y(1)-O(2)	2.590(12)	Y(1)-N(2)	2.29(2)
Y(1)-O(3)	2.514(12)	Y(1)-N(3)	2.338(11)
Y(1)-O(4)	2.457(12)	N(3)-Si(1)	1.714(11)
		N(3)-Si(2)	1.692(12)
		Angles	
O(1)-Y(1)-O(2)	112.2(5)	O(3)-Y(1)-N(1)	116.9(5)
O(1)-Y(1)-O(3)	162.1(5)	O(3)-Y(1)-N(2)	67.8(6)
O(1)-Y(1)-O(4)	65.2(5)	O(3)-Y(1)-N(3)	83.5(5)
O(1)-Y(1)-N(1)	67.0(5)	O(4)-Y(1)-N(1)	99.9(4)
O(1)-Y(1)-N(2)	129.5(6)	O(4)-Y(1)-N(2)	68.0(7)
O(1)-Y(1)-N(3)	82.3(4)	O(4)-Y(1)-N(3)	97.9(4)
O(2)-Y(1)-O(3)	59.2(2)	N(1)-Y(1)-N(2)	104.2(5)
O(2)-Y(1)-O(4)	163.8(4)	N(1)-Y(1)-N(3)	133.3(4)
O(2)-Y(1)-N(1)	65.7(4)	N(2)-Y(1)-N(3)	122.5(5)
O(2)-Y(1)-N(2)	107.2(6)	Y(1)-N(3)-Si(1)	118.4(6)
O(2)-Y(1)-N(3)	97.6(4)	Y(1)-N(3)-Si(2)	121.7(6)
O(3)-Y(1)-O(4)	127.7(5)	Si(1)-N(3)-Si(2)	119.9(7)

[a] estimated standard deviation in parentheses

The cerium complex **9** was also investigated by X-ray crystallography since preliminary photographic work showed that **8** and **9** were not isostructural. Appendix Table IV is a summary of the crystallographic data for Ce(DAC)[N(SiMe$_3$)$_2$]. The diffraction study revealed two independent monomers in the unit cell, unfortunately, one of which was severely disordered. The well-behaved molecule showed the same gross structural features as **8**.

2.4.3 Attempted synthesis of yttrium DAC phenoxide derivatives

Attempts to convert Y(DAC)[N(SiMe$_3$)$_2$] **8** into an alkoxide precursor **10** were investigated in order to isolate a suitable metathesis precursor (Scheme 4).

Scheme 4 Protonolysis of Y(DAC)[N(SiMe$_3$)$_2$] 8 with alcohols

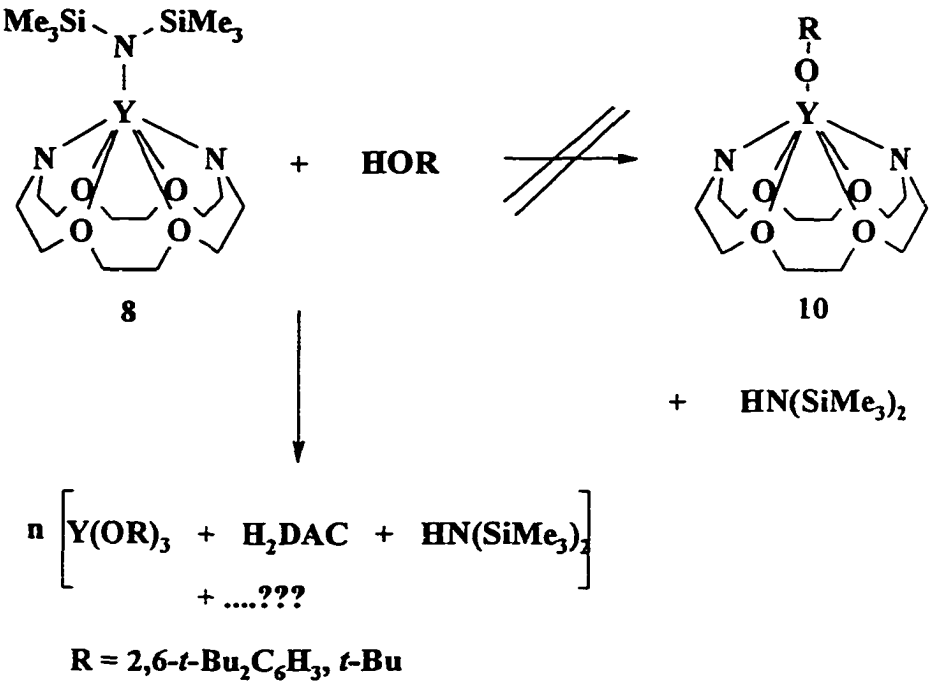

Direct alcoholysis of **8** with 2,6-di-*tert*-butylphenol under conditions of high dilution and slow addition of the alcohol resulted in a clear colourless solution which was evaporated to dryness to afford a hydrocarbon soluble oily white residue. Examination of this material by ^{1}H NMR showed resonances characteristic of free H_2DAC and the tris(phenoxide), Y(OC$_6$H$_3$-2,6-*t*-Bu$_2$)$_3$, as major components of a complex mixture. In a similar manner, reaction of **8** with the less acidic, *tert*-butyl alcohol, also failed to produce the desired alkoxide

precursor. Instead, it afforded a white precipitate in which the toluene soluble material contained free H_2DAC by ^1H NMR. The failure of these reactions may imply that differentiation between the amido DAC and $N(SiMe_3)_2$ group is not possible or that product **10** forms but then undergoes facile ligand redistribution to give $Y(OR)_3$ and DAC containing products.

2.5 Synthesis and characterization of divalent lanthanide complexes of deprotonated 4,13-diaza-18-crown-6 [DAC]

2.5.1 Reaction of H_2DAC with $Yb[(N(SiMe_3)_2]_2\{OEt_2\}_2$[65]

In view of the difficulties in synthesizing the trivalent alkoxide precursors, an alternative pathway involving preparation of divalent lanthanide complexes Ln[DAC] (Ln = Yb, Sm) as potential precursors to trivalent lanthanide alkyls by redox reactions[62] with reducible group 12 metal alkyls (e.g. $HgPh_2$) was investigated. The reaction of the divalent $Yb[N(SiMe_3)_2]_2\{OEt_2\}_2$ with one equivalent of H_2DAC in toluene or THF resulted in isolation of a diamagnetic deep ruby red compound analyzing as $\{Yb[N(SiMe_3)_2](\mu\text{-DAC})\}_2Yb$ **11** by X-ray crystallography (*vide infra*). NMR spectral data revealed the presence of unreacted H_2DAC, along with resonances due to $SiMe_3$ groups and new DAC peaks belonging to the product **11**. After repeated washings with hexanes, followed by recrystallization from a mixture of toluene-hexanes, the crystalline ruby red product was free of H_2DAC. Assignments of the NMR signals were made on the basis of a ^1H-^{13}C COSY experiment (Fig.7). The NMR data for complex **11** are collected in Table 4. Six DAC multiplets and three unique DAC singlets were observed in the ^1H and ^{13}C NMR, respectively, implying a symmetric structure.

However, the presence of an $SiMe_3$ resonance implied that this product was not Ln[DAC]. Analysis of the integrated intensities of the ^1H NMR signals for the DAC ring and the $SiMe_3$ group revealed an empirical proton ratio of 4:3, corresponding to a DAC to $N(SiMe_3)_2$ ratio of 1:1. A structure such as **9** above can be ruled out because the NMR data clearly indicated a diamagnetic compound and therefore divalent ytterbium centre (Yb^{2+}, $4f^{14}$). Since an unambiguous structural assignment was not possible from NMR data alone, a single crystal X-ray diffraction study was carried out.

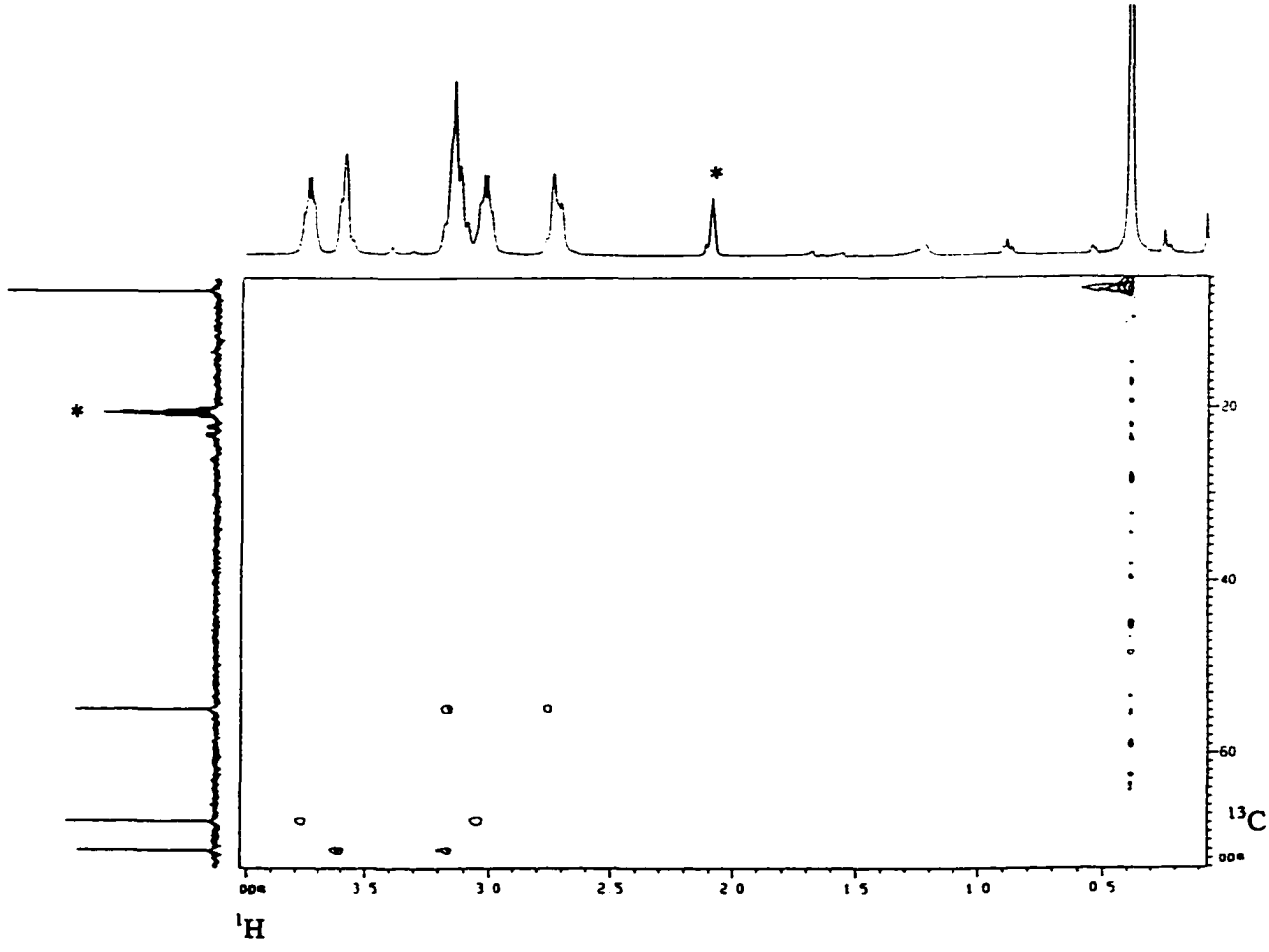

Figure 7 ^1H-^{13}C COSY of {Yb[N(SiMe$_3$)$_2$](μ-DAC)}$_2$Yb 11 (* toluene solvent)

Table 4 NMR data[a] for {Yb[N(Me$_3$Si)$_2$](μ-DAC)}$_2$Yb 11

	^{1}H				^{13}C	
	δ[b]	mult	Int.	Assign[c].	δ[b]	Assign[c].
DAC	3.76	m	4H	C_bH	54.6	C_aH
	3.60	m	4H	C_cH	67.6	C_bH
	3.17	m	8H	C_aH	70.9	C_cH
				C_cH		
	3.02	m	4H	C_aH		
	2.79	m	4H	C_bH		
N(SiMe$_3$)$_2$	0.38	s	18H	SiMe_3	6.4	SiMe_3

[a]Spectrum recorded at 250 MHz (^{1}H) or 62.9 MHz (^{13}C) in C_6D_6 or C_7D_8 at 296 K. [b]δ expressed in ppm. [c]Assignment letters refer to the carbon atoms of the unique $NC_aH_2C_bH_2OC_cH_2$ portion of the DAC ligand (the remaining carbons are related to these by the molecular symmetry).

2.5.2 X-ray structural analysis of $\{Yb[N(SiMe_3)_2](\mu\text{-DAC})\}_2Yb$ 11

The molecular structure of 11 consists of a trinuclear Yb cluster, $\{Yb[N(Me_3Si)_2](\mu\text{-DAC})\}_2Yb$ (Figure 8). Selected bond distances and angles are collected in Table 5, while full crystallographic data are summarised in Appendix Tables V-VII.

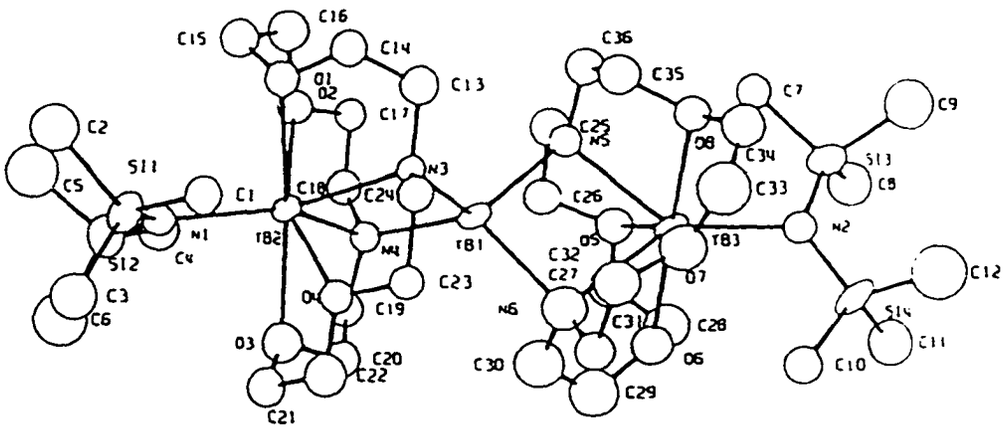

Figure 8 ORTEP drawing of $\{Yb[N(Me_3Si)_2](\mu\text{-DAC})\}_2Yb$ 11

The three Yb atoms and two terminal silylamide N atoms are in a linear arrangement (nonbonding angles: Yb(2)-Yb(1)-Yb(3), 176.9(1)°; N(1)-Yb(2)-Yb(1), 172.4(7)°; N(2)-Yb(3)-Yb(1), 176.9(7)°). Central Yb(1) has a distorted tetrahedral geometry in which the N-Yb(1)-N angles for N belonging to the same DAC unit are compressed (90.4(12) and

93.1(10)°) while the N-Yb(1)-N angles for N belonging to different DAC units are opened (115.5(9) - 122.0(12)°). The dihedral angle between the N(3)-Yb(1)-N(4) and N(5)-Yb(1)-N(6) planes is 89.5°. The Yb(1)-N distances range from 2.34(3) to 2.41(3) Å, considerably shorter than the 2.50(3) to 2.61(3) Å range observed between these same N atoms and the outer metal atoms, Yb(2) and Yb(3). In light of the highly asymmetric Yb-N-Yb bridging, it is reasonable to regard the structure as containing a central YbN_4^{2-} core bonded to two outer $Yb[N(SiMe_2)_2]^+$ cations through the DAC O and N lone pairs as shown schematically in Figure 9.

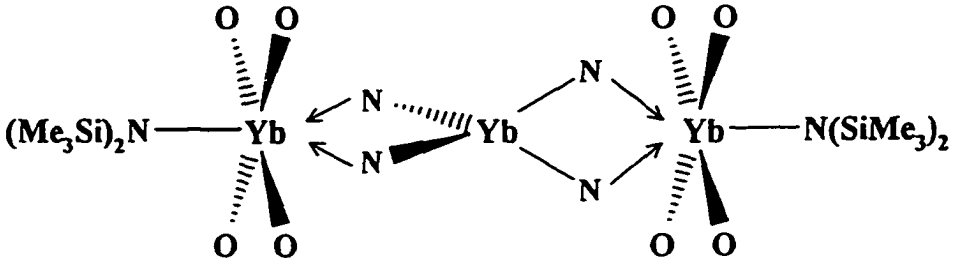

Figure 9 Schematic drawing of the core geometry for $\{Yb[N(Me_3Si)_2](\mu\text{-DAC})\}_2Y$ 11

Table 5 Selected bond (Å) and angles (deg)[a] for $\{Yb[N(Me_3Si)_2](\mu DAC)\}_2Yb$ 11

		Distance	
Yb(1)-N(3)	2.34(3)	Yb(3)-N(2)	2.44(3)
Yb(1)-N(4)	2.38(3)	Yb(3)-N(5)	2.50(3)
Yb(1)-N(5)	2.41(3)	Yb(3)-N(6)	2.59(4)
Yb(1)-N(6)	2.34(5)	Yb(3)-O(5)	2.52(3)
Yb(2)-N(1)	2.43(3)	Yb(3)-O(6)	2.57(3)
Yb(2)-N(3)	2.57(3)	Yb(3)-O(7)	2.56(3)
Yb(2)-N(4)	2.61(3)	Yb(3)-O(8)	2.56(3)
Yb(2)-O(1)	2.56(3)	N(1)-Si(1)	1.67(3)
Yb(2)-O(2)	2.56(3)	N(1)-Si(2)	1.63(3)
Yb(2)-O(3)	2.52(3)	N(2)-Si(3)	1.67(3)
Yb(2)-O(4)	2.49(2)	N(2)-Si(4)	1.70(3)
		Angles	
N(3)-Yb(1)-N(4)	93.1(10)	N(1)-Yb(2)-N(4)	137.0(9)
N(3)-Yb(1)-N(5)	118.9(10)	N(3)-Yb(2)-N(4)	82.8(9)
N(3)-Yb(1)-N(6)	122.0(12)	Yb(2)-N(1)-Si(1)	122(2)
N(4)-Yb(1)-N(5)	115.5(9)	Yb(2)-N(1)-Si(2)	114(2)
N(4)-Yb(1)-N(6)	119.4(13)	Si(1)-N(1)-Si(2)	124(2)
N(5)-Yb(1)-N(6)	90.4(12)	O(5)-Yb(3)-O(6)	62.3(9)
Yb(1)-N(3)-Yb(2)	92.3(9)	O(5)-Yb(3)-O(7)	159.0(11)
Yb(1)-N(4)-Yb(2)	90.6(10)	O(5)-Yb(3)-O(8)	124.8(9)
Yb(1)-N(5)-Yb(3)	93.4(10)	O(5)-Yb(3)-N(2)	98.5(1)
Yb(1)-N(6)-Yb(3)	92.7(14)	O(5)-Yb(3)-N(5)	66.7(10)
O(1)-Yb(2)-O(2)	64.9(8)	O(5)-Yb(3)-N(6)	95.2(11)
O(1)-Yb(2)-O(3)	169.2(9)	O(6)-Yb(3)-O(7)	109.7(11)
O(1)-Yb(2)-O(4)	109.7(8)	O(6)-Yb(3)-O(8)	172.5(9)
O(1)-Yb(2)-N(1)	86.9(9)	O(6)-Yb(3)-N(2)	89.4(10)
O(1)-Yb(2)-N(3)	67.9(9)	O(6)-Yb(3)-N(5)	115.8(9)
O(1)-Yb(2)-N(4)	121.6(8)	O(6)-Yb(3)-N(6)	66.1(12)
O(2)-Yb(2)-O(3)	125.3(10)	O(7)-Yb(3)-O(8)	62.9(10)
O(2)-Yb(2)-O(4)	155.0(8)	O(7)-Yb(3)-N(2)	100.9(11)
O(2)-Yb(2)-N(1)	106.4(9)	O(7)-Yb(3)-N(5)	104.0(11)
O(2)-Yb(2)-N(3)	90.8(8)	O(7)-Yb(3)-N(6)	64.4(12)
O(2)-Yb(2)-N(4)	66.4(10)	O(8)-Yb(3)-N(2)	91.6(10)
O(3)-Yb(2)-O(4)	62.8(9)	O(8)-Yb(3)-N(5)	68.2(9)
O(3)-Yb(2)-N(1)	86.4(11)	O(8)-Yb(3)-N(6)	109.2(12)

O(3)-Yb(2)-N(3)	112.9(10)	N(2)-Yb(3)-N(5)	135.1(10)
O(3)-Yb(2)-N(4)	68.7(10)	N(2)-Yb(3)-N(6)	141.9(12)
O(4)-Yb(2)-N(1)	97.5(8)	N(5)-Yb(3)-N(6)	82.9(12)
O(4)-Yb(2)-N(3)	65.4(8)	Yb(3)-N(2)-Si(3)	117(2)
O(4)-Yb(2)-N(4)	101.0(9)	Yb(3)-N(2)-Si(4)	119(2)
N(1)-Yb(2)-N(3)	140.1(9)	Si(3)-N(2)-Si(4)	125(2)

[a] Estimated standard deviation in parentheses.

The outer Yb atoms are seven-coordinate. The Yb-N(silylamide) distances are equivalent within experimental error at 2.44(3) Å and agree well with the value of 2.46(2) Å predicted from structure **8**[64]. The outer Yb atoms lay within the planes defined by their three surrounding N atoms (displacement of 0.04 Å for both Yb(2) and Yb(3)). The Yb(2/3)-O distances vary from 2.49(2) to 2.57(3) Å which is shorter than the expected distance of 2.63(2) Å predicted from **8**[64]. Overall the molecule has approximate C_{2v} symmetry. A more detailed discussion of bond length variations is not warranted based on the generally poor quality of this structure.

2.5.3 Formation of $\{Yb[N(SiMe_3)_2]\}_2\{\mu\text{-DAC}\}$**12**

Large quantities of $\{Yb[N(Me_3Si)_2](\mu\text{-DAC})\}_2Yb$ **11** were required in order to study its reactivity with reducible group 12 alkyls and a variety of organic substrates. Repeating the reaction of $Yb[N(SiMe_3)_2]_2\{OEt_2\}_2$ and H_2DAC on a preparative scale in a ratio of 3:2 gave an 80 % isolated yield of crystalline **11** (eq 16).

$$3\ Yb[N(SiMe_3)_2]_2\{OEt_2\}_2 + 2\ H_2DAC \rightarrow \{Yb[N(Me_3Si)_2](\mu\text{-}DAC)\}_2Yb \quad (16)$$

11

$$+ \quad 4\ HN(SiMe_3)_2$$

On dropwise addition of H_2DAC to $Yb[N(SiMe_3)_2]_2\{OEt_2\}_2$, both in toluene, the bright brick red colour of the silyamide instantaneously turned black. Formation of **11** was indicated by a colour change to ruby red when most of the H_2DAC was added. The reaction was repeated to investigate the black product. Complex **11** was isolated as the only Yb-containing product at all Yb:H_2DAC ratios below 1.5:1; excess H_2DAC was recovered as well as **11**, at lower ratios. Increasing the ratio to 2:1 resulted in formation of a crystalline black compound $\{Yb[N(SiMe_3)_2]\}_2\{\mu\text{-DAC}\}$**12** (eq 17), relatively free of impurities as analyzed by NMR (Table 6).

$$H_2DAC + 2\ Yb[N(SiMe_3)_2]_2\{OEt_2\}_2 \rightarrow \{Yb[N(SiMe_3)_2]\}_2\{\mu\text{-DAC}\} \quad (17)$$

12

$$+ \quad 2\ HN(SiMe_3)_2$$

Table 6 NMR data[a] for $\{Yb[N(SiMe_3)_2]\}_2\{\mu$-DAC$\}$ 12

	^1H					^{13}C	
	δ^b	Int.	mult.	coupling[c]	Assign[d].	δ^b	Assign[d].
DAC	3.36	8H	t	$^3J_{HH} = 4.7$	C_bH	55.1	C_aH
	3.01	8H	t	$^3J_{HH} = 4.7$	C_aH	68.2	C_bH
	2.87	8H	m		C_cH	73.2	C_cH
$N(SiMe_3)_2$	0.37	36H	s		$SiMe_3$	6.4	$SiMe_3$

[a]Spectrum recorded at 250 MHz (^1H) or 62.9 MHz (^{13}C) in C_6D_6 or C_7D_8 at 296 K. [b]δ expressed in ppm. [c]Coupling constants measured in Hz. [d]Assignment letters refer to the carbon atoms of the unique $NC_aH_2C_bH_2OC_cH_2$ portion of the DAC ligand (the remaining carbons are related to these by the molecular symmetry).

^1H and ^{13}C NMR clearly showed only three sets of DAC resonances and one $SiMe_3$ peak suggesting a highly symmetric structure. Analysis of the ^1H NMR peak integrals for $N(SiMe_3)_2$ and DAC indicated an empirical proton ratio of 3:2, corresponding to $N(SiMe_3)_2$ to DAC ratio of 2:1. Attempts to obtain a crystal structure of this compound were frustrated by extensive disorder in the C_2H_4 backbone of the DAC ligand. However, the general structure of **12** consisting of a bridging DAC ligand between two ytterbium centres, $\{Yb[N(SiMe_3)_2]\}_2\{\mu$-DAC$\}$**12** was suggested by preliminary X-ray analysis and ascertained by NMR. Appendix Table VIII is a summary of the crystallographic data for $\{Yb[N(SiMe_3)_2]\}_2\{\mu$-DAC$\}$**12**.

2.5.4 Reactivity studies of $\{Yb[N(Me_3Si)_2](\mu\text{-DAC})\}_2Yb$ **11** and $\{Yb[N(SiMe_3)_2]\}_2\{\mu\text{-DAC}\}$ **12**

Interconversion of **11** and **12**, as shown in Scheme 5, was observed by NMR. Addition of H_2DAC to a toluene solution containing pure **12** resulted in **11**. Conversely, mixing additional $Yb[N(SiMe_3)_2]_2\{OEt_2\}_2$ to a toluene solution of pure **11** afforded **12**. No evidence of Yb[DAC] was observed in any of these reactions.

Scheme 5 Interconversion of 11 and 12

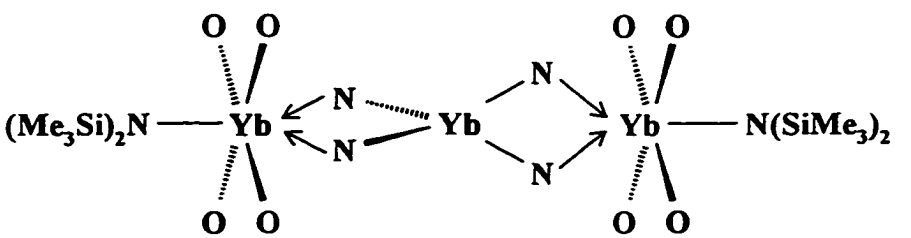

11

(macrocyclic carbons omitted for clarity)

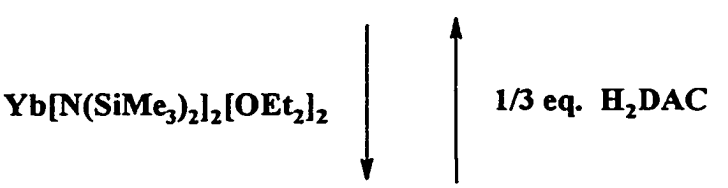

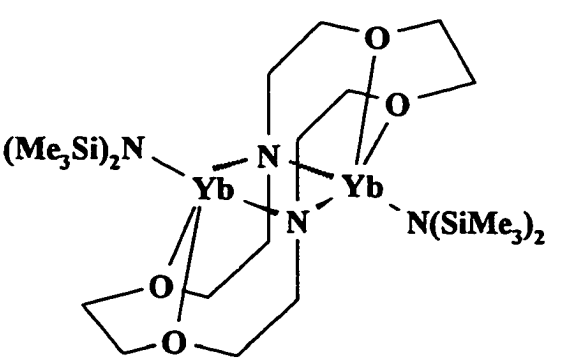

12

It was hoped that oxidation of divalent complexes **11** or **12** might lead to the trivalent ytterbium alkyl complexes, Ln[DAC]R, as shown in the hypothetical reactions in equations 17 and 18, respectively.

$$2\ \underset{\mathbf{11}}{\{[Me_3Si)_2N]Yb^{II}(\mu\text{-DAC})\}_2Yb^{II}} + 3\ Hg^{II}R_2 \rightarrow 4\ Yb^{III}[DAC]R + 3\ Hg^{\circ} + 2\ Yb^{III}[N(SiMe_3)_2]_2R \quad (17)$$

$$\underset{\mathbf{12}}{\{Yb^{II}\ [N(SiMe_3)_2]\}_2\{\mu\text{-DAC}\}} + Hg^{II}R_2 \rightarrow Yb^{III}[DAC]R + Hg^{\circ} + Yb^{III}[N(SiMe_3)_2]_2R \quad (18)$$

R = Ph, CH_2Ph, *t*-Bu

Surprisingly, no reaction was observed between **11** and HgR_2 (R=Ph, CH_2Ph, *t*-Bu), even when the reaction mixture was allowed to stir for 48 hours at ambient temperature. Presumably **11** is too sterically congested for reduction of HgR_2 to occur. The less crowded complex **12** does react with these reagents; however, characterization of the paramagnetic materials by ^1H NMR was precluded by the broad linewidths and complex product mixture. Attempts to grow crystals suitable for X-ray analysis were frustrated by the growth of fine hairy needles. No further attempts were made to characterize the paramagnetic products.

The reactivity of **11** and **12** with mildly acidic organic substrates was explored to determine whether these molecules might lead to interesting organometallic complexes. It was hoped that protonolysis of the $N(SiMe_3)_2$ group with 2,6-di-*t*-butyl phenol or phenylacetylene might result in a viable pathway to divalent lanthanide alkyl or acetylide complexes. However, reaction of the complexes **11** and **12** with the other phenols or phenylacetylene resulted in isolation of insoluble material in which the toluene supernantant contained unreacted alcohol or acetylene. Further investigation of these complexes was abandoned.

2.5.5 Reaction of H_2DAC with divalent $Sm[N(SiMe_3)_2]_2[THF]_2$[66]

Protonolysis of $Sm[N(SiMe_3)_2]_2[THF]_2$ with H_2DAC did not follow the same course as the Yb analogue. On addition of one equivalent of a solution containing H_2DAC to a purple solution of $Sm[N(SiMe_3)_2]_2[THF]_2$, both in toluene, the reaction mixture rapidly turned dark green. After being stirred for 2-3 h, the colour of the solution faded to yellow. A greenish insoluble oily residue (in all solvents) settled to the bottom of the reaction vessel. After workup, recrystallization of the yellow material in a mixture of toluene-hexane resulted in a 79% isolated yield of bright yellow crystals analyzing as trivalent $Sm(DAC)[N(SiMe_3)_2]$ **13**. The identity of **13** was established from ^1H NMR (Table 7), mass spectral data (M/z = 572, M^+), and the crystals of **13** proved to be isostructural with the cerium analogue **9**. It is reasonable to assume that the dark green intermediate is a Sm(II) complex since intense colours are typical of divalent samarium. For example divalent samarium complexes include green SmI_2 and the intensely purple $Sm[N(SiMe_3)_2]_2[THF]_2$; in contrast, trivalent samarium complexes are usually pale yellow as observed for SmI_3 and $Sm[N(SiMe_3)_2]_3$.

Table 7 ^{1}H NMR data[a] for Sm(DAC)[N(SiMe$_3$)$_2$] 13

	Sm[DAC][N(SiMe$_3$)$_2$] 13[d]			
	δ[b]	mult.	Int.	$\upsilon_{1/2}$[c]
DAC	5.7	m	4H	23
	4.5	br	4H	22
	3.4	m	4H	16
	1.9	m	4H	21
	-1.5	m	4H	18
	-4.3	m	4H	21
N(SiMe$_3$)$_2$	1.1	s	18H	6

[a]Spectra recorded at 250 MHz in d_6-benzene or d_8-toluene at 296 K. [b]δ expressed in ppm and [c]$\upsilon_{1/2}$ measured in Hz. No assignment was possible for ^{1}H NMR resonances of this paramagnetic complex. [d]^{13}C spectrum was not observable due to paramagnetism.

Two reasonable pathways for the formation of **13** are proposed in Scheme 6. Path A involves fast protonolysis of Sm[N(SiMe$_3$)$_2$]$_2$[THF] to form Sm[DAC] and 2 equivalents of HN(SiMe$_3$)$_2$ followed by slow reduction of HN(SiMe$_3$)$_2$ to form **13**. Alternatively, path B involves initial protonolysis to give Sm[N(SiMe$_3$)$_2$][HDAC] followed by slow reduction of the remaining DAC N-H bond to afford **13**.

Scheme 6 Proposed pathways for the formation of Sm(DAC)[N(SiMe$_3$)$_2$] 13

Path A

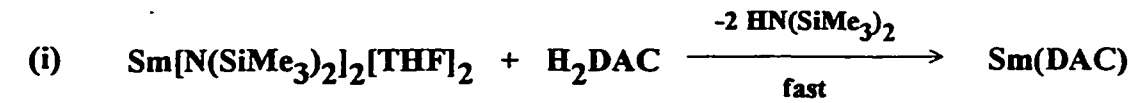

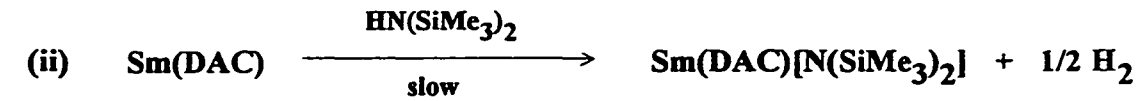

13

Path B

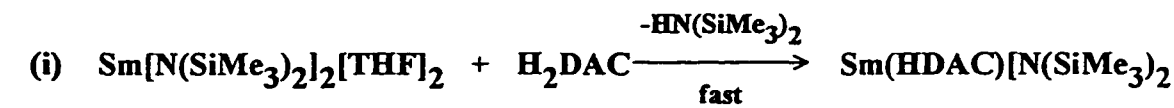

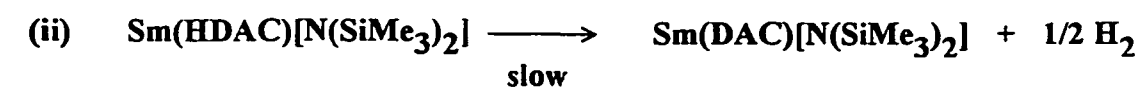

13

Attempts to follow the reaction by ^{1}H NMR were complicated by the low solubility of H_2DAC and the intermediate green complex in d_8-toluene. Nevertheless, path B appears to be the most plausible pathway based on the following supporting evidences: first, it is clear from ^{1}H NMR that HN(SiMe$_3$)$_2$ appears within 10 min of mixing (the first spectrum acquired) and does not change in integrated intensity relative to the methyl peak from d_8-toluene throughout

the experiment. Second, the product peaks do not appear until ca. 2 h after mixing, yet removal of the solvent under vacuum after the first 15 min results in a greenish powder which slowly converts to **11** in the *solid state*. This would seem to rule out reduction of free $HN(SiMe_3)_2$ since this noncoordinating base should be removed with the solvent. Third, the reaction proceeds much more rapidly in d_8-THF than in d_8-toluene; product peaks are evident after 15 min in d_8-THF. If reduction of $HN(SiMe_3)_2$ was actually involved, addition of large excess of a strongly coordinating base such as THF should prevent the second step of path A from occurring. In addition, no reaction was observed between $Sm[N(SiMe_3)_2]_2[THF]_2$ and either $HN(SiMe_3)_2$ or $HNEt_2$ by ^1H NMR at 60°C (24 h); decomposition of $Sm[N(SiMe_3)_2]_2[THF]_2$ to uncharacterized products was observed at higher temperatures. The low solubility of the intermediate green complex and the small relative intensity of H_2 hampered the assignment of these resonances. Although, the obscurity of these resonances may indicate a more complicated pathway than that depicted in path B, the general features of this route are consistent with the experimental observations.

Reduction of an amine N-H bond by divalent samarium to form an amide would appear to be without precedence. Although SmI_2 is well known as a reducing agent in organic chemistry, most examples involve reduction of a carbonyl functional group to give radical anions[6,7]. A more closely related example is the reduction of 2,3,5,6-tetramethylphenol by $(C_5Me_5)_2Sm(THF)_2$ to give a trivalent samarium phenoxide complex **IX** (eq 19)[67].

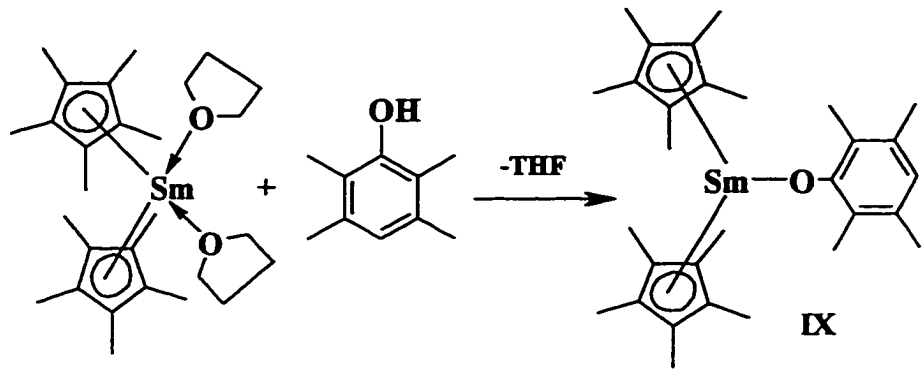

(19)

It is not surprising that reaction of divalent samarium silylamide with H_2DAC did not follow the same course as the ytterbium analog. Considering the sizes of the Yb(II) ion (ionic radii of ca.1.07 Å), and Sm(II) ion (ionic radii ca. 1.20 Å), the latter has a better fit in the cavity of the diaza-18-crown-6 macrocycle (cavity radius ca.1.34 – 1.43 Å)[3]. Even before reduction of the *remaining* amido N-H bond, the samarium forces the flexible macrocycle to adopt a basket shaped geometry, while the smaller ytterbium metal places the macrocycle in a disposition that allows coordination of other ligands above and below the plane defined by the macrocycle. Furthermore, the differences in redox potentials (Sm 1.55 V vs Yb 1.15 V for $Ln^{2+} \rightarrow Ln^{3+} + e^-$)[3] appears to play a large role in dictating the oxidation state and structure of the final product. To address the issue of sizes and redox potentials, it would be interesting to react H_2DAC with divalent europium silylamide because it has a size comparable to samarium and a redox potential lower than Yb (0.43 V).

CHAPTER 3

ORGANOYTTRIUM COMPLEXES CONTAINING DEPROTONATED 4,13-DIAZA-18-CROWN-6 (DAC)

3.1 Introduction

Despite the early difficulties in obtaining a general access into DAC supported organometallic chemistry of the lanthanides and yttrium, attention was drawn towards protonolysis reactions as demonstrated by the success in preparing Ln(DAC)[$N(SiMe_3)_2$] (Ln = Y (**8**), Ce (**9**), and Sm(**13**)). While the bis(trimethylsilylmethyl) ligand, $CH(SiMe_3)_2$ is sterically equivalent to $N(SiMe_3)_2$, the less bulky CH_2SiMe_3 is more suited to stabilize Ln(DAC)R of smaller metals which include yttrium and the later lanthanides from erbium to lutetium. Lappert reported the isolation of $Y(CH_2SiMe_3)_3(THF)_2$[34] as white crystals and this compound serves as valuable precursors to aza-crown stabilized organoyttrium complexes.

3.2 Organoyttrium complexes of deprotonated 4,13-diaza-18-crown-6 (DAC)

3.2.1 Synthesis of Y(DAC)(CH_2SiMe_3) **14**

The protonolysis reaction of $Y(CH_2SiMe_3)_3(THF)_2$ with one equivalent of H_2DAC cleanly affords solvent free Y(DAC)(CH_2SiMe_3) (eq 20). White crystalline complex **14** was isolated in 70% yield after recrystallization from toluene-hexane.

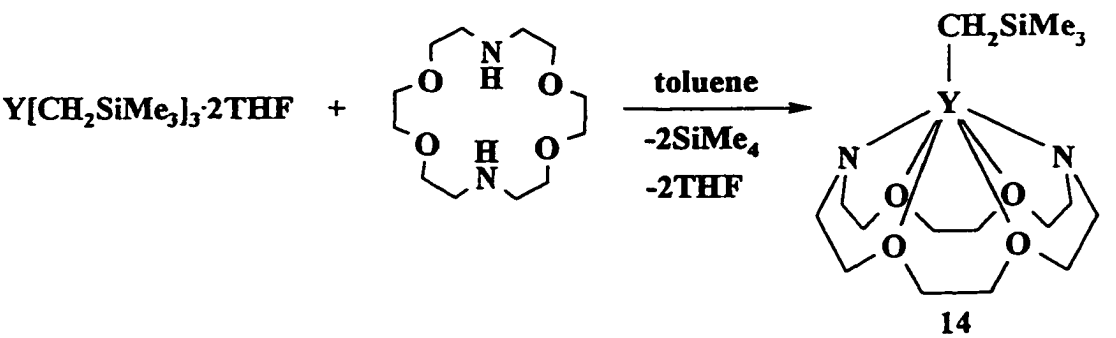

(20)

The NMR spectra of **14** is consistent with a monomeric alkyl structure. As found for Y(DAC)[N(SiMe$_3$)$_2$] **8** the DAC region of the ^{1}H NMR spectrum consists of six multiplets, while only three unique triplets are observed for the DAC carbons in the proton coupled ^{13}C NMR spectrum, consistent with C_{2v} molecular symmetry. Due to yttrium and proton coupling, a characteristic upfield doublet is observed for the alkyl protons. Figure 10 shows the ^{1}H NMR spectrum of **14**. In the ^{13}C NMR, a doublet of triplets is observed for the CH_2 carbon of the alkyl of **14**. Figure 11 shows the proton coupled ^{13}C NMR spectrum of **14**. In addition, the ^{89}Y NMR spectrum of **14** shows a well resolved triplet (Figure 12), effectively ruling out a bridging alkyl structure (Figure 13). The complete set of NMR data are summarized in Table 8 for complex **14**.

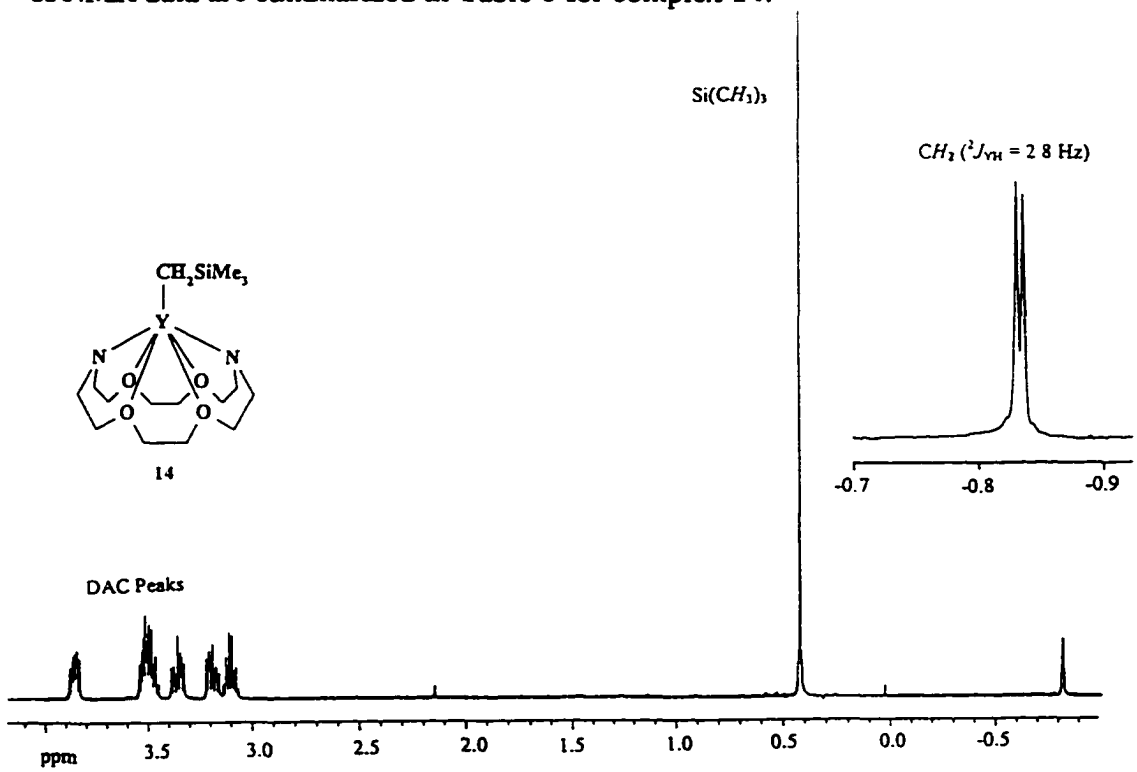

Figure 10 ^{1}H NMR (360 MHz) spectrum of Y(DAC)(CH$_2$SiMe$_3$) 14

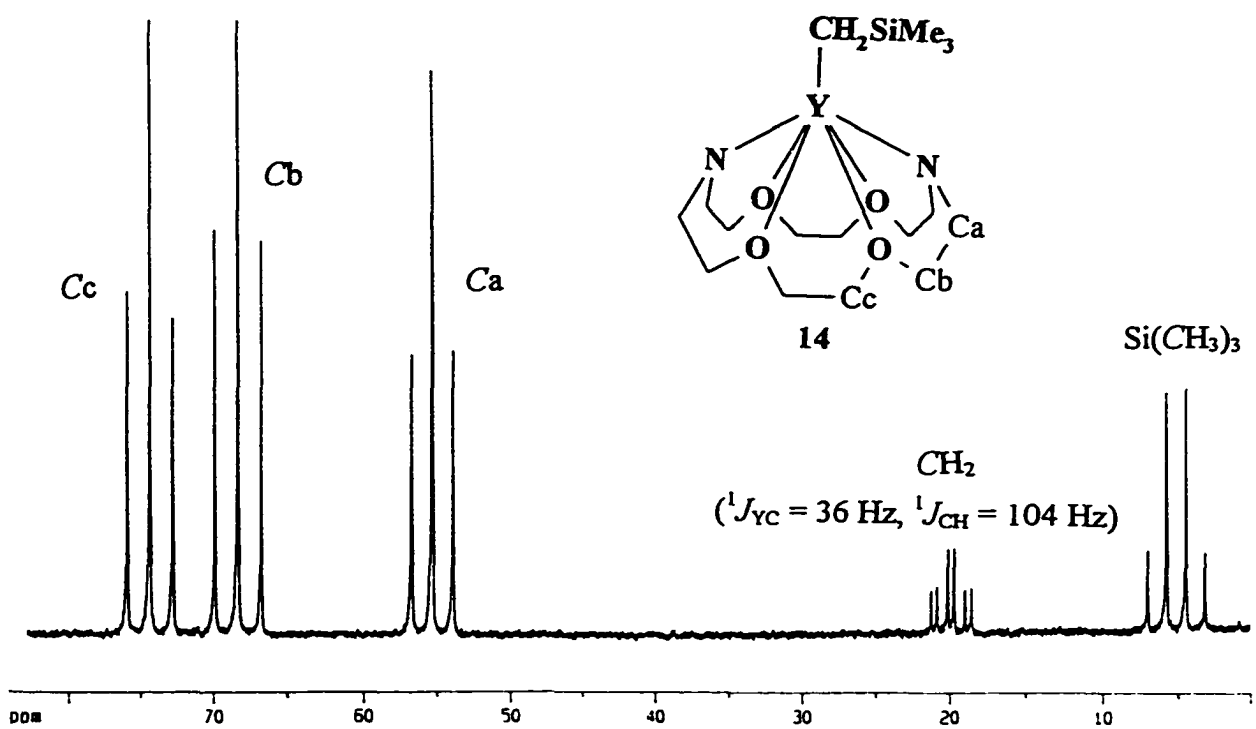

Figure 11 ^{13}C NMR (90.55 MHz) spectrum of Y(DAC)(CH_2SiMe_3) 14

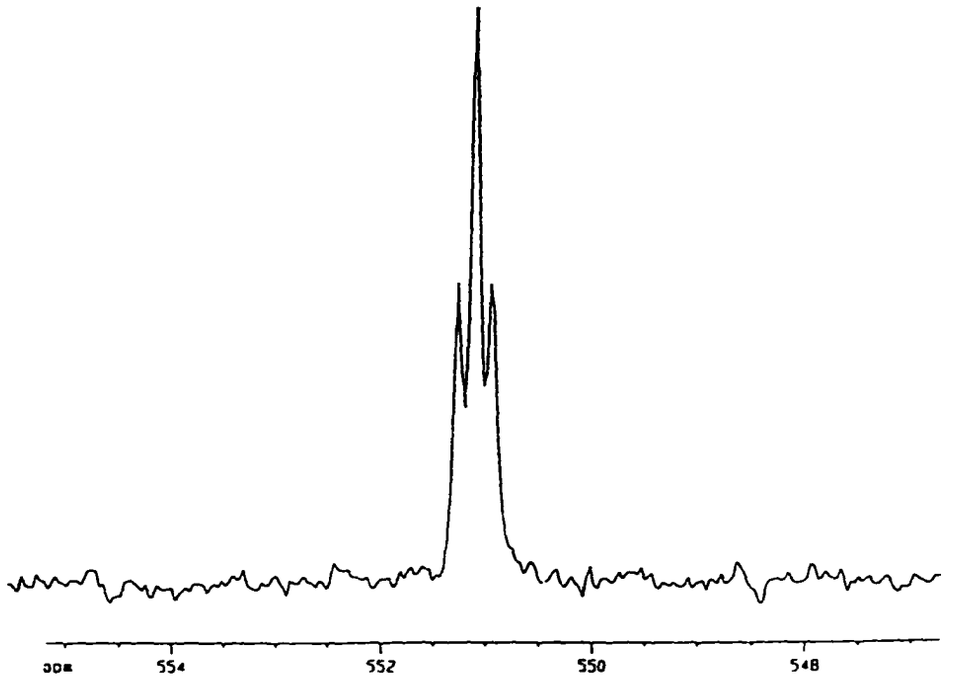

Figure 12 ^{89}Y NMR (17.64 MHz) spectrum of Y(DAC)(CH_2SiMe_3) 14

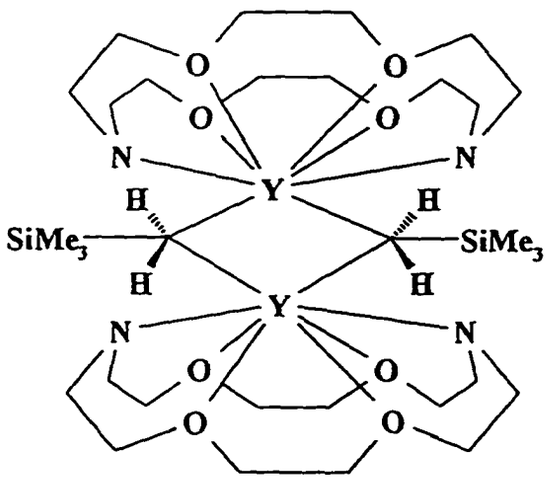

Figure 13 Alternative bridging structure for Y(DAC)(CH_2SiMe_3) complex

Table 8 NMR data[a] for Y(DAC)(CH_2SiMe_3) 14

		δ[b]	mult	Int.	coupling[c]	Assign.[d]
^1H	DAC	3.80	m	4H		C_cH
		3.38	m	8H		C_bH and C_cH
		3.33	m	4H		C_aH
		3.14	m	4H		C_aH
		3.02	m	4H		C_aH
	CH_2SiMe_3	0.31	s	18H		CH_2SiMe_3
	CH_2SiMe_3	-0.84	d	2H	$^2J_{YH}$ = 2.8	CH_2SiMe_3
^{13}C	DAC	74.2	t		$^1J_{CH}$ = 143	C_c
		68.1	t		$^1J_{CH}$ = 145	C_b
		55.2	t		$^1J_{CH}$ = 128	C_a
	CH_2SiMe_3	4.9	q		$^1J_{CH}$ = 114	CH_2SiMe_3
	CH_2SiMe_3	19.4	dt		$^1J_{YC}$ = 36	CH_2SiMe_3
					$^1J_{CH}$ = 104	
^{89}Y		551.2	t		$^2J_{YH}$ = 2.8	

[a]Spectrum recorded at 360 MHz (^1H), 90.55 MHz (^{13}C), or 17.64 MHz (^{89}Y) in d_6-benzene at 296 K. [b]δ expressed in ppm. [c]Coupling constants expressed in Hz. [d]Assignment letters refer to the carbon atoms of the unique $NC_aH_2C_bH_2OC_cH_2$ portion of the DAC ligand (the remaining carbons are related to these by the molecular symmetry).

The ^{89}Y chemical shift of Y(DAC)(CH_2SiMe_3) **14** is far downfield of that in Y(DAC)[$N(SiMe_3)_2$] **8** by +441 ppm, consistent with the strong deshielding effect of alkyls previously noted by Schavarien[68]. The ^{89}Y NMR chemical shifts for a collection of organoyttrium complexes have been correlated with electronic effects of the ligand and an estimated group contribution can be assigned to a variety of common ligands. The numerical value (either positive or negative) for each contributing group is additive, giving a reasonable approximation of the ^{89}Y chemical shift. This guide is particularly useful because the spectral width (+1000 to –500 ppm) in ^{89}Y NMR can make it difficult to locate the signal from the baseline noise. Table 9 summarizes the estimated group contributions determined from the ^{89}Y chemical shifts of the series of organoyttrium complexes collected in Table 10.

Table 9 ^{89}Y NMR group contribution estimates[68]

Group	Shift Contribution (ppm)
Cp*	-100
$OCEt_3$	16
OC_6H_3-*t*-Bu_2	56
OC_6H_2-*t*-Bu_2Me	57
OSi-*t*-$Bu_2(CH_2)_3NMe_2$[69]	90
OSi-*t*-$BuAr'_2$[69]	99/109
$N(SiMe_3)_2$	190
DAC[a]	211
$CH(SiMe_3)_2$	298
CH_2SiMe_3	340

[a]This work.

Table 10 ^{89}Y NMR for a series of organoyttrium complexes

Compound	[a]C.N.	[b]δ	Ref.
$Y[CH(SiMe_3)_2]_3$	3	895	68
$Y[N(SiMe_3)_2]_3$	3	570	68
$Y(DAC)(CH_2SiMe_3)$	7	551	this work
$Y[OSi\text{-}t\text{-}BuAr'][N(SiMe_3)_2]_2$	4	479	69
$Y(DAC)[N(SiMe_3)_2]$	7	401	this work
$Y[OSi\text{-}t\text{-}Bu(CH_2)_3NMe_2]_3$	5	269	69
$Y(OSiMe_2\text{-}t\text{-}Bu)_3(THF)_3$	6	267	70
$Y[OSi\text{-}t\text{-}BuAr'][OC_6H_3\text{-}t\text{-}Bu_2]_2$	4	221	69
$Y_5O(O\text{-}i\text{-}Pr)_{13}$	6	218,214	70
$Y[OC_6H_2\text{-}t\text{-}Bu_2Me]_3$	3	171	68
$Y[OC_6H_3\text{-}t\text{-}Bu_2]_3$	3	168	68
$Y_3(O\text{-}t\text{-}Bu)_9(HO\text{-}t\text{-}Bu)_2$	6	167	71
$\{Y[OCH_2CH_2OMe]_3\}_{10}$	6	135	70
$YCp^*_2[CH(SiMe_3)_2]$	7	79	68
$Y[OCEt_3]_3$	3	48	71
$Y[OCMeEt\text{-}i\text{-}Pr]_3$	3	46	71
$YCp'_2Me(THF)$	8	40	72
$Y[OCMe_2\text{-}i\text{-}Pr]_3$	3	37	71
$YCp^*[OC_6H_3\text{-}t\text{-}Bu_2]_2$	5	21	68
YCl_3 (aq)	6?	0[c]	68
$[YCp'_2(\mu\text{-}Me)]_2$	8	-15	72
$[YCp_2(\mu\text{-}H)]_3(\mu\text{-}H)\}\{Li(THF)_4$	9	-67	72
$[YCp'_2(\mu\text{-}CC\text{-}t\text{-}Bu)]_2$	8	-74	72
$[YCp'_2(\mu\text{-}H)(THF)]_2$	9	-92	72
$[YCp'_2(\mu\text{-}Cl)]_2$	8	-97	72
$YCp'_2Cl(THF)$	8	-103	72
$YCp^*_2[OC_6H_3\text{-}t\text{-}Bu_2]$	7	-129	68
$YCp'_2(\mu\text{-}Cl)_2K(THF)_2$	8	-324	72
$YCp'_3(THF)$	10	-371	72

Note: Cp, Cp*, Cp' and Ar' refer to C_5H_5, C_5Me_5, C_5H_4Me and o-$C_6H_4CH_2NMe_3$, respectively. [a]C.N. refers to the coordination number. [b] δ is in ppm. [c]YCl_3 is the reference standard. The contribution of Cl- should not be considered 0 because YCl_3 in water will have coordinated water molecules.

3.2.2 Structural characterisation of Y(DAC)(CH_2SiMe_3) **14**

Hydrogen-to-metal agostic interactions are important because they may precede hydrogen transfer processes from ligand to metal such as in *o*-metallation and alkyl decomposition reactions[1]. Complexes exhibiting agostic interaction are often sterically and electronically unsaturated and receive some electron density from the agostic C-H bond[28b]. We were interested in determining whether **14** contained an agostic alkyl group in order to assess the electronic and steric saturation of the metal centre in this complex. This is particularly significant because this bonding mode might inhibit reactivity.

One of the quickest spectroscopic methods to determine whether a complex has an agostic interaction is by NMR spectroscopy. A C-H bond involved in an agostic interaction with a metal centre typically has an $^1J_{CH}$ coupling constant value in the range of 40 – 80 Hz, whereas the typical value for a classical sp^3 C-H bond is exemplified by $^1J_{CH}$ of $SiMe_4$ = 117 Hz[26]. The observation of a low $^1J_{CH}$ coupling constant value for **14** (102 Hz) does not provide compelling evidence for an agostic interaction between the α-CH_2 proton and yttrium. In the range of $^1J_{CH}$ from 80 to 105 Hz, the predictability of NMR spectroscopy is reduced. Comparable values in this region have been found for a series of complexes and X-ray crystallographic studies have shown that for some complexes agostic interactions are present, while for others, they are absent (Table 11).

Table 11 Compounds with borderline $^1J_{CH}$ values in determining agostic interactions

Compound	[a]Coupling	Agostic	Ref.
(OEP)Lu[CH($SiMe_3$)$_2$]	95	No	45d
{LuCp*[CH($SiMe_3$)$_2$]Cl_2}Li(TMEDA)	93	No	73
Mg[CH($SiMe_3$)$_2$]$_2$	100.8	No	74
Cp*La[CH($SiMe_3$)$_2$]$_2$	100	Yes	75
Cp*La[CH($SiMe_3$)$_2$]$_2$(THF)	92	Yes	75
Cp*$_2$Y[CH($SiMe_3$)$_2$]	84.2	Yes	26

[a]Coupling constants $^1J_{CH}$ measured in Hz.

The uncertainty regarding the presence of an α-agostic CH interaction, as well as the possibility of an agostic β-Si-Me to yttrium bond[68], prompted an investigation of the solid-state structure of **14** by X-ray crystallography (Figure 14). Crystallographic details are found in Appendix Tables IX-XI, while selected bond distances and angles are collected in Table 12.

Table 12 Selected bond distances (Å) and angles (deg)[a] for Y(DAC)(CH_2SiMe_3) 14

	Distances		
Y(1)-O(1)	2.622(11)	Y(1)-N(1)	2.272(2)
Y(1)-O(2)	2.442(13)	Y(1)-N(2)	2.26(2)
Y(1)-O(3)	2.431(12)	Y(1)-C(13)	2.45(2)
Y(1)-O(4)	2.534(11)		
	Angles		
N(1)-Y(1)-N(2)	111.0(5)	Y(1)-C(13)-Si(1)	126.4(8)
N(1)-Y(1)-C(13)	137.4(6)	N(2)-Y(1)-C(13)	111.5(6)

[a]Estimated standard deviation in parentheses.

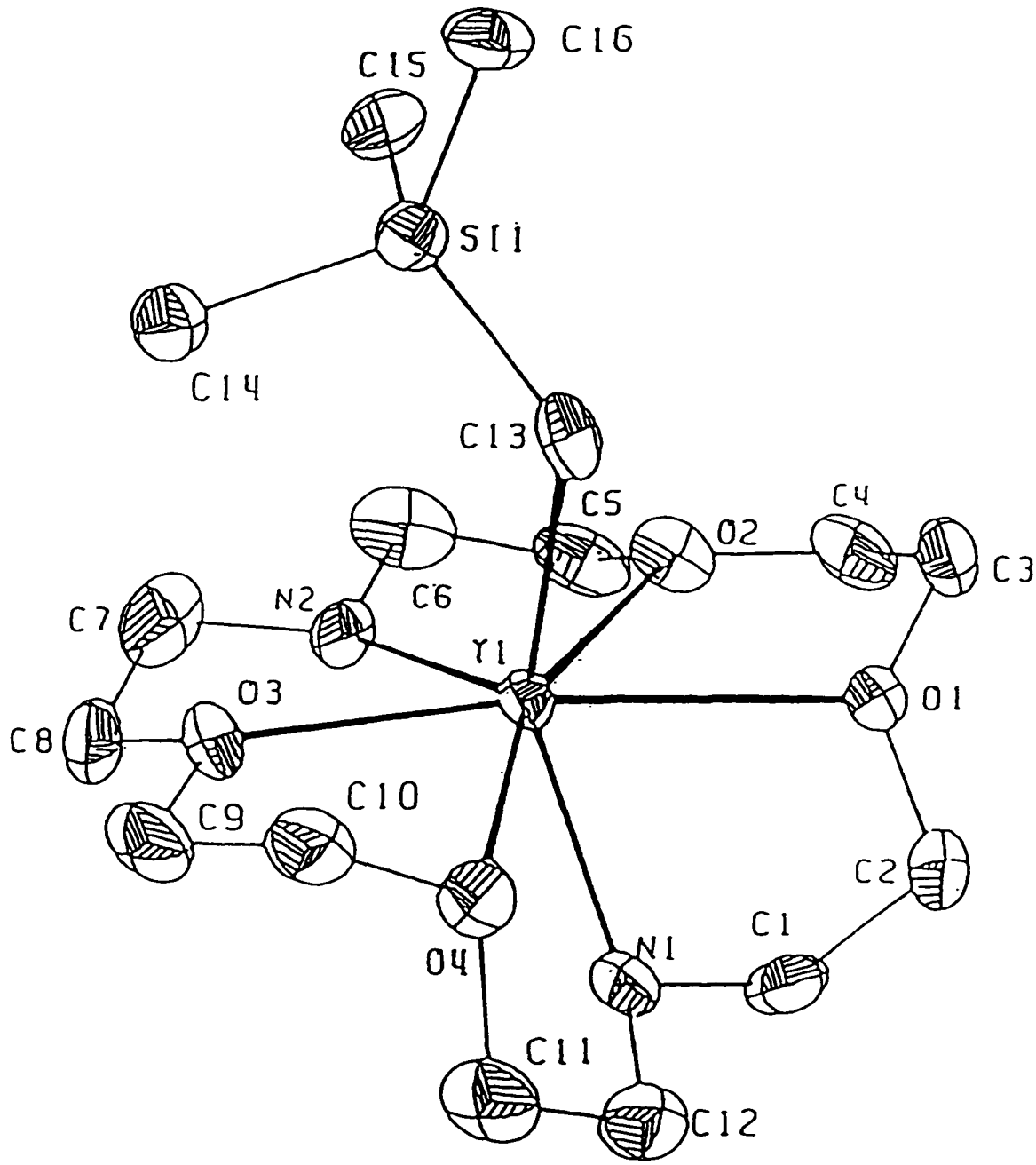

Figure 14 ORTEP drawing of Y(DAC)(CH_2SiMe_3) 14

The structure of **14** is monomeric as suggested by NMR spectroscopy; the nearest intermolecular contacts are > 3.5 Å. The bonding geometry about Y is similar to that in Y(DAC)[N(SiMe$_3$)$_2$] **8**. It can be viewed as consisting of primary trigonal planar coordination of the anionic groups (alkyl C and amido N; sum of the angles about Y for the YN$_2$C unit is 359.9°) with secondary coordination of the four ether O above and below the YN$_2$C plane. The DAC N-Y and O-Y distances are very similar to those found in **8**. The Y-C distance of 2.45(2) Å is comparable to that found in (C$_5$Me$_5$)$_2$Y[CH(SiMe$_3$)$_2$] (2.468(7)Å)[26], the only other structurally characterized neutral yttrium alkyl containing a seven-coordinate yttrium centre. Significantly, the long Y(1)•••Si(1) (3.84(2) Å) and Y(1)•••C(14)-C(16) (4.38(2), 4.38(2), and 5.49(2) Å) distances rule out any β- or γ-agostic interactions. Attempts to refine H(13a) and H(13b) isotropically resulted in an unreasonably short C(13)-H(13b) distance of 0.82(11) Å but the Y(1)•••H(13a, 13b) nonbonding distance did not shorten significantly from the calculated (fixed) distance of 2.92 Å. This distance is far longer than that observed in compounds believed to contain an α-CH agostic interaction and would appear to rule out this type of bonding[26, 75].

3.2.3 Thermal decomposition studies of Y(DAC)(CH$_2$SiMe$_3$) 14

Complex **14** slowly decomposes (weeks) at room temperature but is stable indefinitely at –30 °C in the solid state. In d_6-benzene solution, **14** decomposes more rapidly producing a marginally soluble precipitate and TMS. The ultimate fate of the Y(DAC) moiety is not known with certainty although the presence of at least 15 ^{13}C resonances in the DAC region strongly suggests metallation of the DAC ligand. Alternatively, C-D

activation of solvent (d_6-benzene or d_8-toluene) is also a potential decomposition pathway; however, incorporation of deuterium into the TMS produced was not observed. The two decomposition pathways are illustrated in Scheme 7.

Scheme 7 Possible decomposition pathways for the Y(DAC)(CH_2SiMe_3) 14

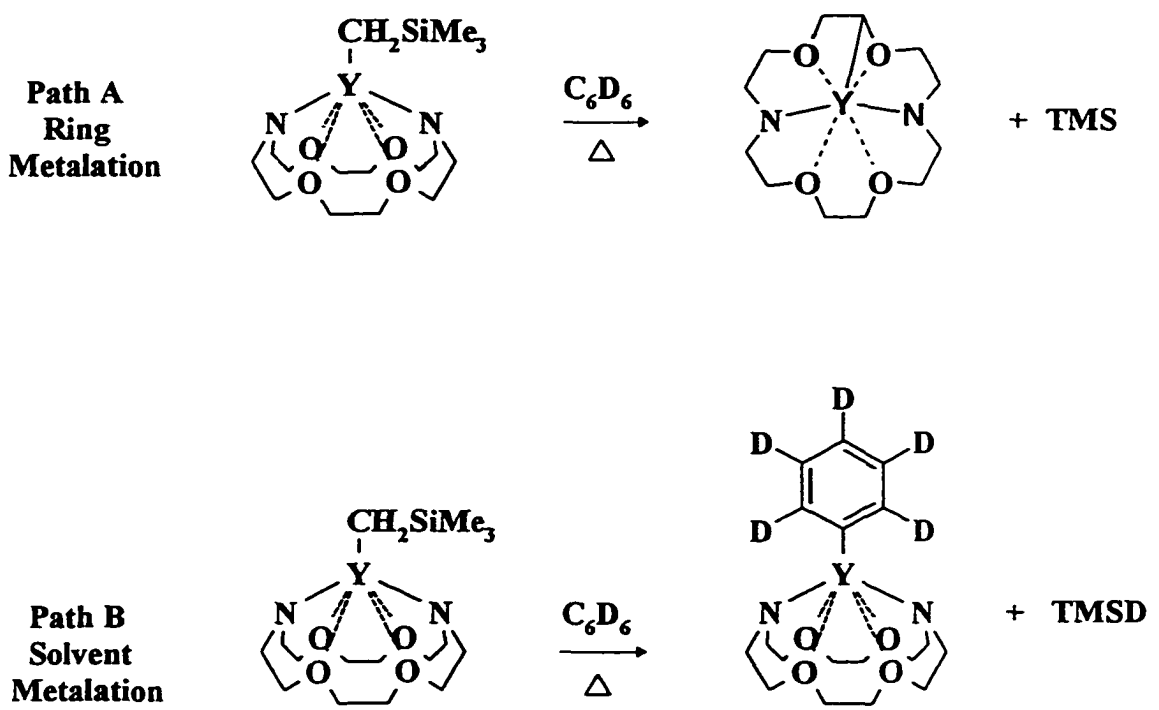

Both pathways are well documented in the literature. For instance, Fryzuk has previously reported a similar decomposition mode to Path A. As shown in equation 21, the amido phosphine complexes, $Ln(PNP^{Me})_2R$ (PNP^{Me} = $N(SiMe_2CH_2PMe_2)_2$; Ln =Y, R=Ph, CH_2Ph; Ln = Lu, R = Ph) undergo thermal decomposition by intramolecular metallation[47]. Presumably, the presence of an electronegative atom next to a methylene group provides a low energy metallation pathway by stabilizing the resulting carbanion.

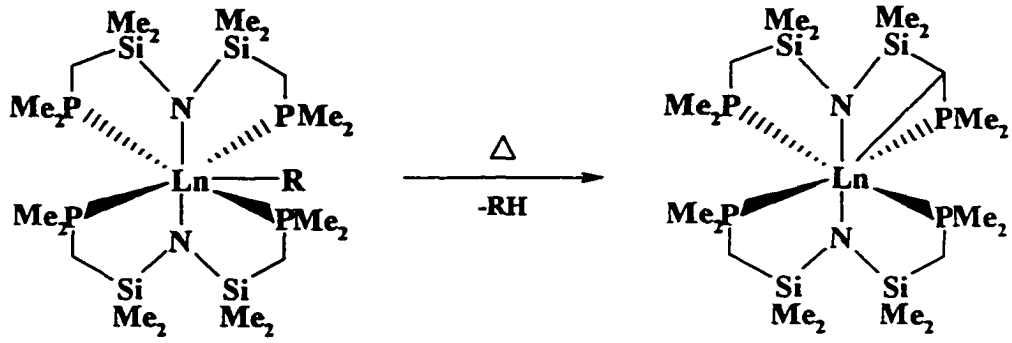

(21)

X

XI

Ln = Y, R = Ph, CH_2Ph
Ln = Lu, R = Ph

Activation of C-H bonds by organometallic complexes has been an area of extensive research and several comprehensive articles are available[76]. The simplest case of C-H activation is given in Path B. When the solvent is a stronger acid than the conjugate acid of the alkyl group, intermolecular metallation is thermodynamically favourable and frequently occurs. The acid strength of C-H bonds increases in the hybridization order

$sp^3 < sp^2 < sp$, as for example, CH_3CH_3 (pKa ~ 50) < $CH_2{=}CH_2$ (pKa ~ 45) < CH≡CH (pKa ~ 25)[77].

It is somewhat surprising that complex **14** is more stable than $Y(PNP^{Me})_2CH_2Ph$ **X**[47], given the lower steric shielding anticipated from the DAC ligand. The higher stability of **14** may be explained by electronic differences between the PNP and DAC ligands, since the soft phosphorus donors of the former ligand are expected to coordinate more weakly to a lanthanide centre than the hard oxygen donors of DAC[47]. Fryzuk has previously presented kinetic evidence which suggests that phosphine dissociation must occur, driving the decomposition of $Y(PNP^{Me})_2(CH_2Ph)$[47].

In contrast to the $Ln(PNP^{Me})_2R$ **X** series[47], the thermal decomposition of **14** does not follow simple first-order kinetics. The decomposition kinetics of **14** were monitored by measuring the decrease in concentration of the starting alkyl relative to TMS in the ^1H NMR at 35°C, 55°C, 75°C, and 85°C. A plot of relative amount of $Y(DAC)(CH_2SiMe_3)$ remaining against time shows essentially zero order kinetics over this temperature range.

In zero order kinetics, the rate of substrate consumption is dependent on the concentration of the catalyst but it is independent of the substrate concentration. This is typical of heterogeneous and enzyme catalyzed reactions. At high substrate concentrations the rate of consumption follows zero order kinetics as the catalyst is saturated with substrate. When the catalyst and substrate concentrations are similar, the rate no longer follows zero order kinetics[78]. For a temperature of 75°C, zero order kinetic were followed until the amount of alkyl remaining decreased to about 15% of its original concentration (Figure 15).

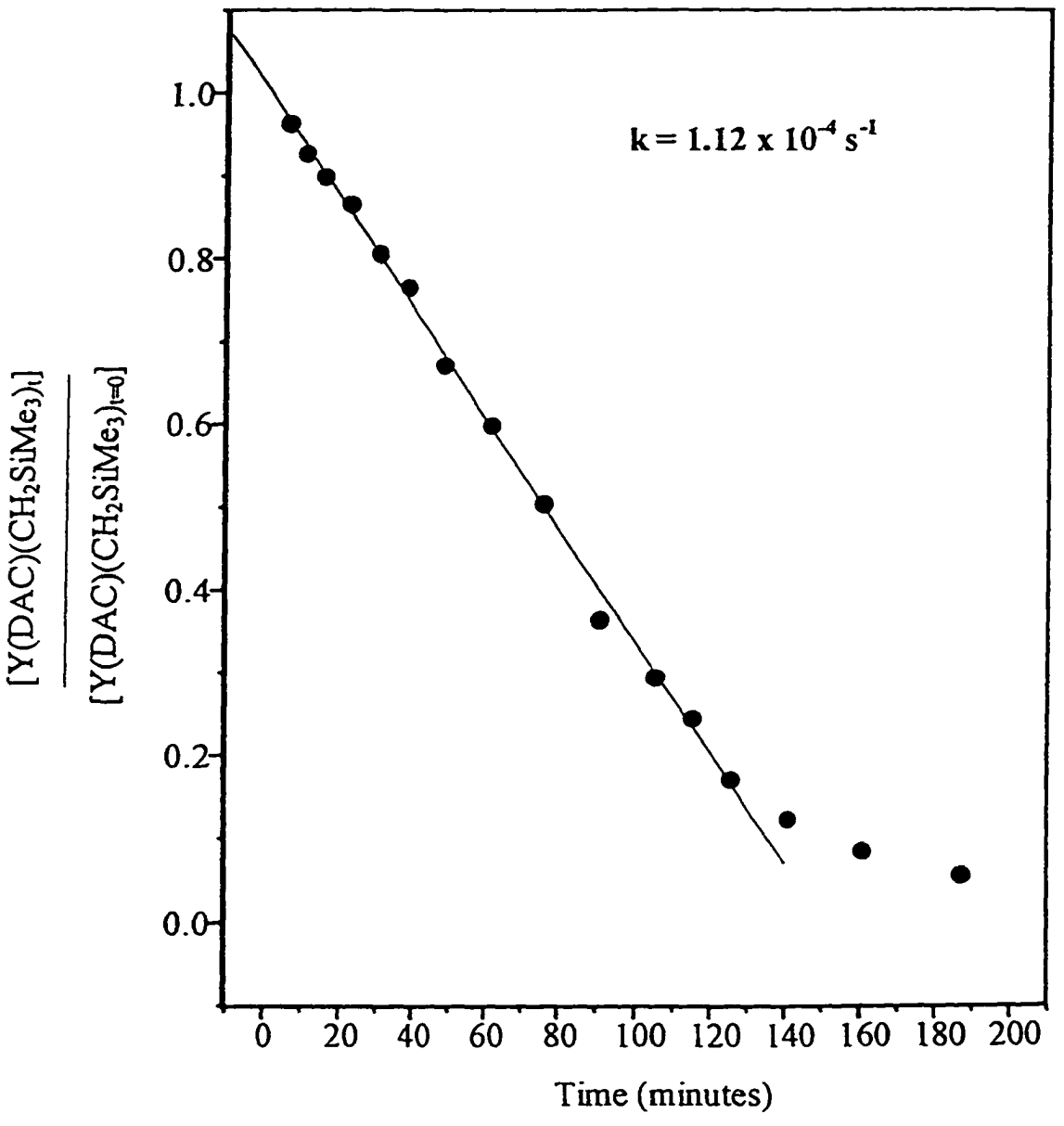

Figure 15 Thermal decomposition of Y(DAC)(CH_2SiMe_3) 14 in d_6-benzene at 75°C

Since the decomposition of Y(DAC)(CH_2SiMe_3) **14** could also occur at the glass surface of the NMR tube to yield zero order kinetics, subsequent kinetic experiments were carried out using NMR tubes that were meticulously cleaned with one of a variety of agents (HNO_3, HCl, H_2O_2/base, followed by repeated rinsing with water and acetone) and oven dried for varying lengths of time at different temperatures. Additionally, the use of new NMR tubes (flame sealed) and NMR tubes pretreated with Me_2SiCl_2[79] were expected to provide a smooth surface and prohibit the glass surface from participating in the decomposition of **14**. However, the different treatments of NMR tubes did not change the rate of decay of **14**; but, the rate was affected by the *age* of the sample of **14** was isolated. These results may suggest that the decomposition is autocatalytic and occurs at the surface of a colloidal Y(DAC) metallation product. The same behaviour is obtained throughout the 35-85°C range and the dependence of the rate constant (k) on temperature affords an E_a activation value of 79 kJ mol^{-1} from the Arrhenius plot (Figure 16).

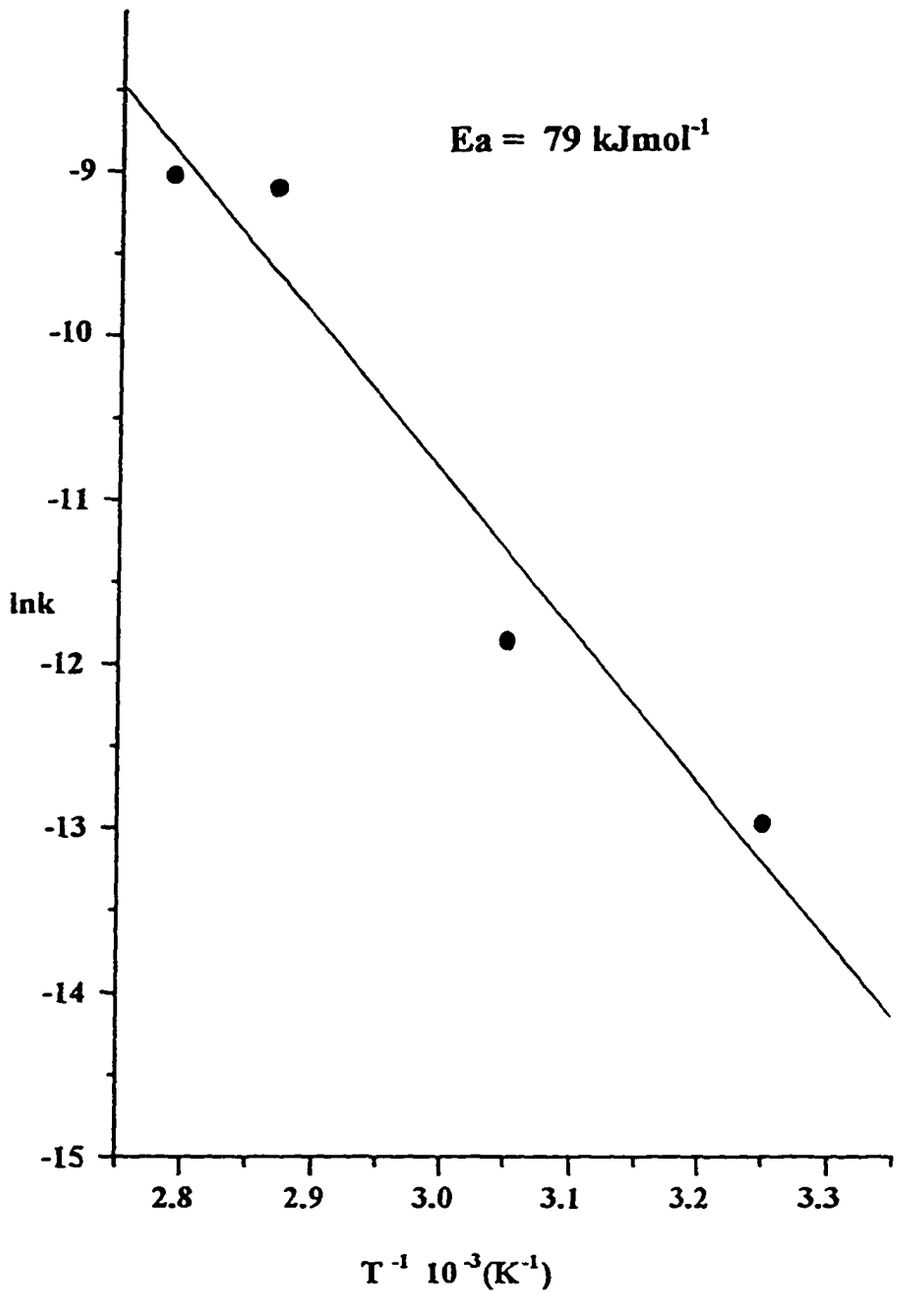

Figure 16 Arrhenius plot for the decomposition of Y(DAC)(CH_2SiMe_3) 14

3.3 Reactivity of Y(DAC)(CH_2SiMe_3) 14

3.3.1 Reaction of Y(DAC)(CH_2SiMe_3) 14 with small molecules

In contrast to the wealth of fascinating reaction chemistry obtained from the alkyl complexes of cyclopentadienyl and its derivatives with small molecules[18-27], no reaction was observed when a toluene solution of Y(DAC)(CH_2SiMe_3) **14** was treated with excess CO, ethylene, or H_2 at 4 atm. In all cases, the NMR spectra showed resonances primarily due **14**. Similarly, Schavarien has found that organolanthanide complexes of the type Ln(OEP)[$CH(SiMe_3)_2$] for M = Lu and Y are inert towards these molecules[10]. We have found that the reactivity of an organoyttrium complex containing an aza-crown macrocycle can be increased by modifying the coordination environment around the metal centre. By utilizing a macrocycle with a single anionic amido group, the yttrium dialkyls derived from it do react with CO (see Section 5.3.4).

3.3.2 Reaction of Y(DAC)(CH_2SiMe_3) 14 with phenylacetylene

The reaction of **14** with one equivalent of phenylacetylene in d_6-benzene produced a deep purple solution consisting of an equilibrium between an uncoupled alkynide-bridged dimer [(DAC)Y(μ-C≡CPh)]$_2$ **15** and a carbon coupled *Z*-1,4-diphenylbutatrienediyl [(DAC)Y]$_2$(μ-PhC=C=C=CPh) **16** (eq 22). The identities of these products were determined by NMR and IR spectroscopy, hydrolysis studies and ultimately by X-ray crystallography. White crystals of **15** were isolated from a mixture of toluene and hexanes, while deep purple crystals of **16** formed from slow evaporation of benzene. Dissolution of either pure **15** or **16** generated an

identical mixture to that obtained in the initial reaction demonstrating that these complexes are in equilibrium.

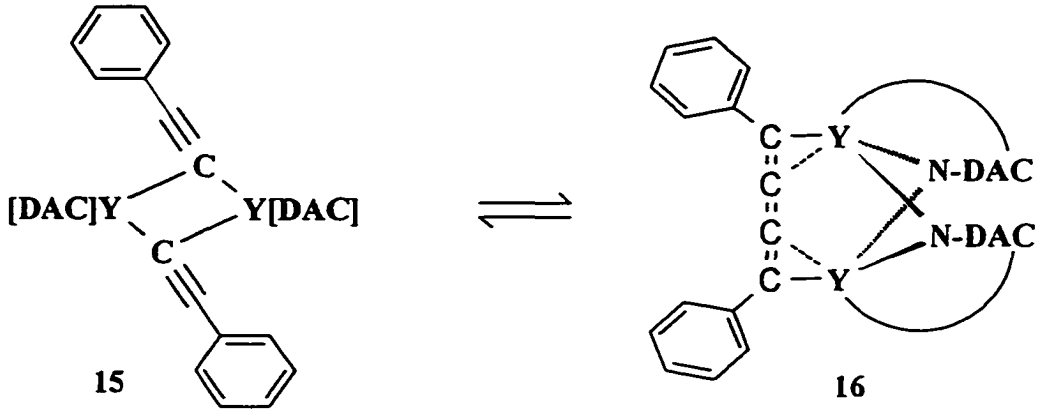

(22)

The ambient temperature ^{1}H NMR spectrum of the reaction mixture shows two sets of aryl resonances. The ortho, meta, and para protons of complex **16** are observed as sharp peaks (δ 7.71, 7.29, and 7.01 ppm, respectively), while the aryl resonances due to **15** appear as broad signals (7.63, 7.11, and 7.01 ppm) (Table 13). The ^{13}C NMR spectrum of complex **16** shows a diagnostic downfield yttrium coupled doublet for the α-carbon for the butatrienediyl fragment at 196.5 ppm ($^{1}J_{YC}$ = 38.6 Hz), while the β carbon is at 169.5 ppm with a smaller coupling constant ($^{2}J_{YC}$ = 4 Hz). The solid state IR spectrum of **15** shows the characteristic weak C≡C vibration at 2035cm^{-1}, while in **16**, the absence of this peak and the presence of a medium intensity band at 1592 cm^{-1} provides strong evidence of a reduction in bond order to C=C.

Table 13 **^{1}H NMR data[a] for the aromatic region of [(DAC)Y(μ-C≡CPh)]$_2$ 15 and [(DAC)Y]$_2$(μ-*Z*-PhC=C=C=CPh) 16**

		δ[b]	mult.	Int.	coupling[c]	Assign.
15	aryl	7.63	br m	4H		ortho-*H*
		7.11	br m	4H		meta-*H*
		7.01[d]	t	2H	$^3J_{HH}$ = 8.0	para-*H*
16	aryl	7.71	d	4H	$^3J_{HH}$ = 7.5	ortho-*H*
		7.29	t	4H	$^3J_{HH}$ = 7.5	meta-*H*
		7.01[d]	t	2H	$^3J_{HH}$ = 8.0	para-*H*

[a]Spectrum recorded at 360 MHz in C_6D_6 at 296 K. [b]δ expressed in ppm. [c]Coupling constant expressed in Hz. [d]Resonances are overlapping

This is not the first example of an alkynide coupling process since Teuben earlier reported an equilibrium between colourless [Cp*$_2$La(μ-C≡CMe)]$_2$ **XII** and red (Cp*$_2$La)$_2$(μ-*E*-MeC=C=C=CMe) **XIII** (eq 23)[80]. The spectroscopic results obtained for [(DAC)Y(μ-C≡CPh)]$_2$ **15** and the *Z*-1,4-diphenylbutatrienediyl [(DAC)Y]$_2$(μ-PhC=C=C=CPh) **16** are comparable to Teuben's system[80] (Table 14). Several other examples of alkynide coupling have been reported and some of these have been characterized by X-ray crystallography[80, 81, 82]. However, in all previously reported cases the stereochemistry of the metallated butatrienediyl complex is *E*. In the present case, the stereochemistry of the butatrienediyl group was established by hydrolysis experiments.

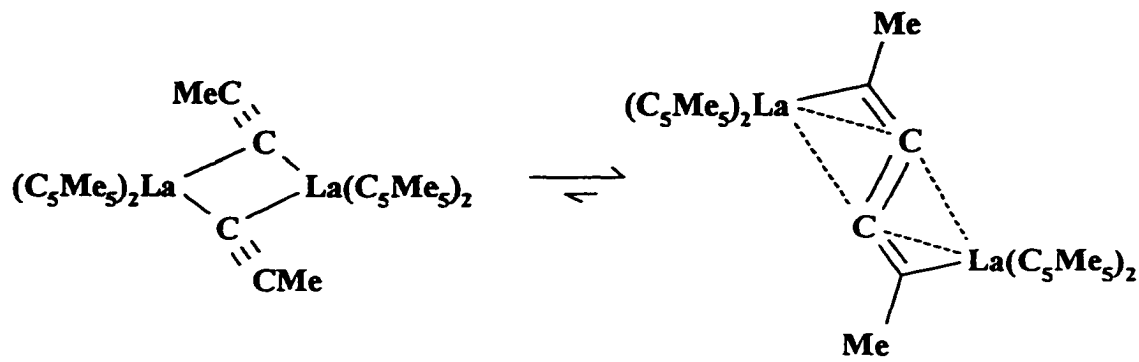

XII XIII (23)

Table 14 Comparative $^{13}C\{^1H\}$ NMR data[a] for uncoupled and coupled acetylides

$Cp^*_2La[(\mu\text{-}C_\alpha{\equiv}C_\beta Me)]_2$ **XII**[a]				$(Cp^*_2La)_2(\mu\text{-}E\text{-}MeC_\alpha{=}C_\beta{=}C_\beta{=}C_\alpha Me)$ **XIII**[a]			
δ[c]	mult	coupling[d]	Assign.	δ[c]	mult	coupling[d]	Assign.
156.2	s	-	C_α	208.5	s	-	C_α
117.0	s	-	C_β	153.9	s	-	C_β
[(DAC)Y(μ-$C_\alpha{\equiv}C_\beta$Ph)]$_2$ **15**[b]				[(DAC)Y]$_2$(μ-*Z*-Ph$C_\alpha{=}C_\beta{=}C_\beta{=}C_\alpha$Ph) **16**[b]			
150.1	s	n/a[e]	C_α	196.5	d	$^1J_{YC} = 38.4$	C_α
n/a[e]	-	-	C_β	169.5	d	$^2J_{YC} = 4$	C_β

[a]Spectra referenced in C_7D_8 at 263 K (**XII**), C_7D_8 at 294 K (**XIII**), or [b]C_6D_6 at 298 K (**15** and **16**. [c]δ expressed in ppm. [d]Coupling constant measured in Hz. [e]n/a not observed.

3.3.3 Hydrolysis of an equilibrium mixture of [(DAC)Y(μ-C≡CPh)]$_2$ **15** and [(DAC)Y]$_2$(μ-*Z*-PhC=C=C=CPh) **16**

Hydrolysis of a benzene solution prepared from pure crystals of either **15** or **16** produced phenylacetylene and a mixture of the *Z* and *E*-isomers of 1,4-diphenyl-3-buten-1-yne **17**, from the head-to-head dimerization of phenylacetylene, in a 85:15 *Z*:*E* ratio. The observation of phenylacetylene and the enyne isomers provided supporting evidence for the presence of both bridging alkynide **15** and butatrienediyl **16** in solution. Other possible hydrolysis products, shown in Figure 17, include the *Z* and *E*-isomers of 1,4-diphenylbutatriene **18** and 2,4-diphenyl-3-buten-1-yne **19**. Analysis of the ^{1}H NMR of the hydrolysis products showed an acetylenic proton resonance at 2.9 ppm belonging to phenylacetylene and two distinct pairs of doublets between 6 and 7 ppm having coupling constants of 12 and 16 Hz. Although, olefinic protons are usually further upfield around 5 ppm, the delocalization of electron density through the conjugated π-system deshields these protons. While the butatriene isomers (*E*/*Z*-**18**) can be eliminated as potential hydrolysis products on the basis that they contain uncoupled protons, the other possibilities were not as easily rejected because the observed coupling constants are within the typical range for $^3J_{HH}$ of *cis* or *trans*-alkenes (*E*/*Z*-**17**) and $^1J_{HH}$ geminal alkene protons (**19**).

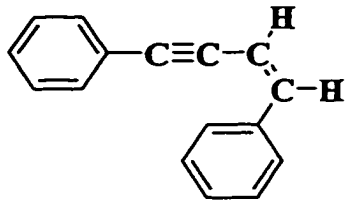

Z-17

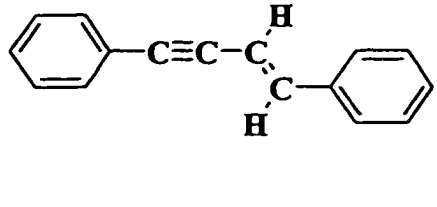

E-17

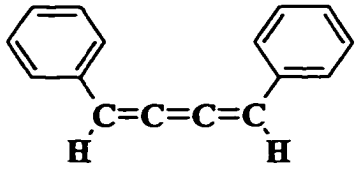

Z-18

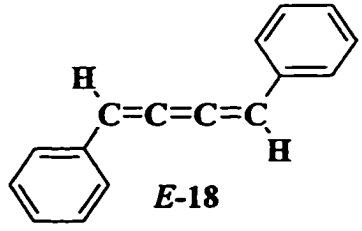

E-18

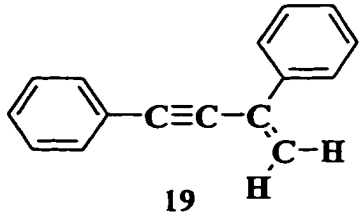

19

Figure 17 Possible hydrolysis products from reaction of Y(DAC)(CH_2SiMe_3) 14 and phenylacetylene

Nakamura revealed that the titanium (III) complex, $(C_5Me_5)_2TiCl_2$/i-PrMgBr, catalyzed the dimerization of phenylacetylene, exclusively giving the head-to-tail isomer, 2,4-diphenyl-3-buten-1-yne **19** [87] and the geminal coupling constant ($^2J_{HH}$) was reported to be 8 Hz. Hydrolysis of Teuben's $(Cp^*_2La)_2(\mu$-E-MeC=C=C=CMe) **XIII** produced exclusively the *E*-isomer of the 1,4-disubstituted enyne giving $^3J_{HH}$ =16 Hz [80]. For the *t*-butyl analogue, a mixture of *E* and *Z*-1,4 disubstituted enynes were formed after hydrolysis confirming the coupling constant for the *E*-isomer and giving $^3J_{HH}$ = 12 Hz for the *Z*-isomer. Evans also reported $^3J_{HH}$ = 16 Hz for the *E*-1,4-diphenyl-3-buten-1-yne (*E*-**17**) [81c]. The ^{1}H NMR data for the olefinic protons of several disubstituted enynes, collected in Table 15, clearly establish the hydrolysis products as *E* and *Z*-**17**.

Table 15 ^{1}H NMR data for disubstituted-3-buten-1-yne

Product	Stereo.	δ[a]	Assign.	mult	J_{HH}[b]	Ref.
2,4-diphenyl	geminal	5.74	=C*H*	d	8	87
		5.95	=C*H*	d	8	
1,4-dimethyl	*E*	5.45	=C*H*	d	15.6	80
		6.01	=C*H*(Me)	m	n/a	
1,4-di-*t*-butyl	*Z*	5.47	=C*H*	d	12	80
		5.57	=C*H*(t-Bu)	d	12	
1,4-di-*t*-butyl	*E*	5.50	=C*H*	d	16	80
		6.15	=C*H*(t-Bu)	d	16	
1,4-diphenyl	*Z*-**17**	5.79	=C*H*	d	12	This work
		6.41	=C*H*(Ph)	d	12	
1,4-diphenyl	*E*-**17**	6.32	=C*H*	d	16	This work
		6.97	=C*H*(Ph)	d	16	81c

[a]δ measured in ppm. [b]Coupling constant measured in Hz; n/a not observed

A mechanism for the formation of a 1,4-disubstituted enyne from the hydrolysis of a dimetallated butatrienediyl was originally proposed by Teuben[80]. Assuming yttrium is primarily bound to the terminal C atoms of the C_4 bridge, the first hydrolysis affords the metallated butatriene. This species can follow two competing pathways: it may rapidly undergo a second hydrolysis to give the butatriene *Z*-**18** or it may rearrange via a 1,3-metal shift prior to hydrolysis to ultimately afford the 1,4-disubstituted enyne *Z*-**17**. Scheme 8 shows the proposed mechanism using $[(DAC)Y]_2(\mu$-*Z*-PhC=C=C=CPh) **16** as the example.

Scheme 8 Proposed mechanism for the formation of *Z*-1,4-diphenyl-3-buten-1-yne

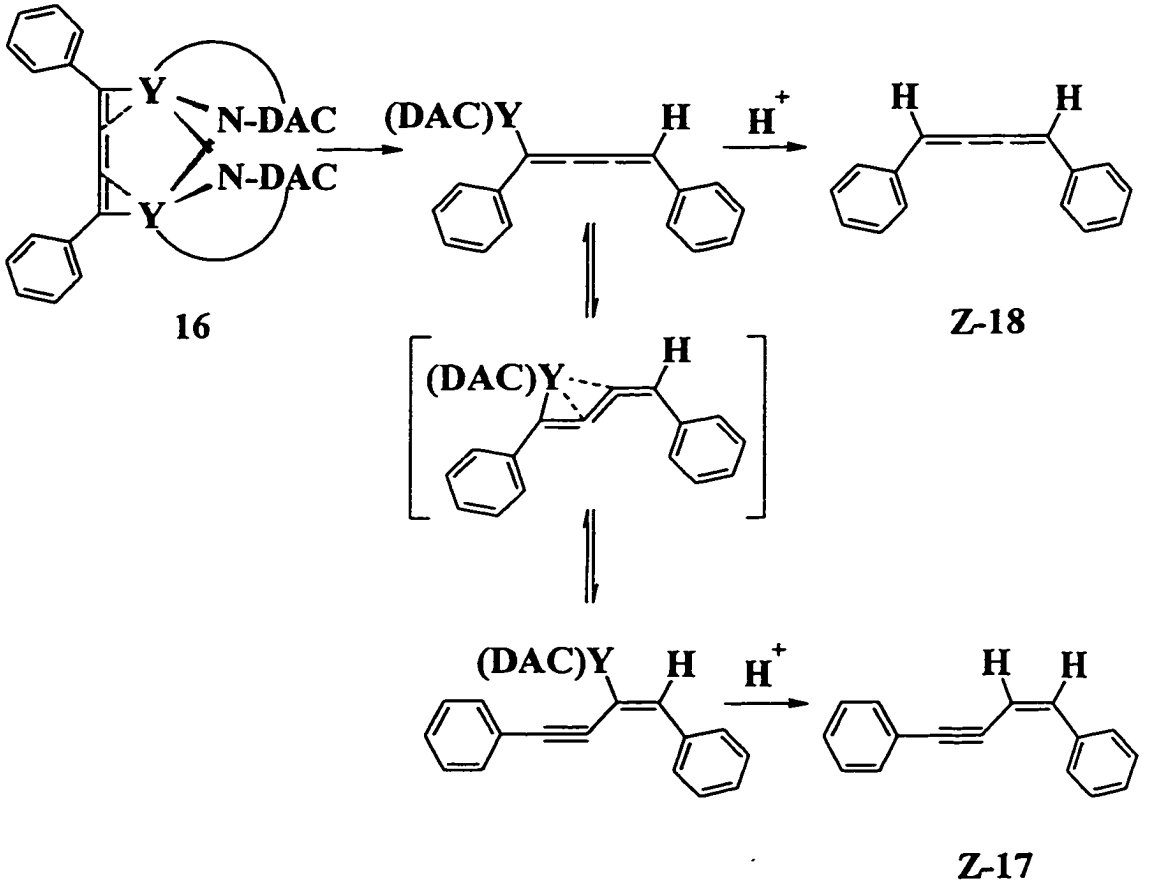

The second hydrolysis (at the terminal carbon) and 1,3-metal shift are competitive pathways which determine the enyne/butatriene ratio. Since no butatriene was detected, the 1,3-metal shift must be faster than the second hydrolysis. While, the hydrolysis of **16** should exclusively form the *Z*-enyne, consistent with the structure found by X-ray crystallography (*vide infra*), the presence of the *E*-enyne may reflect isomerization of the *Z*-isomer. In fact, this isomerization was found to be slow at room temperature , but it occurs within 4 days at 50°C to give a 20:80 equilibrium ratio of *Z*:*E* isomers. In order to confirm the identity of $[(DAC)Y(\mu\text{-}C{\equiv}CPh)]_2$ **15** and the stereochemistry of $[(DAC)Y]_2(\mu\text{-}Z\text{-}PhC{=}C{=}C{=}CPh)$ **16**, X-ray crystallographic analysis of these complexes were performed.

3.3.4 X-ray structural analysis of $[(DAC)Y(\mu\text{-}C{\equiv}CPh)]_2$ 15

An ORTEP drawing of **15** is given in Figure 18. A summary of crystallographic data is collected in Appendix Table XII- XIV and selected bond distances and angles are collected in Table 16.

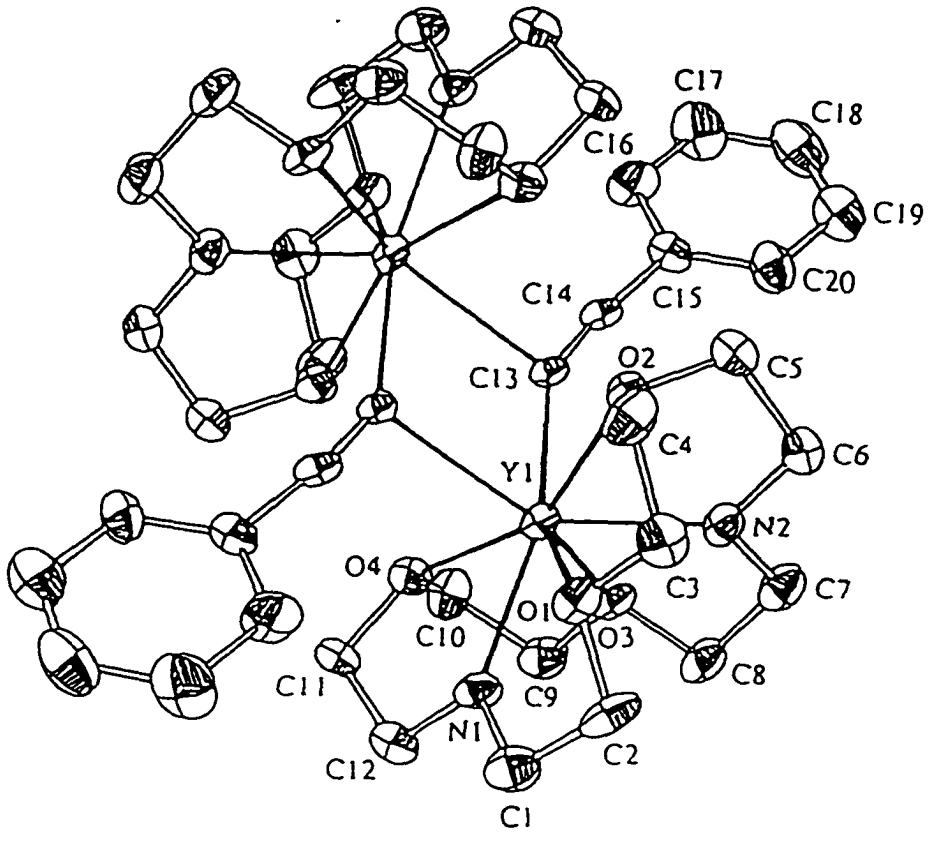

Figure 18 ORTEP drawing of [(DAC)Y(μ-C≡CPh)]$_2$ 15

Table 16 Selected bond distances and angles[a] for [(DAC)Y(μ-C≡CPh)]$_2$ 15

		Distances	
Y(1)-O(1)	2.637(6)	Y(1)-N(1)	2.279(12)
Y(1)-O(2)	2.536(7)	Y(1)-N(2)	2.275(8)
Y(1)-O(3)	2.509(6)	Y(1)-C(13)	2.601(9)
Y(1)-O(4)	2.500(7)	Y(1)'-C(13)	2.627(12)
		C13(3)-C(14)	1.197(13)
		Angles	
Y(1)-C(13)-Y(1)'	101.9(4)	Y(1)'-C(13)-C(14)	104.0(9)
C(13)-Y(1)-C(13)'	78.1(4)	C(13)-C(14)-C(15)	173.5(10)

[a]Estimated standard deviations in parentheses and primed atoms are related by inversion of symmetry.

The structure of **15** (Figure 18) reveals a centrosymmetric dimer with asymmetric bridging alkynide groups. The asymmetry is particularly clear from the difference between the angles Y(1)-C(13)-C(14) and Y(1)'-C(13)-C(14) of 148.7(8) and 104.0(9)°, respectively (Δ_{ang} = 44.7°). The Y(1)-C(13) and Y(1)'-C(13) bridging distances of 2.603(13) and 2.627(12) Å, respectively are not highly asymmetric (Δ_{dist} = 0.024 Å). The values for these asymmetry parameters fall within the range observed for structurally characterized lanthanide dimers ([$Cp_2Er(\mu$-C≡C^{t}Bu)]$_2$, Δ_{ang} = 34°, Δ_{dist} = 0.05 Å [81a]; [$(C_5H_4Me)_2Sm(\mu$-C≡C^{t}Bu)]$_2$, Δ_{ang} = 39°, Δ_{dist} = 0.00 Å [81b]; [$(C_5H_4{}^tBu)_2Sm(\mu$-C≡CPh)]$_2$, Δ_{ang} = 58.2°, Δ_{dist} = 0.057 Å [84]; [{PhC(NSiMe$_3$)$_2$}$_2$Y(μ-C≡CH)]$_2$, Δ_{ang} = 61.4°, Δ_{dist} = 0.047 Å [85]). The alkyne β-C (C(14)) exhibits one short and one long contact with yttrium C(14)-Y(1) (3.69(2) Å); C(14)-Y(1)' (3.15(2) Å). However, the short C≡C bond length of 1.197(13) Å, effectively rules out any significant π- interaction between the alkyne C≡C and yttrium (cf. free PhC≡CH, 1.208 Å from microwave spectroscopy[86]). The Y-C(alkynide) distances in **15** are both considerably longer than the longest previously reported for the other structurally characterized bridging alkynide complexes[81-85]; bond lengths of this type span the range 2.44-2.556 Å, after correction for differences in metal ionic radii[64].

3.3.5 X-ray structural analysis of [(DAC)Y]$_2$(μ-*Z*-PhC=C=C=CPh) **16**

An X-ray crystallographic investigation of **16** was also carried out. Although disorder within the CH_2CH_2 backbone of the DAC ligand prevented satisfactory refinement of the structure, connectivity within this molecule was established and two important differences

from the C_5Me_5 analogs were evident[80-82]. First, the butratrienediyl fragment was clearly in a *Z* conformation, with both yttrium atoms on the same side of the C_4 chain. Second, one nitrogen from each DAC ligand was located in a bridging site between two yttrium centres. A sketch of the core geometry from preliminary X-ray crystallography is given in Figure 19 and Appendix Table XV lists the crystallographic parameters for [(DAC)Y]$_2$(μ-*Z*-PhC=C=C=CPh) **16.**

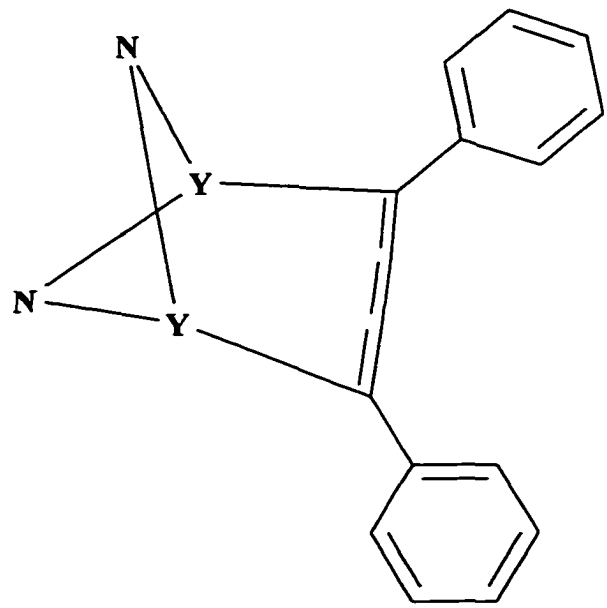

Figure 19 Sketch of the core geometry [(DAC)Y]$_2$(μ-Z-PhC=C=C=CPh) 16

3.3.6 Solution and equilibrium studies of [(DAC)Y(μ-C≡CPh)]$_2$ **15** and [(DAC)Y]$_2$(μ-*Z*-PhC=C=C=CPh) **16**

The purple solution containing [(DAC)Y(μ-C≡CPh)]$_2$ **15** and [(DAC)Y]$_2$(μ-*Z*-PhC=C=C=CPh) **16** bleached to colourless (conversion to **15**) when heated, but the purple colour was regenerated on cooling. In d_8-THF the dimetallated butatrienediyl **16** does not simply form a **16**•THF adduct, instead the carbon-carbon bond is cleaved to afford the colourless monoacetylide complex, Y(DAC)(C≡CPh)(THF) **20**. NMR spectral data for **20** is simplified by C_{2v} symmetry. As noted earlier for all DAC complexes with C_{2v} symmetry, the ^{1}H NMR shows six DAC multiplets, while the carbon has three unique ^{13}C resonances. Additionally, resonances for the acetylide carbons C_α (attached directly to yttrium) and C_β are clearly observable, showing as doublets due to ^{89}Y coupling ($^1J_{YC}$ = 47 Hz; $^2J_{YC}$ of 9.7 Hz, respectively. Table 17 summarizes the NMR data for **20**.

The rapid bleaching during heating indicates that the equilibrium between [(DAC)Y(μ-C≡CPh)]$_2$ **15** and [(DAC)Y]$_2$(μ-*Z*-PhC=C=C=CPh) **16** is established within seconds. In contrast 14 days were required for equilibrium to be reached with the C_5Me_5 system [(C_5Me_5)$_2$La(μ-C≡CMe)]$_2$ **XII** ⇌ [(C_5Me_5)$_2$La]$_2$(μ-*E*-MeC=C=C=CMe) **XIII**[80]. Although the ambient temperature ^{1}H NMR spectrum of the DAC region is complicated from the envelope of resonances extending from 2.5 - 4.5 ppm, the aromatic region (7-7.8 ppm) is much easier to interpret and provides an appropriate set of resonances to probe the position of the equilibrium (Figure 20).

Table 17 NMR data[a] for Y(DAC)(C≡CPh)(THF) 20

		δ[b]	mult	Int.	coupling[c]	Assign[d]
^{1}H	DAC	4.20	m	4H		C_cH
		4.10	m	4H		C_cH
		3.86	m	4H		C_bH
		3.78	m	4H		C_bH
		3.40	m	4H		C_aH
		2.92	m	4H		C_aH
	Y-C_α≡C_β-Ph	7.12	d	2H	$^3J_{HH}$ = 7.4	ortho-aryl
		7.01	t	2H	$^3J_{HH}$ = 7.4	meta-aryl
		6.89	t	1H	$^3J_{HH}$ = 7.1	para-aryl
^{13}C{^{1}H}	Y-C_α≡C_β-Ph	149	d		$^1J_{YC}$ = 47	C_α
		105	d		$^2J_{YC}$ = 9.7	C_β
	DAC	76.5	s			C_c
		72.2	s			C_b
		58.2	s			C_a

[a]Spectrum recorded at 360 MHz (^{1}H) or 90.55 MHz (^{13}C {^{1}H}) in C_4D_8O at 296 K. [b]δ expressed in ppm. [c]Coupling constants expressed in Hz. [d]Assignment letters refer to the carbon atoms of the unique $NC_aH_2C_bH_2OC_cH_2$ portion of the DAC ligand (the remaining carbons are related to these by the molecular symmetry).

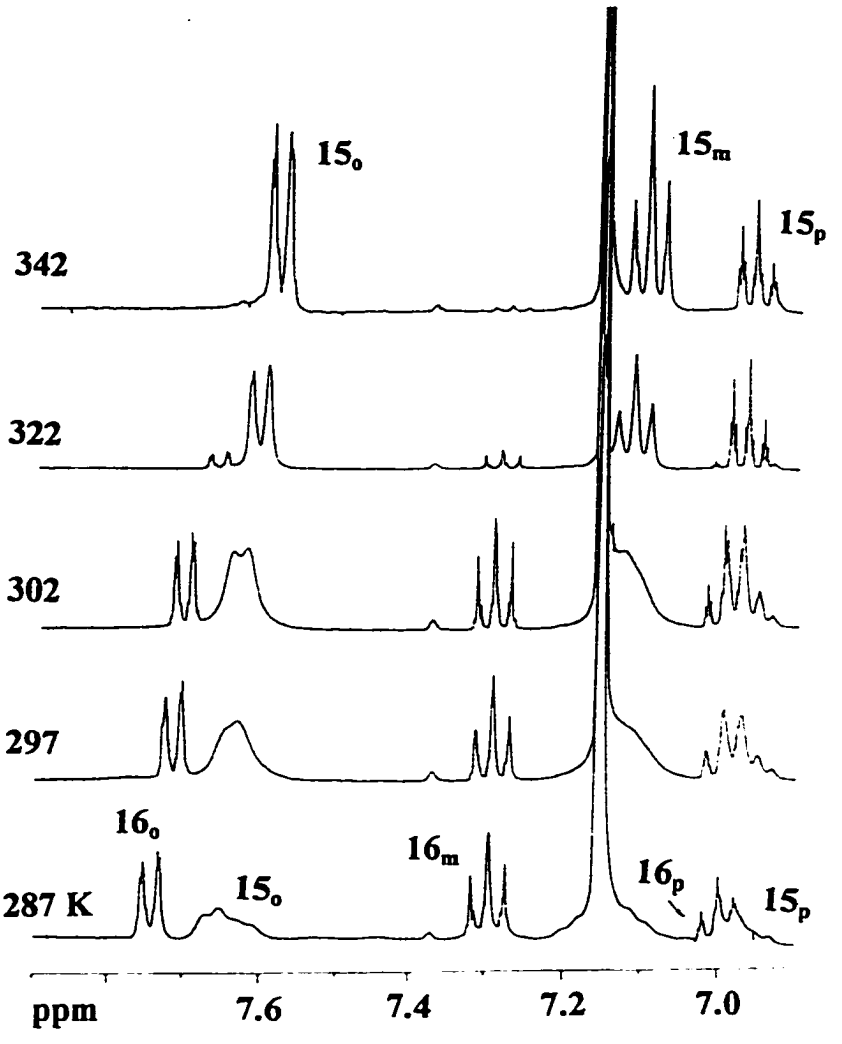

Figure 20 VT-NMR of the equilibrium between [(DAC)Y(μ-C≡CPh)]$_2$ 15 ⇌ [(DAC)Y]$_2$(μ-*Z*-PhC=C=C=CPh) 16

At 342 K, only the bridging acetylide **15** is observed as indicated by the presence of sharp resonances for the ortho (15_o :7.6 ppm), meta (15_m:7.3 ppm), and para (15_p: 7.1 ppm) aryl protons. On cooling to 322 K, the presence of the coupled product **16** becomes apparent, but the equilibrium still lies on the side of **15**. Further cooling to ambient temperature broadens the ortho and meta resonances of **15** and the latter merges into the benzene reference peak. Interestingly, at 287 K the ortho resonance (15_o: 7.63 ppm) belonging to **15** begins to split into

two sets of doublets while those of **16** remain sharp (16_o: *o*-aryl, 16_m: *m*-aryl, 16_p: *p*-aryl). Unfortunately, lower temperatures are not possible because d_6-benzene solidifies due to its high melting point (6.8°C). A plot of ln K_{eq} versus 1/T (Figure 21) yields the thermodynamic parameters, $\Delta H° = -67.0 \pm 2.0$ kJ mol^{-1} and $\Delta S° = -228 \pm 8$ Jmol^{-1}K^{-1} to give a K_{eq} value of 0.68 for **15** ⇌ **16** at 298K. The position of equilibrium between **15** and **16** is strongly temperature dependent due to the large negative entropy term. In contrast, a small entropy value was observed between **XII** and **XIII**, leading to nearly temperature independent behaviour in the C_5Me_5 system[80]. As the previous example shows, a large negative entropy term is unlikely to arise from simple alkynide coupling. However, the entropy term can easily be accounted for if the dimeric alkynide is involved in a second equilibrium with monomeric terminal alkynides (eq 24). Dissociation of **15** is not surprising given the exceptionally long (vide supra) and therefore weak Y-C (alkynide) bonds. The set of equilibria given in equation 24 are also consistent with the observation, previously discussed, that THF leads to complete cleavage of the coupled product and formation of a monomeric terminal alkynide **20**.

2 (YDAC)(C≡CPh) ⇌ [(DAC)Y(μ-C≡CPh)]$_2$ ⇌ [(DAC)Y]$_2$(μ-*Z*-PhC=C=C=CPh) (24)

15 **16**

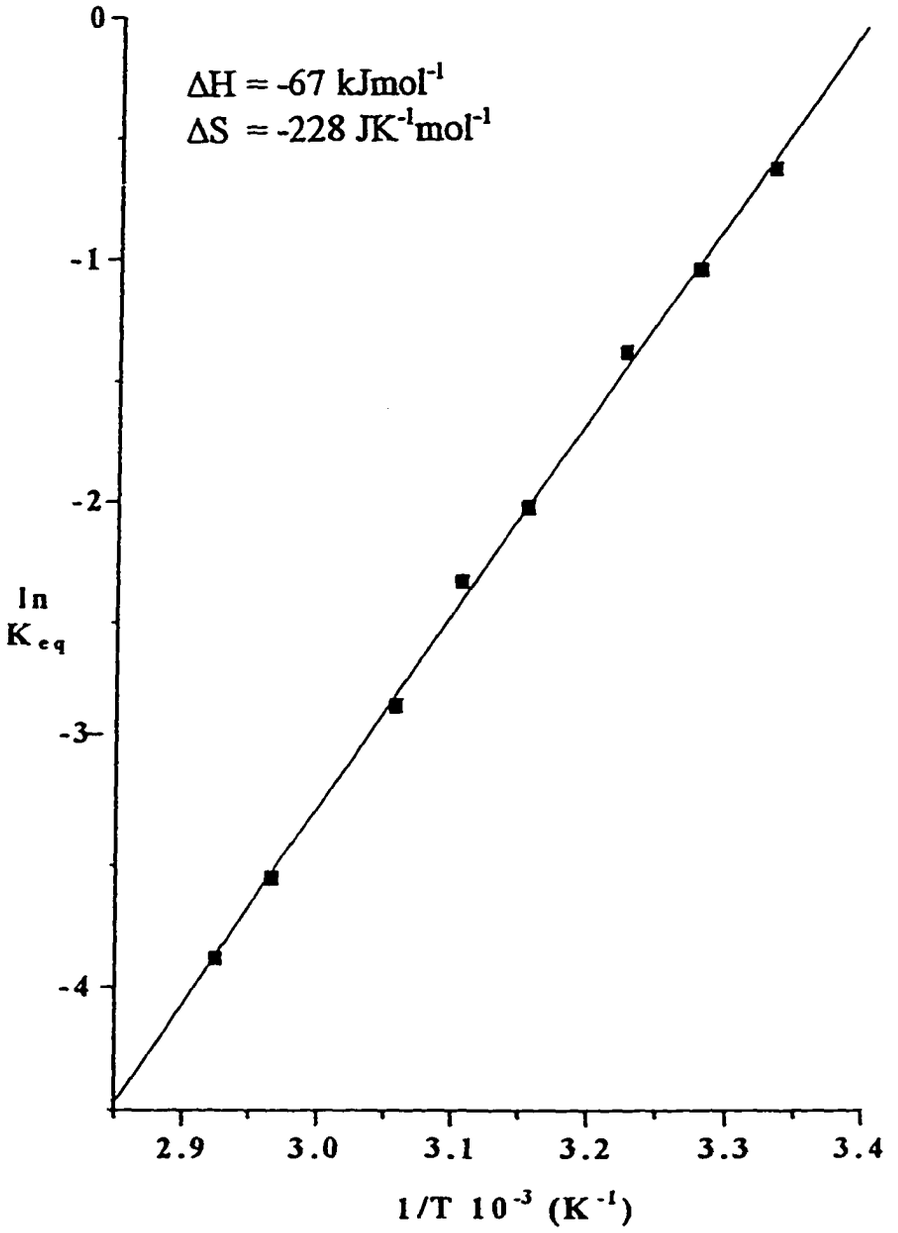

Figure 21 Thermodynamic plot for the equilibrium between 15 ⇌ 16

.3.7 Cross coupling reactions

While low temperature ^{1}H NMR provided strong evidence for the dissociation of **15**, even more compelling evidence has been obtained from cross over experiments. The reaction of *p*-tolylacetylene with Y(DAC)(CH_2SiMe_3) **14** affords the analogous bridging uncoupled and coupled acetylides [(DAC)Y(μ-C≡CTol)]$_2$ **21** and [(DAC)Y]$_2$(μ-Z-TolC=C=C=CTol) **22**, respectively and isolation of crystalline **21** followed the same procedure as that for **15**. Dissociation of the bridging acetylides is evident because mixing (separately dissolved) crystals of **15** and **21** in d_6-benzene results in the cross coupled products [(DAC)Y]$_2$(μ-Z-PhC=C=C=CTol) **23** and [(DAC)Y(μ-C≡CTol)(μ-C≡CPh)] **24**. Analysis of ^{1}H NMR of the mixture is complicated by overlapping aryl and methyl peaks from the presence of multiple products, but hydrolysis clearly shows a near statistical distribution of 1,4-disubstituted-3-buten-1-yne products as observed by GC/MS and ^{1}H NMR (Table 18). No attempts were made to isolate X-ray quality crystals of the cross coupled products.

Table 18 GC and ^{1}H NMR[a] data for alkynide cross coupling reactions

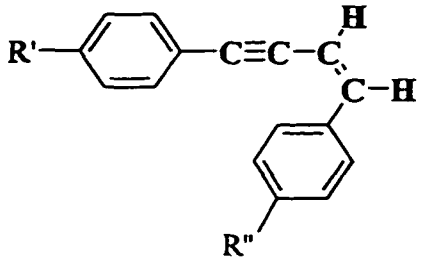

	R'	R"	GC ratio	^{1}H δ[b]	coupling[c]	Assign
Z-17	H	H	0.280[e]	5.79	$^3J_{HH}$ = 12	=CH
				6.41		=CH(Ph)
Z-25	Me	Me	0.261[e]	5.82	$^3J_{HH}$ = 12	=CH
				6.45		=CH(PhMe)
Z-26	H	Me	0.152[d]	5.78	$^3J_{HH}$ = 12	=CH
				6.38		=CH(PhMe)
Z-27	Me	H	0.307[d]	5.83	$^3J_{HH}$ = 12	=CH
				6.41		=CH(Ph)

[a]Spectrum recorded at 360 MHz in C_6D_6. [b]Chemical shift expressed in ppm. [c]Coupling measure in Hz. [d]Regiochemistry of Z-26 and Z-27 tentatively assigned by NMR. No distinction was possible by GC. [e]The *E*-isomers were not detected by GC.

3.3.8 The effect of steric and electronic factors on alkynide coupling.

Since steric factors are reported to favour alkynide coupling[80,81], the DAC system appears to be less congested than the C_5Me_5 system because in the latter equilibrium lies exclusively in favour of the coupled product. In order to assess electronic effects in the coupling reaction, the equilibrium constants (298 K) and relevant thermodynamic parameters were determined for the coupling of four *para*-substituted phenylacetylene substrates (Table 19).

Table 19 Thermodynamic parameters and K_{eq} values for (DAC)Y complexes with substituted phenylacetylenes

Substituent	Equilibrium[a]	$K_{eq\,298}$	σ_p[83]	$\Delta G°_{298}$[b]	$\Delta H°$[b]	$\Delta S°$[b]
para-Cl	**28 ⇌ 29**	3.66	0.24	-3.18	-74.7	-240
para-H	**15 ⇌ 16**	0.688	0	0.926	-67.0	-228
para-Me	**21 ⇌ 22**	0.210	-0.14	3.87	-59.9	-214
para-OMe	**30 ⇌ 31**	0.135	-0.28	4.96	-45.7	-170

[a]Equilibrium is from uncoupled bridged dimer to coupled butatriene. [b]Units reported in $kJmol^{-1}$ for $\Delta G°$ and $\Delta H°$ or $Jmol^{-1}K^{-1}$ for $\Delta S°$.

A plot of $\Delta G°_{298}$ against the Hammett σ_p parameter gives the expected straight line relationship for the equilibrium between the uncoupled alkynide dimer and the coupled butatriene complex for these para-substituted phenylacetylenes (Figure 22).

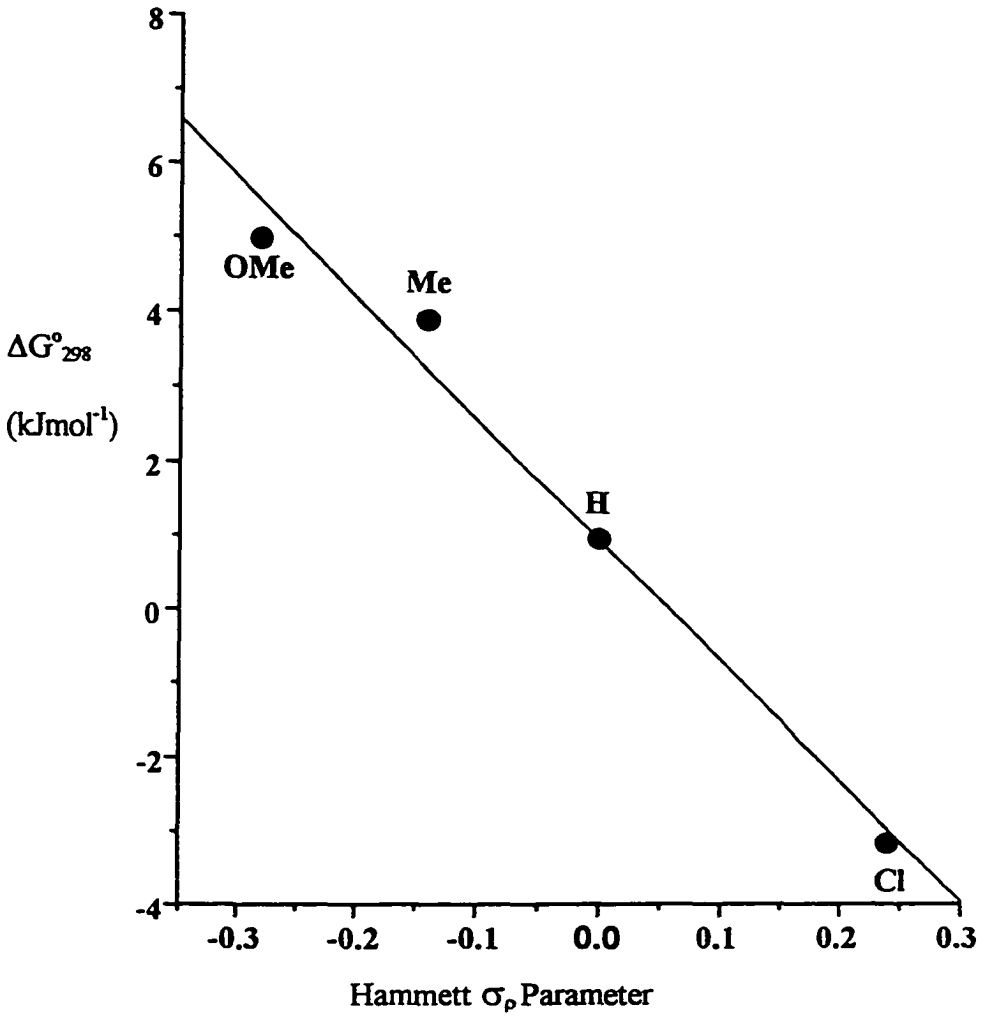

Figure 22 Plot of ΔG°_{298} against the Hammett σ_p parameter

It is clear from this data that electron withdrawing groups favour alkynide coupling. This result can be rationalized by comparing the relative extent of carbanion stabilization in the alkynide (uncoupled) and butatrienediyl (coupled) species. X-ray crystallographic studies have in all cases shown that the metals are most strongly bonded to the terminal carbons of the

butatrienediyl fragment indicating that these carbons have the most carbanionic character[80-82]. Resonance and inductive stabilization are expected to be greater for a carbanion α to the aromatic ring compared to carbanions in the β position, such as those found in an alkynide group. Therefore, electron withdrawing groups lower the ground state energy of the butatrienediyl *more* than that of the alkynide thereby increasing the exothermicity of the coupling reaction. In contrast, electron donating groups favour the formation of uncoupled bridging acetylide by destabilizing the α-carbanion more relative to that at the β-position. It is also interesting to note that ΔS° is least negative with electron donating substituents (ie. OMe) and most negative with electron withdrawing groups (ie. Cl). Assuming that the uncoupled acetylide exists in a monomer-dimer equilibrium then the least negative ΔS° value will be observed when the dimer form is predominant. Since electron donating groups such as methoxy will increase the negative charge on the β-carbon to a small degree, stronger acetylide bridging is to be expected in this case. Therefore, the observed trend in ΔS° is entirely consistent with a monomer-dimer equilibrium for the acetylide form.

3.3.9 Polymerization with bifunctional acetylenes.

Since electronic factors have been demonstrated to play a major role in the coupling of acetylides, it was of some interest to investigate the possibility of poly-enyne formation. The bifunctional 4,4'-diethynylbiphenyl[88] is an intriguing substrate because it has two functional ends which should each couple with another monomer of the substrate. The reaction of 4,4'-diethynylbiphenyl with two equivalents of Y(DAC)(CH_2SiMe_3) **14** (separately dissolved) in d_6-benzene at ambient temperature resulted in the formation of an

insoluble orange precipitate and the supernatant gave H_2DAC. Similarly, the reaction of 1,4-diethynyl benzene[88] with 2 equivalents of $Y(DAC)(CH_2SiMe_3)$ 14 also produced an insoluble orange precipitate.

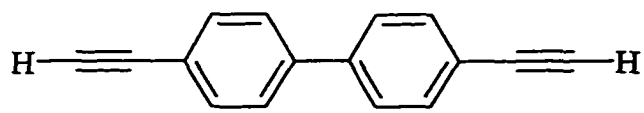

4,4'-diethynyl biphenyl

1,4-diethynyl benzene

The observation of colour and the low solubility of these precipitates suggest the formation of oligomeric material. Additionally, the orange colour does not disappear after hydrolysis, suggesting that the organic fragment is highly conjugated (a poly-enyne). Although mass spectral data of these oligomers might provide information of the number of units in the polymer, we have not determined its nature (bridging or coupled acetylides). Further characterization of these insoluble oligomeric materials were not performed, but work in this area is still continuing.

CHAPTER 4

ORGANOZIRCONIUM COMPLEXES CONTAINING 4,13-DIAZA-18-CROWN-6 (DAC)

4.1 Introduction

The pioneering work of Ziegler and Natta on ethylene and propylene polymerization catalyzed by $TiCl_3/AlEt_3$ heterogenous systems pointed out the utility of early transition metal alkyls as catalysts for olefin polymerization[89]. The modern direction of research is towards soluble organometallic complexes that provide well-defined single site catalysts affording greater control of polymer properties. Lanthanide metallocene complexes such as $(C_5Me_5)_2LuMe$ show high activity in the polymerization of ethylene, but the reaction with propene produces only oligomers[23]. Cationic group 4 metal alkyls L_2MR^+ (M = Ti, Zr, and Hf; R = alkyl; L = ligand) are isoelectronic with neutral lanthanide and group 3 complexes L_2LnR, however their chemistry and reactivity are different[51]. One significant difference is their calculated ground state geometry. The $(C_5H_5)_2ZrMe^+$ is pyramidal which is less sterically congested and hence more reactive, than the analogous lanthanide complex which is trigonal[52]. In addition, the inherent nature of the lanthanide complexes to form bridging structures results in reduced polymerization activity[22,23], while the higher electrophilicity of the cationic group 4 alkyls and the presence of a vacant site cis to a highly polarized $M^{\delta+}—C^{\delta-}$ bond may also increase reactivity[51]. These cationic group 4 complexes are attracting considerable industrial interest because recent work has demonstrated their important role as the active species in the original Ziegler-Natta polymerization systems[51,90]. Work by Jordan has demonstrated impressive stoichiometric insertion chemistry[91], while others have explored the catalytic activity of these systems[52, 90, 92]. There are several general routes to generate these cationic complexes from their parent neutral dialkyl complexes. Common routes include oxdative

cleavage of the M-R bond (eq 25), protonolysis (eq 26), and alkyl abstraction by a strong Lewis acid (eq 27)[93].

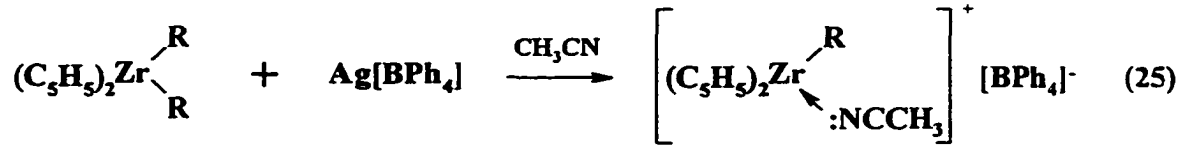

$$(C_5H_5)_2ZrR_2 + Ag[BPh_4] \xrightarrow{CH_3CN} [(C_5H_5)_2ZrR(:NCCH_3)]^+ [BPh_4]^- \quad (25)$$

R = alkyl, aryl

+ Ag° + 1/2 R-R

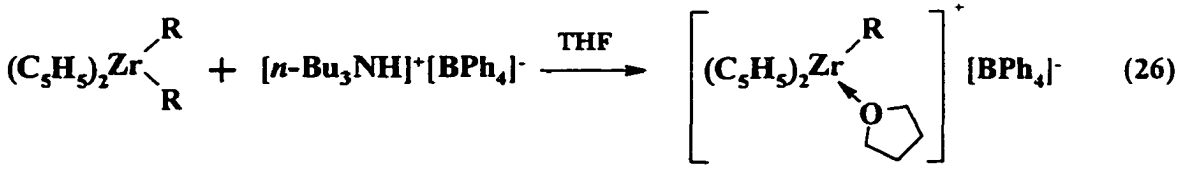

$$(C_5H_5)_2ZrR_2 + [n\text{-}Bu_3NH]^+[BPh_4]^- \xrightarrow{THF} [(C_5H_5)_2ZrR(O)]^+ [BPh_4]^- \quad (26)$$

R = alkyl, aryl

+ R-H + n-Bu_3N

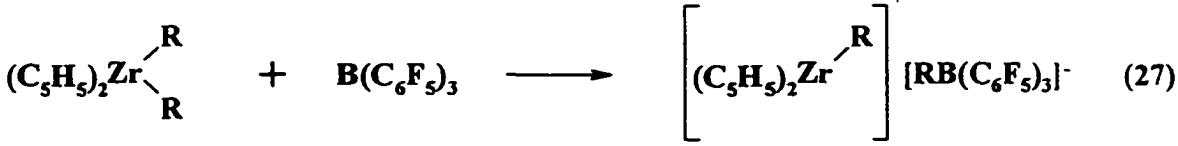

$$(C_5H_5)_2ZrR_2 + B(C_6F_5)_3 \longrightarrow [(C_5H_5)_2ZrR]^+ [RB(C_6F_5)_3]^- \quad (27)$$

R = alkyl,

While a large excess (greater than 100 fold) of aluminium alkyls or MAO (methylaluminoxane) are the methods primarily used in the industrial polymerization systems, $B(C_6F_5)_3$ has been employed increasingly to generate group 4 alkyl cations

because only equimolar amounts are required. One advantage of the latter Lewis acid is the ability to perform spectroscopic measurements without interference from the co-catalyst[93].

The development of group 4 cationic complexes, like that of the lanthanides and yttrium, has been dominated by cyclopentadienyl type ancillary ligation[51, 52, 90]. More recent work has focused on the use of tetraaza macrocycles[94], porphyrins[95], and acyclic Shiff base[96] as stabilizing ligands. As noted earlier, the DAC system is the approximate steric equivalent to two C_5Me_5 ligands; however, DAC offers greater flexibility and a variable donor array. While the presence of donors may increase electron donation to the metal centre and consequently reduce reactivity, the saturated framework of DAC avoids problems associated with alkyl migration which are common in unsaturated systems such as porphyrins and Schiff base macrocycles. The successful synthesis of Y(DAC)(CH_2SiMe_3) **14** suggested that preparation of the isoelectronic Zr(DAC)$(R)^+$ cations should be possible. An investigation of the reactivity of Zr(DAC)$(R)^+$ should provide valuable insights into the ancillary ligand effects for this important class of organometallic molecules.

4.2 Organozirconium complexes of 4,13-diaza-18-crown-6 (DAC)

4.2.1 Synthesis and NMR characterization of *cis* and *trans*-Zr(DAC)$(CH_2Ph)_2$ 32

The protonolysis reaction of $Zr(CH_2Ph)_4$[97] with one equivalent of H_2DAC proceeds smoothly in toluene to afford a 1:4 mixture of Zr(DAC)$(CH_2Ph)_2$ ***cis*-32** and ***trans*-32** (Scheme 9). The isomers are difficult to separate by fractional crystallization, but small

quantities of pure isomers can be separated manually (*cis*-**32** is pale yellow and rectangular; *trans*-**32** is orange and cubic shaped).

Scheme 9 Preparation of zirconium dibenzyl complexes stabilized by DAC

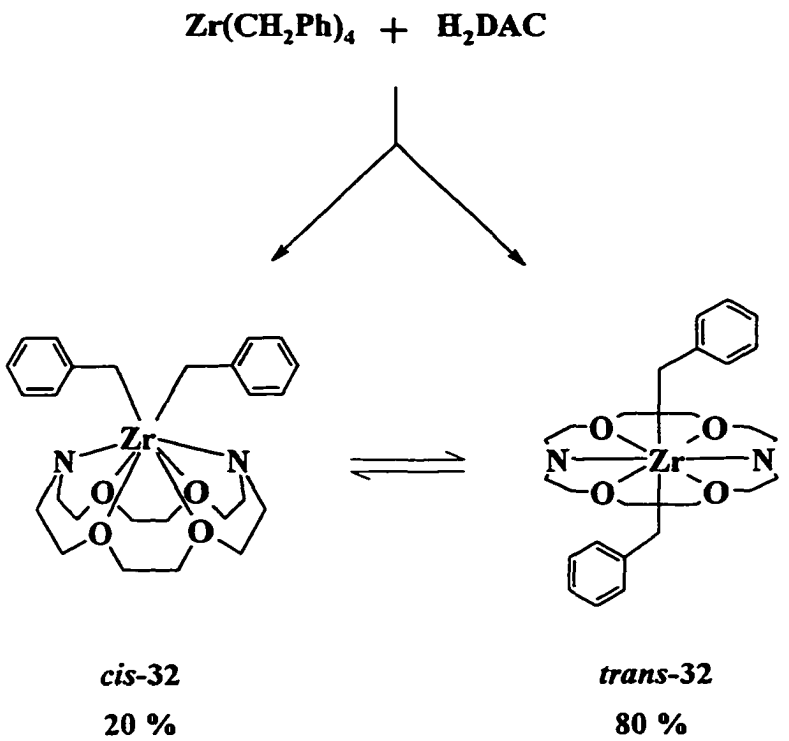

cis-**32** 20 %

trans-**32** 80 %

The NMR spectra of *cis*-**32** are consistent with a monomeric dialkyl structure with C_{2v} molecular symmetry. The DAC region consists of six well resolved multiplets in the ^{1}H NMR spectrum due to inequivalent endo and exo hydrogens on each of the three unique DAC carbons signals in ^{13}C NMR(Table 20).

Table 20 NMR data[a] for *cis*-Zr(DAC)(CH_2Ph)$_2$ 32

		δ[b]	mult	Int.	coupling[c]	Assign[d].
^1H	Aryl	7.22 - 7.31	m	8H		*o*, *m*-aryl
		6.84	tt	2H	$^3J_{HH}$ = 7.0 $^4J_{HH}$ = 1.5	*p*-aryl
	DAC	3.57, 3.15[e]	m	8H		C_cH
		3.40, 2.84[e]	m	8H		C_bH
		3.05[f]	m	8H		C_aH
	CH_2Ph	2.46	s	4H		CH_2Ph
^{13}C	Aryl	154.65	s			*ipso*-aryl
		127.64	s			*o*-aryl
		126.83	s			*m*-aryl
		118.67	s			*p*-aryl
	DAC	73.90	s			C_c
		72.01	s			C_b
		56.26	s			C_a
	CH_2Ph	60.02	t[g]		$^1J_{CH}$ = 119	CH_2Ph

[a]Spectrum recorded at 360 MHz (^1H) or 90.55 MHz (^{13}C {^1H}) in C_6D_6 296 K. [b]δ expressed in ppm. [c]Coupling constants expressed in Hz. [d]Assignment letters refer to the carbon atoms of the unique $NC_aH_2C_bH_2OC_cH_2$ portion of the DAC ligand (the remaining carbons are related to these by the molecular symmetry). [e]Exo and endo protons not assigned. [f]Partially overlapping resonances. [g]Gated carbon-proton coupling.

Due to the D_{2h} molecular symmetry of the solution structure, the *trans*-isomer is expected to show three CH_2 multiplets in the ^1H NMR spectrum since the exo and endo protons on each unique DAC carbon are equivalent. At ambient temperature, however, ***trans*-32** shows six broad resonances in both the ^1H and $^{13}C\{^1H\}$ NMR. When the temperature is raised these resonances coalesce between 30°C and 50°C and re-emerge as three new resonances at 70°C (Table 21). This variable temperature NMR behaviour is more clearly illustrated by the $^{13}C\{^1H\}$ NMR spectrum (Figure 23).

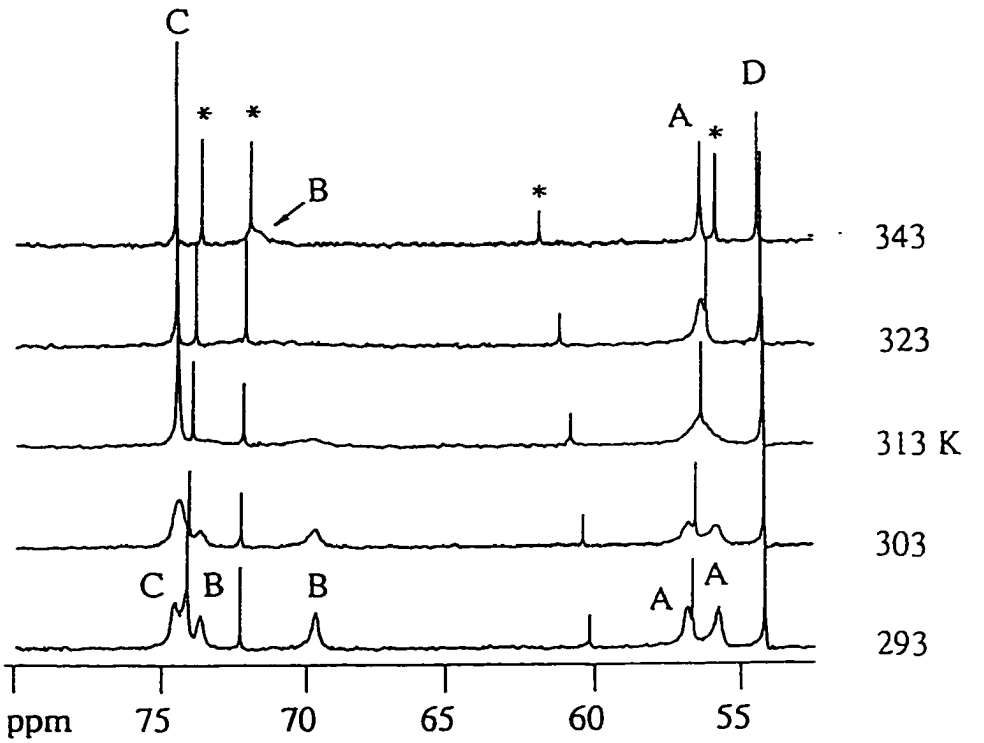

Trans-**32**: (A) NC_aH_2; (B) $NCH_2OC_bH_2$; (C) OC_cH_2; (D) CH_2Ph

Cis-**32**: Impurity denoted by *.

Figure 23 Variable temperature $^{13}C\{^1H\}$ NMR of the DAC region of *trans*-32

Table 21 NMR data[a] for *trans*-Zr(DAC)(CH_2Ph)$_2$ 32

		δ[b]	Mult	Int.	Coupling[c]	Assign[d]
^1H	Aryl	7.11	t	4H	$^3J_{HH}$ = 7.3	*m*-aryl
		6.81	br d	4H	$^3J_{HH}$ = 7.8	*o*-aryl
		6.72	t	2H	$^3J_{HH}$ = 7.3	*p*-aryl
	DAC	3.52	t	8H	$^3J_{HH}$ = 5.2	C_bH
		3.37	br s	8H		C_cH
		3.11	t	8H	$^3J_{HH}$ = 5.2	C_aH
	CH_2Ph	1.74	s	4H		CH_2Ph
^{13}C	Aryl	155.28	s			*ipso*-aryl
		127.49	s			*o*-aryl
		125.85	s			*m*-aryl
		117.70	s			*p*-aryl
	DAC	74.45	s			C_c
		71.60	s			C_b
		56.12	s			C_a
	CH_2Ph	54.16	t[e]		$^1J_{CH}$ = 120	CH_2Ph

[a]Spectrum recorded at 360 MHz (^1H) or 90.55 MHz (^{13}C {^1H}) in C_6D_6 at 343 K. [b]δ expressed in ppm. [c]Coupling constants expressed in Hz. [d]Assignment letters refer to the carbon atoms of the unique $NC_aH_2C_bH_2OC_cH_2$ portion of the DAC ligand (the remaining carbons are related to these by the molecular symmetry). [e]Gated carbon-proton coupling.

The results obtained from VT-NMR suggests that the lower molecular symmetry, apparent in the room temperature NMR spectrum of ***trans*-32**, is due to asymmetric coordination of the DAC ligand. The solid state structure of ***trans*-32** shows a seven coordinate, distorted bipyramidal structure with at least one dangling oxgen donor (*vide infra*). This suggests that the dynamic process observed by VT-NMR involves rapid dissociation and reassociation of the DAC oxygens. From the coalescence temperature of the DAC resonances due to NC_aH_2 (A) (T_c = 308 K, $\delta\upsilon$ = 100 Hz) and $NCH_2C_bH_2O$ (B) (T_c = 323 K, $\delta\upsilon$ = 366 Hz), a free energy of activation for this process of $^a\Delta G^{\ddagger} = 62 \pm 2$ kJmol^{-1} was estimated[98].

$^a\Delta G^{\ddagger}$ was calculated from the coalescence temperature (T_c) using the equal-population, two site exchange equation: $\Delta G^{\ddagger} = (1.912 \times 10^{-2})T_c[9.972 + \log(T_c/\delta\upsilon)]$ in kJmol^{-1}, where $\delta\upsilon$ is the separation of the resonances in Hz and T_c is in K. The error in $\Delta G^{\ddagger}$ of ± 2 kJmol^{-1} was estimated by assuming liberal errors of ± 5 K in T_c and ± 5 Hz in $\delta\upsilon$.

4.2.2 X-ray structural analysis of *cis* and *trans*-Zr(DAC)$(CH_2Ph)_2$ **32**

The ZORTEP[99] drawing of ***cis*-32** is shown in Figure 24 and selected bond distances and angles are collected in Table 22. A complete summary of the crystallographic data for ***cis*-32** are given in Appendix Tables XVI-XVIII. The zirconium centre is eight coordinate with all four ether oxygens of the DAC ligand coordinated. The coordination geometry may be described as a highly distorted square antiprism (Figure 25). The most significant features of the structure are the open Zr-CH_2-C_{ipso} angles (123.7(5) and 128.3(6)° for Zr-C13-C15 and Zr-C14-C20, respectively), indicating strictly η^1-benzyl coordination[100]. The Zr-N distances (2.124(6) and 2.119(7) Å) are very similar to those found in seven-coordinate Y(DAC)(CH_2SiMe_3) (2.27(2) and 2.26(2) Å) after correcting for the 0.12 Å larger ionic radius of the Y^{3+} ion[64]. However, the Zr-C bond lengths are long by the same comparison (***cis*-32**: 2.417(7) and 2.389(6)Å; Y(DAC)(CH_2SiMe_3): 2.45(2) Å). Unlike the Y-O distances in Y(DAC)(CH_2SiMe_3) which were found to span a wide range (2.431(13) to 2.622(11) Å), the four Zr-O distances (2.466(6) to 2.477(5) Å) in ***cis*-32** are very nearly identical to one another.

The ZORTEP drawing of ***trans*-32** is shown in Figure 6. A summary of the crystallographic data is summarized in Appendix Table XIX. Attempts to refine the X-ray crystal structure of ***trans*-32** were hindered by thermal disorder from the macrocyclic ring atoms, especially in the vicinity of the uncoordinated oxygen atom (O3). As a result the bond angles and bond distances are not reliable and do not warrant further discussion. The distorted belt arrangement in ***trans*-32** shows zirconium is too small to coordinate all six donors in a planar array without introducing strain in the macrocyclic ring. Despite the

fact that zirconium appears to fit the macrocycle better in the *cis* geometry, the *trans* isomer is the most stable isomer in solution.

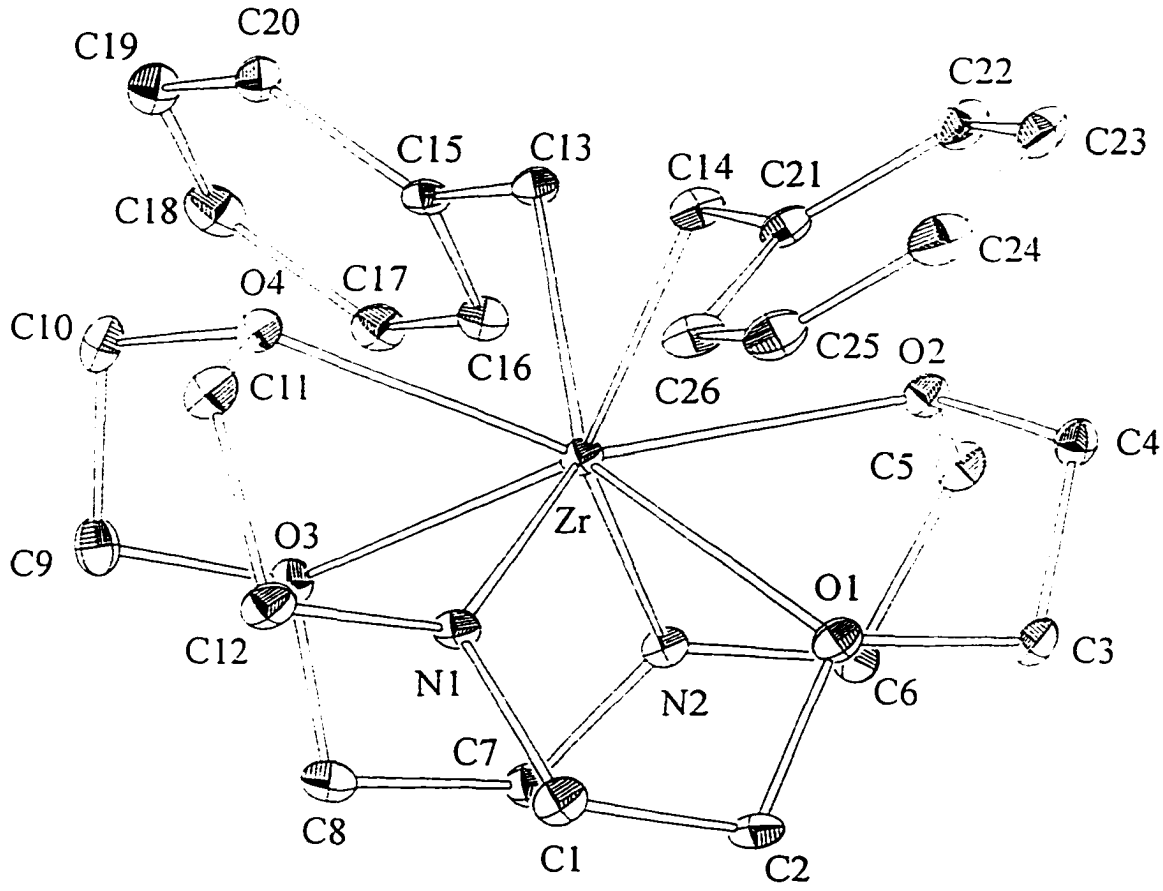

Figure 24 ZORTEP drawing of *cis*-Zr(DAC)(CH_2Ph)$_2$ 32 showing side view

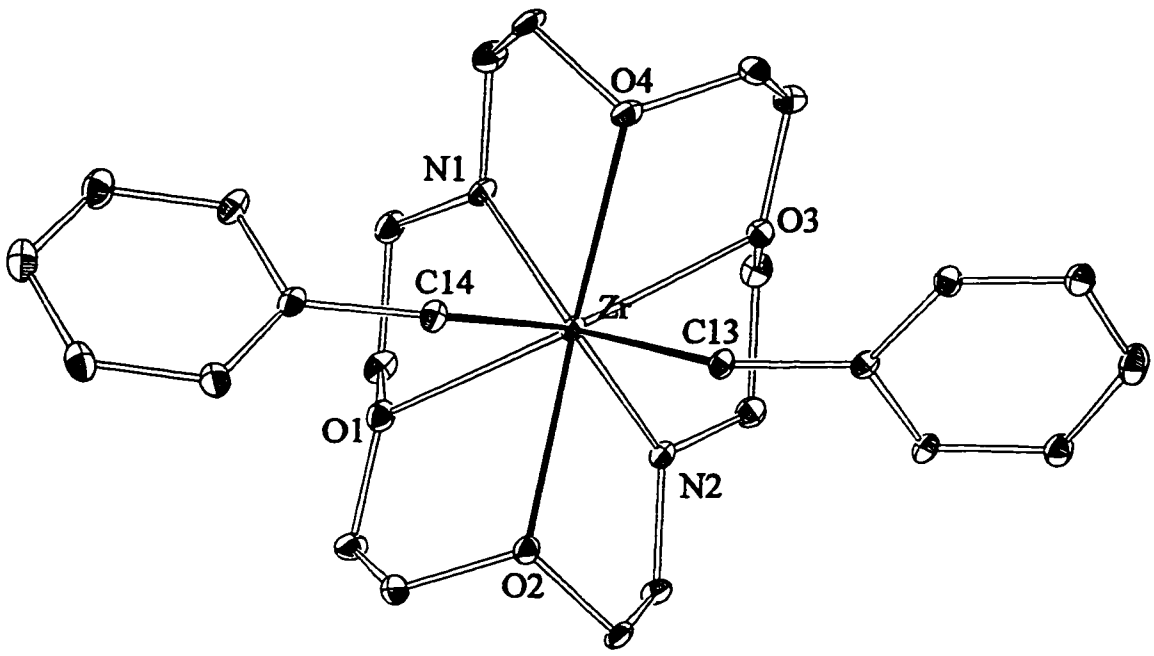

Figure 25 ZORTEP drawing of *cis*-Zr(DAC)$(CH_2Ph)_2$ 32 showing the top view

Table 22 Selected distances (Å) and angles (deg)[a] for *cis*-Zr(DAC)(CH_2Ph)$_2$ 32

		Distances	
Zr(1)-O(1)	2.471(5)	Zr(1)-O(2)	2.466(6)
Zr(1)-O(3)	2.477(5)	Zr(1)-O(4)	2.470(5)
Zr(1)-N(1)	2.119(7)	Zr(1)-N(2)	2.2124(6)
Zr(1)-C(13)	2.417(7)	Zr(1)-C(14)	2.389(8)
		Angles	
O(1)-Zr(1)-O(2)	65.3(2)	O(1)-Zr(1)-O(3)	128.4(2)
O(1)-Zr(1)-O(4)	131.4(2)	O(1)-Zr(1)-N(1)	68.4(2)
O(1)-Zr(1)-N(2)	81.8(2)	O(1)-Zr(1)-C(13)	143.2(2)
O(1)-Zr(1)-C(14)	81.4(2)	O(2)-Zr(1)-O(3)	130.8(2)
O(2)-Zr(1)-O(4)	148.8(2)	O(2)-Zr(1)-N(1)	133.7(2)
O(2)-Zr(1)-N(2)	68.9(2)	O(2)-Zr(1)-C(13)	79.1(2)
O(2)-Zr(1)-C(14)	75.5(2)	O(3)-Zr(1)-O(4)	64.6(2)
O(3)-Zr(1)-N(1)	81.1(2)	O(3)-Zr(1)-N(2)	67.9(2)
O(3)-Zr(1)-C(13)	82.0(2)	O(3)-Zr(1)-C(14)	144.5(2)
O(4)-Zr(1)-N(1)	68.8(2)	O(4)-Zr(1)-N(2)	132.4(2)
O(4)-Zr(1)-C(13)	76.8(2)	O(4)-Zr(1)-C(14)	81.3(2)
N(1)-Zr(1)-N(2)	106.5(2)	N(1)-Zr(1)-C(13)	145.5(3)
N(1)-Zr(1)-C(14)	96.3(3)	N(2)-Zr(1)-C(13)	94.4(2)
N(2)-Zr(1)-C(14)	144.2(3)	C(13)-Zr(1)-C(14)	80.8(3)
Zr(1)-C(13)-C(15)	123.7(5)	Zr(1)-C(14)-C(21)	128.3(6)

[a] Estimated standard deviation in parentheses.

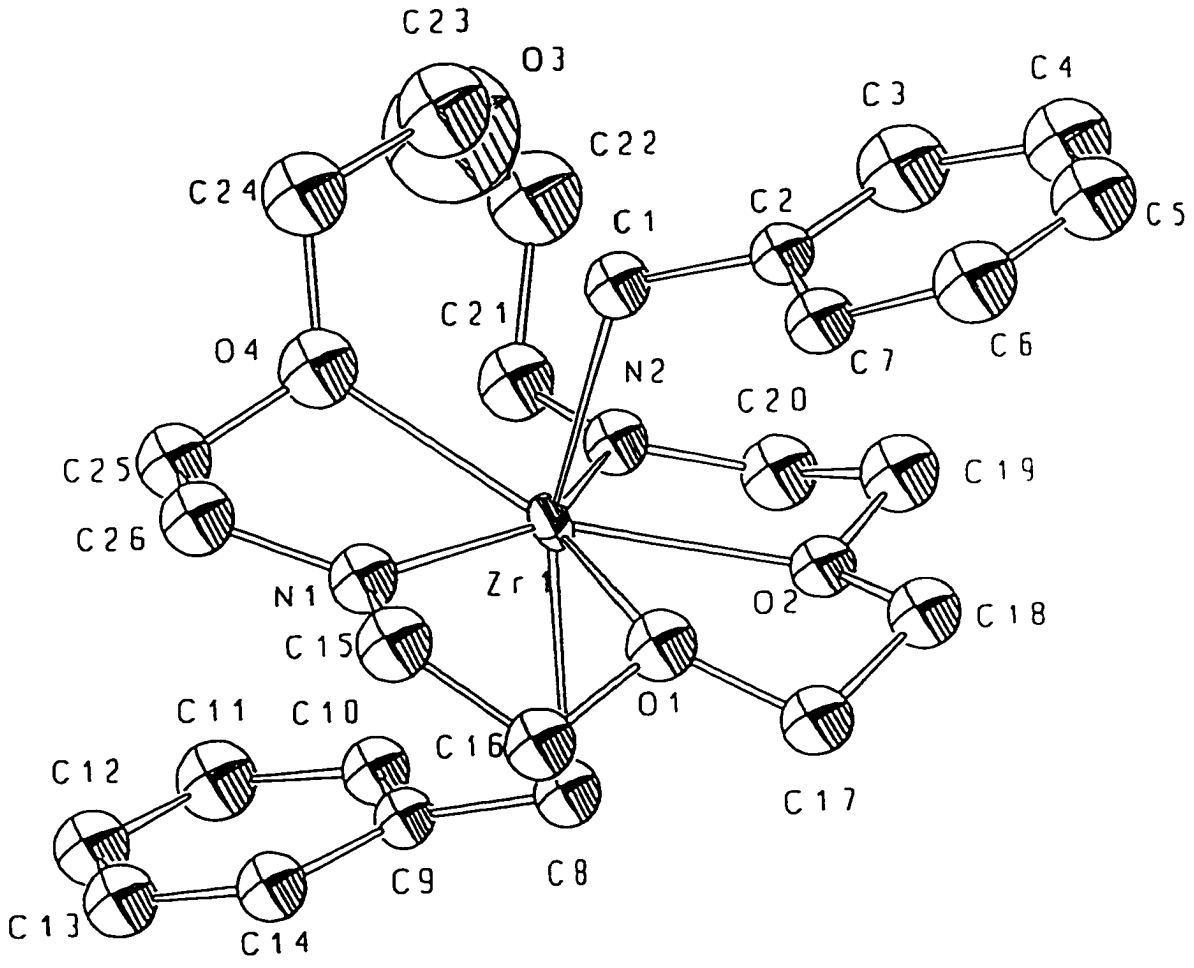

Figure 26 ZORTEP drawing of *trans*-Zr(DAC)(CH_2Ph)$_2$ 32

4.2.3 Isomerization of $Zr(DAC)(CH_2Ph)_2$ *cis* -**32** ⇌ *trans*-**32**

Pure *cis*-**32** and *trans*-**32** slowly undergo isomerization to a *cis:trans* 1:4 mixture when redissolved. Isomerization proceeds more rapidly in d_6-benzene (days) than in d_8-THF (weeks). The slower rate of isomerization in d_8-THF could be due to strong solvent coordination which enforces a high coordination number at zirconium and prevents rearrangement on steric grounds. A possible pathway for *cis-trans* isomerization could involve an unimolecular process in which one benzyl group passes through the DAC ring. However, it is more likely that this rearrangement proceeds by a bimolecular process involving alkyl transfer between two zirconium centres. While the former case appears at least theoretically possible given the NMR and structural evidence for oxygen dissociation in *trans*-**32**, steric crowding in the transition state probably makes this unlikely.

4.2.4 General route to organozirconium dialkyl complexes

In order to gain more general access to other alkyl and aryl complexes, the preparation of $Zr(DAC)Cl_2$ was investigated. Attempts to prepare the dichloride from $ZrCl_4$ and M_2DAC (M = Li, Na, and K) failed to yield clean products due to the high stability of crown-ether-alkali metal complexes (see Section 2.3.2 for further discussion). However, the reaction of one equivalent of H_2DAC with $Zr(CH_2Ph)_2Cl_2 \bullet 2OEt_2$[101] in toluene produced a marginally soluble powder, presumed to be polymeric $[Zr(DAC)Cl_2]_x$ **33**. No attempt was made to fully characterize this compound because of its very low solubility. *In situ* alkylation of **33** with an alkyl lithium reagent, LiR (R = CH_2SiMe_3, **34**; CH_2CMe_3 **35**) exclusively afforded *cis*-$Zr(DAC)(R)_2$ (eq 28). The NMR data for these new complexes are consistent

with a C_{2v} symmetry since six DAC proton multiplets are observed for the three unique DAC carbons (Table 23). Isomerization was not observed for *cis*-Zr(DAC)$(R)_2$ of **34** and **35** over a period of weeks in d_6-benzene. Presumably, the larger size of CH_2SiMe_3 and CH_2CMe_3 relative to CH_2Ph make isomerization impossible. The mechanism for isomerization cannot be resolved because both unimolecular and bimolecular processes are expected to be hindered by the larger alkyl groups.

$$Zr(CH_2Ph)_2Cl_2 + H_2DAC \xrightarrow{\text{toluene}} [Zr(DAC)Cl_2]_x \quad \text{(presumed)}$$

33

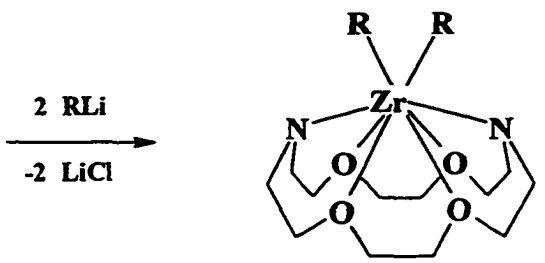

34, R = CH_2SiMe_3

35, R = CH_2CMe_3

(28)

Table 23 NMR data[a] for *cis*-Zr(DAC)(CH_2SiMe_3)$_2$ 34 and *cis*-Zr(DAC)(CH_2CMe_3)$_2$ 35

	cis-Zr(DAC)(CH_2SiMe_3)$_2$ **34**				*cis*-Zr(DAC)(CH_2CMe_3)$_2$ **35**			
^{1}H	δ[b]	mult	Int.	Assign[c].	δ[b]	mult	Int.	Assign[c]
DAC[d]	3.47	m	4H	C_oH	3.50	s	4H	C_oH
	3.12	m	4H	C_oH	3.13[e]	s	4H	C_oH
	3.05	m	4H	C_bH	3.13[e]	s	4H	C_bH
	2.93	m	4H	C_aH	2.99	s	4H	C_aH
	2.68	m	4H	C_bH	2.74	s	4H	C_bH
	2.51	m	4H	C_aH	2.54	s	4H	C_aH
$CH_2(XMe_3)$	0.43	s	18H	$SiMe_3$	1.49	s	18H	CMe_3
	-1.39	s	4H	CH_2	0.09	s	4H	CH_2
^{13}C	δ		δ	δ	δ		δ	δ
DAC	71.5 C_c		67.5 C_b	52.9 C_a	71.4C_c		67.4 C_b	52.9 C_a
$CH_2(XMe_3)$	4.93 $SiMe_3$		-9.85 CH_2[f]		37.6 CMe_3		33.0 $CMe3$	23.0 CH_2[f]
$^1J_{CH}$			103 Hz					100 Hz

[a]Spectrum recorded at 360 MHz (^{1}H) or 90.55 MHz (^{13}C) in C_6D_6 296 K. [b]δ expressed in ppm. [c]Assignment letters refer to the carbon atoms of the unique $NC_aH_2C_bH_2OC_cH_2$ portion of the DAC ligand (the remaining carbons are related to these by the molecular symmetry). [d]Exo and endo protons not assigned. [e]Partially overlapping resonances. [f]Gated carbon-proton coupling.

4.2.5 Thermal stability of $Zr(DAC)(R)_2$

All organozirconium dialkyl complexes supported by DAC ligation are stable indefinitely both in solution (benzene) and in the solid state at room temperature. At higher temperatures, a solution of a 1:4 mixture ***cis*** and ***trans*-32** (R = CH_2Ph) decomposes to uncharacterizable products after a week at 70°C, while the other alkyls (R = CH_2SiMe_3, **34**; CH_2CMe_3 **35**) are stable indefinitely even at this elevated temperature. As noted earlier, one common decomposition pathway involves metallation of the DAC ring. This decomposition mode must involve approach of a carbanionic α-carbon of the alkyl to a suitable CH_2 of the macrocycle forming a four-centre transition state. However, steric congestion created by the larger neopentyl alkyls provides the kinetic barrier to this mode of decomposition.

4.2.6 Reactivity of $Zr(DAC)(R)_2$ complexes

No insertion product was observed in the reaction of $Zr(DAC)(R)_2$ (R = CH_2Ph, ***cis*-32**, ***trans*-32**; R = CH_2SiMe_3 **34**; R = CH_2CMe_3 **35**) with unsaturated substrates such as CO, H_2, acetylenes, olefins, and nitriles. Attempts to use more acid substrates such as phenylacetylene also failed to yield new products. This result provides further evidence that the coordination environment around the metal is extremely congested and reactivity can only be obtained by reducing the steric bulk (assuming that electron donation from the macrocylic donors has little effect on reactivity). No attempt was directed towards preparing $Zr(DAC)(Me)_2$ complexes.

4.3 Cationic organozirconium complexes

4.3.1 Synthesis and NMR characterization of $[Zr(DAC)(CH_2Ph)]^+[BPh_4]^-$ 36

Direct protonolysis of either ***cis*-32** or ***trans*-32** with one equivalent of $[n\text{-}Bu_3NH]^+[BPh_4]^-$ in toluene cleanly afforded $[Zr(DAC)(CH_2Ph)]^+[BPh_4]^-$ **36** (eq. 29) as a marginally soluble pale yellow precipitate in quantitative yield. The product is insoluble in CH_2Cl_2, but highly soluble in strongly coordinating solvents such as THF and pyridine. In d_8-THF, the NMR spectra of **36** consists of 6 multiplets due to the presence of endo and exo protons on each of the three unique carbons, consistent with a C_{2v} molecular symmetry (Table 24).

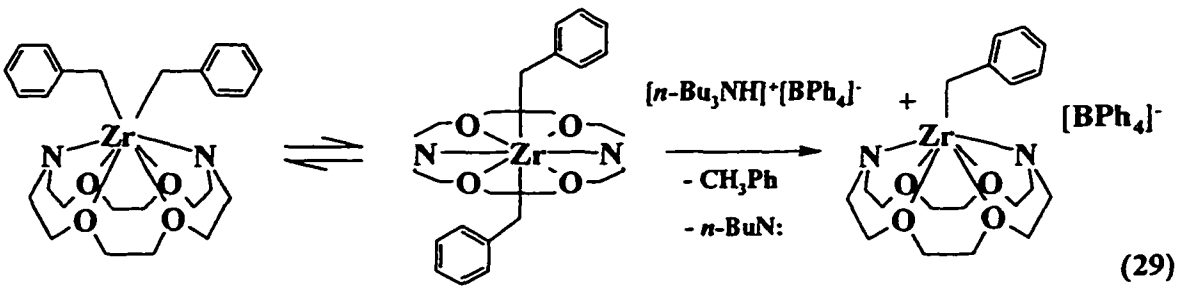

(29)

cis-32 *trans*-32 36

Table 24 NMR data[a] for $[Zr(DAC)(CH_2Ph)]^+[BPh_4]^-$ 36

		δ[b]	mult	Int.	coupling[c]	Assign[d].
^1H	Aryl	7.31	br m	8H		*o*-aryl BPh_4^-
		6.98	t	2H	$^3J_{HH} = 7.5$	*m*-aryl (benzyl)
		6.90	t	8H	$^3J_{HH} = 7.4$	*m*-aryl BPh_4^-
		6.76	tt	4H	$^3J_{HH} = 7.3$ $^4J_{HH} = 1.0$	*p*-aryl BPh_4^-
		6.74	m	2H		*o*-aryl (benzyl)
		6.63	tt	1H	$^3J_{HH} = 7.3$ $^4J_{HH} = 1.0$	*p*-aryl (benzyl)
	DAC[e]	3.90, 3.77	m	4H, 4H		C_cH
		3.77, 3.05	m	4H, 4H		C_bH
		3.64, 3.08	m	4H, 4H		C_aH
	CH_2Ph	1.87	s	2H		CH_2Ph

^{13}C		δ[b]		
	BPh_4^-	137.16 (*o*-aryl)	125.92 (*m*-aryl)	122.09 (*p*-aryl)
	CH_2Ph	128.09 (*o*-aryl)	127.43 (*m*-aryl)	120.44 (*p*-aryl)
		59.11 (CH_2Ph)		
	DAC	76.13 C_c	73.49 C_b	53.18 C_a

[a]Spectrum recorded at 360 MHz (^1H) or 90.55 MHz (^{13}C) in C_4D_8O 296 K. [b]δ expressed in ppm. [c]Coupling measured in Hz. [d]Assignment letters refer to the carbon atoms of the unique $NC_aH_2C_bH_2OC_cH_2$ portion of the DAC ligand (the remaining carbons are related to these by the molecular symmetry). [e]Exo and endo protons not assigned.

The failure of **36** to dissolve in weakly coordinating solvents precluded any reactions with weakly coordinating substrates such as ethylene, CO, and H_2. As a result, no further studies were carried out on this complex.

4.3.2 Synthesis and NMR characterization of $[Zr(DAC)(CH_2Ph)]^+[B(CH_2Ph)(C_6F_5)_3]^-$ **37**

Treatment of either ***cis*-32** or ***trans*-32** with the strong Lewis acid, $B(C_6F_5)_3$ in toluene yielded $[Zr(DAC)(CH_2Ph)]^+[B(CH_2Ph)(C_6F_5)_3]^-$ **37** as a bright yellow oil which readily dissolves in THF or CH_2Cl_2 (eq 30). Attempts to grow crystals of **37** from a variety of common solvents or a mixture of solvents were not successful as the product either remained soluble or separated as an immiscible oil.

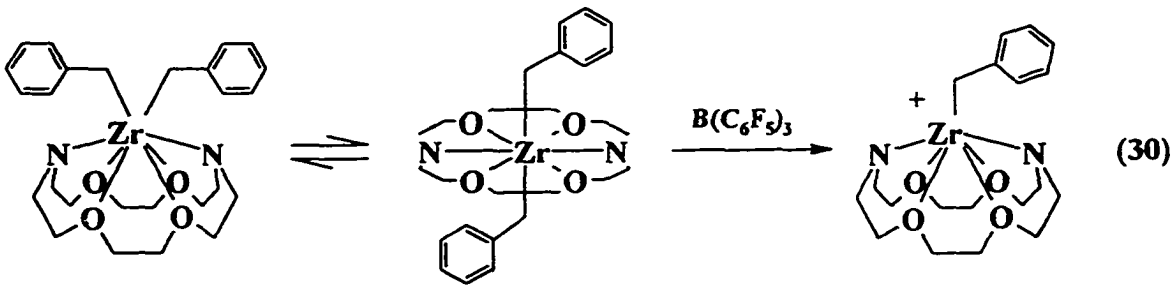

(30)

***cis*-32** ***trans*-32** $[B(CH_2Ph)(C_6F_5)_3]^-$

37

The ^1H NMR spectrum recorded in CD_2Cl_2 (Table 25) shows the presence of inequivalent *exo* and *endo* protons on each of the three unique DAC carbons. Figure 27 shows the ^1H-^{13}C COSY NMR spectrum of 37. In comparison to *cis*-32, the $ZrCH_2$ proton resonance of the cation 37 shifts 0.26 ppm upfield, while in comparison to *trans*-32 the same signal moves downfield by 0.46 ppm. This anomaly is due to the differences in geometries and the coordination numbers amongst the complexes.

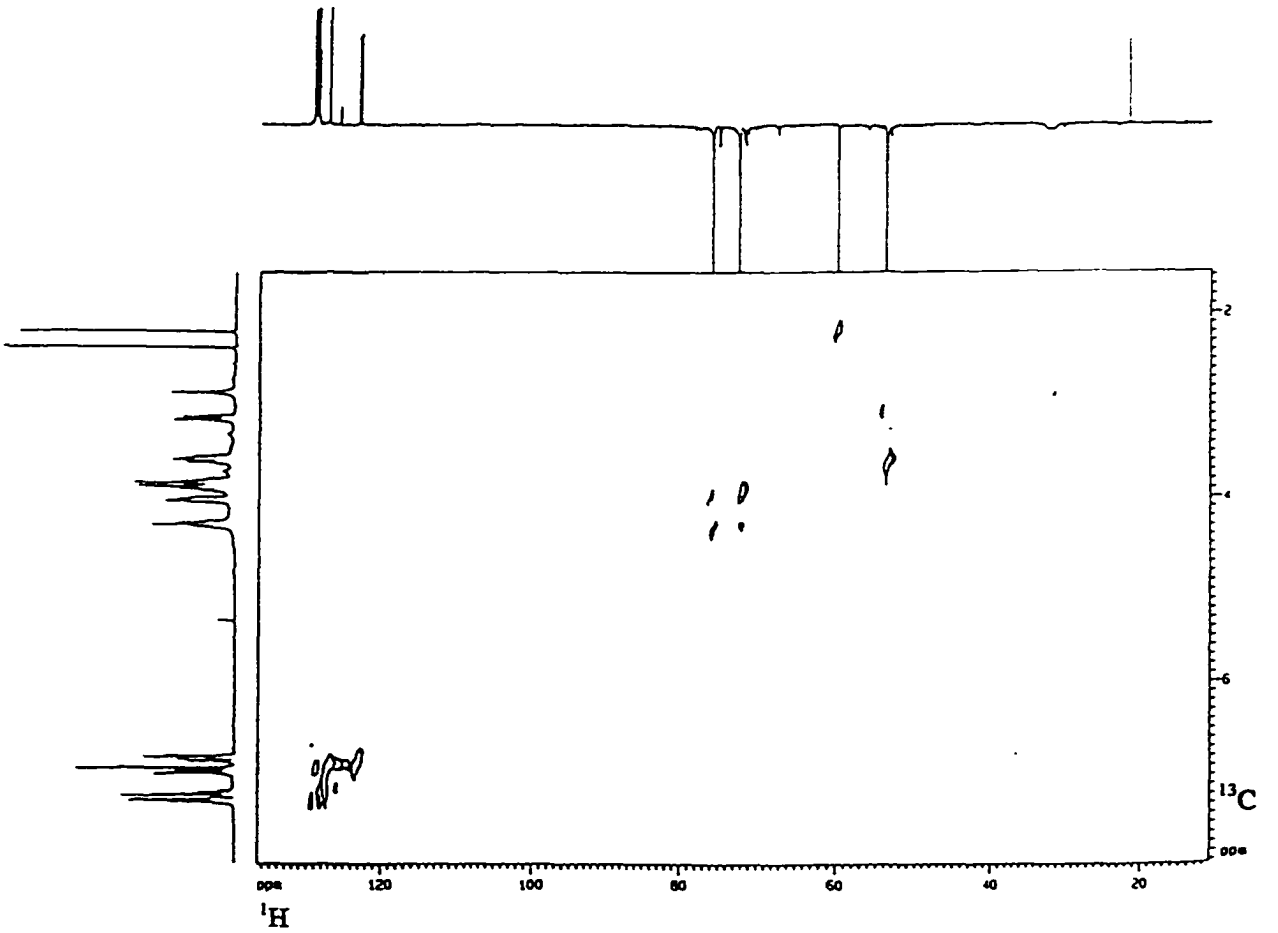

Figure 27 ^1H-^{13}C COSY NMR spectrum of $[Zr(DAC)(CH_2Ph)]^+[B(CH_2Ph)(C_6F_5)_3]^-$ 37

Table 25 NMR data[a] for $[Zr(DAC)(CH_2Ph)]^+[B(CH_2Ph)(C_6F_5)_3]^-$ 37

		δ[b]	mult	Int.	coupling[c]	Assign[d].
^1H	Aryl	6.78 - 6.98	m	10H		aryl
	DAC[e]	4.29, 4.02	m	4H, 4H		C_cH
		3.88	m	8H		C_bH
		3.58, 3.13	m	4H, 4H		C_aH
	CH_2Ph	2.86	br s	2H		BCH_2Ph
		2.20	s	2H		$ZrCH_2Ph$

^{13}C		δ[b]		
	$(C_6F_5)_3$	148.0 (*o*-aryl *C*F) $^1J_{CF}$ = 228	137.88 (*p*-aryl *C*F) $^1J_{CF}$ = 243	136.90 (*m*-aryl *C*F). $^1J_{CF}$ = 228
	Benzyl aryl	148.9 (ipso)		
	$B(CH_2Ph)$	144.4 (ipso)		
	DAC	75.78 C_c	72.33 C_b	53.81 C_a
	CH_2Ph	59.80 $ZrCH_2$ $^1J_{CH}$ = 127	32.40 BCH_2	

[a]Spectrum recorded at 360 MHz (^1H) or 90.55 MHz (^{13}C) in CD_2Cl_2 296 K. [b]δ expressed in ppm. [c]Coupling measured in Hz. [d]Assignment letters refer to the carbon atoms of the unique $NC_aH_2C_bH_2OC_cH_2$ portion of the DAC ligand (the remaining carbons are related to these by the molecular symmetry). [e]Exo and endo protons not assigned.

The presence of a benzyl group bound to boron is clearly evident by the broad singlet at δ 2.86 ppm and the presence of two sets of benzyl proton and carbon resonances. A number of NMR parameters that have been cited as evidence for an η^2-CH_2Ph interaction are notably absent. Specifically, upfield shifts of the benzyl ipso carbon and the ortho proton resonances to ca. 137.5 ppm and less than 6.40 ppm[102], respectively, and an unusually large $^1J_{CH}$ value (> 140 Hz) for the benzyl CH_2 group[103a] are not observed for **37** (benzyl ipso carbon, δ 148.9 ppm; ortho benzyl proton, δ 6.78 – 6.85; benzyl CH_2, $^1J_{CH}$ = 127 Hz).

Further structural characterization without X-ray analysis can be obtained from ^{19}F NMR. In particular, Horton has shown that cation-anion interactions from coordination of the $RB(C_6F_5)_3^-$ anion with the cationic d^0 metal centre can be detected by measuring the difference in ppm between the *meta*- and *para*- fluorine resonances ($\Delta\delta_{m,p} = \delta_mF - \delta_pF$). A value of less than 3 ppm has been shown to indicate no significant interactions while a value greater than 3 ppm is an indication of anion coordination[103a]. In the case of $[Zr(DAC)(CH_2Ph)]^+$ $[B(CH_2Ph)(C_6F_5)_3]^-$ **37**, the small $\Delta\delta_{m,p}$ value of 2.9 ppm (free anion, 2.7 ppm) indicates there is no significant cation-anion interaction. Further evidence can be obtained from the presence of an upfield carbon resonance at 144.4 ppm of $B(CH_2Ph)(C_6F_5)_3$(free anion, 148.6 ppm, coordinated anion, 161.0 ppm)[103a] in the ^{13}C NMR spectrum (Table 25).

4.3.3 Catalytic reactivity of $[Zr(DAC)(CH_2Ph)]^+[B(CH_2Ph)(C_6F_5)_3]^-$ **37**

Although no reaction was observed between **37** in toluene and an excess of ethylene or 1-hexene, the reaction of **37** with a more acidic substrate, *p*-tolylacetylene led to slow catalytic production of 1,4-di-*p*-tolyl-3-buten-1-yne (*Z*:*E* ratio = 85:15) at an initial rate of 2 turnovers/h. Horton has previously reported the catalytic dimerization of *p*-tolylacetylene by $(C_5H_5)_2ZrMe^+$ to yield 2,4-di-*p*-tolyl-3-buten-1-yne by a simple insertion/protonolysis cycle (Scheme 10)[103b]. It is possible that an equivalent cycle is operative for **37** (Scheme 11) given that insertion of olefin units are very common for group 4 metals (eg, Ziegler-Natta polymerization)[51,52]. Since insertion leading to the 1,4-substituted enyne causes more steric congestion at the metal centre, the 2,4 substitution should be expected for a more congested metal centre. However based on a comparison of M-C(benzyl) distances from X-ray analysis, the substituted $Zr(Me_3SiC_5H_4)_2(CH_2Ph)_2$ [104] (average M-C, 2.307 Å)) is less sterically crowded than *cis*-$Zr(DAC)(CH_2Ph)_2$ **32** (average M-C, 2.403(7) Å). Thus it follows that the less substituted cyclopentadienyl cation $(C_5H_5)_2ZrMe^+$ investigated by Horton is considerably less crowded than $Zr(DAC)(CH_2Ph)^+$ **37**. Given this result, the production of 1,4 substituted enyne by the DAC system is very surprising, but it is possible that the DAC backbone is flexible enough to allow electronic factors to dictate the head-to-head regiochemistry. Perhaps the formation of either isomer is promoted by a favourable π-interaction between the alkynyl group and the metal (Horton's system)[103b] or, through an ortho-aryl C-H agostic interaction (DAC system).

Scheme 10 Horton's proposed catalytic cycle for the dimerization of *p*-tolylacetylene

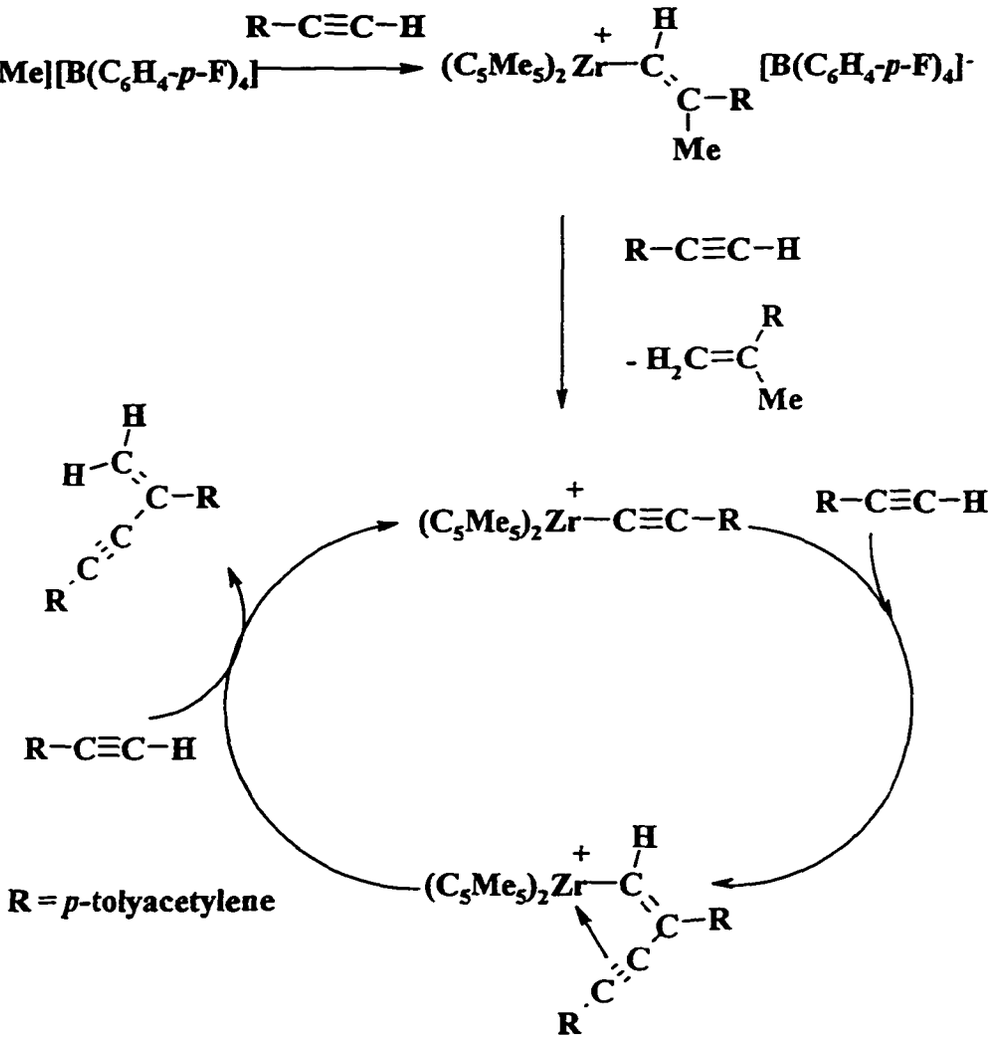

Scheme 11 Proposed catalytic[a] cycle for the dimerization of *p*-tolylacetylene by $[Zr(DAC)(CH_2Ph)]^+[B(CH_2Ph)(C_6F_5)_3]^-$ 37

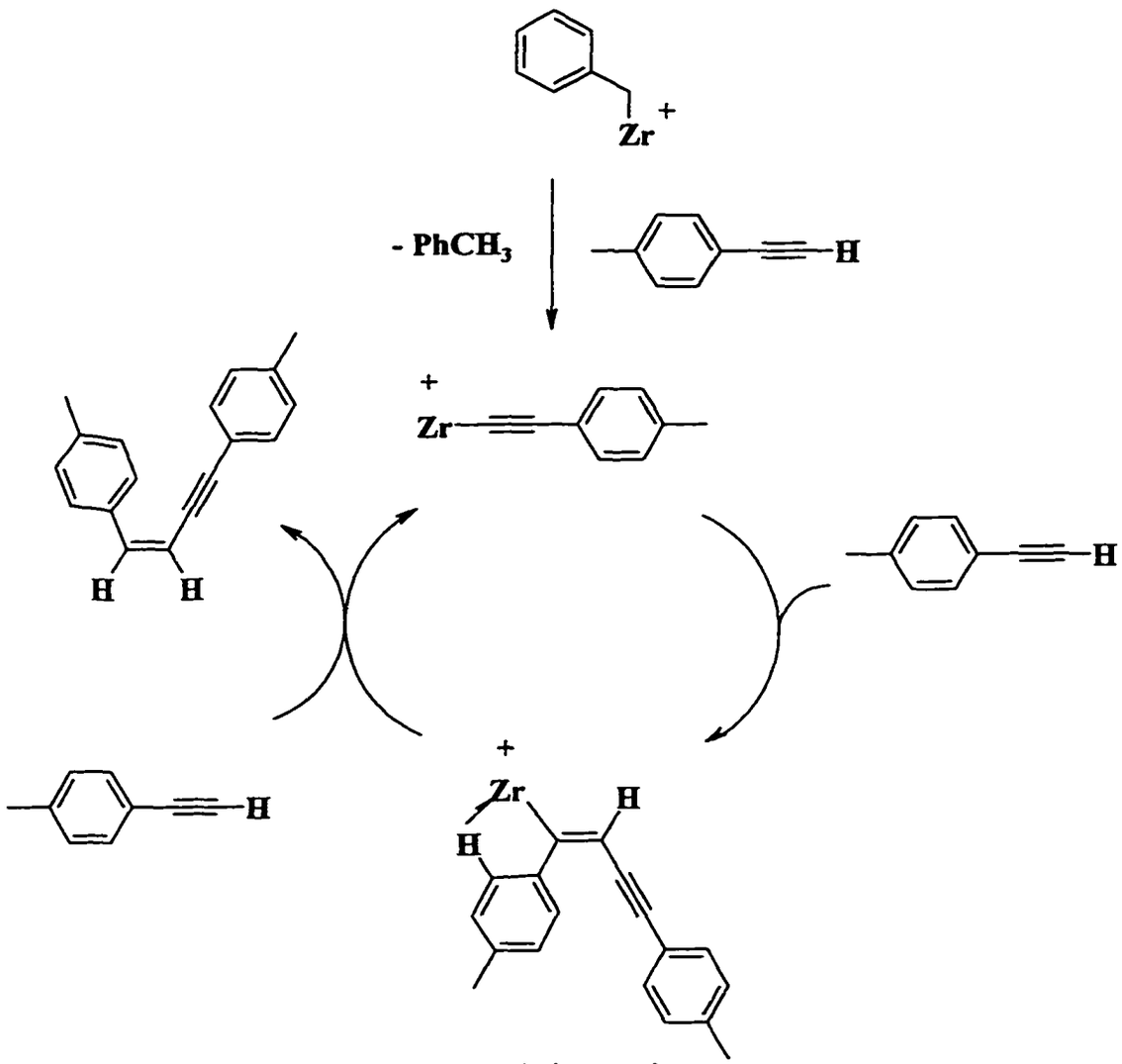

agostic interaction
favours 1,4-diphenyl-3-buten-1-yne

[a]DAC is omitted for clarity.

An alternative mechanism is also possible in the DAC system. The regioselective and stereoselective production of 1,4-di-*p*-tolyl-3-buten-1-yne (Z:E ratio = 85:15) is very similar to that found previously for the dimerization of phenylacetylene by Y(DAC)(CH_2SiMe_3) **14**. Since the cationic zirconium complex **37** is isoelectronic with the neutral yttrium complex **14**, these results suggest that the dimerization of *p*-tolylacetylene by Zr(DAC)(CH_2Ph)$^+$ **37** could occur through a coupling/protonolysis pathway (see Section 3.3.3). No attempt has been directed towards isolating the butratrienediyl of the zirconium species because our interest was focused on determining the catalytic reactivity at the time.

4.3.4 Stoichiometric reactivity of [Zr(DAC)(CH_2Ph)]$^+$[B(CH_2Ph)(C_6F_5)$_3$]$^-$ **37**.

Cation **37** reacts with one equivalent of *t*-butyl-isonitrile (*t*-BuNC) in methylene chloride to produce [Zr(DAC)(N(t-Bu)CH=CHPh)]$^+$[B(CH_2Ph)(C_6F_5)$_3$]$^-$ **38** (eq 31).

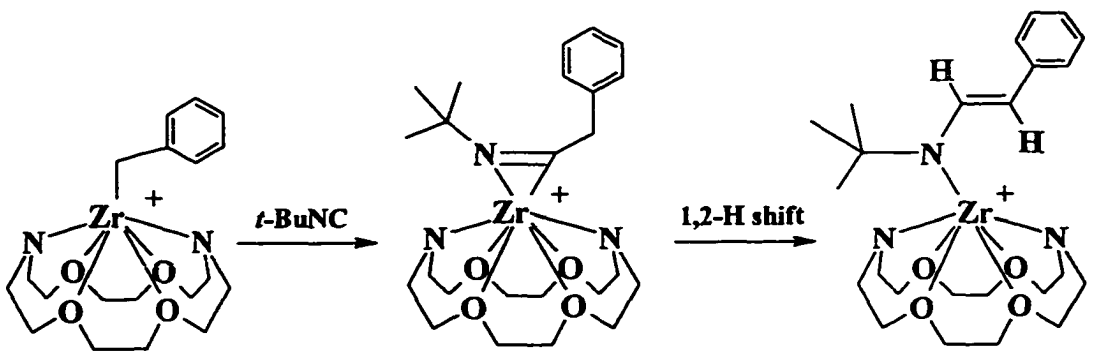

37 **39** **38** (31)

The ^{1}H NMR spectrum of **38** (CD_2Cl_2) clearly shows one alkenyl resonances at 6.42 ($^3J_{HH}$ = 14 Hz) ppm while the corresponding resonance at 7.14 ppm, buried by the aromatic peaks, is observable in the ^{1}H-^{1}H COSY spectrum (Figure 28). The corresponding ^{13}C resonances obtained from ^{1}H-^{13}C COSY at 111.2 and 135.0 ppm, respectively are present in the typical region for alkenes (Figure 29). The large $^3J_{HH}$ coupling constant ($^3J_{HH}$ = 14 Hz) suggests a *trans* sterochemistry around the double bond. ^{19}F NMR data ($\Delta\delta_{mp}$ = 3.0 ppm) indicate that the anion is not coordinated to the cation in CD_2Cl_2.

Formation of vinylamide complex **38** is likely to arise from a rapid 1,2-proton rearrangement of the η^2-iminoacyl group, $[Zr(DAC)(N(t\text{-}Bu)=CCH_2Ph)]^+[B(CH_2Ph)(C_6F_5)_3]^-$ **39** formed by initial insertion of the isonitrile into the zirconium-carbon bond (eq 31). Unfortunately only the presence of vinlyamide **38** was detectable by NMR by spectroscopy. Complex **38** is marginally soluble in benzene and very soluble in THF and CH_2Cl_2.

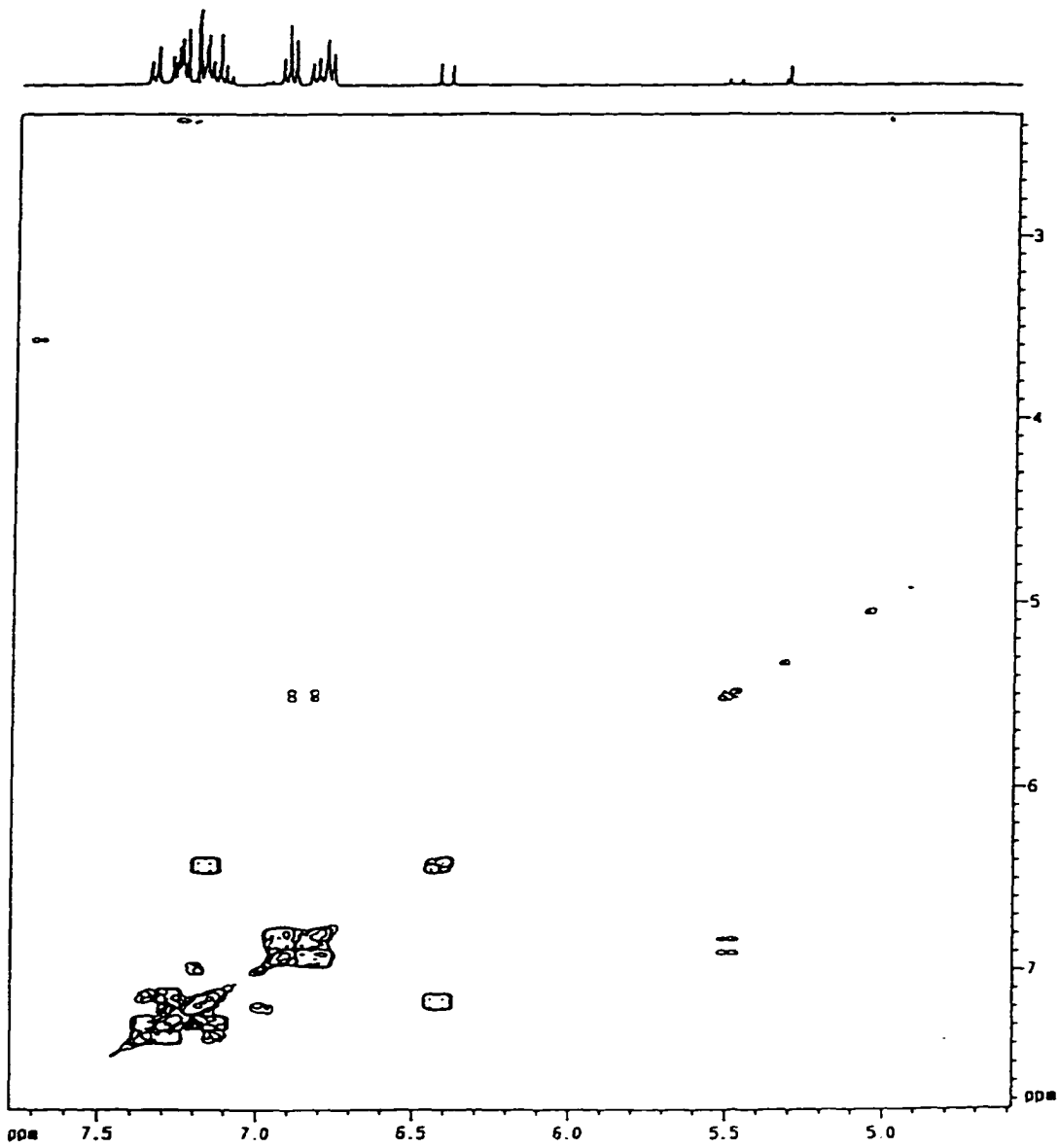

Figure 28 ^{1}H-^{1}H COSY of $[Zr(DAC)(N(t\text{-}Bu)CH{=}CHPh)]^{+}[B(CH_2Ph)(C_6F_5)_3]^{-}$ 38

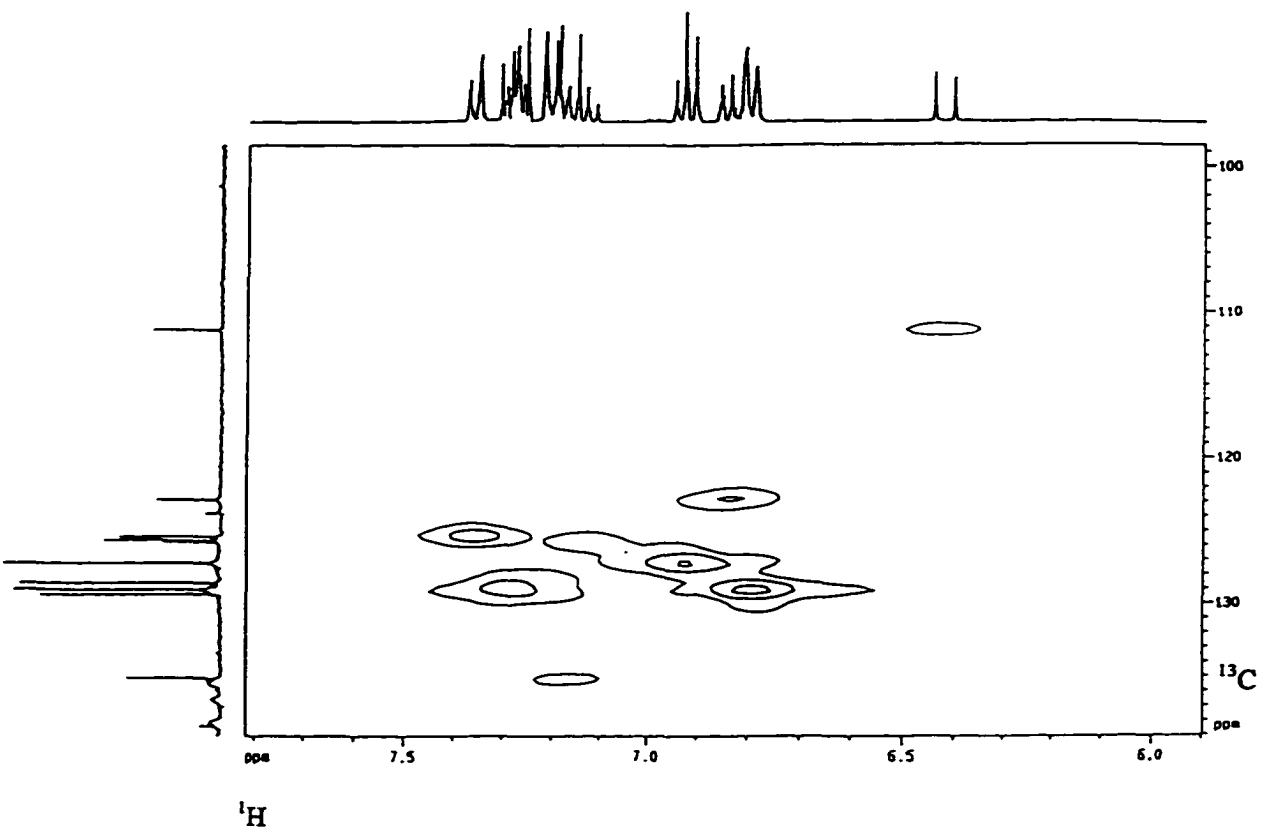

Figure 29 ^{1}H-^{13}C COSY of [Zr(DAC)(N(t-Bu)CH=CHPh)]$^{+}$[B(CH$_2$Ph)(C$_6$F$_5$)$_3$]$^{-}$ 38

Table 26 NMR data[a] for $[Zr(DAC)(N(t\text{-}Bu)CH{=}CHPh)]^+[B(CH_2Ph)(C_6F_5)_3]^-$ 38

		δ[b]	mult	Int.	coupling[c]	Assign.
^1H	Aryl[d]	7.37 – 7.25	m	5H		*aryl*-B
		6.79 – 6.95	m	5H		*aryl*-benzyl
	Alkenyl	7.14	d	1H	$^3J_{HH}$ =14	NC*H*=CH
		6.42	d	1H	$^3J_{HH}$ =14	NCH=C*H*
	CH_2Ph	2.86	br s	2H		B$C\!H_2$Ph
	t-Butyl	1.29	s	9H		C*Me*$_3$
^{13}C			δ[b]			
	$(C_6F_5)_3$	148.6 (*o*-aryl *C*F) $^1J_{CF}$ = 241.1		137.9 (*p*-aryl *C*F) $^1J_{CF}$ = 244.1		136.8 (*m*-aryl *C*F) $^1J_{CF}$ = 245.5
	$NC_xH{=}C_yH$	135.04 C_x		111.16 C_y		
	$N(CMe_3)$	58.46 *C*Me$_3$		30.15 C*Me*$_3$		
	BCH_2Ph	32.28		32.40 B$C\!H_2$		

[a]Spectrum recorded at 360 MHz (^1H) or 90.55 MHz (^{13}C) in CD_2Cl_2 296 K. [b]δ expressed in ppm. [c]Coupling measured in Hz. [d]Aryl reasonances not assigned. Aryl carbon resonances and DAC resonances not shown.

CHAPTER 5

YTTRIUM DIALKYL COMPLEXES

SUPPORTED BY AZA-CROWN MACROCYCLES

5.1 Introduction

Over the last two decades, the organometallic chemistry of the lanthanides and yttrium has become an area of intense research, dominated primarily by pentamethyl cyclopentadienyl C_5Me_5 ancillary ligation[18-27]. Recent introduction of other ligand systems such as porphyrins[44], tris(pyrazolylborates)[48], and benzamidinates[49] has also resulted in a wealth of interesting chemistry, however, very few dialkyl complexes have been reported. For the C_5Me_5 system, major obstacles to preparing the elusive $(C_5Me_5)LnR_2$ (R = alkyl or aryl) complexes are facile ligand redistribution to $(C_5Me_5)_2LnR$, formation of intermolecularly bridged oligomeric products, and salt complexation[105]. While the first two problems can be minimized by employing sterically bulky monoanionic ligands with multidentate coordination, the last problem can be eliminated by avoiding metathetical routes. Protonolysis of $Y(CH_2SiMe_3)_3 \bullet 2THF$[34] by H_2DAC[60,61] to prepare stable yttrium alkyl complex was demostrated in Chapter 3. Thus it seems possible that a similar route using the aza-crown ethers, aza-18-crown-6 (HMAC) and aza-15-crown-5 (H-15-AC-5)[106] could by used to isolate stable dialkyl complexes of yttrium.

Aza-18-crown-6 (HMAC) and aza-15-crown-5 (H-15-AC-5) can be purchased for $125 and $103 (Can.) per gram, respectively, from Aldrich. However, the ligands are easily synthesized from inexpensive starting materials in over 70% overall yields by template synthesis[106].

5.2 Organoyttrium dialkyl complexes stabilized by deprotonated aza-crown ligation

5.2.1 Synthesis and NMR characterization of *trans*-Y(MAC)(CH_2SiMe_3)$_2$ 40

Protonolysis of Y(CH_2SiMe_3)$_3$•2THF[34] with HMAC in toluene results in colourless crystal of *trans*-Y(MAC)(CH_2SiMe_3)$_2$ **40** in high yield (eqn 31).

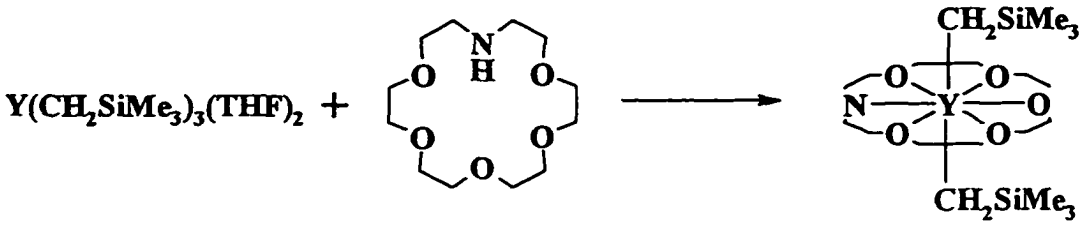

40 (31)

In d_8-THF, the ^{1}H NMR MAC region (3.0 – 4.1 ppm) shows only six proton multiplets (Table 27), clearly indicating a *trans*-dialkyl geometry of C_{2v} symmetry. The *cis*-isomer would possess C_s symmetry and must therefore display 12 proton resonances due to inequivalent exo and endo protons on the six unique carbons. The presence of two equivalent dialkyls is confirmed by the observation of only one set of CH_2 and $SiMe_3$ resonances of the appropriate intensity. In the ^{13}C NMR spectrum, the coupling constants associated with CH_2 group directly bonded to yttrium are observed ($^1J_{YC}$ = 32.4 Hz and $^1J_{CH}$ 102.7 Hz), while two-bond Y-H coupling ($^2J_{YH}$) is not evident in the ^{1}H NMR. However, a well-resolved ^{1}H NMR spectrum obtained in d_6-benzene (Table 27) clearly shows

this coupling ($^2J_{YH}$ = 2.5 Hz). These values are very similar to the coupling parameters found for the same alkyl group in Y(DAC)(CH_2SiMe_3) **14** ($^1J_{YC}$ = 39 Hz, $^1J_{CH}$ = 102 Hz, $^2J_{YH}$ = 2.8 Hz). Interestingly in d_6-benzene the MAC region does not show a simple pattern of six proton multiplets. Instead, two well-resolved triplets, a multiplet, and a singlet with an overlapping multiplet are observed with a ratio of 4:4:4:12, respectively (Figure 30). The solvent-dependent change in solution structure suggested by NMR prompted us to investigate the solid-state structure of this complex by X-ray crystallography.

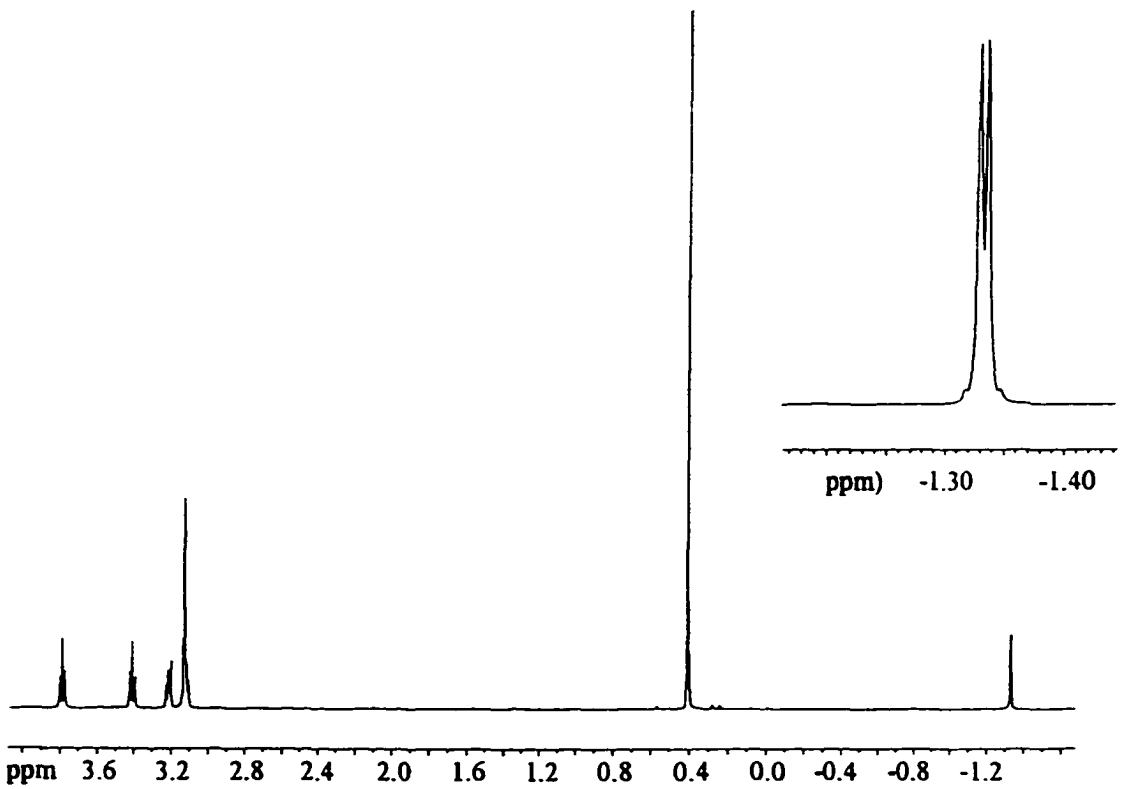

Figure 30 ^{1}**H NMR spectrum of *trans*-Y(MAC)(CH_2SiMe_3)$_2$ 40**

Table 27 NMR data[a] for *trans*-Y(MAC)(CH_2SiMe_3)$_2$ 40

	40 (d_8-THF)				40 (d_6-benzene)			
^{1}H	δ[b]	mult	Int.	Assign	δ[b]	mult	Int.	Assign
MAC[c]	4.02	m	4H	C*H*$_2$	3.79 $^3J_{HH}$ = 5.5	t	4H	C*H*$_2$
	3.88	m	4H	C*H*$_2$				
	3.86	m	4H	C*H*$_2$	3.44 $^3J_{HH}$ = 5.5	t	4H	C*H*$_2$
	3.79	m	4H	C*H*$_2$	3.22	m	4H	C*H*$_2$
	3.70	m	4H	C*H*$_2$	3.13[d]	s	12H	C*H*$_2$
	3.19	m	4H	C*H*$_2$				
$CH_2(SiMe_3)$	-0.16	s	18H	Si*Me*$_3$	0.41	s	18H	Si*Me*$_3$
	-1.59	s	4H	C*H*$_2$	-1.33 $^2J_{YH}$ = 2.5	d	4H	C*H*$_2$
^{13}C	δ[b]				δ[b]			
MAC[c]	76.99	72.01	71.59		76.71	70.95	70.44	
	70.44	69.36	56.76		69.42	68.38	56.08	
$CH_2(SiMe_3)_2$	5.13				5.44			
*C*H$_2$SiMe3	19.84 dt *C*H$_2$[e]	$^1J_{YC}$ = 32.4 $^1J_{CH}$ = 103			20.24 d *C*H$_2$	$^1J_{YC}$ = 34.2 $^1J_{CH}$ = 101		

[a]Spectrum recorded at 360 MHz (^{1}H) or 90.55 MHz (^{13}C) in C_4D_8O or C_6D_6 296 K. [b]δ expressed in ppm. [c]MAC resonances not assigned. [d]Partially overlapping resonances. [e]Gated carbon-proton coupling.

5.2.2 X-ray structural analysis of *trans*-Y(MAC)(CH_2SiMe_3)$_2$ **40**

The ORTEP drawing of *trans*-**40** is shown in Figure 31. All crystallographic details are summarized in Appendix Tables XX- XXII and selected bond distances and angles are collected in Table 28.

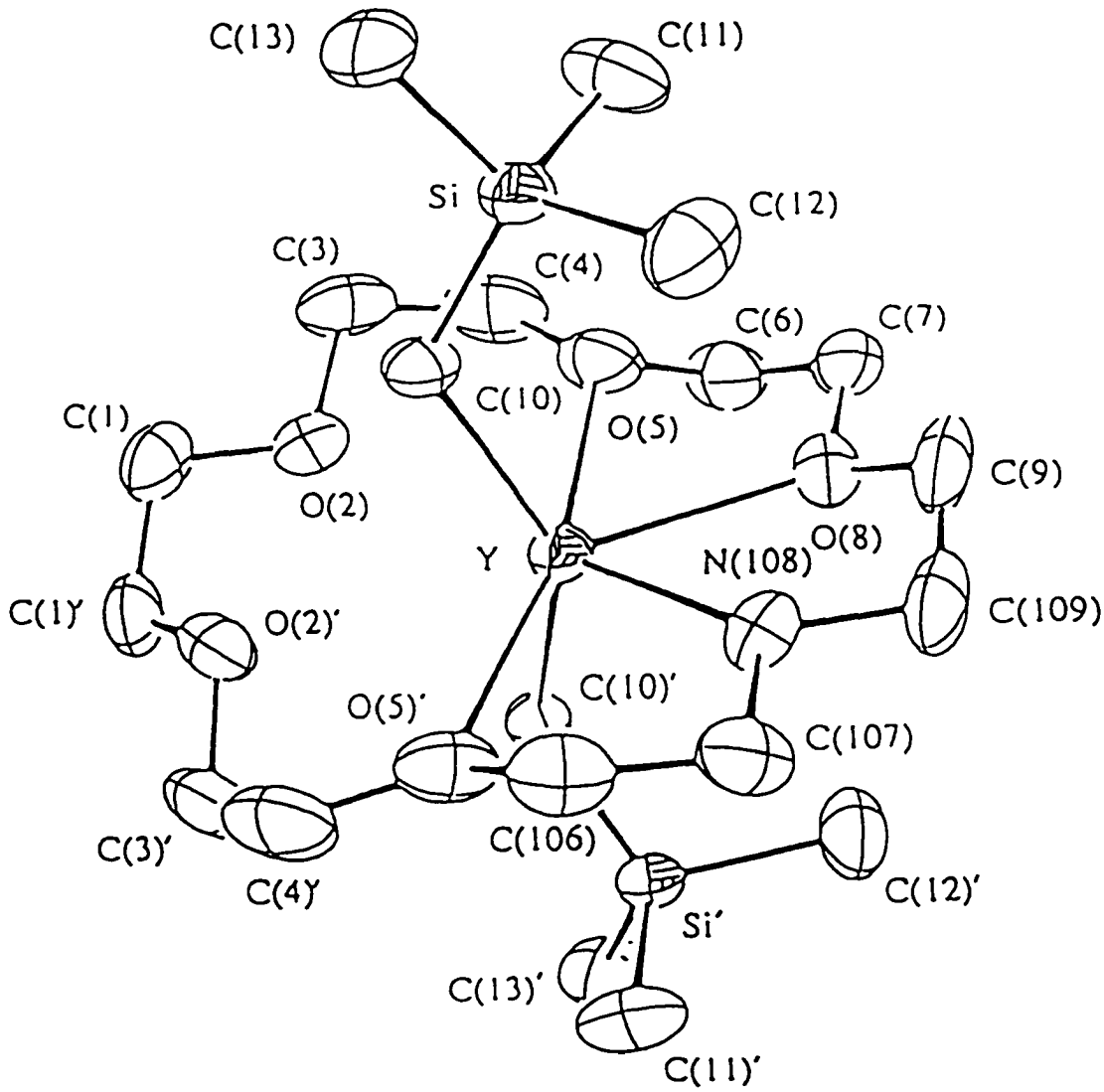

Figure 31 ORTEP drawing of *trans*-Y(MAC)(CH_2SiMe_3)$_2$ 40 at 213K

Table 28 Selected bond distances (Å) and angles (deg)[a] for *trans*-Y(MAC)(CH_2SiMe_3)$_2$ 40

		Distances	
Y-N(108)	2.253(10)	Y-O(8)	2.482(8)
Y-O(2)	3.033(3)	Y-C(10)	2.461(4)
Y-O(5)	2.605(3)		
		Angles	
N(108)-Y-C(10)	109.8(5)	C(10)-Y-C(10)'	144.55(13)
N(108)-Y-C(10)'	100.0(5)	Y-C(10)-Si	125.25(20)

[a] Estimated standard deviation in parentheses.

The structure of *trans*-**40** consists of *trans* alkyl groups as suggested by NMR spectroscopy. The yttrium centre lies on a crystallographic 2-fold axis which passes through the midpoint of the C(1)-C(1)' and C(9)-C(109) bonds. The resulting disorder between N(108) and O(8) was successfully modeled but the yttrium-donor distances associated with these atoms are necessarily unreliable. The nearest intermolecular contacts are >3.5 Å. The Y--O(2) and Y--O(2)' distances (not depicted as a bond in Figure 31) must represent relatively weak interactions as they ~0.5 Å longer than the other Y-O bonds. Thus the coordination number of Y might be described as either 6 or 8 depending upon whether these weak interactions are counted. It is easy to envision that these weak donors might be displaced by competitive donors perhaps explaining the structural changes detected by NMR spectroscopy in d_8-THF versus d_6-benzene solution.

The arrangement about Y may be described as distorted from hexagonal bipyramidal, by the displacement of O(2) and O(2)' away from Y in the equatorial plane, accompanied by a complimentary tilting of the other vertices, especially the apical carbon atoms C(10) and C(10)'. Apart from the long Y-O(2) distances, the other bond distances to Y fall in the expected ranges (compared to those found for Y(DAC)[$N(SiMe_3)_2$] **8** and Y(DAC)(CH_2SiMe_3) **14**). The shortest bonds to Y, Y-N (108) and Y-O(8) are anti with respect to the long Y-O(2) and Y-O(2)' vectors. The Y-C distance (2.461(4) Å) and Y-C-Si angle (125.25(20)°) are very similar to those found in Y(DAC)(CH_2SiMe_3) (2.45(2) Å and 126.4(8)°). There is no evidence for agostic interactions between the alkyl α-CH_2 or $SiMe_3$ groups and the metal centre.

5.2.3 Thermal stability of *trans*-Y(MAC)($CH_2SiMe_3)_2$ **40**.

In contrast to Y(DAC)($CH_2SiMe_3)_2$ **14**, *trans*-Y(MAC)($CH_2SiMe_3)_2$ **40** is thermally stable for more than one week in d_6-benzene solution at room temperature. The major decomposition pathway for **14** was previously shown to involve metallation of the DAC backbone (Chapter 3). Since, the MAC ligand should be susceptible to a similar attack, the much slower rate of decomposition may be attributable to the greater ring strain in **40** than in the more flexible DAC complex. The notable distortion toward a six-coordinate geometry, observed in the solid state, illustrates that the macrocycle in **40** is unable to achieve a geometry which allows all five oxygens to coordinate. It therefore seems reasonable to assume that approach of the carbanionic α-carbon of the alkyl to a suitable CH_2 group of the MAC ligand will be difficult in this coordination geometry.

5.2.4 Reactivity of *trans*-Y(MAC)(CH_2SiMe_3)$_2$ **40**

The reaction of a toluene solution of **40** with CO proceeds smoothly to yield *trans*-Y(MAC)(OC($SiMe_3$)=CH_2)$_2$ **41** (eq 32).

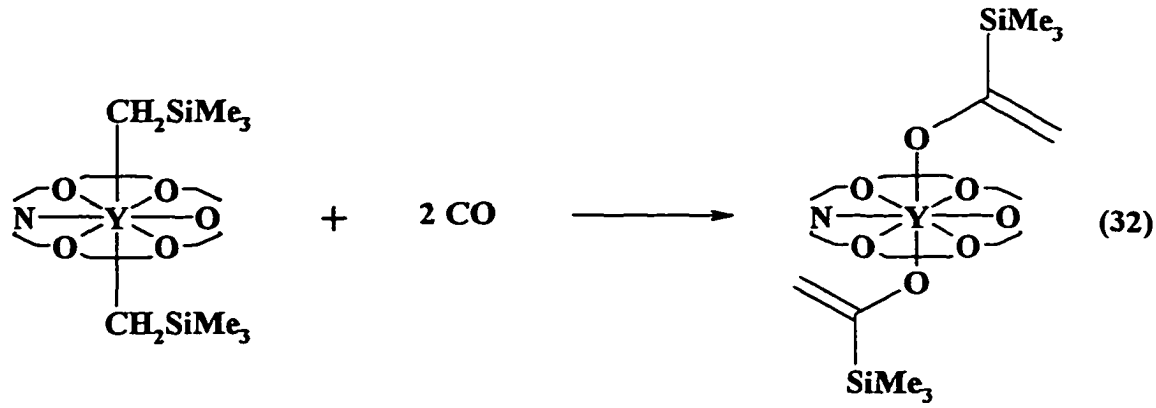

(32)

40 **41**

The ^{1}H NMR spectrum of **41** in d_6-benzene shows two alkenyl coupled doublets at δ 4.70 and δ 4.44 ppm ($^2J_{HH}$ = 2.2 Hz) which belong to the ^{13}C resonance at δ 93.86 ppm as observed by ^{1}H-^{13}C COSY (Figure 32). These features are consistent with a terminal =CH_2 group formed by $SiMe_3$ migration of the initial acyl insertion product (Scheme 12). This is not the first case of $SiMe_3$ migration; similar acyl to enolate rearrangements have been observed following CO insertion into the thorium alkyl bonds of Th(C_5Me_5)$_2$Cl(CH_2SiMe_3)[107] and Th(C_5H_5)$_3$(CH_2SiMe_3)[108]. A summary of the NMR spectral data for **41** is provided in Table 29.

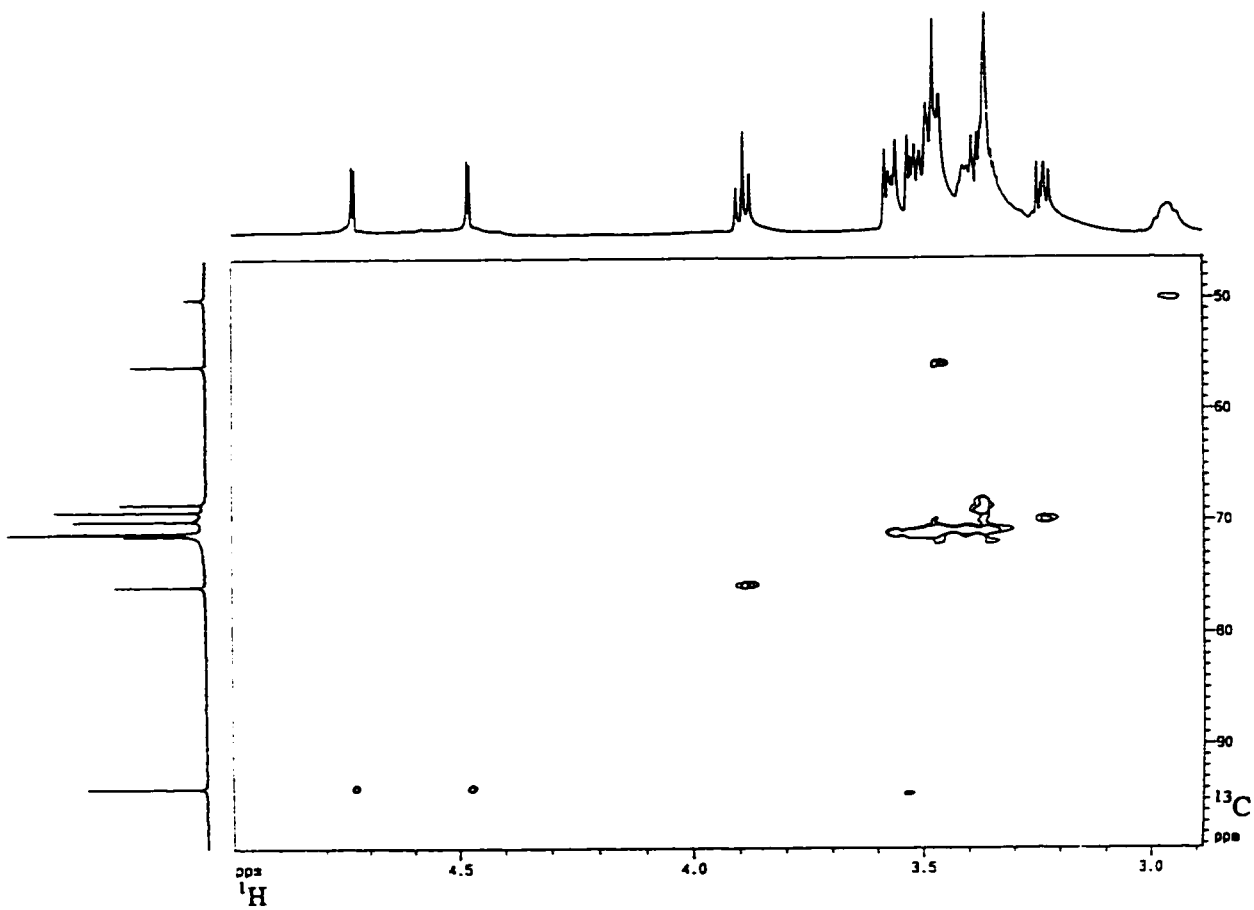

Figure 32 ^{1}H-^{13}C COSY Y(MAC)(OC(SiMe$_3$)=CH$_2$)$_2$ 41

Scheme 12 Mechanism for the formation of Y(MAC)(OC(SiMe$_3$)=CH$_2$)$_2$ 41

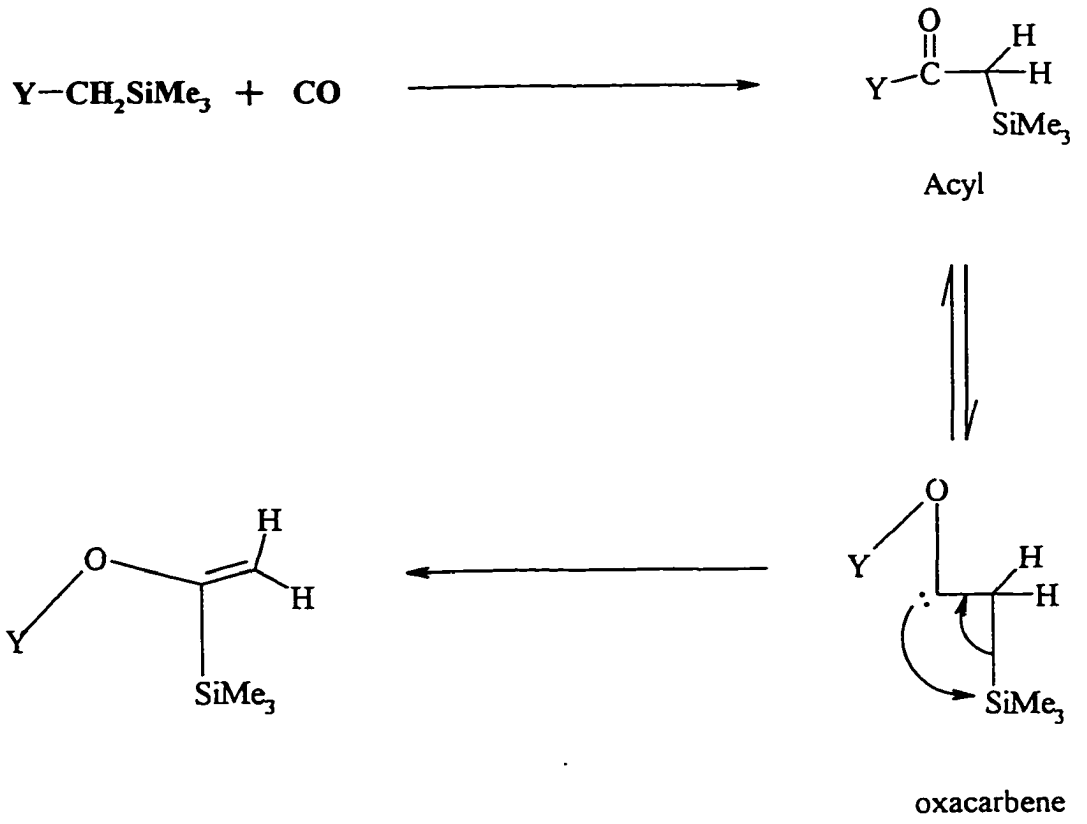

Table 29 NMR data[a] for Y(MAC)(OC(SiMe$_3$)=CH$_2$)$_2$ 41

^{1}H		δ[b]	mult	Int.	coupling[c]	Assign.
	Alkenyl	4.70	d	2H	$^2J_{HH}$ = 2.2	=C*H*$_a$H$_b$[d]
		4.44	d	2H	$^3J_{HH}$ = 2.2	=CH$_a$*H*$_b$[d]
	MAC[e]	3.85	m	4H		C*H*$_2$
		3.55 - 3.32	m	16H		C*H*$_2$
		3.19	m	4H		C*H*$_2$
	SiMe$_3$	0.38	s	18H		Si*Me*$_3$

^{13}C		δ[b]					
	OC(SiMe$_3$)=	176.33 d (O*C*) $^2J_{YC}$ = 4.5		93.86 (C=*C*H$_2$)		-1.38 (Si*Me*$_3$)	
	MAC[e]	75.71	71.01	69.85	69.00	68.33	55.98

[a]Spectrum recorded at 360 MHz (^{1}H) or 90.55 MHz (^{13}C) in C$_6$D$_6$ 296 K. [b]δ expressed in ppm. [c]Coupling measured in Hz. [d]Stereochemistry relative to the SiMe$_3$ group has not been assigned for H$_a$ and H$_b$. [e]MAC resonances have not been assigned.

While Y(DAC)(CH_2SiMe_3) **14** has been previously shown to be inert towards CO, the reactivity of *trans*-Y(MAC)(CH_2SiMe_3)$_2$ **40** can be explained by electronic changes resulting from the replacement of a negative amido group in DAC with an oxygen donor in MAC. In fact, the solid state structure of **14** (*vide supra*) have shown that two amido and four oxygen donors are coordinated. In contrast, only one amido and three oxygen donors that are strongly bonded to yttrium in **40**. It is possible therefore that **40** is more reactive because the yttrium centre is less electron rich. This electronic difference is more significant than steric effects because both Y(DAC)(CH_2SiMe_3) **14** and *trans*-Y(MAC)(CH_2SiMe_3)$_2$ **40** are sterically equivalent. The Y-C bond lengths (**14**: 2.45(2) Å cf. ***trans*-40**: 2.461(4) Å) are similar within experimental error. However, it is surprising in view of the ease of CO insertion that a toluene solution of *trans*-Y(MAC)(CH_2SiMe_3)$_2$ **40** does not react with H_2 or ethylene (2 atm, 1 week at room temperature). This striking difference would also appear to be electronic in origin since all these substrates present similar steric demands.

5.2.5 Synthesis and NMR characterization of *cis*-Y(15-AC-5)(CH_2SiMe_3)$_2$ **42**

Direct protonation of Y(CH_2SiMe_3)$_3$•2THF [34] with H-15-AC-5[106] in toluene results in a viscous oily residue after removal of the solvent. Recrystallization of the residue in a mixture of toluene and hexane affords colourless crystals of *cis*-Y(15-AC-5)(CH_2SiMe_3)$_2$ **42** in 12.4 % yield (eq 33).

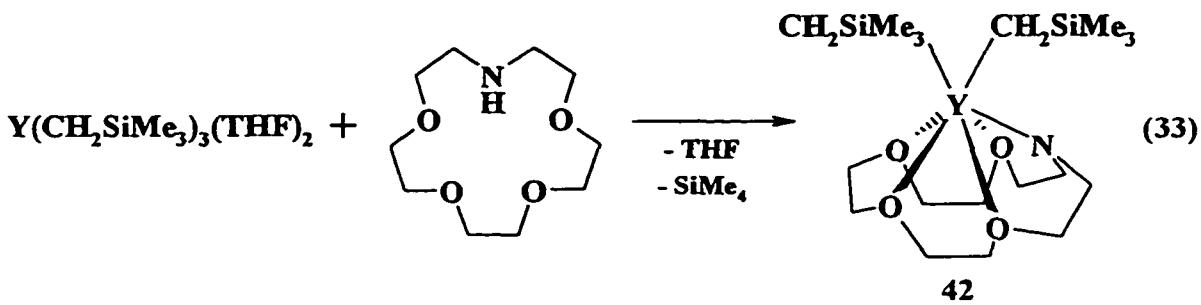

(33)

The ^{1}H NMR spectrum showed 10 proton mulitplets due to the presence of inequivalent exo and endo protons on the five unique carbon atoms, which is consistent with a C_s geometry. The observation of one set of CH_2 and $SiMe_3$ resonances with the appropriate intensity is consistent with the presence of two equivalent dialkyls. The upfield ^{1}H NMR chemical shift for the CH_2 (δ -0.73 ppm) group directly bonded to yttrium in **42** is consistent with the carbanionic character of the CH_2SiMe_3 ligand as found for Y(DAC)(CH_2SiMe_3) **14** (δ -0.84 ppm) and *trans*-Y(MAC)(CH_2SiMe_3)$_2$ **40** (δ -1.33 ppm in d_6-benzene). Additionally, the coupling constants associated with the CH_2 group ($^2J_{YH}$ = 2.8 Hz and J_{YC} = 35.4 Hz) (Table 30) are comparable to those found for **14** and **40**.

By decreasing the macrocyclic ring cavity by ~0.5 Å[55a], the geometry of the dialkyls is forced into a *cis*-orientation. It appears from the ^{1}H NMR data that all four oxygen donors of the macrocycle coordinate to yttrium. Unfortunately, an attempt to carry out a X-ray crystallographic analysis of **42** was not successful because the complex decomposed rapidly in the X-ray beam. The reactivity and structural assessments of *cis*-Y(15-AC-5)(CH_2SiMe_3)$_2$ **42** are currently continuing.

Table 30 NMR data[a] for *cis*-Y(15-AC-5)(CH_2SiMe_3)$_2$ 42

		δ[b]	mult	Int.	coupling[c]	Assign.
^{1}H	MAC[d]	4.24	m	2H		CH_2
		3.53	m	2H		CH_2
		3.83	m	2H		CH_2
		3.30	m	2H		CH_2
		3.22	m	2H		CH_2
		3.10	m	2H		CH_2
		3.02	m	4H		CH_2
		2.67	m	4H		CH_2
	CH_2SiMe_3	0.52	s	18H		SiMe_3
		-0.73	s	4H	$^1J_{YH}$=2.8	CH_2

^{13}C	δ[b]				
[d]MAC	72.82	69.26	66.98	65.22	54.45
CH_2SiMe_3	24.08 (CH_2) ; $^1J_{YC}$ = 35.4		5.39 (SiMe_3)		

[a]Spectrum recorded at 360 MHz (^{1}H) or 90.55 MHz (^{13}C) in C_6D_6 296 K. [b]δ expressed in ppm. [c]Coupling measured in Hz. [d]MAC resonances have not been assigned.

5.3 Cationic organoyttrium complexes of deprotonated aza-18-crown-6 (MAC)

While cationic group 4 (titanium and zirconium) metal complexes have been extensively studied due to their role in olefin polymerization, cationic group 3 and lanthanide alkyls have not been explored in detail[51,52]. The difficulty involved in preparing the parent dialkyl complexes is one large reason for this lack of study. The first and only lanthanide alkyl cation known, $[La(C_5Me_5)\{CH(SiMe_3)_2\}]^+[BPh_4]^-$ was reported by Schavarien[109]. The ease of access to *trans*-$Y(MAC)(CH_2SiMe_3)_2$ **40** and the success of preparing $[Zr(DAC)(CH_2Ph)]^+[BR_4]^-$ **(36 and 37)** suggested that an alkyl cation stabilized by aza-crown macrocycles could be synthesized.

5.3.1 Synthesis and characterization of $[Y(MAC)(CH_2SiMe_3)]^+$ $[B(CH_2SiMe_3)(C_6F_5)_3]^-$ **43**

The attempted protonolysis of *trans*-$Y(MAC)(CH_2SiMe_3)_2$ **40** with $[n\text{-}Bu_3NH]^+[BPh_4]^-$ in either THF or toluene resulted in the precipitation of a white insoluble material. The toluene soluble residue was found to contain primarily HMAC by ^1H NMR. The product may be thermally sensitive and further attempts will be required to better handle the product. However, *trans*-$Y(MAC)(CH_2SiMe_3)_2$ **40** appears to undergo alkyl abstraction with $B(C_6F_5)_3$ in d_8-THF to produce a colourless solution of the cationic species $[Y(MAC)(CH_2SiMe_3)]^+[B(CH_2SiMe_3)(C_6F_5)_3]^-$ **43** (eq 34). The cationic species can be directly generated in d_8-THF which is surprising since the boron Lewis acid should form a strong complex with d_8-THF.

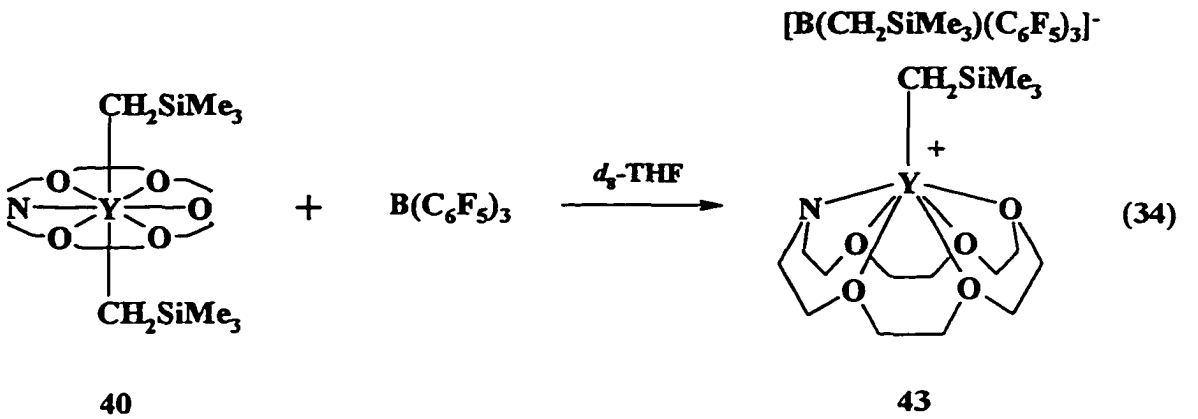

40 43 (34)

Nevertheless, the ^{1}H NMR spectrum of the cation **43**, generated *in situ*, indicates that alkyl transfer has occurred. Two signals due to the methylene group of the CH_2SiMe_3 ligand are distinguishable: one is well resolved showing coupling to ^{89}Y and downfield from the parent dialkyl complex (**43**: δ -1.16, $^{2}J_{YH}$ = 3.2 Hz cf. **40**: δ -1.59, $^{2}J_{YH}$ = 2.5 Hz), while the other signal at δ 0.12 ppm shows broadening due to ^{11}B coupling consistent with the anion $[(CH_2SiMe_3)B(C_6F_5)_3]^-$. The ^{19}F NMR spectrum of **43** shows that the anion is noncoordinating since the difference in ppm between the resonances due to fluorine in the *meta* and *para* positions ($\Delta\delta_{m,p} = \delta_mF - \delta_pF$)[103] is found to be 2.5 ppm. Table 31 summarizes the NMR data collected for **43**. Attempts to isolate pure **43** were unsuccessful even in the presence of a Lewis base such as THF and PMe_3. Decomposition appears to occur over a period of a few minutes at room temperature in d_8-THF, as shown by the growth of resonances due to $SiMe_4$. The high stability of $[La(C_5Me_5)\{CH(SiMe_3)_2\}]^+[BPh_4]^-$ [109] may be due to the strong coordination of the anion; however, displacement of $[BPh_4]^-$ by THF produces a stable complex, $[La(C_5Me_5)\{CH(SiMe_3)_2\}(THF)_3]^+[BPh_4]^-$ [109]. While it has previously been shown

that fluorine substitution of phenyl groups in the tetraphenylborate anion destabilizes the cationic alkyl complexes by decreasing the coordinating ability of the anion [109], it is not clear why a cation such as **43** should be so unstable in the presence of a good donor such as THF. Perhaps, decomposition involves metallation of the MAC ring or attack on THF, but attempts to confirm the decomposition product were hampered by the complexity of the product mixture. Preparation of **43** in different NMR solvents was also attempted. In CD_2Cl_2 and BrC_6D_5, the decomposition of **43** is fast resulting in the formation of an insoluble precipitate, presumably due to halide abstraction from the solvent. However, in d_5-pyridine the cation appears to be more stable, surviving for days. The initial ^1H and ^{13}C NMR spectra (moments after mixing in d_5-pyridine) clearly show two different complexes. One product is the starting material (**40**: for α-CH_2 group: ^1H, δ -1.25 ppm, $^2J_{YH}$ = 2.2 Hz; ^{13}C δ 19.70 ppm, $^1J_{YC}$ = 33.2 Hz) and the other is presumably the cation (**43**: for α-CH_2 group: ^1H, δ 0.87 ppm, $^2J_{YH}$ = 2.9 Hz; ^{13}C δ 24.25 ppm, $^1J_{YC}$ = 41.4 Hz). Resonances due to the starting material disappear as time progresses. On further standing at room temperature, the observation of $SiMe_4$ is evident. ^{19}F NMR suggests no cation-anion interaction from $\Delta\delta_{m,p}$ = 1.5 ppm. The increased stability of the cation in pyridine is not surprising since pyridine (33)* is a stronger donor than THF (20)*. Table 31 is a summary comparing the NMR resonance of the parent dialkyl complex and the cation in d_5-pyridine.

---

* Numbers in parentheses are Gutmann's donor numbers which measure the basicity or donor ability of a solvent. These are negative enthalpy (- ΔH) values obtained from the reaction of the donor solvent with $SbCl_5$ [110].

Table 31 Comparative NMR data[a] between dialkyl 40 and cation 43 in d_5-pyridine

	trans-Y(MAC)(CH_2SiMe_3)$_2$ **40**				*trans*-[Y(MAC)(CH_2SiMe_3)]$^+$ **43**			
^{1}H NMR	δ[b]	mult	Int	Coupling[c]	δ[b]	mult	Int.	Coupling[c]
MAC[d]	4.01	t	4H	$^3J_{HH}$ = 5.5	4.0 - 3.5	s	16 H	
	3.78	m	4H		3.24	m	4H	
	3.72	m	4H		3.12	m	4H	
	3.67	m	4H					
	3.56	m	4H					
	3.35	t	4H	$^3J_{HH}$ = 5.5				
$CH_2Si\mathit{Me}_3$	0.25	s	18H		0.21	s	9H	
$C\mathit{H}_2SiMe_3$	-1.25	d	4H	$^2J_{YH}$ = 2.2	0.87	d	2H	$^2J_{YH}$ = 2.8
$BCH_2Si\mathit{Me}_3$[e]	-	-	-	-	-0.22	s	9H	
^{13}C NMR	δ[b]				δ[b]			
MAC	76.41	71.30		70.87	75.40	70.65		70.13
	69.76	68.63		56.28	69.94	69.27		55.27
CH_2SiMe_3	19.70 ($\mathit{C}H_2$) $^1J_{YC}$ = 33.2			5.46 ($SiMe_3$)	24.95 ($\mathit{C}H_2$) $^1J_{YC}$ = 41.4			5.27 ($SiMe_3$)
BCH_2SiMe_3[e]					1.17 ($Si\mathit{Me}_3$)			$\mathit{C}H_2$?

[a]Spectra recorded at 360 MHz (^{1}H) or 90.55 MHz (^{13}C) in d_5-C_5D_5N 296 K. [b]δ expressed in ppm. [c]Coupling measured in Hz. [d]MAC ligand is not assigned. [e]Broad BCH_2 peak not observed and peak assignments are tentative.

Decomposition of the cation generated in d_5-pyridine results in the predominant formation of a highly symmetric structure in which the ^{1}H NMR spectrum consists of a singlet and two triplets for the protons of the six unique MAC carbons, along with resonances due to $SiMe_4$ and (CH_2SiMe_3). Thermolysis of **40** in d_5-pyridine gave a very similar set of NMR resonances to those observed during decomposition of the cation **43**. The decomposition may involve double *o*-metallation of two pyridine ligands to form **44** or from insertion of pyridine to afford **45**. It is possible that the pathway to these products involves a rapid alkyl exchange between $[BR(C_6F_5)_3]^-$ and the cation to regenerate **40** thus explaining the similarity of the decomposition products observed with **40** (Scheme 13). ^{1}H NMR spectrum does not clearly show evidence for DCH_2SiMe_3 byproduct and the presence of yttrium-carbon coupling is not observed in the ^{13}C NMR. These results along with the relative ratio of MAC and CH_2SiMe_3 protons in the ^{1}H NMR seem to suggest **45** as the most likely decomposition product. Although *o*-metallation of pyridine by other organolanthanide complexes has been observed[29], the insertion of pyridine into these complexes is without precedence. Thus neither of the two decomposition products can be ruled out without further analysis.

Scheme 13 Possible thermal decomposition product for $[Y(MAC)(CH_2SiMe_3)]^+$ $[B(CH_2SiMe_3)(C_6F_5)_3]^-$ 43 in d_5-pyridine

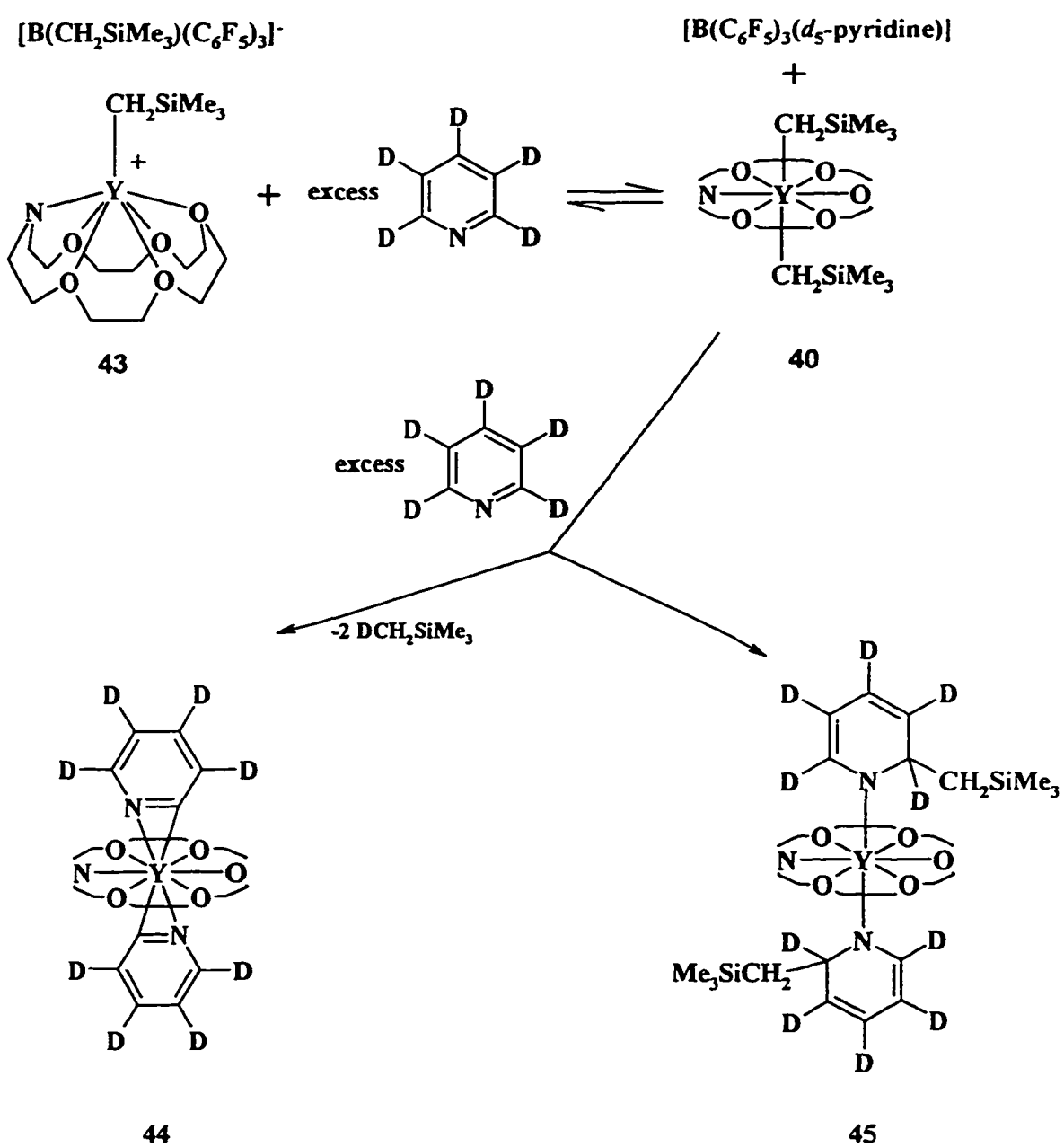

CHAPTER 6

CONCLUSIONS AND FUTURE DIRECTIONS

6.1 General routes to organometallic complexes containing aza-crown ligands

A convenient pathway into yttrium and zirconium complexes stabilized by aza-crown macrocycles was demonstrated by the protonolysis route. Given the monomeric structure of the organoyttrium and organozirconium complexes, deprotonated 4,13-diaza-18-crown-6 (DAC) **1**, aza-18-crown-6 (MAC) **2**, and aza-15-crown-5 (15-AC-5) **3** are capable of satisfying the steric requirements of the yttrium and zirconium (DAC) centres in a similar manner to that for C_5Me_5. The unique feature of the aza-crown macrocycle systems compared with C_5Me_5 is their flexible geometry and variable donor complement which led to *trans* geometries of the alkyls, such as in *trans*-Zr(DAC)$(CH_2Ph)_2$ **32** and *trans*-Y(MAC)$(CH_2SiMe_3)_2$ **40**, which are not possible for the cyclopentadienyl sytstems. The monoanionic macrocycle has shown the ability to stabilize organoyttrium dialkyls with respect to both metallation and ligand redistribution. Although, the protonolysis route has provided access into organoyttrium and orgaonozirconium complexes, the chemistry is limited. A general pathway to organometallic complexes of the lanthanide series, in particular the earlier metals, containing an unrestricted range of alkyls and aryls is desperately required to provide access to potentially more reactive complexes. The future goal is to explore possible pathways to gain entry to these complexes.

One possible general route to organoyttrium complexes containing DAC as an ancillary ligand is by use of $Y[N(SiMe_3)_2]_2Cl{\bullet}2THF$[111]. After initial protonolysis, $[Y(DAC)(Cl)]_x$ can be produced and subsequent metathesis with an alkyl lithium reagent should afford the organoyttrium complex. Several drawbacks to using this silylamide precursor have recently been discovered. The polymeric $[Y(DAC)Cl]_x$ is insoluble in

hydrocarbon solvent which makes the metathesis step difficult. Work is continuing to convert the chloride to a (hopefully) more soluble derivative such as the 2,6-di-*t*-butylphenoxide. The phenoxide may also provide a good NMR probe to assist complex characterization. Furthermore, the reaction of $Y[N(SiMe_3)_2]_2OAr$ with H_2DAC should afford a more soluble monomeric complex and the reaction with alkyl lithium reagents should result in clean elimination of insoluble LiOAr, giving soluble organoyttrium complexes.

A more general route into a variety of alkyl and aryl organometallic complexes encompassing all lanthanides, group 3 (yttrium), and group 4 (zirconium) involves the preparation of $TMS_2(DAC)$ **46** (TMS = $SiMe_3$) followed by stoichiometric halide exchange with $LnCl_3$ (Ln = lanthanides and yttrium) or $ZrCl_4$ to produce $[Ln(DAC)Cl]_x$ or $[Zr(DAC)Cl_2]_x$ and volatile TMSCl. In a similar manner, the preparation of TMS(MAC) **47** and TMS(15-AC-5) **48** also can lead to $Ln(MAC)Cl_2$ and $Ln(15\text{-}AC\text{-}5)Cl_2$. Derivatization to the more soluble phenoxide may again provide better NMR characterization of the product (Scheme 14).

Early attempts to prepare the silylated macrocycles from the reaction of H_2DAC, HMAC, or H-15-AC-5 with a 2-fold excess of TMSCl and a 10 fold excess of triethylamine failed to yield clean product. Presumably, the amine group of the unreacted macrocycle may compete with triethylamine for HCl. However, results have shown that deprotonation of the corresponding macrocycle with a stoichiometric quantity of *n*-butyl lithium followed by an *in situ* reaction with a stoichiometric equivalent of TMSCl affords, after workup, silylated macrocycle as a colourless oil. No attempt was made to purify this product.

Scheme 14 A proposed general route to aza-crown organometallic complexes

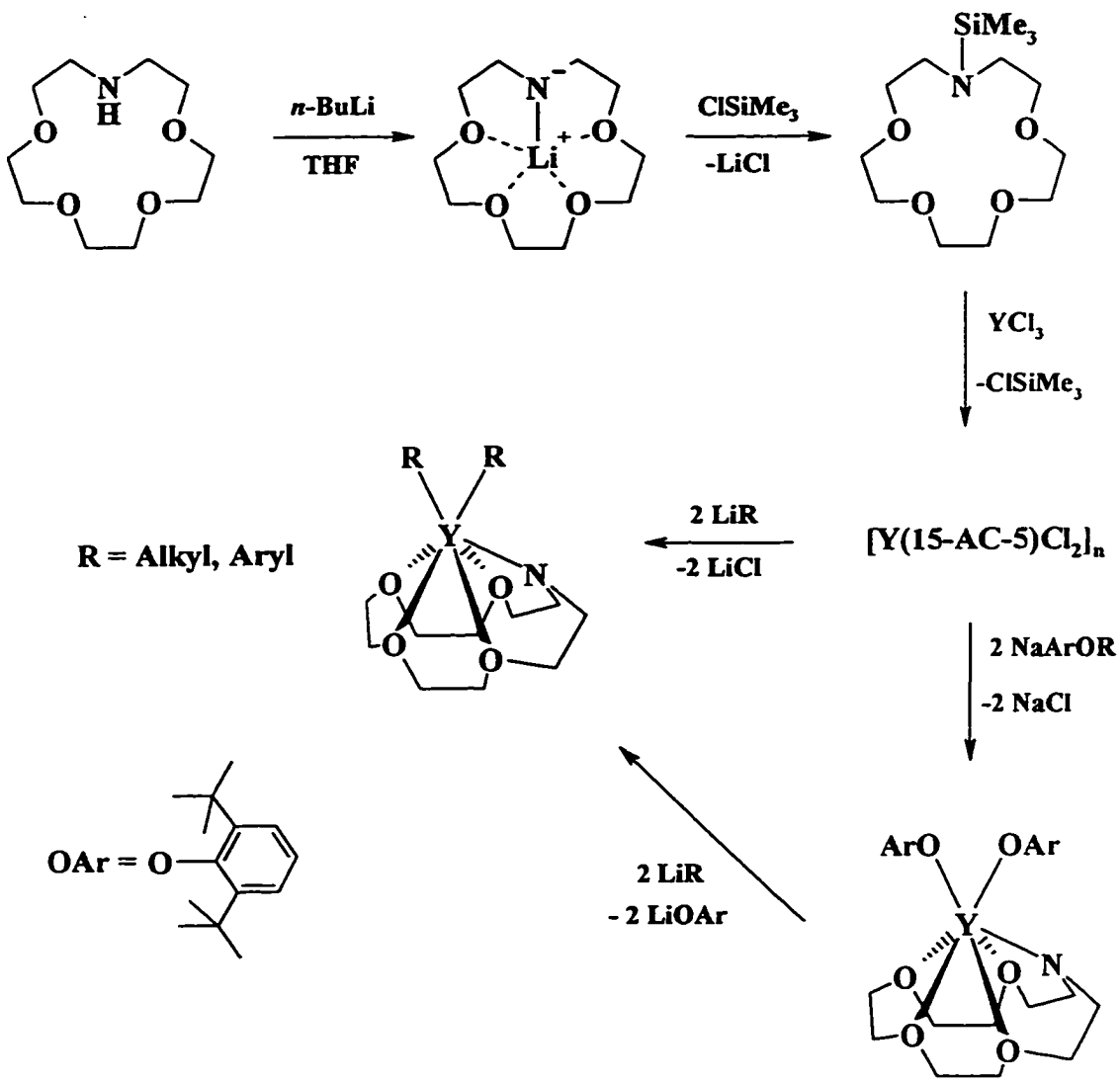

Preliminary reactions of TMS(MAC) with YCl_3 resulted in a white precipitate which is only marginally soluble in THF. However, *in situ* reaction of the presumed $[Y(MAC)Cl_2]_x$ with 2 equivalents of LiR (R = CH_2SiMe_3) in THF resulted in a low yield production of the *cis*-$Y(MAC)(CH_2SiMe_3)_2$ (^1H NMR (C_6D_6) ***cis*-40**: upfield signal at −1.05 $^1J_{YH}$ = 2.5 Hz; cf. ***trans*-40**: -1.33 $^1J_{YH}$ = 2.5 Hz), along with other side products. This result is very interesting because the protonolysis route resulted in the exclusive formation of the *trans*-dialkyl **40**. Further investigation of this reaction is warranted as a general method to the *cis*-dialkyls.

6.2 Potential for unique chemistry

Although the synthesis and reactivity of metallacylobutane, metallacyclopropene, and benzyne complexes of group 4 (titanium[112] and zirconium[113]) have been extensively studied, the analogs of the lanthanides have not been investigated. Exclusive production of *cis*-dialkyl complexes of the lanthanides affords an opportunity to study these novel complexes. Several possible strategies for preparing the metallacyclobutane[114], metallacyclopropene[115], and benzyne[113b] based on the successful routes used in zirconium and titanium chemistry are shown in eqs. 35-37. These complexes should be more reactive than the dialkyls due to the increase in metallacyclic strain and decrease in steric bulk. Furthermore the organometallic chemistry of group 5 metals (tantalum and niobium) and the actinides (uranium and thorium) containing aza-crown macrocycles has not been explored but may be expected to yield a wealth of interesting chemistry particulary since a range of oxidation states are accessible.

Metallacyclobutane[114]

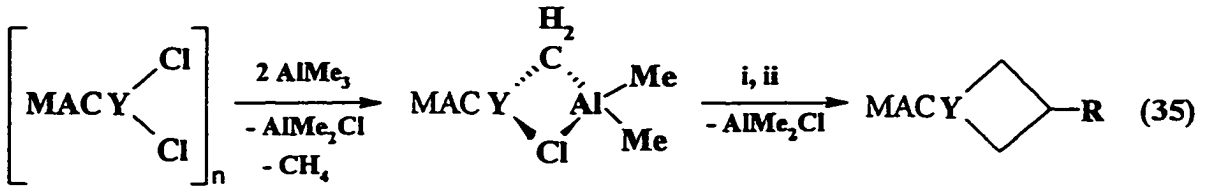

(35)

i : $RC(H)=CH_2$

ii : 4-vinylpyridine-styrene comonomer

Metallacyclopropene[115]

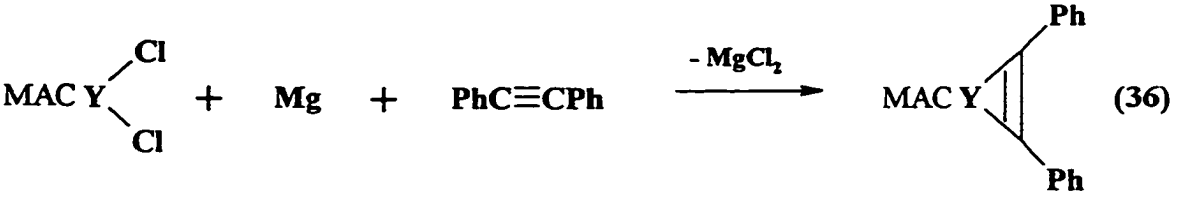

(36)

Benzyne[113b]

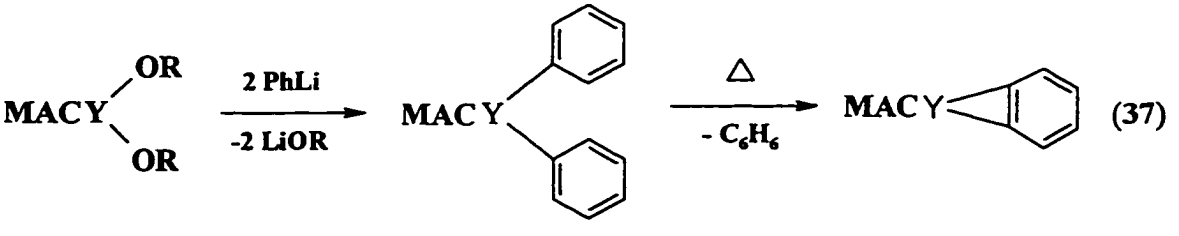

(37)

CHAPTER 7

Experimental

7.1 General procedures

All manipulations were carried out under an argon atmosphere, with the rigorous exclusion of oxygen and water, using standard glovebox (Braun MB150-GII) or Schlenk techniques, except as noted in the text. Tetrahydrofuran (THF), diethyl ether, hexane and toluene were dried by distillation from sodium benzophenone ketyl under argon immediately prior to use. Anhydrous metal trichlorides (Ce and Y) were prepared from the hydrated salts by prolonged reflux in neat $SOCl_2$ followed by vacuum distillation and drying at 150 °C (10^{-2} torr) for 16 to 20 h. Anhydrous SmI_2 was prepared from Sm powder and CH_2I_2 in THF solution [116]. THF of solvation was removed by heating at 150 °C for 16 h. Ytterbium diiodide was prepared from Yb metal chips and NH_4I in liquid ammonia[65]. Hexamethyldisilazane was purchased from Aldrich and dried by distillation from sodium metal. Lanthanide silylamides, $Ln[N(SiMe_3)_2]_3$ (Ln = Ce and Y)[63], $Sm[N(SiMe_3)_2]_2[THF]_2$[67], $Yb[N(SiMe_3)_2]_2[OEt_2]_2$[65], $Y[N(SiMe_3)_2]_2Cl\bullet 2THF$[111], yttrium phenoxide $Y(OC_6H_3\text{-}2,6\text{-}t\text{-}Bu)_3$[41], and the zirconium alkyls, $Zr(CH_2Ph)_4$[97] and $Zr(CH_2Ph)_2Cl_2[OEt_2]_2$[101] were prepared as reported in the literature. Neopentyl chloride was prepared from neopentyl alcohol using PCl_5 and DMF at 150 °C for 1h; the alkyl halide was distilled and used without further purification[117]. The gases CO, H_2, ethylene were passed through a Ridox ® column and molecular sieves (4 Å). Tris(pentafluorophenyl) boron was a gift from Boulder Scientific Co. All other chemicals were of reagent grade, unless otherwise specified.

^{1}H, ^{13}C, ^{19}F, ^{29}Si and ^{89}Y NMR spectra were recorded on a Varian 90 MHz, Bruker WM-250 MHz, Bruker AMX-300, or Bruker AMX-360 MHz spectrometer. Spectra were recorded in C_6D_6, C_7D_8, or C_4D_8O solvent, previously distilled from sodium under argon, or in CD_2Cl_2 or C_5D_5N dried and stored over 4Å molecular sieves, using 5 mm tubes fitted with a teflon valve (Brunfeldt). All solvents were thoroughly degassed prior to use. All two dimensional spectra (^{1}H-^{1}H COSY and ^{1}H-^{13}C COSY) were recorded on the Bruker AMX-360 MHz spectrometer. ^{29}Si spectra were recorded using DEPT or INEPT pulse sequences as appropriate. ^{1}H and ^{13}C NMR spectra were referenced to residual solvent resonances; ^{19}F, ^{29}Si, and ^{89}Y were referenced to C_6F_6, external TMS and 3M YCl_3 in D_2O, respectively. Mass spectra were recorded on a Finnigan 3300 or a Kratos Concept H spectrometer using chemical ionization or electron impact (70 eV) sources. Gas chromatograms were performed on a Varian 3700 GC. Infrared spectra were recorded on a Bruker IFS 25 FT-IR instrument as nujol mulls or neat oils on NaCl plates. X-ray crystallographic details are given in Appendix. Melting points were recorded using a Reichert hot stage and are not corrected. Elemental analyses were performed by Canadian Microanalytical, Delta, B.C., Canada, or Atlantic Microanalytical, Atlanta, GA, USA. Analytical results were generally low in C despite repeated recrystallizations and clean NMR spectra. We have observed this problem many times in lanthanide complexes containing silicon.

4,13-Diaza-18-crown-6 (H_2DAC) Method 1 (Kulstad and Malmsted route[60]):

1,2-bis(2-azidoethoxyethane) (4) A two-neck 1 L round bottom flask containing 1,2-bis(2-chloroethoxy)ethane (73.75 g, 0.394 mol), NaN_3 (104 g, 1.6 mol), Aliquot 336* (14 g) and 300 mL water were stirred vigorously for 22 h at 90 °C. The reaction was cooled then washed (2 x 100 mL) with water followed by extraction with diethyl ether (3 x 100 mL) and dried over anhydrous $MgSO_4$. Evaporation of the solvent afforded crude 4 as an orange oil which was used without further purification. The yield was quantititative. ^{1}H NMR (360 MHz, $CDCl_3$): δ 3.64 (t, 8H, $OCH_2CH_2N_3$ $^3J_{HH}$ = 4.8 Hz), 3.63 (s, 8H OCH_2CH_2O), 3.35 (t, 8H, $OCH_2CH_2N_3$, $^3J_{HH}$ = 4.9 Hz). ^{13}C NMR (90.56 MHz, $CDCl_3$): δ 70.60 (OCH_2CH_2O), 70.00 ($OCH_2CH_2N_3$), 50.54 ($OCH_2CH_2N_3$).

1,8-diamino-3,6-dioxaoctane (5). A two-neck 1L round bottom flask equipped with an efficient condenser was flushed for 2 min with argon. To this flask was added 250 mL dry THF and $LiAlH_4$ (10.03 g, 0.264 mol). To a pressure equalizing dropping funnel was added 4 (20 g, 0.10 mol) in 150 mL dry THF. The dropping funnel was stoppered and 4 was *slowly* added to the stirred suspension of $LiAlH_4$ in the round bottom flask at O °C. The reaction is exothermic as frothing of the solution was observed. After addition of 4, the dropping funnel was removed and the round bottom flask was stoppered. The reaction was heated to reflux

---

* Aliquot 336 is a phase transfer surfactant

under argon for 16 h, cooled, and quenched with water (200 mL) at 0 °C. A gelatinous white precipitate was observed after the addition of about 50 mL of water. On further addition of water, the gelatinous material became very viscous and another 100 mL of THF was added to the reaction mixture. Addition of water was continued until no more hydrogen evolution was observed. The white precipitate containing aluminium salts was removed by suction filtration. The soluble diamine was Soxlet extracted from the aluminium salts with THF from the mother liquor for 24 h. After this time, the THF extract was evaporated under reduced pressure and the diamine was dried by addition of benzene for azeotropic removal of water with a Dean-Stark trap. Crude **5** was obtained after evaporation of benzene and was used without further purification. ^{1}H NMR (90 MHz, $CDCl_3$): δ 3.62 (s, 4H, OCH_2CH_2O), 3.41 (t, 4H, $OCH_2CH_2NH_2$, $^3J_{HH}$ = 6.3 Hz), 2.84 (t, 4H, $OCH_2CH_2NH_2$, $^3J_{HH}$ = 6.3 Hz), 1.32 (s, 4H, NH_2).

1,2-bis(2-iodoethoxyethane) (6) A one-neck 1L round bottom flask containing NaI (330 g, 2.20 mol) in 200 mL of acetone was added 1,2-bis(2-choloroethoxyethane) (190 g, 1.016 mol) in 500 mL acetone. The reaction mixture was refluxed for 3 days. The mixture was allowed to cool before filtration of the sodium salts. Acetone was evaporated under reduced pressures and the resulting dark orange oily residue was dissolved in CH_2Cl_2 (500 mL) and washed with 10 % w/v sodium thiosulfate solution (5 x 200 mL). The organic layer was dried over anhydrous $MgSO_4$. Evaporation of the solvent gave crude **6** as a pale yellow oil.

Yield: Quantitative. No further purification was necessary. ^{1}H NMR (90 MHz, $CDCl_3$): 3.78 (t, 4H), 3.64 (s, 4H), 3.25 (t, 4H).

Cyclization to form H_2DAC A two-neck 1L round bottom flask containing **6** (12.6 g, 0.0851 mol) in 150 ml of acetonitrile and 5-fold excess of anhydrous Na_2CO_3 (46.2 g, 0.436 mol) was fitted with a condenser and a pressure equalizing dropping funnel which was charged with **5** (31.5 g, 0.0851 mol) in 50 mL acetonitrile. The diamine **5** was added dropwise over three hours to a vigorously stirred boiling solution of **6** and a suspension of Na_2CO_3. After addition of **5**, the reaction mixture was stirred under reflux for an additional 18 h. Removal of the sodium salts by suction filtration was followed by evaporation of the solvent under reduced pressure. The resulting dark orange–red oily residue was dissolved in a boiling solution of acetone and *p*-dioxane (100 mL, 1:1 mixture) and allowed to cool overnight at –5 °C. White crystals presumed to be the sodium iodide complex of the macrocycle were isolated (51.5 g). The crystals were redissolved in water (100 ml) and extracted with $CHCl_3$ by continuous extraction for 22 h. Chloroform was evaporated under reduced pressure to give a dark red residue. Recrystallization of the residue from hexanes gave yellow coloured H_2DAC. Yield: 4.56 g (20.5 %). Mp. 109-110°C; lit: 115-116°C[61]. ^{1}H NMR (250 MHz, C_6D_6): δ 3.41 (t, 8H, OCH_2CH_2N, $^3J_{HH}$ = 4.7 Hz), 3.30 (s, 8H, OCH_2CH_2O), 2.68 (t, 8H, , OCH_2CH_2N, $^3J_{HH}$ = 4.7 Hz), 2.27 (br s, 2H, N*H*). ^{13}C NMR (62.9 MHz, C_6D_6): δ 70.60 (OCH_2CH_2O), 70.42 (OCH_2CH_2N), 49.53 (OCH_2CH_2N).

4,13-Diaza-18-crown-6 (H_2DAC). Method 2 (Gokel route[61]):

N,N'-Dibenzyl-4,13-diaza-18-crown-6 (7). To a 3-neck 2L round bottom flask equipped with an efficient condenser and an overhead stirrer was added 5-fold excess of Na_2CO_3 (38.8 g, 0.366 mol), half an equivalent of NaI (5.45 g, 0.037 mol), 1,2-bis(2-iodoethoxyethane) **6** (27.1 g, 0.0731mol), benzylamine (7.82 g, 0.0.732 mol), and 1.5 L acetonitrile. The solution was mechanically stirred and heated at reflux for 21 h. After this time, the flask was allowed to cool and the sodium salts were filtered from the solution. The solvent was evaporated under reduced pressure and the solid yellow-orange residue was recrystallized in a refluxing mixture of 1:1 acetone, *p*-dioxane (250 mL). After overnight cooling at –5 °C, white crystals presumed to be sodium iodide complex of the dibenzyl protected macrocycle were isolated (95 g). The crystals were dissolved in water (500 mL) and $CHCl_3$ (400 ml) and extracted with $CHCl_3$ (3 x 75 ml). The combined organic phases were dried over $MgSO_4$ and evaporated under reduced pressure to give crude **7**. Recrystallization of **7** from hexane (500 mL) and ethanol (100 mL) afforded pale yellow crystals of **7**. Yield: 11.2 g (63.5 %). Mp: 80 - 81.5°C. ^{1}H NMR (360 MHz, $CDCl_3$): δ 7.3 - 7.25 (m, 10H, aryl), 3.67 (s, 4H, CH_2Ph), 3.63 (s, t overlapping, 12H OCH_2CH_2O and OCH_2CH_2N), 2.82 (t, 8H, NCH_2CH_2O, $^3J_{HH}$ = 5.88 Hz), NH resonance not observed. ^{13}C NMR (90.55 MHz. $CDCl_3$): 139.6 (ipso), 129.8 (aryl), 128.1 (aryl), 126.8 (aryl), 70.66 (OCH_2CH_2O),70.0 (OCH_2CH_2NH), 59.9 (CH_2Ph), 53.7 (OCH_2CH_2NH)

Deprotection of N,N'-dibenzyl 4,13-diaza-18-crown-6 A dark yellow solution of 7 (11.0 g, 0.0249 mol) in 250 mL absolute ethanol and 10% Pd/C catalyst (1 g) was shaken on a Parr series 3300 hydrogenation apparatus at 60 psi and ambient temperature for 3 days. The first attempt at deprotection of 7 failed to give H_2DAC, but a much cleaner sample of 7 (9.5 g, 0.0215 mol) was recovered and the hydrogenation was repeated (this suggests that 7 must be decolourised with charcoal followed by recrystallization from ethanol prior to hydrogenation). The solution was filtered through celite and the solvent was evaporated under reduced pressure to give crude off white H_2DAC. Recrystallization of this residue from hexane afforded pure H_2DAC. Yield: 5.15 g (91.4 %). The physical properties and NMR spectral data are similar to that reported above. H_2DAC was dried over 4 Å molecular sieves prior to use.

Y(DAC)[N(SiMe$_3$)$_2$] (8) In the glovebox, H_2DAC (1.00 g, 3.81 mmol) and Y[N(SiMe$_3$)$_2$]$_3$ (2.16 g , 3.81 mmol) were dissolved in 50 mL toluene. The solution was stirred vigorously overnight. Removal of the solvent under reduced pressure produced a white powder. Recrystallization from a toluene-hexane mixture produced colourless crystals of **8**. Yield: 1.54 g (79.4 %). Mp: dec. 148-149 °C. MS (EI): m/z 508 (M^+), 494 (M^+ - CH_3), 466 (M^+ - C_2H_3O), 348 (M^+ - N(SiMe$_3$)$_2$), 305 (M^+ - N(SiMe$_3$)$_2$ - C_2H_3O). Anal. Calcd for $C_{18}H_{42}N_3O_4Si_2Y$: C, 42.42; H, 8.31; N, 8.25. Found: C, 41.56; H, 8.37; N, 8.01. NMR data are found in Table 2.

Ce(DAC)[N(SiMe$_3$)$_2$] (9) Reaction of H_2DAC (0.250 g , 0.953 mmol) with Ce[N(SiMe$_3$)$_2$]$_3$ (0.591 g , 0.953 mmol) according to the procedure outlined for **8**, afforded **9** as a yellow microcrystalline powder. Yield: 0.36 g (67 %). Mp: dec. 140°C. MS (EI): m/z 560 (M^+), 545 (M^+ - CH_3), 517 (M^+ - C_2H_3O), 399 (M^+ - N(SiMe$_3$)$_2$), 356 (M^+ - N(SiMe$_3$)$_2$ - C_2H_3O). Anal. Calcd for $C_{18}H_{42}N_3O_4Si_2Ce$: C, 38.55; H, 7.55; N, 7.49. Found: C, 37.71; H, 6.78; N, 7.26. NMR data are found in Table 2.

Attempted preparation of Y(DAC)(OC$_6$H$_3$-*t*-Bu$_2$) (10) Method 1: In the glovebox, complex **8** (0.10 g, 0.20 mmol) was dissolved in 250 mL of toluene in a 500 mL Erlenmyer flask fitted with a dropping funnel. A solution of freshly sublimed 2,6-di-*tert*-butylphenol (0.041 g, 0.20 mmol) in 100 mL of toluene was placed in the dropping funnel and slowly added to the vigorously stirred solution of **8** over 6 h. At the end of this period, the solvent was removed from the clear, colorless reaction mixture to produce an oily white solid. Examination of this material by ^{1}H NMR (C_6D_6) showed free H_2DAC and Y(OC$_6$H$_3$-2,6-*t*-Bu$_2$)$_3$ [41] [δ 7.25 (d, 6H, *m*-arylC*H*, $^3J_{HH}$ = 7.8 Hz), 6.82 (t, 3H, *p*-arylC*H*, $^3J_{HH}$ = 7.8 Hz), 1.51 (s, 54H, C*Me*$_3$)] as major components of the complex mixture. Reaction of **8** with *tert*-butanol was carried out in an analogous fashion. In this case, white precipitate formed immediately while the toluene supernatant contained free H_2DAC by ^{1}H NMR. Method 2: To a solution of H_2DAC (0.500g, 1.91 mmol) in 50 mL toluene was added by cannula two equivalents of Li[N(SiMe$_3$)$_2$] (0.637 g, 3.81 mmol) in 50 mL toluene. The slightly turbid yellow solution was cannula

filtered into a suspension of $Y(OC_6H_3\text{-}2,6\text{-}t\text{-}Bu_2)_3$ in 50 mL toluene and the resulting highly turbid orange-yellow solution was heated at 70°C overnight. The yellow supernatant containing a white precipitate was filtered and the solvent was removed under reduced pressure. NMR spectroscopy showed that this toluene soluble product consisted of $Y(OC_6H_3\text{-}2,6\text{-}t\text{-}Bu_2)$, DAC peaks were not detected.

$\{Yb[N(SiMe_3)_2]\ (\mu\text{-DAC})\}_2Yb$ (11) In the glovebox, H_2DAC (0.250 g , 0.953 mmol)

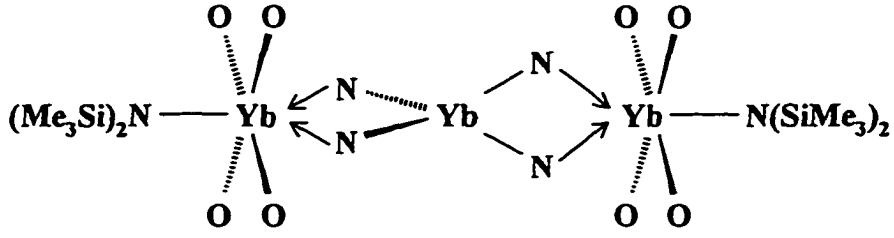

macrocyclic carbons omitted for clarity

and $Yb[N(SiMe_3)_2]_2[OEt_2]_2$ (0.812 g , 1.43 mmol) were dissolved in 50 mL toluene. The deep red solution was stirred vigorously overnight. Removal of the solvent under reduced pressure produced a red-brown powder. Recrystallization from a toluene-hexane mixture produced ruby red crystals of **11** (0.52 g , 80 %). Mp: dec. 170 °C. Anal. Calcd for $C_{36}H_{84}N_6O_8Si_4Yb_3$: C, 31.78; H, 6.22; N, 6.18. Found: C, 31.50; H, 5.99; N, 6.13. NMR data for **11** are summarized in Table 4.

Attempted derivatization of 11. To a bright red solution of **11** (0.042 g, 0.0309 mmol) in 0.5 mL d_6-benzene was added a solution of HOC_6H_3-2,6-*t*-Bu_2 (0.013 g, 0.063 mmol) in 0.5 mL d_6-benzene. The turbid red solution was mixed vigorously by pipette. The solution was filtered through celite and transferred to a NMR tube fitted with a teflon valve (Brunfeldt). ^{1}H NMR spectroscopy of the orange solution showed unreacted phenol as the major compound in solution. Similarily, the reaction of **11** (0.030 g, 0.022 mmol) in 0.5 mL of d_6-benzene with 0.072 mL of a 0.610 M solution of phenylacetylene in d_6-benzene (0.068 g, 0.044 mmol) resulted in a red precipitate while the benzene soluble orange fraction contained unreacted phenylacetylene as the major component.

Attempted oxidation of 11 with HgR_2. To a stirred solution of **11** (0.210g. 0.154 mmol) in 30 mL toluene was added dropwise one and a half equivalent of $Hg(CH_2Ph)_2$ (0.088 g, 0.230 mmol). After allowing the slightly turbid ruby red solution to stir for one day, the solution was filtered through celite and the solvent was removed under reduced pressure. No change in ^{1}H NMR spectrum of **11** was observed. Similarily the reaction of **11** (0.15 g, 0.11mmol) in 15 mL toluene with one and a half equivalents of $Hg(Ph)_2$ (0.063 g, 0.165 mmol) in 15 mL toluene was allowed to stir for 3 days and the major component was found to be unreacted **11** by ^{1}H NMR. The reaction of **11** (0.050g, 0.0359 mmol) in 10 mL toluene with one and a half equivalent of $Hg(t\text{-}Bu)_2$ (0.017g, 0.054 mmol), following the same course of events as above, similarly resulted in unreacted **11** as the major soluble component.

{Yb[N(SiMe$_3$)$_2$]}$_2${μ-DAC} (12) This complex was prepared as described for **11** above using a 1:2 ratio of H_2DAC (0.250 g, 0.950 mmol) and Yb[N(SiMe$_3$)$_2$]$_2$[OEt$_2$]$_2$ (1.08 g , 1.91 mmol). Black crystals of **12** were obtained by recrystallization from a toluene-hexane mixture at -30 °C. Yield: 0.15 g (17 %). m.p. 170 °C. Anal. Calcd for $C_{24}H_{60}N_4O_4Si_4Yb_2$: C, 31.08; H, 6.53; N, 6.04. Found: C, 30.19; H, 6.26; N, 5.89. NMR data are collected in Table 6.

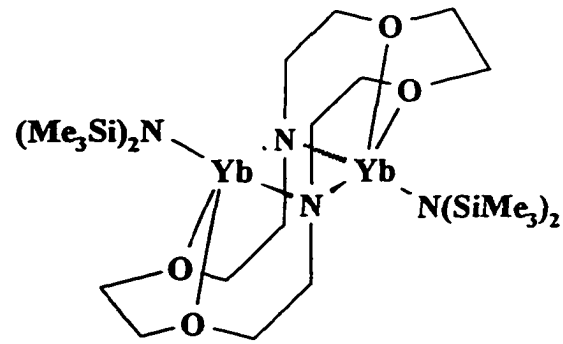

Attempted derivatization of 12. To a black solution of **12** (0.065 g, 0.0701 mmol) in 10 mL toluene was added a solution of HO-C$_6$H$_3$-2,6-*t*-Bu$_2$ (0.029 g, 0.14 mmol) in 5 mL toluene. On addition of the phenol, the black solution immediately turned ruby red. The reaction mixture was allowed to stir for several hours. After the first hour, the solution turned black-green and after another hour the solution faded to a permanent light green colour. Removal of the solvent under reduced pressure resulted in a green residue which was difficult to redissolve in d_6-benzene. Filtration of the green precipitate into a NMR tube gave a yellow coloured supernatant that contained unreacted phenol by ^{1}H NMR. The reaction of **12** with phenylacetylene followed the same course of events as that of the phenol.

Attempted oxidation of 12 with HgR_2. To a stirring black solution of **12** (0.111 g,. 0.120 mmol) in 5 mL toluene was added dropwise one equivalent of a solution containing $Hg(CH_2Ph)_2$ (0.046 g, 0.120 mmol) in 5 mL toluene. The colour of the mixture turned brown immediately and the solution was allowed to stir for three days. Solvent was removed under reduced pressure and the brown residue was redissolved in d_6-benzene. The resulting ^1H NMR spectrum of the sample clearly indicated paramagnetic species in solutions by the presence of broad peaks from 10 to –30 ppm. Similarly, the reaction of **12** with one equivalent of $Hg(Ph)_2$ or $Hg(t\text{-}Bu)_2$ resulted in paramagnetic species in solution. Attempts to grown X-ray quality crystals for structural analysis were hampered from the isolation of fine hairy needles. No further attempts at characterizing these products were pursued.

Interconversion of (11) and (12) A solution of **11** (0.030 g , 0.022 mmol) in 10 mL toluene was added to a stirred solution of $Yb[N(SiMe_3)_2]_2[OEt_2]_2$ (0.013 g , 0.022 mmol) in 10 mL toluene dropwise. The bright brick red colored solution quickly faded to a clear black. The solvent was removed under reduced pressure and the residue completely redissolved in C_6D_6. The ^1H NMR of this solution was identical with that of pure **12**. A solution of **12** (0.030 g , 0.032 mmol) was dissolved in 10 mL toluene and added to a stirred solution of H_2DAC (0.003 g , 0.01 mmol) in 2 mL toluene. The solution rapidly changed colour from black to ruby red. After stirring for 2 h, the solvent was removed and the residue completely redissolved in C_6D_6. The ^1H NMR of this solution was identical to that reported for pure **11**

with the exception that resonances due to a small amount of free H_2DAC were present. H_2DAC can be removed from this product by repeated washing with hexane.

$Sm(DAC)[N(SiMe_3)_2]$ (13) Reaction of H_2DAC (0.125 g , 0.447 mmol) and *divalent* $Sm[N(SiMe_3)_2]_2[THF]_2$ (0.293 g , 0.447 mmol) in 50 mL toluene resulted in an initial purple solution which faded to green and finally yellow after stirring for 2.5 h. The yellow supernatant was filtered through celite to remove a black viscous oil which could not be characterized by NMR because it was insoluble in all solvents. This yellow solution was evaporated to dryness and recrystallized from a toluene-hexane mixture at -30 °C. Bright yellow crystals of **13** were isolated by filtration and dried under vacuum. Yield: 0.214 g (78.7 %). m.p. dec. 175 °C. MS (EI) m/z 572 (M^+), 557 (M^+ - CH_3), 529 (M^+ - C_2H_3O), 411 (M^+ - $N(SiMe_3)_2$), 368 (M^+ - $N(SiMe_3)_2$ - C_2H_3O). ^1H NMR data for 13 are summarized in Table 7. Anal. Calcd for $C_{18}H_{42}N_3O_4Si_2Sm$: C, 37.86; H, 7.41; N, 7.35. Found: C, 37.42; H, 7.36; N, 7.15.

$Y(CH_2SiMe_3)_3 \bullet 2THF$[34] To a suspension of anhydrous YCl_3 (2.77 g, 14.2 mmol) in 50 mL of an 1:1:1 THF:ether:hexane mixture at 0 °C was added by cannula a solution of $LiCH_2SiMe_3$[118] (4 g, 42.6 mmol) in 50 mL of 1:1:1 THF:ether:hexane mixture. On addition of the lithium reagent, white YCl_3 slowly disappeared and the colourless suspension became clear. When all of the $LiCH_2SiMe_3$ was added a white precipitate due to LiCl instantly emerged from the solution. The mixture was allowed to stir for another 30 minutes and

after this time the solvent was removed under vacuum at 0 °C. The Schlenk flask containing an oily white residue was promptly transferred to the glove box for workup. After addition of hexane, the LiCl precipitate was filtered and the solution was concentrated under vacuum. The solution was cooled to -30 °C overnight. White crystals analyzing for $Y(CH_2SiMe_3)_3 \bullet 2THF$ was isolated. Yield: 5.3 g (75.6 %). ^1H NMR (C_6D_6, 360 MHz): δ 3.93 (m, 8H, $C_aH_2C_bH_2O$ for THF) , 1.29 (m, 8H, $C_aH_2C_bH_2O$ for THF), 0.29 (s, 27, Si*Me*3), -0.71 (d, 6H, CH_2SiMe_3. $^2J_{YH} = 2.6$ Hz). $^{13}C\{^1H\}$ NMR (C_6D_6, 90.55 MHz): 55.0 (s, $C_aH_2C_bH_2O$), 25.0 (s, $C_aH_2C_bH_2O$), 33.7 (d, CH_2SiMe_3, $^1J_{YC} = 36$ Hz), 4.6 (s, $SiMe_3$).

Y(DAC)(CH_2SiMe_3) (14) A solution of H_2DAC (0.200 g, 0.762 mmol) in 20 mL of toluene was added dropwise over 10 min to a vigorously stirred solution of $Y(CH_2SiMe_3)_3(THF)_2$[34] (0.377 g, 0.762 mmol) in 20 mL of toluene. The colourless solution was stirred for 30 min followed by removal of the solvent under reduced pressure. Recrystallization of the resulting white powder from a toluene-hexane mixture produced white crystals of **14**. Yield: 0.310 g (70 %). Mp. dec. 120 °C. ^{29}Si NMR (49.69 MHz) δ -1.9 (s, *Si*Me_3). ^1H, ^{13}C, and ^{89}Y NMR data are found in Table 8. Anal. Calcd for $C_{16}H_{35}N_2O_4SiY$: C, 44.03; H, 8.08; N, 6.42. Found: C, 43.00; H, 7.81; N, 6.35.

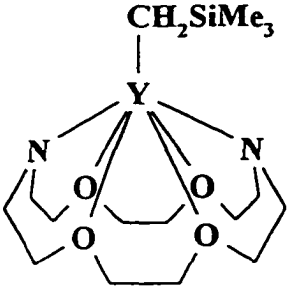

Thermal decomposition kinetics of 14. The thermal decomposition of **14** was performed at 35 °C, 55 °C, 75 °C, and 85 °C. For each temperature, pure **14** (approximately 20 mg) was dissolved in d_6-benzene and transferred to a NMR tube fitted with a teflon valve (Brunfeldt). The decomposition was followed by ^{1}H NMR a Bruker AMX-360 MHz spectrometer after varying lengths of time giving the rate constants 2.31×10^{-6}, 7.00×10^{-6}, 1.12×10^{-4}, and 1.21×10^{-4}, respectively. From the Arrehnius equation : $\ln k = \ln A - E_a/RT$, a plot of ln k against 1/T gave a slope of $-Ea/R$.

Siliconization of the NMR tubes. A 5mm NMR tube that can be fitted with a teflon valve (Brunfeldt) was first treated with 10% HF followed by several rinses with deionised water and oven dried for 1-2 h. After it was cooled, the tube was treated with 3% v/v Me_2SiCl_2 in toluene followed by oven drying at 120 °C for 48 h. This proceduce is a modification of that given in: *Model 303 Static Mercury Dropping Electrode Operating and Service Manual*; EG+G Princeton Applied Research: Princeton, NJ, 1984.

Attempted reaction of 14 with small molecules. A solution of **14** (0.050 g, 0.115 mmol) in 0.75 mL d_6-benzene was placed in a NMR tube fitted with a teflon valve (Brunfeldt). After cooling in liquid nitrogen, the sample was degassed and allowed to warm to room temperature under an atmosphere of CO prior to sealing. **14** was observed unchanged in the ^{1}H and ^{13}C NMR spectrum. After several days a precipitate was

observed in the NMR tube and the NMR spectrum was consistent with decomposition of **14**. Similarly, no reaction was observed between **14** and H_2 or ethylene .

[{DAC)Y(μ-C≡CPh)]$_2$ (15) A solution of phenylacetylene (1.79 mL of a 0.513 M solution in benzene, 0.917 mmol) was added to a colourless solution of Y(DAC)(CH_2SiMe_3) (0.40 g, 0.92 mmol) in 25 mL benzene with stirring. The clear purple solution of the reaction mixture was layered with hexane and allowed to stand at room temperature until white crystals of **15** slowly deposited. Yield :0.260 g (63.4 %). Mp: 120 °C dec. IR (Nujol, KBr): 2047 cm^{-1} (m, $\upsilon_{C\equiv C}$). ^1H NMR (C_6D_6, 360 MHz, 302 K): envelope of DAC resonaces extends from 4.5-2.5 ppm. Aryl resonances are summarized in Table 13. $^{13}C\{^1H\}$ NMR (90.55 MHz): δ 150.1 (*C*≡CPh), Ph*C*≡C not observed, DAC resonances (tentative): 75.7 (br, partially obscured) 74.3 (br), 71.6 (br). Anal. Calcd for $C_{40}H_{58}N_4O_8Y_2$: C, 53.34; H, 6.49; N, 6.22. Found: C, 53.61; H, 6.60; N, 5.62.

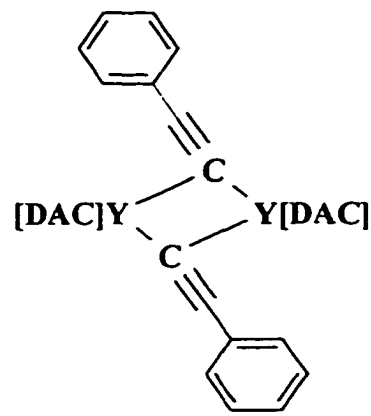

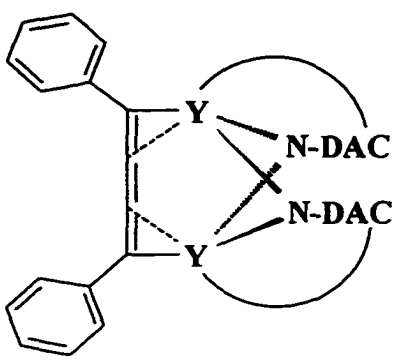

[(DAC)Y]$_2$(μ-(Z)-PhC=C=CPh) (16). The above reaction was repeated except that slow evaporation of the resulting purple solution gave blue-purple needles (0.280 g, 67.8 %) as a benzene solvate (1.5 equiv). Mp: 90 °C dec. IR (Nujol, KBr): 1592, 1542 cm^{-1} (m, $\upsilon_{C=C}$). ^{1}H NMR (C_6D_6, 360 MHz, 302 K) **16**: envelope of DAC resonances extends from δ 4.5 – 2.5 ppm. Aryl resonances are reported in Table 13. ^{13}C{^{1}H} NMR (90.55 MHz) δ 196.5 (d, C=*C*Ph, $^1J_{YC}$ = 38.4 Hz), 169.5 (d, *C*=CPh, J_{YC} = 4.0 Hz), DAC resonances (tentative): 75.9, 75.5, 73.7, 70.5, 69.6, 68.4, 68.3, 67.6, 58.3, 58.1, 56.2, 53.7. Anal. Calcd for $C_{49}H_{67}N_4O_8Y_2$: C, 57.82; H, 6.64; N, 5.50. Found: C, 57.75; H, 6.63; N, 5.36.

Hydrolysis of (15) or (16). In the glove box a solution of pure crystals of **15** (10 mg) or **16** (15 mg) in 0.7 mL d_6-benzene was place in a 10 mL vial and capped. The vial was taken out of the glove box and under argon degassed water was added. The purple colour rapidly disappeared and an insoluble solid was noted in the colourless solution. The benzene layer was carefully removed and filtered through a layer of celite and $MgSO_4$. The initial ^{1}H NMR spectrum showed the exclusive formation of the *Z*-1,4-di-phenyl-3-buten-1-yne **17**, but after several hours isomerization was observed by the formation of the *E*-isomer giving a ratio of 85:15 (*Z*:*E*). After 4 days at 50 °C, the ratio was found to be 20:80 (*Z*:*E*). ^{1}H NMR data are

summarized in Table 15. GC/MS(CI): m/z 204 (M^+)

Y(DAC)(C≡CPh) •THF (20) Crystals of **15** (0.020 g, 0.022 mmol) were placed in an NMR tube tube fitted with a teflon valve (Brunfeldt). Under an atmosphere of argon outside of the glove box, dry, degassed d_8-THF (0.50 mL) was added by syringe and the sample was degassed by three freeze thaw-pump-thaw cycles. The sample was allowed to warm to ambient temperature and the NMR spectra of the clear colourless solution were recorded. NMR data are summarized in Table 17.

[{DAC)Y(μ-C≡CTol)]$_2$ (21) A solution of *p*-tolylacetylene (0.370 mL of a 0.248 M solution in benzene, 0.0917 mmol) was added to a solution of Y(DAC)(CH_2SiMe_3) (0.040 g, 0.0917 mmol) in 10 mL benzene. The reagents were vigorously mixed by pipette action and the appearance of the purple colour due to the presence of [(DAC)Y](μ-(Z)-TolC=C=CTol) **22** developed slowly. The reaction mixture was layered with hexane and allowed to stand at room temperature until white crystals of **21** slowly deposited. Yield :0.025 g (59.5 %). Complex **21**; ^{1}H NMR (C_6D_6, 360 MHz): δ 7.56 (br m, *o*-arylC*H*, 4H), 6.95 (br m, *m*-arylC*H*, 4H), 2.06 (s, 6H, CH_3). $^{13}C\{^1H\}$ NMR (90.56 MHz): δ 147.4 (*C*≡CTol), 106.9 (C≡*C*Tol), 21.24 (*C*H$_3$), DAC resonances (tentative): 75.6 (br, overlapping), 74.6 (br), 71.5 (br), 69.6 (br overlapping), 58.1 (br, overlapping), 56.3 (br obscured and overlapping). Complex **22**; ^{1}H NMR (C_6D_6, 360 MHz): δ 7.68 (d, *o*-arylC*H*, 4H, $^3J_{HH}$ = 7.5 Hz), 7.12 (d, *m*-arylC*H*, 4H,

$^3J_{HH}$ = 7.5 Hz, partially obscured), envelope of DAC resonances extend from 4.5- 2.5 ppm, 2.20 (s, 6H, CH_3). $^{13}C\{^1H\}$ NMR (90.56 MHz) δ 195.0 (d, C=*C*Tol, $^1J_{YC}$ = 37.8 Hz), 168.7 (s, *C*=CTol), 21.16 (CH_3), DAC resonances (tentative): 75.8, 75.6, 73.8, 70.48, 69.3, 68.5, 68.4, 67.6, 58.3, 58.1, 56.3, 53.7.

Cross coupling reaction. In separate vials pure crystals of [{DAC)Y(μ-C≡CPh)]$_2$ **15** (10 mg, 0.011 mmol) and [{DAC)Y(μ-C≡CTol)]$_2$ **21** (10 mg, 0.011 mmol) were each dissolved in 0.5 mL d_6-benzene. The clear purple solutions were combined and vigorously mixed by pipette action. Neither ^1H or ^{13}C NMR of this new purple coloured solution was informative so the solution was hydrolyzed with degassed water under an atmosphere of argon. ^1H NMR and GC/MS confirmed the presence of a mixture of 1,4-diphenyl-3-buten-1-yne **Z-17** (R_t = 24.24 min) 1,4, di-*p*-toly-3-buten-1-yne **Z-25** (R_t = 27.49 min) 1-phenyl-4-*p*-tolyl-3-buten-1-yne **Z-26** (R_t = 25.81 min), 1-*p*-tolyl-4-phenyl-3-buten-1-yne **Z-27** (R_t= 25.96 min) along with phenylacetylene (R_t = 4.11) and *p*-tolylacetylene (R_t = 6.80 min). The presence of these organic compounds suggest the presence of [{DAC)Y(μ-C≡CPh)]$_2$ **15**, [(DAC)Y]$_2$(μ-*Z*-PhC=C=CPh) **16**). [{DAC)Y(μ-C≡CTol)]$_2$ **21**, [(DAC)Y](μ-*Z*-TolC=C=CTol) **22**, [(DAC)Y](μ-*Z*-PhC=C=CTol) **23**, [{DAC)Y(μ-C≡CTol) (μ-C≡CPh)]$_2$ **24**. ^1H NMR data and GC results for the enynes produced by hydrolysis of the cross coupling reaction are summarized in Table 18.

***Para*-chlorophenylacetylene**[119] To a 200 mL Schlenk flask cooled at 0°C and flushed with nitrogen, was first added PCl_5 (6.4 g, 30.7 mmol) followed by careful addition of *p*-chloroacetophenone (5 g, 32.4 mmol). The flask was fitted with a condenser and the reaction mixture was heated to 70 °C under nitrogen for 3 h. The flask was cooled and the condenser replaced by a short path distillation apparatus to remove volatile $POCl_3$ (bp. 103 °C, 760 mm Hg) at 30 - 40 °C and 0.8 mm Hg from the chlorostyrenes, 1-(4-chlorophenyl)-1-chloroethylene and 1-(4-cholorophenyl)-1,1-dichloroethylene. After removal of the phosphorus oxychloride by-product, the chorostyrenes were collected (60-70°C, 0.8 mm Hg). Yield: 4.4 g. To a clean 250 mL round bottom flask were added the chlorostyrenes (4.4 g) and KOH (6 g) previously dissolved in absolute ethanol (18 g, 25% solution). The reaction flask was fitted with a condenser and the mixture was heated to reflux for 4 h. The contents of the flask were then immediately transferred while hot into a 1 L beaker containing ~100 ml ice. The solution was extracted with diethyl ether (3 x 100 mL), dried over $MgSO_4$, and evaporated to a volume of about 20 mL (20 °C, 22 mm Hg). The solution was transferred to a 100 mL Schlenk flask and the remaining ether was removed (20 °C, 22 mm Hg). The crude *p*-chlorophenylacetylene was vacuum sublimed (70 °C, 0.8 mm Hg) giving pure compound. Yield: 0.67g (15%). ^{1}H NMR (360 MHz, C_6D_6): δ 7.03 (d, 2H, *o*-aryl*H*, $^3J_{HH}$ = 8.8 Hz), 6.80 (d, 2H, *m*-aryl*H*, $^3J_{HH}$ = 8.6 Hz), 2.65 (s, 1H, ≡C*H*). ^{13}C NMR (90.56 MHz, C_6D_6): δ 133.5 (*o*-aryl*C*), 128.8 (*m*-aryl*C*), 82.63 (Ph-*C*≡C), 78.62 (C≡*C*H). Pure *p*-chlorophenylacetyene (0.120 g) was diluted with benzene (2.34 ml, 0.376M) and dried over 4Å molecular sieves

prior to use.

[{DAC)Y(μ-C≡CPh-Cl)]$_2$ (28) and [(DAC)Y](μ-(Z)-Cl-PhC=C=CPh-Cl) (29) A solution of *p*-chlorophenylacetylene (0.335 mL (290 mg) of a 0. 376 M solution in benzene, 0.126 mmol) was added to a solution of Y(DAC)(CH_2SiMe_3) (0.055 g, 0.126 mmol) in 10 mL benzene. The reagents were vigorously mixed by pipette action and a dark purple colour due to the presence of [(DAC)Y](μ-*Z*-Cl-PhC=C=CPh-Cl) **29** developed rapidly. Attempts to isolate X-ray quality crystals for structural analysis by slow evaporation of benzene were not successful, since the crystals formed plate-like aggregates. Yield: 15 mg (24.6%). However, the pure crystals were useful for NMR spectroscopy. The presence of **28** and **29** was clearly demonstrated by ^{1}H VTNMR of the aromatic region. ^{1}H NMR (360 MHz, C_6D_6, 348 K) **28**: δ 7.35 (d, 4H, *o*-aryl*H*, $^3J_{HH}$ = 8.4 Hz), 7.03 (d, 4H, *m*-aryl*H*, $^3J_{HH}$ = 8.3 Hz). (303 K) **29**: δ 7.45 (d, 4H, *o*-aryl*H*, $^3J_{HH}$ = 8.3 Hz), 7.24 (d, 4H, *m*-aryl*H*, $^3J_{HH}$ = 8.1 Hz).

***Para*-methoxyphenylacetylene**[120] To a 1L Schlenk flask containing *p*-methoxycinnamic acid (10g, 56.2 mmol) in 200 mL of dry $CHCl_3$ and cooled to 0 °C was added dropwise a solution of bromine (9.6 g, 60.0 mmol) in 200 mL of dry $CHCl_3$ under an atmosphere of nitrogen for a period of about 2 h. After addition, the mixture was allowed to stir at 0 °C for another hour and cyclohexene (50 mL) was added to the reaction mixture to remove excess bromine. The solvent was removed under reduced pressure (20 °C, 22 mm Hg) to give crude pale yellow *p*-methoxy-α,β-dibromocinnamic acid. This product was refluxed in 10% Na_2CO_3

(150 mL) for 2h and the cooled solution was extracted with diethyl ether (3 x 100 ml) which subsequently was dried over $MgSO_4$ followed by solvent removal under reduced pressure (20 °C and 22 mm Hg). The residue containing *p*-methoxy-α-bromocinnamic acid was added to a 1L Schlenk flask containing $KOC(CH_3)_3$ (4.59 g, 41.0 mmol) and *t*-butanol (200 ml) and the reaction mixture was refluxed under an atmosphere of argon for 4 h. The solvent was evaporated under reduced pressure (50 °C, 22 mm Hg). The residue was treated with water (300 mL) and extracted with diethyl ether (3 x 150 mL). The ether extracts were combined and dried over $MgSO_4$. After removal of solvent, crude *p*-methoxyphenylacetylene was obtained which was purified by distillation (70 °C, 0.8 mm Hg). Yield: 0.7 g (9.4 %). ^1H NMR (360 MHz, C_6D_6): δ 6.81 (d, 2H, *o*-aryl*H*, $^3J_{HH}$ = 9 Hz), 6.59 (d, 2H, *m*-aryl*H*, $^3J_{HH}$ = 8.8 Hz), 3.24 (s, 3H, C*H*$_3$), 3.14 (s, 1H, ≡C*H*). ^{13}C NMR (90.56 MHz, C_6D_6): δ 160.1 (*p*-aryl*C*), 136.9 (*o*-aryl*C*), 127.6 (*m*-aryl*C*), 114.3 (C≡*C*H). 104.3 (Ph-*C*≡C), 54.7 (*C*H$_3$0). Pure *p*-methoxyphenylacetyene (0.060 g) was diluted with benzene (1.26 mL, 0.360M) and dried over 4Å molecular sieves prior to use.

[{DAC)Y(μ-C≡CPh-OMe)]$_2$ (30) A solution of *p*-methoxyphenylacetylene (0.191 mL (182 mg) of a 0.360 M solution in d_6-benzene, 0.0688 mmol) was added to a solution of Y(DAC)(CH_2SiMe_3) (0.030 g, 0.0688 mmol) in 0.5 mL d_6-benzene. The reagents were vigorously mixed by pipette action and the colour of the solution was pink due to the small amount of [(DAC)Y](μ-(Z)-MeO-PhC=C=CPh-OMe) **31** formed. The pink solution was

transferred to a NMR tube fitted with a teflon valve (Brunfeldt) and the ^{1}H NMR spectra was recorded. Since this spectra was quite clean, ^{1}H VTNMR was performed on this sample to identify **30** and **31**. ^{1}H NMR (360 MHz, C_6D_6, 283 K) **30**: δ 7.59 and 7.56 (two br d, 4H, *o*-aryl*H* (one set is from **30** and the other set is from the monoacetylide complex, neither could be assigned), 6.79 and 6.71 (two br d, 4H, *m*-aryl*H*). (283 K) **31**: δ 7.80 (d, 4H, *o*-aryl*H*, $^3J_{HH}$ = 8.7 Hz), 6.95 (d, 4H, *m*-aryl*H*, $^3J_{HH}$ = 8.1 Hz).

1,4-diethynylbenzene[121] To a 1L Schlenk flask under nitrogen were added 1,4-dibromobenzene (23.6 g, 0.1 mole), 2-methylbut-3-yn-2-ol (20.2 g, 0.24 mole), dry diethylamine (120 mL), $(PPh_3)_2PdCl_2$ (280mg, 0.400 mmol), and CuI (80 mg, 0.42 mmol). The reaction mixture was heated at reflux for 16 h. After this time, triethylammonium bromide was filtered from the bright orange solution which darkens to brown when left exposed to air. Crude brown crystalline material analyzing for 1,4-bis(2-hydroxy-2-methyl-but-3-ynyl) benzene (8 g, 33%) was isolated after removing the solvent. This material was used without further purification to make the diacetylene. In order to remove the alcohol protecting groups, the diol (8 g, 0.033 mol) was dissolved in a gently boiling solution of sodium (300 mg) in *iso*-propyl alcohol (200 mL) in a tall (30 cm) Schlenk. The reaction mixture was heated without using a condenser and a steady stream of nitrogen was passed through the Schlenk. Over a 4 h period half the volume of *iso*-propyl alcohol along with the acetone byproduct were allowed to evaporate. After the 4 h heating period, the cooled solution was diluted with diethyl ether (200

mL), washed with water (3 x 75 mL), and the organic product was dried over $MgSO_4$. Crude 1,4-diethynylbenzene was obtained after removal of diethyl ether under reduced pressure (20 ° C, 22 mm Hg). Sublimation of this material afforded pure white crystalline product. Yield: 2g (48%). Mp: 91-92 ° C. Pure 1,4-diethynyl benzene (0.100 g) was diluted with benzene (2.0 mL, 0.40 M) and dried over 4Å molecular sieves prior to use.

4,4'-diethynlbiphenyl was prepared by a method similar to 1,4-diethynylbenzene (above). 4,4'-dibromobiphenyl (5g, 0.016 mole), 2-methylbut-3-yn-2-ol (3.1g, 0.037 mole), dry diethylamine (50 mL), $(PPh_3)_2PdCl_2$ (45mg, 0.064 mmol), and CuI (15 mg, 0.079 mmol) yielded 4,4'-bis(2-hydroxy-2-methyl-4-but-3-ynyl) biphenyl which followed deprotection of the acetylene with a gently boiling solution of sodium (300 mg) in *iso*-propyl alcohol (200 ml) gave crude 4,4'-diethynylbiphenyl. After sublimation diacetylene with few impurities were obtained: Yield : 0.150 g (4.7%). Mp: 80-85 °C. ^1H NMR: δ 7.24 (aryl), 3.13 (≡C*H*). 4,4'-ethynyl biphenyl (30 mg) was diluted with benzene (2.29 ml, 0.065 M) and dried over 4Å molecular sieves prior to use.

Poly-enyne In a typical reaction, a solution of $Y(DAC)(CH_2SiMe_3)$ (0.020 g, 0.0459 mmol) in 10 mL benzene was added to half an equivalent of a solution of 1,4-ethynylbenzene (0.115 mL of 0.40 M, 0.0464 mmol) in 10 mL benzene. On addition of the diacetylene, the solution became orange in colour and very turbid. The pale yellow

supernanant contained H_2DAC and the orange precipitate was insoluble in hydrocarbon, THF, and aromatic solvents. The reaction of 4,4'-diethynyl biphenyl (0.176 mL of 0.065 M, 0.0115 mmol) and Y(DAC)(CH_2SiMe_3) (0.010 g, 0.0229 mol) followed the same course of events.

Cis*- and *trans*-Zr(DAC)($CH_2Ph)_2$ (*cis*-/*trans*-32)** A solution of H_2DAC (0.215 g, 0.953 mmol) in 20 mL toluene was added rapidly to a stirred solution of $Zr(CH_2Ph)_4$ (0.434 g, 0.953 mmol) in 20 mL toluene. After stirring for 1 h, the stir bar was removed and the reaction solution was cooled at -30 °C overnight. Pale yellow (cis*-32**) and orange (***trans*-32**) slowly deposited and were collected by decanting the mother liquor. Combined yield: 0.41 g (80 %). Manual separation afforded the pure *cis* and *trans* isomers in a 1:4 ratio. ***cis*-32**: Mp. 85-86 °C. Anal. Calcd for $C_{26}H_{38}N_2O_4Zr$: C, 58.50; H, 7.18; N, 5.24. Found: C, 58.05; H, 7.11; N, 4.95. ***trans*-32**: Mp. 108-110 °C. Anal. Calcd for $C_{26}H_{38}N_2O_4Zr$: C, 58.50; H, 7.18; N, 5.24. Found: C, 57.92; H, 7.15; N, 5.00. Pure samples of ***cis*-** or ***trans*-32** slowly isomerized back to a 1:4 equilibrium mixture over a period of days in d_6-benzene or weeks in d_8-THF. NMR data for *cis* and ***trans*-32** are summarized in Table 20 and 21, respectively.

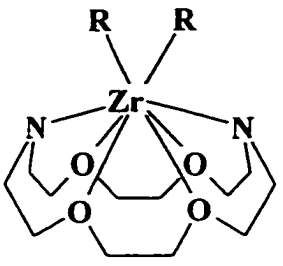

***Cis*-Zr(DAC)R_2 (R = CH_2SiMe_3, *cis*-34; CH_2CMe_3, *cis*-35)** H_2DAC (0.053 g, 0.20 mmol) and $Zr(CH_2Ph)_2Cl_2$ (0.10 g, 0.20 mmol) were separately dissolved in 10 mL of toluene, followed by dropwise addition of the H_2DAC solution to that of the zirconium complex. Immediate precipitation of a white solid, presumed to be polymeric $[Zr(DAC)Cl_2]_x$, **33** was observed. After stirring for 1 h, a solution of the appropriate alkyllithium reagent (2 equiv) was added and the resulting suspension was stirred for a further 30 minutes. This suspension was then filtered through celite and the clear, pale yellow filtrate was concentrated to ca. 2 mL and cooled at -30 °C. Crystals of pure ***cis*-34** (colourless) and ***cis*-35** (pale yellow) were collected by decanting the mother liquors. ***cis*-34**: Yield: 0.097 g (92 %). Mp. dec. 165 °C. ^{29}Si NMR (d_6-benzene, 49.69 MHz): δ 0.24. ***cis*-35**: Yield: 0.080 g (81 %). Mp. dec. 190 °C. Anal. Calcd for $C_{22}H_{46}N_2O_4Zr$: C, 53.51; H, 9.39; N, 5.67. Found: C, 52.49; H, 9.01; N, 5.19. NMR data are collected in Table 23 for both *cis*-**34** and *cis*-35.

$[Zr(DAC)(CH_2Ph)]^+[BPh_4]^-$ (36) Reaction of a mixture of *cis*- and ***trans*-32** (0.060 g, 0.11 mmol) with one equivalent of $[n\text{-}Bu_3NH]^+[BPh_4]^-$ (0.057 g, 0.11 mmol) in benzene resulted in precipitation of **36** as a pale yellow solid. Yield: 0.080 g (95 %). Mp. dec. 180 °C. Anal. Cacld for $C_{43}H_{51}BN_2O_4Zr$: C, 67.79; H, 6.75; N, 3.67. Found: C, 66.80; H, 6.44; N, 3.44. Complex **36** is soluble only in THF. The presence of n-Bu_3N

was evident in the ^1H and ^{13}C NMR spectra. ^1H NMR and ^{13}C NMR (d_8-THF) data for complex **36** are summarized in Table 24.

$[Zr(DAC)(CH_2Ph)]^+[B(CH_2Ph)(C_6F_5)_3]^-$ (37) Reaction of a mixture of ***cis***- and ***trans*-32** (1.00 g, 1.88 mmol) with one equivalent of $B(C_6F_5)_3$ (0.960 g, 1.88 mmol) in benzene resulted in quantitative formation of **37** as a sparingly soluble, bright yellow oil. This oil was freely soluble in d_8-THF and CD_2Cl_2 but we were unsuccessful in crystallizing **37** from these solvents, either neat or as mixtures with toluene or hexane. Satisfactory elemental data could not be obtained, probably due to difficulties in removing trace solvent. ^{19}F NMR (CD_2Cl_2, 338.86 MHz): δ -129.6 (*o*-aryl*F*, d, $^3J_{FF}$ = 22 Hz), -162.9 (*m*-aryl*F*, t, $^3J_{FF}$ = 22 Hz), -165.8 (*p*-aryl*F*, t, $3J_{FF}$ = 21 Hz). Table 25 summarizes the ^1H and ^{13}C NMR data for **37**.

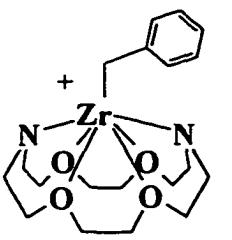

$[B(CH_2Ph)(C_6F_5)_3]^-$

Reaction of 37 with excess *p*-tolylacetylene. An excess of *p*-tolylacetylene (20-fold excess, 2.0 mmol) was added to an Schlenk tube containing a solution of **37** in toluene (0.10 mmol in 20 mL). The solution was stirred vigorously and samples were withdrawn periodically and hydrolyzed for examination by GC to determine the extent of conversion. Catalytic dimerization of *p*-tolylacetylene to an isomeric mixture of 1,4-di-*p*-tolyl-3-buten-1-ynes (*Z*:*E* ratio = 85:15) was observed giving an initial turnover rate of 2 mol enyne/mol

37 • h. The product was identified by comparison of the ^{1}H spectra with literature values for the phenyl analog[122] and by comparison of the GC-MS traces of the hydrolyzed product with an authentic sample.

[Zr(DAC)(N(t-Bu)CH=CHPh)]$^+$[B(CH$_2$Ph)(C$_6$F$_5$)$_3$]$^-$ (38)

A toluene solution of t-butylisonitrile (0.413 mL of a 0.136 M solution; 0.056 mmol) was added to a stirred solution of **37** (generated *in situ* from 0.030 g ***cis-/trans*-32** and 0.029 g B(C$_6$F$_5$)$_3$ in 10 mL toluene). After stirring for 1 h, the volatiles were removed under reduced pressure to yield **38** as a yellow oil. ^{19}F NMR (CD_2Cl_2, 338.86 MHz): δ -129.6 (*o*-aryl*F*, d, $^3J_{FF}$ = 24 Hz), -162.8 (*m*-aryl*F*, m), -165.8 (*p*-aryl*F*, t, $^3J_{FF}$ = 21 Hz). Table 27 summarizes the ^{1}H and ^{13}C NMR data. Not included in Table 26 are the resonaces due to DAC and the ^{13}C resonances from the benzyl group. For these resonances: ^{1}H NMR (CD_2Cl_2, 360 MHz), DAC C*H*$_2$: 4.42 (m, 2H), 4.32(m, 2H), 4.25 (m, 2H), 4.19 (m, 2H), 4.00 (m, 2H), 3.95 (m, 2H), 3.89 (m, 2H), 3.84 (m, 2H), 3.73 (m, 2H), 3.53 (m, 2H), 3.32 (m, 2H). ^{13}C NMR (CD_2Cl_2, 90.55 MHz), *aryl*: 149.9 (*ipso*), 139.1 (*ipso*), 129.0, 127.2, 125.8, 125.4, 122.8; DAC: 77.1 (O*C*H$_2$), 73.6 (O*C*H$_2$), 73.2 (O*C*H$_2$), 69.2 (O*C*H$_2$), 55.1 (N*C*H$_2$), 54.8 (N*C*H$_2$).

Tetraethylene glycol di(*p*-toluenesulphonate). Tetraethylene glycol (36 g, 0.185 mol), CH_2Cl_2 (600 mL) and 2.5-fold excess of triethylamine (46.8 g, 0.463 mol) to an 2L Erlymmer flask and the mixture was cooled at 0°C. To the stirred mixture was added *p*-toluene sulfonyl chloride (70.67 g, 0.371 mol) in small portions. The rate of addition was carefully controlled because the reaction is very exothermic. After this addition was complete, the reaction mixture was stirred for 12 h. The solution was suction filtered to remove triethylammonium chloride. The organic product was washed with 0.1M HCl (3 x 200 mL) to remove unreacted triethylamine, followed by water (5 x 200 mL) and a saturated solution of $NaHCO_3$ (5 x 200 mL). The organic layer was dried over $MgSO_4$, the solution filtered and the solvent evaporated under reduced pressure (30 °C, 22 mm Hg) giving a orange oil for tetraethylene glycol di(*p*-toluenesulphonate). Yield was quantitative. ^{1}H NMR (300 MHz, $CDCl_3$): δ 7.74 (d, 4H, *o*-aryl*H*, $^3J_{HH}$ = 8.4 Hz), 7.28 (d, 4H, *m*-aryl*H*, $^3J_{HH}$ = 8.5 Hz), 4.08 (t, 4H, ArOC*H*$_2$, $^3J_{HH}$ = 4.8 Hz), 3.61 (t, 4H, OC*H*$_2$CH$_2$OAr, $^3J_{HH}$ = 4.8 Hz), 3.49 (s, 8H, C*H*$_2$C*H*$_2$OC*H*$_2$C*H*$_2$), 2.37 (s, 6H, C*H*$_3$). ^{13}C NMR (90.55 MHz, $CDCl_3$): 144.7 (ipso), 132.7 (*para*-aryl), 129.67 (*ortho*-aryl), 127.7 (*meta*-aryl), 70.45, 70.29, 69.14, 68.42 (CH_2), 21.4 (*C*H$_3$).

Mono-Aza-18-Crown-6 (HMAC)[106] A 1.3-fold excess of K-OC$(CH_3)_3$ (29.5 g, 0.263 mol) was weighed into a 1L Schlenk flask in the glove box. Outside the glove box and under an atmosphere of argon, diethanolamine (21.2 g, 0.202 mol) and *t*-butylalcohol

(350 mL) were added to the Schlenk containing K-OC(CH_3)$_3$ giving a slightly turbid solution. A solution of tetraethylene glycol di(*p*-toluenesulphonate) (50.8 g, 0.101 mol) in *p*-dioxane (150 mL) was introduced to the stirred mixture by slow dropwise addition over a period of 2 h at 40 °C. After addition the extremely turbid reaction mixture was allowed to stir for another two hours. The insoluble precipitates were removed by suction filtration and washed with dichloromethane which was combined with the mother solution and the solvent was removed under reduced pressure (50 °C, 22 mm Hg). Water (20 mL) was added to the oily yellow residue and the solution was extracted with hexane (3 x 50 ml) to remove the hexane soluble-byproducts. The aqueous fraction was extracted with CH_2Cl_2 (3 x 100 mL) and the organic solution was dried over $MgSO_4$. The solvent was evaporated under reduced pressure (60 °C, 22 mm Hg) to give crude HMAC. Pure HMAC was obtained by vacuum sublimation (130-140 °C, 0.8 mmHg). Yield: 6.5g (12.2%), ^{1}H NMR (360 MHz, $CDCl_3$): δ 3.56-3.68 (m, 20H), 2.76 (t, 4H, $^3J_{HH}$ = 4.82 Hz), 2.08 (br s, 1H, N*H*). ^{13}C NMR (90.55 MHz, $CDCl_3$): δ 70.71, 70.48, 70.43, 70.56, 70.30, 49.2.

Triethylene glycol di(*p*-toluenesulphonate) This compound was prepared using a method similar to that above using triethylene glycol (50 g, 0.333 mol), *p*-toluenesulfonyl chloride (127 g, 0.666 mol), and 2.5-fold excess of triethylamine (84.2, 0.832 mol) in 400 mL CH_2Cl_2. After workup, a white solid was obtained for triethylene glycol di(*p*-toluenesulphonate). Yield: Quantitative. ^{1}H NMR (360 MHz, $CDCl_3$): δ 7.76 (d, 4H,

o-aryl*H*, $^3J_{HH}$ = 8.4 Hz), 7.31 (d, 4H, *m*-aryl*H*, $^3J_{HH}$ = 8.5 Hz), 4.10 (t, 4H, ArOCH_2, $^3J_{HH}$ = 4.8 Hz), 3.62 (t, 4H, OCH_2CH$_2$OAr, $^3J_{HH}$ = 4.8 Hz), 3.49 (s, 8H, CH_2OCH_2), 2.41 (s, 6H, CH_3). ^{13}C NMR (90.55 MHz, $CDCl_3$): 144.8 (ipso), 132.8 (*para*-aryl), 129.8 (*ortho*-aryl), 127.9 (*meta*-aryl), 70.62, 69.17, 68.66 (CH_2), 21.6 (CH_3).

Mono-Aza-15-Crown-5 (H-15-AC-5)[106] The macrocycle was prepared by a method similar to that for HMAC (above), using triethylene glycol di(*p*-toluenesulphonate) (39.8 g, 0.087 mol), diethanolamine (18.29 g, 0.174 mol), with the exception that $NaOC(CH_3)_3$ was generated *in situ* by the dissolution of 1.3-fold excess sodium (5 g, 0.217 mol) in 400 mL of *t*-butanol. After reaction and workup, distillation (130-140 °C, 0.8 mm Hg) gave a pure viscous oil of H-15-AC-5. Yield: 8 g (42 %). ^{1}H NMR (300 MHz, $CDCl_3$): δ 3.64 (overlapping singlets, 16 H), 2.78 (t, 4H, CH_2NH), NH resonance is not observed.

Y(MAC)(CH$_2$SiMe$_3$)$_2$ (40) A solution of HMAC[106] (0.27 g, 0.10 mmol) in 20 mL of toluene was added dropwise to a vigorously stirred solution of Y(CH$_2$SiMe$_3$)$_3$(THF)$_2$[34], (0.50 g, 0.10 mmol) in 20 mL toluene. The solution was stirred for 1 h followed by removal of the solvent under reduced pressure. Recrystallization of the resulting white powder from a toluene-hexane mixture produced colourless crystals of **40**. Yield: 0.40 g (76 %). Mp: 130 °C dec. ^{1}H and ^{13}C NMR data for **40** in d_8-THF and in d_6-benzene are

summarized in Table 27. $^{29}Si\{^1H\}$ NMR (49.69 MHz, C_6D_6): δ -2.05 ppm.. Anal. Calcd for $C_{20}H_{46}NO_5Si_2Y$: C, 45.70; H, 8.82; N, 2.66. Found: C, 45.57; H, 8.51; N, 2.98.

Y(MAC)(OC(SiMe$_3$)=CH$_2$)$_2$ 41 A solution of **40** (0.030 g, 0.057 mmol) in 0.75 mL d_6-benzene was placed in a NMR tube fitted with a teflon valve (Brunfeldt). After cooling in liquid nitrogen, the sample was degassed and allowed to warm to room temperature under an atmosphere of CO prior to sealing. The NMR spectra showed clean formation of **41**.

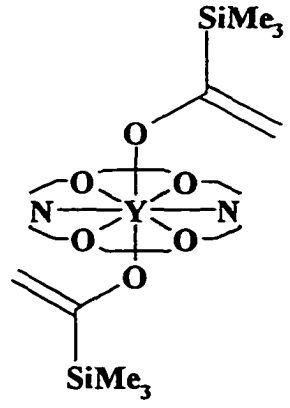

Complex **41** was isolated as a greasy solid after washing with cold hexane. ^1H and ^{13}C NMR data are found in Table 29. IR (Nujol, KBr): 1618, 1567 (w, νC=C) cm^{-1}. Anal. Calcd for $C_{22}H_{46}NO_7Si_2Y$: C, 45.43; H, 7.97; N, 2.41. Found: C, 43.91; H, 7.48; N, 2.87. Despite repeated attempts, no better elemental analysis could be obtained.

Y(15-AC-5)(CH$_2$SiMe$_3$)$_2$ 42 A solution of H-15-AC-5[106] (0.55 g, 2.51 mmol) in 20 mL of toluene was added dropwise to a vigorously stirred solution of $Y(CH_2SiMe_3)_3(THF)_2$[34] (1.24 g, 2.51 mmol) in 20 mL toluene. The solution was stirred for 30 min followed by removal of the solvent under reduced pressure. Recrystallization of the viscous oily residue from a toluene-hexane mixture afforded a small quantity of colourless crystals of **42**. Yield: 0.15 g (12.4 %). NMR data for **42** are summarized in Table 30.

[Y(MAC)(CH_2SiMe_3)]$^+$[B(CH_2SiMe_3)(C_6F_5)$_3$]$^-$ 43 Complex **40** (0.030 g, 0.057 mmol) and B(C_6F_5)$_3$ (0.029 g, 0.057 mmol) were placed in an NMR tube under argon. Dry, degassed d_8-THF (0.50 mL) was added with a syringe and the sample was sealed. The sample was immediately examined by ^{1}H, ^{19}F and ^{13}C{^{1}H} NMR spectroscopy at -10 °C. The reaction mixture contained resonances due to one major product, although minor resonances due to **40**, TMS and other unidentified products were also present. ^{1}H NMR (360 MHz): 3.90-4.15 (16H, macrocycle), 3.45-3.65 (4H, macrocycle), 3.20 (4H, macrocycle), 0.12 (br s, BCH_2SiMe$_3$), -0.06, -0.11 (s, SiMe_3), -1.16 (d, YCH_2SiMe$_3$, $^2J_{YH}$ = 3.2 Hz). ^{19}F NMR (338.38 MHz): -132.4 (d, *o*-aryl-*F*, $^3J_{FF}$ = 20 Hz), -165.2 (t, *p*-aryl-*F*, $^3J_{FF}$ = 21 Hz), -167.7 (br t, *m*-aryl-*F*, $^3J_{FF}$ = 18 Hz). ^{13}C{^{1}H} NMR (90.55 MHz): 74.4, 69.6, 69.0, 68.7, 68.5 (OCH_2, macrocycle), 54.1 (NCH_2, macrocycle), 32.4 (d, YCH_2, $^1J_{YC}$ = 37 Hz), -1.9 (SiMe_3), -2.5 (SiMe_3). The ^{13}C resonance due to the CH_2 group bonded to boron was difficult to assign with confidence due to ^{11}B broadening. The TMS resonance slowly increased over time at the expense of the other SiMe$_3$ resonances and the solution turned brown. The above reaction was repeated with the exception that d_5-pyridine was used as the solvent and ^{1}H, ^{13}C, and ^{19}F NMR data were recorded at ambient temperature. The ^{1}H and ^{13}C NMR data are summarized in Table 31. ^{19}F (338.38 MHz): -131.9 (d, *o*-aryl-*F*, $^3J_{FF}$ = 22 Hz), -160.8 (t, *p*-aryl-*F*, $^3J_{FF}$ = 21 Hz), -162.3 (br t, *m*-aryl-*F*, $^3J_{FF}$ = 21 Hz).

Thermal decomposition of $[Y(MAC)(CH_2SiMe_3)]^+[B(CH_2SiMe_3)(C_6F_5)_3]^-$ 43 A sealed NMR tube containing **43** in d_5-pyridine was heated at 70 °C for 2 weeks. After this period NMR data were collected. ^1H NMR (360 MHz, d_5-pyridine): 3.64 (s, 18H, MAC), 3.58 (t, 3H, MAC, $^3J_{HH}$ = 6.4), 3.10 (t, 3H, MAC, $^3J_{HH}$ = 6.4), 0.91 (s, 4H, CH_2SiMe_3), -0.02 (s,18H, CH_2SiMe_3). ^{13}C NMR (90.55 MHz): 73.06, 71.34, 71.10, 71.81, 70.81, 48.64 (MAC resonances), 0.10 (CH_2SiMe_3), -0.65 (CH_2SiMe_3). ^{19}F NMR (338.38 MHz): -131.9 (d, *o*-aryl-*F*, $^3J_{FF}$ = 22 Hz), -165.3 (t, *p*-aryl-*F*, $^3J_{FF}$ = 20 Hz), -165.9 (br t, *m*-aryl-*F*, $^3J_{FF}$ = 20 Hz). The whole number values for the peak integrals in the ^1H NMR are approximate. Although the NMR data might imply the doubly pyridine inserted product $Y(MAC)(C_5ND_5CH_2SiMe_3)_2$ **45**, the NMR assignments are tentative and further analysis is required to confirm the formation of **45**.

TMSMAC (47) To a solution of HMAC (2.55 g, 9.70 mmol) in 50 mL of THF was added dropwise *n*-BuLi (6.1 mL, 9.76 mmol) in 50 mL of THF at ambient temperature. The clear canary yellow solution was allowed to stir for 30 minutes. On addition of chlorotrimethylsilane (1.3 mL, 10.2 mmol) to this mixture, at ambient temperature, the solution became colourless. After allowing this solution to stir for 2 h, the solvent was removed under reduced pressure. The flask was transferred to the glove box for workup. The residue was extracted with hexane (30 mL), the extract filtered through Celite and the solvent was removed to afford 47 as a very pale yellow oil. ^1H

NMR (360 MHz, C_6D_6): δ 3.49 (overlapping t, 4H, OCH_2CH_2NTMS, $^3J_{HH}$ = 6.3 Hz), 3.47 (overlapping s, 16H, OCH_2CH_2O), 3.06 (t, 4H, OCH_2CH_2NTMS, $^3J_{HH}$ = 6.3 Hz), 0.086 (s, 9H, $SiMe_3$). ^{13}C NMR (90.55 MHz, C_6D_6): (MAC peaks; δ 73.15, 71.55, 71.28, 71.19, 70.92, 48.75), δ 0.173 ($SiMe_3$)

TMS-15-AC-5 (48) The above reaction was repeated using H-15-AC-5 (1.45 g, 6.62 mmol), *n*-BuLi (4.2 mL, 6.72 mmol) and chlorotrimethylsilane (0.89 mL, 7.01 mmol) to give **48** as a pale yellow oil. ^1H NMR (360 MHz, C_6D_6): macrocyclic protons δ 3.60 (t, 4H, $^3J_{HH}$ = 6.6 Hz), 3.45 (m, 8H), 3.33 (s, 4H), 3.07 (t, 4H, $^3J_{HH}$ = 5.9 Hz), 0.11 (s, 9H, $SiMe_3$). ^{13}C NMR (90.55 MHz, C_6D_6): (AC-methylene, δ 73.71, 72.06, 70.71, 70.38, 50.49), δ 0.128 ($SiMe_3$).

APPENDIX

X-RAY CRYSTALLOGRAPHIC DATA

The crystal structures presented in this thesis were solved by Mrs. Kathy Beveridge (complexes **8**, **9**, **11**, and **12**), Dr. Becky Chak (complexes **14**, **15**, and **16**), Professor Dave Berg (*cis*-**32** and *trans*-**32**), and Professor Fredrick Einstein and Mr. Raymond Batchelor (*trans*-**40**). In general the crystallographic data was obtained as follows. Single crystal were loaded in glass capillaries in the glove box, sealed under argon and transferred to a Nonius CAD4F diffractometer equipped with a Ni-filtered Cu Kα radiation. The unit cell was refined using 25 high angle reflections (> 35° in θ), Data were collected using three reference standards measured periodically during data collection. In general, decay of <10 % in the intensity of these standards was observed. Following data reduction, an absorption correction according to an empirical ψ scan was applied. The structure was solved using Patterson or direct methods and refined using SHELX86 or NRCVAX structure solving package. The structural drawings were done using ORTEP[123] or the ZORTEP[99] modification.

Summary of crystallographic data, fractional atomic coordinates with equivalent isotropic temperature factors and the complete lists of bond distances and angles are given in the following tables.

Table I Summary of crystallographic data for Y(DAC)[N(SiMe$_3$)$_2$] 8

empirical formula	$C_{18}H_{42}N_3O_4Si_2Y$
fw	509.6
crystal system	monoclinic
space group	$P2_1/n$ (No. 14)
a (A)	9.471(1)
b (A)	28.786(3)
c (A)	10.567(3)
α (deg)	90
β (deg)	114.45(1)
γ (deg)	90
V (A^3)	2622.5
Z	4
ρ (calcd) (g cm^{-3})	1.291
μ (cm^{-1})	42.81
radiation, λ (A)	Cu K_α, 1.542
temperature	ambient
$2\theta_{max}$ (deg)	60
no. of observed reflections	3682
no. of unique reflcns	2311
no. of parameters	253
R [a]	0.010
R_w [b]	0.124

[a] $R = \Sigma(|F_o| - |F_c|) / \Sigma|F_o|$ [b] $R_w = [\Sigma w(|F_o| - |F_c|)^2 / \Sigma w(|F_o|)^2]^{1/2}$

Table II Fractional atomic coordinates [a] and equivalent isotropic temperature factors [b] for Y(DAC)[N(SiMe$_3$)$_2$] 8

Atom	x/a	y/b	z/c	U_{eq}
Y(1)	22619(12)	34734(4)	-759(11)	504(5)
Si(1)	11.3(5)	397.9(2)	-331.5(4)	7.8(2)
Si(2)	346.9(6)	416.9(2)	-220.1(6)	10.4(3)
O(1)	413(2)	304.6(4)	-72(2)	11.1(8)
O(2)	359(2)	411.0(4)	177(2)	11.7(8)
O(3)	71(2)	411.8(6)	33(2)	12.3(8)
O(4)	131(2)	272.7(4)	-124.8(14)	13.0(7)
N(1)	438.7(14)	322.4(5)	180.8(13)	8.1(6)
N(2)	21(2)	320.0(7)	31(2)	11.8(9)
N(3)	194.9(13)	391.0(4)	-204.1(11)	6.4(5)
C(1)	527(3)	278.6(8)	43(3)	14(2)
C(2)	576(2)	309.4(11)	173(2)	13.8(13)
C(3)	474(3)	347.7(8)	309(2)	14.0(13)
C(4)	500(2)	396.0(7)	303(2)	13.1(11)
C(5)	287(3)	453.2(8)	190(3)	16(2)
C(6)	158(3)	458.7(8)	66(3)	13.9(14)
C(7)	9(4)	399.1(14)	122(3)	17(2)
C(8)	-80(3)	354.7(12)	68(3)	15(2)
C(9)	-65(3)	281.3(11)	-26(2)	16(2)
C(10)	36(4)	245.7(10)	-75(3)	18(2)
C(11)	227(4)	242.4(8)	-167(3)	17(2)
C(12)	335(4)	276.3(8)	-194(2)	15(2)
C(13)	-120(2)	348.6(6)	-328(2)	11.3(10)
C(14)	-85(2)	455.9(7)	-316(2)	12.1(11)
C(15)	1(3)	393.9(7)	-520(2)	11.4(11)
C(16)	520(2)	421.9(6)	-47(2)	10.3(9)
C(17)	419(3)	383.3(10)	-335(2)	16(2)
C(18)	312(3)	477.1(9)	-288(3)	19(2)

[a] x10^n where n = 5 for Y; n = 3 for Si, O, N, C [b] U_{eq} = 1/3 $\Sigma_i\Sigma_j U_{ij} a_i^* a_j^* (a_i \bullet a_j)$ A^2 x10^n where n = 4 for Y; n = 2 for Si, O, N, C.

TABLE III Bond distances(Å) and angles(deg)[a] for Y(DAC)[N(SiMe$_3$)$_2$] 8

Atoms		Distance	Atoms		Distance
O(1)	-Y(1)	2.467(11)	C(4)	-O(2)	1.506(20)
O(2)	-Y(1)	2.590(12)	C(5)	-O(2)	1.431(24)
O(3)	-Y(1)	2.514(12)	C(6)	-O(3)	1.545(26)
O(4)	-Y(1)	2.457(12)	C(7)	-O(3)	1.346(32)
N(1)	-Y(1)	2.283(12)	C(10)	-O(4)	1.443(25)
N(2)	-Y(1)	2.287(15)	C(11)	-O(4)	1.452(27)
N(3)	-Y(1)	2.338(11)	C(2)	-N(1)	1.384(23)
N(3)	-Si(1)	1.714(11)	C(3)	-N(1)	1.449(26)
C(13)	-Si(1)	1.895(18)	C(8)	-N(2)	1.537(30)
C(14)	-Si(1)	1.943(18)	C(9)	-N(2)	1.363(27)
C(15)	-Si(1)	1.957(16)	C(2)	-C(1)	1.535(31)
N(3)	-Si(2)	1.692(12)	C(4)	-C(3)	1.417(23)
C(16)	-Si(2)	1.890(18)	C(6)	-C(5)	1.377(31)
C(17)	-Si(2)	1.885(21)	C(8)	-C(7)	1.503(37)
C(18)	-Si(2)	1.849(22)	C(10)	-C(9)	1.623(38)
C(1)	-O(1)	1.454(24)	C(12)	-C(11)	1.530(36)
C(12)	-O(1)	1.444(23)			

Atoms			Angle	Atoms			Angle
O(2)	-Y(1)	-O(1)	112.2(5)	C(1)	-O(1)	-Y(1)	113.3(12)
O(3)	-Y(1)	-O(1)	162.1(5)	C(12)	-O(1)	-Y(1)	111.8(14)
O(3)	-Y(1)	-O(2)	59.2(4)	C(12)	-O(1)	-C(1)	112.4(17)
O(4)	-Y(1)	-O(1)	65.2(5)	C(4)	-O(2)	-Y(1)	116.1(10)
O(4)	-Y(1)	-O(2)	163.8(4)	C(5)	-O(2)	-Y(1)	124.6(14)
O(4)	-Y(1)	-O(3)	127.7(5)	C(5)	-O(2)	-C(4)	116.3(17)
N(1)	-Y(1)	-O(1)	67.0(5)	C(6)	-O(3)	-Y(1)	112.8(11)
N(1)	-Y(1)	-O(2)	65.7(4)	C(7)	-O(3)	-Y(1)	111.8(17)
N(1)	-Y(1)	-O(3)	116.9(5)	C(7)	-O(3)	-C(6)	115.1(22)
N(1)	-Y(1)	-O(4)	99.9(4)	C(10)	-O(4)	-Y(1)	116.3(15)
N(2)	-Y(1)	-O(1)	129.5(6)	C(11)	-O(4)	-Y(1)	122.2(15)
N(2)	-Y(1)	-O(2)	107.2(6)	C(11)	-O(4)	-C(10)	110.4(21)
N(2)	-Y(1)	-O(3)	67.8(6)	C(2)	-N(1)	-Y(1)	122.8(12)
N(2)	-Y(1)	-O(4)	68.0(7)	C(3)	-N(1)	-Y(1)	115.7(12)
N(2)	-Y(1)	-N(1)	104.2(5)	C(3)	-N(1)	-C(2)	109.6(17)
N(3)	-Y(1)	-O(1)	82.3(4)	C(8)	-N(2)	-Y(1)	118.9(16)
N(3)	-Y(1)	-O(2)	97.6(4)	C(9)	-N(2)	-Y(1)	126.6(17)
N(3)	-Y(1)	-O(3)	83.5(5)	C(9)	-N(2)	-C(8)	109.1(21)
N(3)	-Y(1)	-O(4)	97.9(4)	Si(1)	-N(3)	-Y(1)	118.4(6)
N(3)	-Y(1)	-N(1)	133.3(4)	Si(2)	-N(3)	-Y(1)	121.7(6)
N(3)	-Y(1)	-N(2)	122.5(5)	Si(2)	-N(3)	-Si(1)	119.9(7)

C(13)-Si(1)-N(3)	110.9(6)	C(2) -C(1) -O(1)	107.1(16)
C(14)-Si(1)-N(3)	113.2(7)	C(1) -C(2) -N(1)	105.5(16)
C(14)-Si(1)-C(13)	107.9(9)	C(4) -C(3) -N(1)	115.5(20)
C(15)-Si(1)-N(3)	113.6(8)	C(3) -C(4) -O(2)	102.2(15)
C(15)-Si(1)-C(13)	102.5(9)	C(6) -C(5) -O(2)	106.3(19)
C(15)-Si(1)-C(14)	108.1(9)	C(5) -C(6) -O(3)	107.3(21)
C(16)-Si(2)-N(3)	111.6(7)	C(8) -C(7) -O(3)	107.8(23)
C(17)-Si(2)-N(3)	112.8(9)	C(7) -C(8) -N(2)	109.9(20)
C(17)-Si(2)-C(16)	105.2(10)	C(10)-C(9) -N(2)	109.7(19)
C(18)-Si(2)-N(3)	115.4(10)	C(9) -C(10)-O(4)	108.2(20)
C(18)-Si(2)-C(16)	104.3(10)	C(12)-C(11) -O(4)	103.3(18)
C(18)-Si(2)-C(17)	106.7(14)	C(11)-C(12) -O(1)	108.9(16)

[a]Estimated standard deviations are given in parentheses.

Table IV Summary of crystallographic data for Ce(DAC)[N(SiMe$_3$)$_2$] 9

empirical formula	$C_{18}H_{42}N_3O_2Si_2Ce$
formula weight	560.81
crystal system	monoclinic
space group	$P2_1/n$ (No. 14)
a (Å)	9.557(1)
b (Å)	56.897(8)
c (Å)	10.777(2)
α (deg)	90
β (deg)	114.37(1)
γ (deg)	90
V (Å^3)	5338.0
Z	4
ρ (calcd) (g cm^{-3})	1.395
μ (cm^{-1})	N/A
radiation, λ (Å)	Cu K_α, 1.542
temperature	ambient
$2\theta_{max}$ (deg)	100
no. of observed reflections	4856
no. of unique reflections	2831
no. of parameters	251
R [a]	0.1143
R_w [b]	0.1382

[a] $R = \Sigma(|F_o| - |F_c|) / \Sigma|F_o|$ [b] $R_w = [\Sigma w(|F_o| - |F_c|)^2 / \Sigma w(|F_o|)^2]^{1/2}$

Table V Summary of crystallographic data {[$(Me_3Si)_2N$]Yb(μ-DAC)}$_2$Yb 11

empirical formula	$C_{36}H_{84}N_6O_8Si_4Yb_3$
formula weight	1360.6
crystal system	monoclinic
space group	$P2_1/n$ (No. 14)
a (Å)	19.982(3)
b (Å)	17.870(2)
c (Å)	16.933(3)
α (deg)	90
β (deg)	113.56(1)
γ (deg)	90
V (Å^3)	5542
Z	4
ρ (calcd) (g cm^{-3})	1.630
μ (cm^{-1})	103.45
radiation, λ (Å)	Cu K_α, 1.542
T	ambient
$2\theta_{max}$ (deg)	50
no. of observed reflections	4980
no. of unique reflections	2473
no. of parameters	264
R [a]	0.087
R_w [b]	0.104

[a] $R = \Sigma(|F_o| - |F_c|)/\Sigma|F_o|$ [b] $R_w = [\Sigma w(|F_o| - |F_c|)^2/\Sigma w(|F_o|)^2]^{1/2}$

Table VI Fractional atomic coordinates[a] and equivalent isotropic temperature factors[b] for{[$(Me_3Si)_2N$]Yb(μ-DAC)}$_2$Yb 11

Atom	x/a	y/b	z/c	Ueq
Yb(1)	474.4(13)	1535.0(10)	2518.3(14)	54.8(10)
Yb(2)	-1239.9(10)	1507.2(12)	2688.3(11)	52.2(11)
Yb(3)	2202.6(11)	1454.4(11)	2359.0(13)	56.4(11)
Si(1)	-2654(7)	713(7)	3246(8)	77(7)
Si(2)	-3061(8)	1955(8)	2027(10)	95(8)
Si(3)	3954(8)	2157(7)	2771(9)	90(8)
Si(4)	3639(8)	691(7)	1847(9)	90(9)
O(1)	-80.6(14)	172.8(13)	431(2)	8.4(9)'
O(2)	-85(2)	284.9(14)	318(2)	8.4(9)'
O(3)	-178(2)	107(2)	114(2)	11.3(11)'
O(4)	-103.9(14)	17.4(12)	241(2)	7.0(8)'
O(5)	175(2)	265(2)	153(2)	9.7(10)'
O(6)	163(2)	138(2)	71(2)	11.0(10)'
O(7)	217(2)	17(2)	300(3)	13.7(13)'
O(8)	274.7(14)	134.7(14)	400(2)	8.4(9)'
N(1)	-246(2)	136.3(14)	266(2)	6.4(9)'
N(2)	341(2)	143(2)	233(2)	7.4(10)'
N(3)	7.1(14)	103.3(14)	353(2)	5.1(8)'
N(4)	-64(2)	219(2)	178(2)	6.6(9)'
N(5)	157(2)	229(2)	302(2)	7.2(10)'
N(6)	95(2)	78(2)	174(3)	13(2)'
C(1)	-185(2)	7(2)	391(3)	8.9(14)'
C(2)	-298(3)	115(3)	408(4)	15(2)'
C(3)	-334(3)	-1(3)	265(4)	13(2)'
C(4)	-264(3)	266(2)	158(3)	12(2)'
C(5)	-354(3)	257(3)	252(4)	19(3)'
C(6)	-378(4)	159(3)	112(5)	20(3)'
C(7)	353(2)	282(2)	332(3)	8.8(14)'
C(8)	418(3)	275(3)	200(4)	14(2)'
C(9)	491(3)	192(3)	371(4)	18(3)'
C(10)	288(2)	-5(2)	147(3)	9(2)'
C(11)	389(3)	96(3)	98(4)	16(2)'
C(12)	447(4)	11(4)	262(4)	20(3)'
C(13)	44(2)	145(2)	438(3)	10(2)'
C(14)	-8(2)	150(2)	485(3)	8.9(13)'
C(15)	-110(2)	249(2)	437(3)	10(2)'
C(16)	-63(3)	306(3)	411(3)	12(2)'

C(17)	-35(2)	320(2)	83(3)	7.7(14)'
C(18)	-69(2)	303(2)	190(3)	9(2)'
C(19)	-109(2)	205(2)	83(3)	8.9(14)'
C(20)	-127(2)	123(2)	74(3)	9(2)'
C(21)	-203(3)	32(3)	108(3)	10(2)'
C(22)	-141(3)	-20(3)	164(3)	12(2)'
C(23)	-34(2)	-21(2)	290(3)	7.2(13)'
C(24)	4(2)	24(2)	376(3)	8.1(13)'
C(25)	149(3)	309(2)	268(3)	11(2)'
C(26)	118(3)	305(2)	170(3)	10(2)'
C(27)	150(3)	271(3)	57(4)	14(2)'
C(28)	187(3)	215(3)	39(4)	14(2)'
C(29)	92(4)	107(3)	27(4)	16(3)'
C(30)	53(3)	102(3)	76(5)	16(2)'
C(31)	106(2)	3(2)	170(3)	10(2)'
C(32)	147(3)	-13(3)	276(4)	12(2)'
C(33)	270(3)	4(3)	388(5)	18(3)'
C(34)	311(3)	62(3)	432(3)	12(2)'
C(35)	224(3)	161(3)	437(3)	11(2)'
C(36)	199(2)	235(2)	401(3)	10(2)'

[a] $x10^n$ where n = 4 for Yb, Si ; n = 3 for O, N, C

[b] U_{eq} = 1/3 $\Sigma i \Sigma j U_{ij} a_i^* a_j^* (a_i . a_j)$ A^2 $x10^n$ where n = 3 for Yb, Si; n = 2 for O, N, C. Primed values indicate that U_{iso} is given $T = \exp(-8\pi^2 U_{iso} \sin^2\theta/\lambda^2)$

estimated standard deviations in parentheses

Table VII Bond distances (Å) and angles (deg)[a] for {[$(Me_3Si)_2N$]Yb(μ-DAC)}$_2$Yb 11

Atoms	Distance	Atoms	Distance
N(3)-Yb(1)	2.34(3)	C(20)-O(3)	1.45(5)
N(4)-Yb(1)	2.38(3)	C(15)-O(1)	1.50(4)
N(5)-Yb(1)	2.41(3)	C(14)-O(1)	1.43(4)
N(6)-Yb(1)	2.34(5)	C(16)-O(2)	1.50(5)
O(1)-Yb(2)	2.56(3)	C(21)-O(3)	1.42(4)
O(2)-Yb(2)	2.56(3)	C(22)-O(4)	1.38(5)
O(3)-Yb(2)	2.52(3)	C(23)-O(4)	1.48(4)
O(4)-Yb(2)	2.49(2)	C(26)-O(5)	1.46(5)
N(1)-Yb(2)	2.43(3)	C(27)-O(5)	1.50(6)
N(3)-Yb(2)	2.57(3)	C(28)-O(6)	1.62(6)
N(4)-Yb(2)	2.61(3)	C(29)-O(6)	1.41(6)
O(5)-Yb(3)	2.52(3)	C(32)-O(7)	1.39(5)
O(6)-Yb(3)	2.57(3)	C(34)-O(8)	1.48(5)
O(7)-Yb(3)	2.56(3)	C(35)-O(8)	1.47(5)
O(8)-Yb(3)	2.56(3)	C(13)-N(3)	1.52(5)
N(2)-Yb(3)	2.44(3)	C(24)-N(3)	1.49(4)
N(5)-Yb(3)	2.50(3)	C(18)-N(4)	1.52(4)
N(6)-Yb(3)	2.59(4)	C(19)-N(4)	1.51(5)
N(1)-Si(1)	1.67(3)	C(25)-N(5)	1.53(5)
C(1)-Si(1)	1.92(4)	C(36)-N(5)	1.56(5)
C(2)-Si(1)	1.94(6)	C(30)-N(6)	1.58(7)
C(3)-Si(1)	1.86(5)	C(31)-N(6)	1.37(5)
N(1)-Si(2)	1.63(3)	C(14)-C(13)	1.54(6)
C(4)-Si(2)	1.84(5)	C(16)-C(15)	1.56(6)
C(5)-Si(2)	1.85(7)	C(18)-C(17)	1.48(5)
C(6)-Si(2)	1.75(6)	C(20)-C(19)	1.50(5)
N(2)-Si(3)	1.67(3)	C(22)-C(21)	1.54(5)
C(7)-Si(3)	1.91(5)	C(24)-C(23)	1.57(5)
C(8)-Si(3)	1.88(6)	C(26)-C(25)	1.53(6)
C(9)-Si(3)	1.98(6)	C(28)-C(27)	1.35(6)
N(2)-Si(4)	1.70(3)	C(30)-C(29)	1.36(8)
C(10)-Si(4)	1.92(4)	C(32)-C(31)	1.66(6)
C(11)-Si(4)	1.81(6)	C(34)-C(33)	1.34(6)
C(12)-Si(4)	1.95(6)	C(36)-C(35)	1.44(5)
C(17)-O(2)	1.49(4)	C(33)-O(7)	1.46(6)

Atoms	Angle	Atoms	Angle
N(4)-Yb(1)-N(3)	93.1(10)	N(6)-Yb(3)-O(7)	64.4(12)
N(5)-Yb(1)-N(3)	118.9(10)	N(6)-Yb(3)-O(8)	109.2(12)
N(5)-Yb(1)-N(4)	115.5(9)	N(6)-Yb(3)-N(2)	141.9(12)
N(6)-Yb(1)-N(3)	122.0(12)	N(6)-Yb(3)-N(5)	82.9(12)
N(6)-Yb(1)-N(4)	119.4(13)	C(1)-Si(1)-N(1)	115(2)
N(6)-Yb(1)-N(5)	90.4(12)	C(2)-Si(1)-N(1)	112(2)
O(2)-Yb(2)-O(1)	64.9(8)	C(2)-Si(1)-C(1)	105(2)
O(3)-Yb(2)-O(1)	169.2(9)	C(3)-Si(1)-N(1)	117(2)
O(3)-Yb(2)-O(2)	125.3(10)	C(3)-Si(1)-C(1)	99(2)
O(4)-Yb(2)-O(1)	109.7(8)	C(3)-Si(1)-C(2)	107(3)
O(4)-Yb(2)-O(2)	155.0(8)	C(4)-Si(2)-N(1)	112(2)
O(4)-Yb(2)-O(3)	62.8(9)	C(5)-Si(2)-N(1)	117(3)
N(1)-Yb(2)-O(1)	86.9(9)	C(5)-Si(2)-C(4)	101(3)
N(1)-Yb(2)-O(2)	106.4(9)	C(6)-Si(2)-N(1)	117(2)
N(1)-Yb(2)-O(3)	86.4(11)	C(6)-Si(2)-C(4)	104(3)
N(1)-Yb(2)-O(4)	97.5(8)	C(6)-Si(2)-C(5)	103(3)
N(2)-Yb(3)-O(5)	98.5(10)	C(7)-Si(3)-N(2)	112(2)
N(2)-Yb(3)-O(6)	89.4(10)	C(8)-Si(3)-N(2)	115(2)
N(2)-Yb(3)-O(7)	100.9(11)	C(8)-Si(3)-C(7)	105(2)
N(3)-Yb(2)-O(1)	67.9(9)	C(9)-Si(3)-N(2)	116(2)
N(3)-Yb(2)-O(2)	90.8(8)	C(9)-Si(3)-C(7)	103(2)
N(3)-Yb(2)-O(3)	112.9(10)	C(9)-Si(3)-C(8)	105(3)
N(3)-Yb(2)-O(4)	65.4(8)	C(10)-Si(4)-N(2)	111(2)
N(3)-Yb(2)-N(1)	140.1(9)	C(11)-Si(4)-N(2)	114(2)
N(4)-Yb(2)-O(1)	121.6(8)	C(11)-Si(4)-C(10)	111(2)
N(4)-Yb(2)-O(2)	66.4(10)	C(12)-Si(4)-N(2)	114(2)
N(4)-Yb(2)-O(3)	68.7(10)	C(12)-Si(4)-C(10)	102(2)
N(4)-Yb(2)-O(4)	101.0(9)	C(12)-Si(4)-C(11)	104(3)
N(4)-Yb(2)-N(1)	137.0(9)	C(14)-O(1)-Yb(2)	118(3)
N(4)-Yb(2)-N(3)	82.8(9)	C(15)-O(1)-Yb(2)	104(2)
O(6)-Yb(3)-O(5)	62.3(9)	C(15)-O(1)-C(14)	122(3)
O(7)-Yb(3)-O(5)	159.0(11)	C(16)-O(2)-Yb(2)	120(2)
O(7)-Yb(3)-O(6)	109.7(11)	C(17)-O(2)-Yb(2)	116(2)
O(8)-Yb(3)-O(5)	124.8(9)	C(17)-O(2)-C(16)	111(3)
O(8)-Yb(3)-O(6)	172.5(9)	C(20)-O(3)-Yb(2)	110(2)
O(8)-Yb(3)-O(7)	62.9(10)	C(21)-O(3)-Yb(2)	111(3)
N(2)-Yb(3)-O(8)	91.6(10)	C(21)-O(3)-C(20)	117(4)
N(5)-Yb(3)-O(5)	66.7(10)	C(22)-O(4)-Yb(2)	125(3)
N(5)-Yb(3)-O(6)	115.8(9)	C(23)-O(4)-Yb(2)	122(2)
N(5)-Yb(3)-O(7)	104.0(11)	C(23)-O(4)-C(22)	109(3)
N(5)-Yb(3)-O(8)	68.2(9)	C(26)-O(5)-Yb(3)	117(3)
N(5)-Yb(3)-N(2)	135.1(10)	C(27)-O(5)-Yb(3)	123(3)
N(6)-Yb(3)-O(5)	95.2(11)	C(27)-O(5)-C(26)	103(3)
N(6)-Yb(3)-O(6)	66.1(12)	C(28)-O(6)-Yb(3)	105(2)

C(29)-O(6)-Yb(3)	121(4)	C(28)-C(27)-O(5)	103(5)
C(29)-O(6)-C(28)	121(4)	C(27)-C(28)-O(6)	107(5)
C(32)-O(7)-Yb(3)	114(3)	C(30)-C(29)-O(6)	114(6)
C(33)-O(7)-Yb(3)	116(3)	C(29)-C(30)-N(6)	117(6)
C(33)-O(7)-C(32)	119(5)	C(32)-C(31)-N(6)	98(4)
C(34)-O(8)-Yb(3)	113(3)	C(31)-C(32)-O(7)	105(5)
C(35)-O(8)-Yb(3)	112(2)	C(34)-C(33)-O(7)	119(6)
C(35)-O(8)-C(34)	117(4)	C(33)-C(34)-O(8)	111(5)
Si(1)-N(1)-Yb(2)	122(2)	C(36)-C(35)-O(8)	107(4)
Si(2)-N(1)-Yb(2)	114(2)	C(35)-C(36)-N(5)	110(4)
Si(2)-N(1)-Si(1)	124(2)	C(19)-N(4)-C(18)	105(3)
Si(3)-N(2)-Yb(3)	117(2)	Yb(3)-N(5)-Yb(1)	93.4(10)
Si(4)-N(2)-Yb(3)	119(2)	C(25)-N(5)-Yb(1)	117(2)
Si(4)-N(2)-Si(3)	125(2)	C(25)-N(5)-Yb(3)	112(3)
Yb(2)-N(3)-Yb(1)	92.3(9)	C(36)-N(5)-Yb(1)	116(2)
C(13)-N(3)-Yb(1)	109(2)	C(36)-N(5)-Yb(3)	111(2)
C(13)-N(3)-Yb(2)	111(2)	C(36)-N(5)-C(25)	106(3)
C(24)-N(3)-Yb(1)	129(3)	Yb(3)-N(6)-Yb(1)	92.7(14)
C(24)-N(3)-Yb(2)	108(2)	C(30)-N(6)-Yb(1)	106(3)
C(24)-N(3)-C(13)	106(3)	C(31)-N(6)-Yb(3)	109(3)
Yb(2)-N(4)-Yb(1)	90.6(10)	C(31)-N(6)-C(30)	104(4)
C(18)-N(4)-Yb(1)	121(2)	C(14)-C(13)-N(3)	111(3)
C(18)-N(4)-Yb(2)	108(3)	C(13)-C(14)-O(1)	114(4)
C(19)-N(4)-Yb(1)	121(2)	C(16)-C(15)-O(1)	106(4)
C(19)-N(4)-Yb(2)	109(2)	C(19)-C(20)-O(3)	109(4)
C(30)-N(6)-Yb(3)	109(3)	C(22)-C(21)-O(3)	110(4)
C(31)-N(6)-Yb(1)	134(4)	C(20)-C(19)-N(4)	107(4)
C(15)-C(16)-O(2)	100(3)	C(23)-C(24)-N(3)	108(3)
C(18)-C(17)-O(2)	104(3)	C(26)-C(25)-N(5)	108(3)
C(17)-C(18)-N(4)	109(3)	C(21)-C(22)-O(4)	107(4)
C(25)-C(26)-O(5)	102(4)	C(24)-C(23)-O(4)	106(3)

[a]Estimated standard deviation in parentheses

Table VIII Summary of crystallographic data for $\{Yb[(N(SiMe_3)_2]\}_2(\mu$-DAC) 12

empirical formula	$C_{24}H_{42}N_4O_4Si_4Yb_2$
formula weight	909
crystal system	triclinic
space group	P1
a (Å)	12.148(4)
b (Å)	15.110(4)
c (Å)	11.266(5)
α (deg)	77.57(3)
β (deg)	93.71(3)
γ (deg)	106.03(2)
V (Å^3)	1940.9
Z	2
ρ (calcd) (g cm^{-3})	1.56
radiation, λ (Å)	Cu K_α, 1.542
temperature	ambient
$2\theta_{max}$ (deg)	110
no. of observed reflections	3007
R [a]	0.255
R_w [b]	0.255

[a] $R = \Sigma(|F_o| - |F_c|) / \Sigma|F_o|$ [b] $R_w = [\Sigma w(|F_o| - |F_c|)^2 / \Sigma w(|F_o|)^2]^{1/2}$

Table IX Summary of crystallographic data for Y(DAC)(CH_2SiMe_3) 14

empirical formula	$C_{16}H_{35}N_2O_4SiY$
formula weight	436.46
crystal system	monoclinic
space group	$P2_1/n$ (No. 14)
a (Å)	9.709(5)
b (Å)	11.704(6)
c (Å)	19.523(6)
α (deg)	90
β (deg)	97.63(4)
γ (deg)	90
V (Å^3)	2198.7
Z	4
ρ (calcd) (g cm^{-3})	1.319
μ (cm^{-1})	27.40
radiation, λ (Å)	MoKα, 0.70932
temperature	ambient
$2\theta_{max}$ (deg)	45
no. of observed reflections	2851
no. of unique reflections	1402
no. of parameters	219
R [a]	0.088
R_w [b]	0.118

[a] $R = \Sigma(|F_o| - |F_c|) / \Sigma|F_o|$ [b] $R_w = [\Sigma w(|F_o| - |F_c|)^2 / \Sigma w(|F_o|)^2]^{1/2}$

Table X Fractional atomic coordinates [a] and equivalent isotropic temperature factors [b] for Y(DAC)(CH_2SiMe_3) 14

Atom	x/a	y/b	z/c	U_{eq}
Y(1)	48338(15)	25574(14)	19373(8)	415(6)
Si(1)	68651(54)	17384(44)	4508(30)	534(21)
N(1)	4427(13)	2765(12)	3050(8)	52(5)
N(2)	3517(17)	3777(12)	1231(8)	63(7)
O(1)	4191(13)	592(10)	2453(7)	60(5)
O(2)	2665(12)	1662(12)	1428(8)	69(6)
O(3)	6119(13)	4266(9)	1711(7)	68(6)
O(4)	7036(11)	2925(12)	2760(7)	63(5)
C(1)	3337(24)	1981(19)	3228(11)	73(9)
H(1a)	321(0)	210(0)	376(0)	50(0)'
H(1b)	237(0)	217(0)	290(0)	50(0)'
C(2)	3727(20)	730(16)	3114(11)	66(9)
H(2a)	283(0)	20(0)	314(0)	50(0)'
H(2b)	455(0)	48(0)	351(0)	50(0)'
C(3)	3310(22)	-70(16)	1987(12)	74(10)
H(3a)	387(0)	-37(0)	158(0)	50(0)'
H(3b)	295(0)	-79(0)	225(0)	50(0)'
C(4)	2084(23)	631(20)	1675(13)	88(11)
H(4a)	142(0)	83(0)	206(0)	50(0)'
H(4b)	150(0)	18(0)	125(0)	50(0)'
C(5)	1579(23)	2425(21)	1152(14)	91(10)
H(5a)	83(0)	198(0)	79(0)	50(0)'
H(5b)	106(0)	277(0)	156(0)	50(0)'
C(6)	2275(23)	3365(22)	796(13)	90(10)
H(6a)	156(0)	406(0)	69(0)	50(0)'
H(6b)	257(0)	304(0)	32(0)	50(0)'
C(7)	4116(27)	4739(21)	943(14)	95(12)
H(7a)	446(0)	449(0)	46(0)	50(0)'
H(7b)	334(0)	540(0)	85(0)	50(0)'
C(8)	5322(27)	5190(17)	1412(13)	83(11)
H(8a)	496(0)	570(0)	181(0)	50(0)'
H(8b)	595(0)	571(0)	112(0)	50(0)'
C(9)	7428(24)	4586(21)	2099(13)	90(11)
H(9a)	811(0)	93(0)	76(0)	50(0)'
H(9b)	727(0)	521(0)	249(0)	50(0)'
C(10)	8033(22)	3543(21)	2433(12)	84(10)
H(10a)	889(0)	377(0)	282(0)	50(0)'
H(10b)	840(0)	301(0)	205(0)	50(0)'
C(11)	6706(20)	3404(21)	3411(13)	86(10)
H(11a)	643(0)	429(0)	334(0)	50(0)'

H(11b)	760(0)	333(0)	380(0)	50(0)'
C(12)	5551(22)	2789(19)	3636(12)	83(9)
H(12a)	586(0)	193(0)	378(0)	50(0)'
H(12b)	520(0)	322(0)	407(0)	50(0)'
C(13)	6335(15)	1397(14)	1300(11)	56(7)
H(13a)	582(0)	58(0)	123(0)	50(0)'
H(13b)	730(0)	131(0)	164(0)	50(0)'
C(14)	7836(18)	3126(18)	487(10)	63(8)
H(14a)	721(0)	379(0)	68(0)	50(0)'
H(14b)	806(0)	335(0)	-2(0)	50(0)'
H(14c)	880(0)	304(0)	83(0)	50(0)'
C(15)	5312(21)	1892(19)	-226(10)	72(9)
H(15a)	461(0)	251(0)	-6(0)	50(0)'
H(15b)	479(0)	108(0)	-30(0)	50(0)'
H(15c)	564(0)	217(0)	-70(0)	50(0)'
C(16)	8033(21)	649(17)	118(11)	74(9)
H(16a)	752(0)	-17(0)	9(0)	50(0)'
H(16c)	825(0)	90(0)	-39(0)	50(0)'
H(16b)	899(0)	59(0)	47(0)	50(0)'

Estimated standard deviations are given in parentheses.
Coordinates x 10^n where n = for
Temperature parameters x 10^n where n = for
U_{eq} = the equivalent isotropic temperature parameter.
$U_{eq} = 1/3\ \Sigma_i\Sigma_j U_{ij} a_i^* a_j^* (a_i . a_j)$
Primed values indicate that U_{iso} is given
$T = \exp-(8\pi^2 U_{iso} \sin^2 \theta/\lambda^2)$

Table XI Bond distances(Å) and bond angles (deg)[a] Y(DAC)(CH_2SiMe_3) 14

Atoms		Distance	Atoms		Distance
N(1)	-Y(1)	2.273(15)	C(2)	-O(1)	1.433(23)
N(2)	-Y(1)	2.261(15)	C(3)	-O(1)	1.397(23)
O(1)	-Y(1)	2.622(11)	C(4)	-O(2)	1.443(25)
O(2)	-Y(1)	2.442(13)	C(5)	-O(2)	1.433(25)
O(3)	-Y(1)	2.431(12)	C(8)	-O(3)	1.411(25)
O(4)	-Y(1)	2.534(11)	C(9)	-O(3)	1.440(25)
C(13)	-Y(1)	2.451(17)	C(10)	-O(4)	1.426(22)
C(13)	-Si(1)	1.843(20)	C(11)	-O(4)	1.463(25)
C(14)	-Si(1)	1.876(21)	C(2)	-C(1)	1.538(29)
C(15)	-Si(1)	1.876(19)	C(4)	-C(3)	1.506(31)
C(16)	-Si(1)	1.880(18)	C(6)	-C(5)	1.509(35)
C(1)	-N(1)	1.477(25)	C(8)	-C(7)	1.484(33)
C(12)	-N(1)	1.472(25)	C(10)	-C(9)	1.471(32)
C(6)	-N(2)	1.461(27)	C(12)	-C(11)	1.450(27)
C(7)	-N(2)	1.417(28)			

Atoms	Angle	Atoms	Angle
N(2)-Y(1)-N(1)	111.0(5)	C(15)-Si(1)-C(14)	107.2(9)
O(1)-Y(1)-N(1)	69.3(4)	C(16)-Si(1)-C(13)	114.6(9)
O(1)-Y(1)-N(2)	130.2(5)	C(16)-Si(1)-C(14)	106.2(9)
O(2)-Y(1)-N(1)	100.6(5)	C(16)-Si(1)-C(15)	106.7(10)
O(2)-Y(1)-N(2)	68.7(5)	C(1)-N(1)-Y(1)	112.3(11)
O(2)-Y(1)-O(1)	62.7(4)	C(12)-N(1)-Y(1)	122.6(12)
O(3)-Y(1)-N(1)	104.2(5)	C(12)-N(1)-C(1)	108.1(16)
O(3)-Y(1)-N(2)	68.3(5)	C(6)-N(2)-Y(1)	120.1(13)
O(3)-Y(1)-O(1)	161.4(4)	C(7)-N(2)-Y(1)	121.0(14)
O(3)-Y(1)-O(2)	135.7(5)	C(7)-N(2)-C(6)	112.6(19)
O(4)-Y(1)-N(1)	67.4(4)	C(2)-O(1)-Y(1)	111.5(10)
O(4)-Y(1)-N(2)	129.8(5)	C(3)-O(1)-Y(1)	113.2(11)
O(4)-Y(1)-O(1)	97.5(4)	C(3)-O(1)-C(2)	114.3(14)
O(4)-Y(1)-O(2)	160.0(4)	C(4)-O(2)-Y(1)	125.3(13)
O(4)-Y(1)-O(3)	64.2(4)	C(5)-O(2)-Y(1)	115.9(12)
C(13)-Y(1)-N(1)	137.4(6)	C(5)-O(2)-C(4)	110.3(17)
C(13)-Y(1)-N(2)	111.5(6)	C(8)-O(3)-Y(1)	116.1(12)
C(13)-Y(1)-O(1)	84.0(5)	C(9)-O(3)-Y(1)	123.8(13)
C(13)-Y(1)-O(2)	95.4(5)	C(9)-O(3)-C(8)	114.5(16)
C(13)-Y(1)-O(3)	90.6(5)	C(10)-O(4)-Y(1)	111.6(12)
C(13)-Y(1)-O(4)	84.7(5)	C(11)-O(4)-Y(1)	110.6(10)
C(14)-Si(1)-C(13)	110.7(8)	C(11)-O(4)-C(10)	115.7(15)
C(15)-Si(1)-C(13)	111.0(8)	C(2)-C(1)-N(1)	111.2(17)

C(1)-C(2)-O(1)	110.5(16)	C(5)-C(6)-N(2)	111.1(19)
C(4)-C(3)-O(1)	110.1(15)	C(8)-C(7)-N(2)	111.8(20)
C(3)-C(4)-O(2)	105.5(17)	C(7)-C(8)-O(3)	109.0(16)
C(6)-C(5)-O(2)	106.0(17)	C(11)-C(12)-N(1)	107.3(18)
C(9)-C(10)-O(4)	111.4(18)	C(10)-C(9)-O(3)	106.9(16)
C(12)-C(11)-O(4)	109.9(17)	Si(1)-C(13)-Y(1)	126.4(8)

[a]Estimated standard deviations are given in parentheses.

Tablee XII Summary of crystallographic data for [(DAC)Y(μ-C≡CPh)]$_2$ 15

empirical formula	$C_{40}H_{58}N_4O_8Y_2$
formula weight	900.74
crystal system	triclinic
space group	P$\underline{1}$ (No. 2)
a (Å)	10.032(3)
b (Å)	11.7932(14)
c (Å)	9.410(2)
α (deg)	73.32(1)
β (deg)	88.28(2)
γ (deg)	85.72(2)
V (Å^3)	1063.5
Z	2
ρ (calcd) (g cm^{-3})	1.406
μ (cm^{-1})	42.32
radiation, λ (Å	Cu K$_\alpha$, 1.542
temperature	ambient
$2\theta_{max}$ (deg)	100
no. of observed reflections	2196
no. of unique reflections	1993
no. of parameters	244
R [a]	0.076
R_w [b]	0.080

[a] $R = \Sigma(|F_o| - |F_c|) / \Sigma|F_o|$ [b] $R_w = [\Sigma w(|F_o| - |F_c|)^2 / \Sigma w(|F_o|)^2]^{1/2}$

Table XIII Fractional atomic coordinates and and equivalent isotropic temperature factors[b] for $[(DAC)Y(\mu\text{-}C{\equiv}CPh)]_2$ 15

Atom	x/a	y/b	z/c	U_{eq}
Y(1)	1598(7)	4135(6)	15921(8)	464(4)
O(1)	74(7)	1309(6)	1156(7)	66(3)
O(2)	-1807(6)	3105(6)	145(8)	63(3)
O(3)	275(7)	3710(6)	4120(6)	59(3)
O(4)	2167(6)	4415(6)	1996(7)	61(3)
N(1)	1964(8)	2123(7)	2421(9)	62(3)
N(2)	-1622(8)	2736(7)	3063(9)	61(3)
C(1)	1992(13)	827(10)	2752(14)	83(5)
C(2)	552(14)	485(9)	2552(12)	79(5)
C(3)	-1241(12)	1031(10)	797(13)	78(5)
C(4)	-1736(14)	2080(12)	-377(14)	85(6)
C(5)	-3044(11)	3322(11)	922(13)	73(5)
C(6)	-2933(11)	2688(10)	2544(14)	79(5)
C(7)	-1656(13)	2614(11)	4657(13)	79(5)
C(8)	-229(13)	2681(10)	5163(12)	78(5)
C(9)	1535(11)	3985(10)	4579(11)	71(5)
C(10)	2050(12)	4868(11)	3261(13)	78(5)
C(11)	3398(10)	3734(10)	1895(14)	73(5)
C(12)	3270(11)	2430(11)	2697(13)	78(5)
C(13)	-867(10)	5576(8)	1158(9)	46(3)
C(14)	-1758(11)	6237(9)	1387(11)	57(4)
C(15)	-2898(10)	6937(9)	1811(11)	58(4)
C(16)	-2968(14)	8143(10)	1293(14)	93(6)
C(17)	-4046(14)	8818(13)	1777(14)	120(8)
C(18)	-4992(13)	8248(14)	2774(14)	98(7)
C(19)	-4941(13)	7024(14)	3213(14)	95(7)
C(20)	-3865(11)	6370(11)	2738(12)	76(5)

Estimated standard deviations are given in parentheses.

[a]Coordinates $x10^n$ where n = 5,4,4,4 for Y,O,N,C.

Temperature parameters $x10^n$ where n = 4,3,3,3 for Y,O,N,C.

[b]U_{eq} = the equivalent isotropic temperature parameter. $U_{eq} = 1/3\ \Sigma_i\Sigma_j U_{ij} a_i^* a_j^* (a_i.a_j)$.

$T = \exp-(8\pi^2 U_{iso} \sin^2\theta/\lambda^2)$

Table XIV Bond distances (Å) and angles (deg)[a] for [(DAC)Y(μ-C≡CPh)]$_2$ 15

Atoms	Distance	Atoms	Distance
O(1) -Y(1)	2.637(6)	C(12) -N(1)	1.436(14)
O(2) -Y(1)	2.536(7)	C(6) -N(2)	1.428(14)
O(3) -Y(1)	2.509(6)	C(7) -N(2)	1.465(14)
O(4) -Y(1)	2.500(7)	C(2) -C(1)	1.56(2)
N(1) -Y(1)	2.279(8)	C(4) -C(3)	1.47(2)
N(2) -Y(1)	2.275(8)	C(6) -C(5)	1.50(2)
C(13) -Y(1)	2.601(9)	C(8) -C(7)	1.54(2)
C(13) -Y(1)'	2.627(12)	C(10) -C(9)	1.48(2)
C(2) -O(1)	1.461(12)	C(12) -C(11)	1.52(2)
C(3) -O(1)	1.454(13)	C(14) -C(13)	1.197(13)
C(4) -O(2)	1.426(14)	C(15) -C(14)	1.47(2)
C(5) -O(2)	1.465(12)	C(16) -C(15)	1.36(2)
C(8) -O(3)	1.438(12)	C(20) -C(15)	1.364(14)
C(9) -O(3)	1.437(13)	C(17) -C(16)	1.44(2)
C(10) -O(4)	1.437(13)	C(18) -C(17)	1.38(2)
C(11) -O(4)	1.438(12)	C(19) -C(18)	1.38(2)
C(1) -N(1)	1.467(13)	C(20) -C(19)	1.42(2)

Atoms	Angle	Atoms	Angle
O(2) -Y(1)-O(1)	63.0(2)	C(9) -O(3)-Y(1)	117.8(5)
O(3) -Y(1)-O(1)	123.2(2)	C(9) -O(3)-C(8)	111.6(8)
O(3) -Y(1)-O(2)	131.0(2)	C(10)-O(4)-Y(1)	113.8(6)
O(4) -Y(1)-O(1)	128.2(2)	C(11)-O(4)-Y(1)	112.6(6)
O(4) -Y(1)-O(2)	155.2(2)	C(11)-O(4)-C(10)	115.0(8)
O(4) -Y(1)-O(3)	65.5(2)	C(1) -N(1)-Y(1)	125.7(7)
N(1) -Y(1)-O(1)	64.6(3)	C(12)-N(1)-Y(1)	126.2(6)
N(1) -Y(1)-O(2)	127.4(3)	C(12)-N(1)-C(1)	108.1(8)
N(1) -Y(1)-O(3)	82.6(2)	C(6) -N(2)-Y(1)	125.1(7)
N(1) -Y(1)-O(4)	66.9(3)	C(7) -N(2)-Y(1)	122.5(7)
N(2) -Y(1)-O(1)	80.1(2)	C(7) -N(2)-C(6)	110.3(8)
N(2) -Y(1)-O(2)	67.0(3)	C(2) -C(1)-N(1)	108.2(9)
N(2) -Y(1)-O(3)	67.1(3)	C(1) -C(2)-O(1)	105.7(9)
N(2) -Y(1)-O(4)	132.6(3)	C(4) -C(3)-O(1)	104.8(9)
N(2) -Y(1)-N(1)	107.9(3)	C(3) -C(4)-O(2)	110.2(10)
C(13) -Y(1)-C(13)'	78.1(4)	C(6) -C(5)-O(2)	110.2(9)
C(13) -Y(1)-O(1)	149.2(3)	C(5) -C(6)-N(2)	110.8(9)
C(13)'-Y(1)-O(1)	93.3(3)	C(8) -C(7)-N(2)	108.6(9)
C(13) -Y(1)-O(2)	86.3(3)	C(7) -C(8)-O(3)	105.5(9)
C(13)'-Y(1)-O(2)	77.4(3)	C(10)-C(9)-O(3)	104.7(8)

C(13)	-Y(1)-O(3)	77.4(2)	C(9)	-C(10)-O(4)	111.5(9)
C(13)'	-Y(1)-O(3)	140.6(4)	C(12)	-C(11)-O(4)	110.5(9)
C(13)	-Y(1)-O(4)	79.6(3)	C(11)	-C(12)-N(1)	108.5(8)
C(13)'	-Y(1)-O(4)	80.1(4)	C(14)	-C(13)-Y(1)	148.7(8)
C(13)	-Y(1)-N(1)	145.8(3)	C(14)	-C(13)-Y(1)'	104.0(9)
C(13)'	-Y(1)-N(1)	101.8(4)	Y(1)	-C(13)-Y(1)'	101.9(4)
C(13)'	-Y(1)-N(2)	89.5(3)	C(15)	-C(14)-C(13)	173.5(10)
C(13)'	-Y(1)-N(2)	142.7(4)	C(16)	-C(15)-C(14)	119.8(10)
C(2)	-O(1)-Y(1)	103.8(6)	C(20)	-C(15)-C(14)	119.5(9)
C(3)	-O(1)-Y(1)	114.8(6)	C(20)	-C(15)-C(16)	120.6(10)
C(3)	-O(1)-C(2)	111.0(8)	C(17)	-C(16)-C(15)	119.3(12)
C(4)	-O(2)-Y(1)	117.9(7)	C(18)	-C(17)-C(16)	120.2(13)
C(5)	-O(2)-Y(1)	108.7(6)	C(19)	-C(18)-C(17)	119.2(12)
C(5)	-O(2)-C(4)	115.9(8)	C(20)	-C(19)-C(18)	119.8(12)
C(8)	-O(3)-Y(1)	107.2(6)	C(19)	-C(20)-C(15)	120.7(12)

[a]Estimated standard deviations parentheses.

Table XV Summary of crystallographic data for [(DAC)Y]$_2$(μ-*Z*-PhC=C=C=CPh) 16

empirical formula	$C_{40}H_{58}N_4O_8Y_2$
formula weight	900.73
crystal system	monoclinic
space group	$P2_1/n$ (No. 14)
a (Å)	12.301(7)
b (Å)	24.037(7)
c (Å)	20.106(22)
α (deg)	90
β (deg)	107.72(7)
γ (deg)	90
V (Å^3)	5663.0
Z	4
ρ (calcd) (g cm^{-3})	1.391

Table XVI Summary of crystallographic data for *cis*-Zr(DAC)(CH_2Ph)$_2$ 32

empirical formula	$C_{26}H_{38}N_2O_4Zr$
formula weight	533.81
crystal system	monoclinic
space group	$P2_1/c$ (No. 14)
a (Å)	20.178(3)
b (Å)	7.805(2)
c (Å)	16.711(2)
α (deg)	90
β (deg)	104.350(9)
γ (deg)	90
V (Å^3)	2549.5
Z	4
ρ (calcd) (g cm^{-3})	1.391
μ (cm^{-1})	38.34
radiation, λ (Å)	Cu K_α, 1.542
temperature	ambient
$2\theta_{max}$ (deg)	100
no. of observed reflections	2663
no. of unique reflections	2447
no of parameters	298
R [a]	0.0634
R_w [b]	0.0754

[a] $R = \Sigma(|F_o| - |F_c|) / \Sigma |F_o|$ [b] $R_w = [\Sigma w(|F_o| - |F_c|)^2 / \Sigma w(|F_o|)^2]^{1/2}$

Table XVII Fractional atomic coordinates [a] and equivalent isotropic temperature factors [b] for *cis*-Zr(DAC)(CH_2Ph)$_2$ 32

Atom	x/a	y/b	z/c	U_{eq}
Zr(1)	24352(3)	2864(9)	2060(4)	432(4)
O(1)	1396(3)	-1043(7)	-673(3)	62(2)
O(2)	1518(3)	-277(6)	911(3)	56(2)
O(3)	3630(3)	-764(8)	503(3)	58(2)
O(4)	3271(3)	2307(7)	-125(3)	61(2)
N(1)	2520(3)	-49(8)	-1023(4)	51(3)
N(2)	2543(3)	-2184(8)	757(4)	52(2)
C(1)	2088(5)	-1299(12)	-1607(5)	70(4)
C(2)	1632(5)	-2273(10)	-1180(5)	63(3)
C(3)	870(4)	-1676(12)	-327(5)	67(4)
C(4)	835(5)	-457(11)	372(6)	62(4)
C(5)	1713(4)	1595(11)	1533(5)	59(3)
C(6)	2106(4)	-3006(10)	1213(5)	61(3)
C(7)	3134(4)	-3319(11)	775(5)	62(3)
C(8)	3594(5)	-2521(11)	282(6)	68(4)
C(9)	4147(5)	144(14)	208(7)	78(5)
C(10)	3983(5)	2024(14)	289(6)	76(4)
C(11)	3131(5)	2609(12)	-1027(5)	73(4)
C(12)	2953(5)	852(13)	-1446(5)	75(4)
C(13)	2872(4)	1785(10)	1495(4)	51(3)
C(14)	1727(4)	2779(11)	-59(5)	62(3)
C(15)	3499(4)	1259(10)	2125(4)	49(3)
C(16)	565(4)	-346(11)	2494(5)	59(4)
C(17)	4156(5)	-841(13)	3097(5)	70(4)
C(18)	4699(6)	325(16)	3331(7)	86(5)
C(19)	4659(5)	1911(13)	2971(6)	73(4)
C(20)	4060(4)	2396(12)	2383(5)	61(3)
C(21)	1156(4)	3153(10)	-789(5)	59(3)
C(22)	521(5)	3770(11)	-683(6)	75(4)
C(23)	-14(5)	4223(12)	-1374(8)	85(5)
C(24)	89(6)	4118(14)	-2200(8)	92(5)
C(25)	689(6)	3507(14)	-2285(6)	88(5)
C(26)	1231(5)	2988(11)	-1607(5)	71(4)

Estimated standard deviations are given in parentheses

[a]Coordinates x10^n where n = 5,4,4,4 for Zr,O,N,C.

Temperature parameters x10^n where n = 4,3,3,3 for Zr,O,N,C.

[b]U_{eq} = the equivalent isotropic temperature parameter.

$U_{eq} = 1/3 \sum_i \sum_j U_{ij} a_i^* a_j^* (a_i . a_j)$

$T = \exp-(8B^2 U_{iso} \sin^2 \theta/\lambda^2)$

Table XVIII Bond distances(Å) and angles(deg)[a] for *cis*-ZrDAC(CH_2Ph)$_2$ 32

Atoms	Distance	Atoms	Distance
O(1) -Zr(1)	2.471(5)	C(2) -C(1)	1.503(12)
O(2) -Zr(1)	2.466(6)	C(4) -C(3)	1.522(13)
O(3) -Zr(1)	2.477(5)	C(6) -C(5)	1.529(11)
O(4) -Zr(1)	2.470(5)	C(8) -C(7)	1.520(12
N(1) -Zr(1)	2.119(7)	C(10) -C(9)	1.517(14)
N(2) -Zr(1)	2.124(6)	C(12) -C(11)	1.540(13)
C(13) -Zr(1)	2.417(7)	C(15) -C(13)	1.489(10)
C(14) -Zr(1)	2.389(8)	C(21) -C(14)	1.484(11)
C(2) -O(1)	1.437(10)	C(16) -C(15)	1.388(11)
C(3) -O(1)	1.417(9)	C(20) -C(15)	1.419(10)
C(4) -O(2)	1.454(10)	C(17) -C(16)	1.412(12)
C(5) -O(2)	1.447(9)	C(18) -C(17)	1.403(14)
C(8) -O(3)	1.418(10)	C(19) -C(18)	1.370(14)
C(9) -O(3)	1.444(11)	C(20) -C(19)	1.407(12)
C(10) -O(4)	1.448(10)	C(22) -C(21)	1.421(12)
C(11) -O(4)	1.483(10)	C(26) -C(21)	1.418(12)
C(1) -N(1)	1.497(10)	C(23) -C(22)	1.416(13)
C(12) -N(1)	1.438(11)	C(24) -C(23)	1.448(16)
C(6) -N(2)	1.451(9)	C(25) -C(24)	1.342(14)
C(7) -N(2)	1.480(10)	C(26)- C(25)	1.424(12)

Atoms	Angle	Atoms	Angle
O(2) -Zr(1) -O(1)	65.3(2)	N(2) -Zr(1) -O(4)	132.4(2)
O(3) -Zr(1) -O(1)	128.4(2)	N(2) -Zr(1) -N(1)	106.5(2)
O(3) -Zr(1) -O(2)	130.8(2)	C(13) -Zr(1) -O(1)	143.2(2)
O(4) -Zr(1) -O(1)	131.4(2)	C(13) -Zr(1) -O(2)	79.1(2)
O(4) -Zr(1) -O(2)	148.8(2)	C(13) -Zr(1) -O(3)	82.0(2)
O(4) -Zr(1) -O(3)	64.6(2)	C(13) -Zr(1) -O(4)	76.8(2)
N(1) -Zr(1) -O(1)	68.4(2)	C(13) -Zr(1) -N(1)	145.5(3)
N(1) -Zr(1) -O(2)	133.7(2)	C(13) -Zr(1) -N(2)	94.4(2)
N(1) -Zr(1) -O(3)	81.1(2)	C(14) -Zr(1) -O(1)	81.4(2)
N(1) -Zr(1) -O(4)	68.8(2)	C(14) -Zr(1) -O(2)	75.5(2)
N(2) -Zr(1) -O(1)	81.8(2)	C(14) -Zr(1) -O(3)	144.5(2)
N(2) -Zr(1) -O(2)	68.9(2)	C(14) -Zr(1) -O(4)	81.3(2)
N(2) -Zr(1) -O(3)	67.9(2)	C(14) -Zr(1) -N(1)	96.3(3)

C(14) -Zr(1) -N(2)	144.2(3)	C(25)-C(26) -C(21)	119.8(9)
C(14) -Zr(1) -C(13)	80.8(3)	C(6) -C(5) -O(2)	109.4(6)
C(2) -O(1) -Zr(1)	106.0(4)	C(5) -C(6) -N(2)	107.5(6)
C(3) -O(1) -Zr(1)	121.0(4)	C(8) -C(7) -N(2)	109.9(7)
C(3) -O(1) -C(2)	113.5(6)	C(7) -C(8) -O(3)	104.7(7)
C(4) -O(2) -Zr(1)	115.5(5)	C(10) -C(9) -O(3)	104.6(7)
C(5) -O(2) -Zr(1)	111.6(4)	C(9) -C(10) -O(4)	108.5(7)
C(5) -O(2) -C(4)	115.0(6)	C(12) -C(11) -O(4)	106.6(7)
C(8) -O(3) -Zr(1)	106.5(5)	C(11) -C(12) -N(1)	108.2(7)
C(9) -O(3) -Zr(1)	121.2(5)	C(15) -C(13) -Zr(1)	123.7(5)
C(9) -O(3) -C(8)	112.3(7)	C(21) -C(14) -Zr(1)	128.3(6)
C(10) -O(4) -Zr(1)	116.6(5)	C(16) -C(15) -C(13)	122.3(7)
C(11) -O(4) -Zr(1)	111.1(4)	C(20) -C(15) -C(13)	121.1(7)
C(11) -O(4) -C(10)	115.3(6)	C(20) -C(15) -C(16)	116.6(7)
C(1) -N(1) -Zr(1)	122.6(5)	C(17) -C(16) -C(15)	122.4(8)
C(12) -N(1) -Zr(1)	128.4(5)	C(18) -C(17) -C(16)	119.0(9)
C(12) -N(1) -C(1)	109.0(6)	C(19) -C(18) -C(17)	120.5(10)
C(6) -N(2) -Zr(1)	128.3(5)	C(20) -C(19) -C(18)	119.7(9)
C(7) -N(2) -Zr(1)	123.2(5)	C(19) -C(20) -C(15)	121.8(8)
C(7) -N(2) -C(6)	108.4(6)	C(22) -C(21) -C(14)	120.3(8)
C(2) -C(1) -N(1)	110.3(7)	C(26) -C(21) -C(14)	121.8(8)
C(1) -C(2) -O(1)	105.8(6)	C(26) -C(21) -C(22)	117.8(8)
C(4) -C(3) -O(1)	106.1(6)	C(23) -C(22) -C(21)	120.7(10)
C(25) -C(24) -C(23)	117.8(10)	C(24) -C(23) -C(22)	120.3(10)
C(3) -C(4) -O(2)	108.5(7)	C(26) -C(25) -C(24)	123.5(10)

[a]Estimated standard deviations in parentheses.

Table XIX Summary of crystallographic data for *trans* -Zr(DAC)$(CH_2Ph)_2$ 32

empirical formula	$C_{26}H_{38}N_2O_4Zr$
formula weight	533.81
crystal system	monoclinic
space group	Pn (No. 14)
a (Å)	8.5754(7)
b (Å)	23.5325(11)
c (Å)	12.9259(13)
α (deg)	90
β (deg)	91.569(13)
γ (deg)	90
V (Å^3)	2608.4
Z	4
ρ (calcd) (g cm^{-3})	1.36
μ (cm^{-1})	37.5
radiation, λ (Å)	Cu K_α, 1.542
temperature	ambient
$2\theta_{max}$ (deg)	100
no. of observed reflections	2825
no. of unique reflections	2565
no. of parameters	413
R [a]	0.088
R_w [b]	0.110

[a] $R = \Sigma(|F_o| - |F_c|) / \Sigma|F_o|$ [b] $R_w = [\Sigma w(|F_o| - |F_c|)^2 / \Sigma w(|F_o|)^2]^{1/2}$

Table XX Summary of crystallographic data for *trans*-Y(MAC)(CH_2SiMe_3)$_2$ 40

empirical formula	$C_{20}H_{46}NO_5Si_2Y_2$
formula weight	525.68
crystal system	monoclinic
space group	C2/c
a (Å)	18.487(3)
b (Å)	11.030(2)
c (Å)	13.908(3)
α (deg)	90
β (deg)	101.50(2)
γ (deg)	90
V (Å^3)	2779.1
Z	4
ρ (calcd) (g cm^{-3})	1.256
μ (cm^{-1})	22.0
radiation, λ (Å)	Cu K_α, 0.70932
temperature	213 K
$2\theta_{max}$ (deg)	50
no. of observed reflections	2466
no. of unique reflections	1400
no. of parameters	152
R [a]	0.039
R_w [b]	0.038

[a] $R = \Sigma(|F_o| - |F_c|) / \Sigma|F_o|$ [b] $R_w = [\Sigma w(|F_o| - |F_c|)^2 / \Sigma w(|F_o|)^2]^{1/2}$

Table XXI **Fractional atomic coordinates [a] and equivalent isotropic temperature factors [b] for *trans*-Y(MAC)(CH_2SiMe_3)$_2$ 40 at 213 K.**

Atom	x	y	z	U_{iso} \eq[a]
Y	0.00000	0.21572(5)	0.25000	0.0342
Si	0.19237(6)	0.23626(10)	0.19106(9)	0.0386
C1	-0.03675(22)	-0.1331(4)	0.2165(3)	0.053
O2	-0.03988(15)	-0.0298(3)	0.15604(21)	0.045
C3	-0.1086(3)	-0.0175(4)	0.0902(3)	0.061
C4	-0.0990(3)	0.0786(5)	0.0201(3)	0.071
O5	-0.07832(15)	0.1876(3)	0.07375(22)	0.054
C6	-0.0613(10)	0.2626(10)	-0.0023(9)	0.054
C7	-0.0751(10)	0.3800(12)	0.0388(9)	0.053
O8	-0.0296(9)	0.3896(7)	0.1356(6)	0.044
C9	-0.0424(9)	0.4976(11)	0.1845(13)	0.065
C106	0.0665(10)	0.2996(11)	0.4792(9)	0.054
C107	0.0660(11)	0.4135(12)	0.4220(9)	0.053
N108	0.0230(11)	0.3976(9)	0.3236(7)	0.039
C109	0.0145(8)	0.5149(10)	0.2755(13)	0.065
C10	0.10680(20)	0.1515(4)	0.1815(3)	0.036
C11	0.2386(3)	0.2647(4)	0.3215(3)	0.066
C12	0.1731(3)	0.3866(4)	0.1297(4)	0.067
C13	0.26505(22)	0.1613(4)	0.1345(3)	0.057
H11	-0.0747	-0.1297	0.2539	0.056(4)
H12	-0.0423	-0.2044	0.1776	0.056(4)
H31	-0.1462	0.0048	0.1248	0.063(4)
H32	-0.1214	-0.0918	0.0567	0.063(4)
H41	-0.1440	0.0909	-0.0251	0.071(4)
H42	-0.0615	0.0558	-0.0144	0.071(4)
H61	-0.0921	0.2477	-0.0641	0.059(4)
H62	-0.0111	0.2529	-0.0077	0.059(4)
H71	-0.0604	0.4415	-0.0013	0.057(4)
H72	-0.1260	0.3889	0.0402	0.057(4)
H91	-0.0399	0.5643	0.1420	0.058(4)
H92	-0.0899	0.4950	0.2012	0.058(4)
H561	0.1048	0.3049	0.5354	0.059(4)
H562	0.0202	0.2948	0.4993	0.059(4)
H571	0.0480	0.4797	0.4543	0.057(4)
H572	0.1152	0.4294	0.4153	0.057(4)
H591	-0.0016	0.5739	0.3165	0.058(4)
H592	0.0600	0.5398	0.2598	0.058(4)

H101	0.1208	0.0750	0.2106	0.041(4)
H102	0.0888	0.1412	0.1133	0.041(4)
H111	0.2827	0.3093	0.3227	0.097(6)
H112	0.2065	0.3097	0.3539	0.097(6)
H113	0.2499	0.1893	0.3539	0.097(6)
H121	0.2179	0.4306	0.1348	0.101(6)
H122	0.1398	0.4309	0.1605	0.101(6)
H123	0.1519	0.3747	0.0625	0.101(6)
H131	0.3075	0.2117	0.1426	0.092(6)
H132	0.2778	0.0855	0.1655	0.092(6)
H133	0.2467	0.1488	0.0666	0.092(6)

[a] U_{eq} is the mean of the principal axes of the displacement ellipsoid.

Table XXII **Bond distances(Å) and angles(deg)[a] for *trans*-Y(MAC)(CH_2SiMe_3)$_2$ 40 at 213 K**

Atoms	Distance	Atoms	Distance
Y-O2	3.033(3)	Y-O5	2.605(3)
Y-O8	2.482(8)	Y-N108	2.253(10)
Y-C10	2.461(4)	Si-C10	1.819(4)
Si-C11	1.872(4)	Si-C12	1.866(5)
Si-C13	1.879(5)	C1-C1'	1.486(8)
C1-O2	1.411(5)	O2-C3	1.416(5)
C3-C4	1.474(7)	C4-O5	1.426(6)
O5-C6	1.427(14)	C6-C7	1.459(18)
C7-O8	1.442(16)	O8-C9	1.415(17)
C9-C109	1.488(22)	C106-O5'	1.477(13)
C106-C107	1.486(18)	C107-N108	1.450(17)
N108-C109	1.451(15)		

Atoms	Angles	Atoms	Angles
O2-Y-O2'	53.55(7)	O2-Y-O5	56.39(8)
O2-Y-O5'	109.92(9)	O2-Y-O8	114.19(20)
O2-Y-N108	176.3(5)	O2-Y-C10	73.82(11)
O2-Y-C10'	76.40(11)	O2'-Y-O8	165.80(22)
O2'-Y-N108	126.2(3)	O5-Y-O5'	166.31(10)
O5-Y-O8	58.58(23)	O5-Y-N108	123.5(3)
O5-Y-C10	86.56(11)	O5-Y-C10'	89.51(11)
O5'-Y-O8	134.87(24)	O5'-Y-N108	70.1(3)
O8-Y-N108	66.5(3)	O8-Y-C10	93.8(4)
O8-Y-C10'	112.3(4)	N108-Y-C10	109.8(5)
N108-Y-C10'	100.0(5)	C10-Y-C10'	146.55(13)
C10-Si-C11	112.26(21)	C10-Si-C12	109.85(20)
C10-Si-C13	115.31(20)	C11-Si-C12	107.63(22)
C11-Si-C13	104.71(20)	C12-Si-C13	106.63(23)
C1'-C1-O2	107.3(3)	Y-O2-C1	119.12(23)
Y-O2-C3	107.62(24)	C1-O2-C3	112.8(3)
O2-C3-C4	106.6(4)	C3-C4-O5	108.4(4)
Y-O5-C4	129.3(3)	Y-O5-C6	117.7(6)
C4-O5-C6	100.2(6)	O5-C6-C7	98.2(11)
C6-C7-O8	108.4(11)	Y-O8-C7	123.7(7)
Y-O8-C9	112.3(8)	C7-O8-C9	112.8(12)

O8-C9-C109	111.0(12)	Y-O5'-C106	105.0(5)
C4'-O5'-C106	119.7(5)	O5'-C106-C107	115.2(11)
C106-C107-N108	110.3(11)	Y-N108-C107	123.7(8)
Y-N108-C109	126.2(8)	C107-N108-C109	108.4(10)
C9-C109-N108	105.7(10)	Y-C10-Si	125.25(20)

[a]Estimated standard deviations in parentheses

REFERENCES

1. Cotton, F.A.; Wilkinson, G.,"*Advanced Inorganic Chemistry*", 5th Ed., Wiley Interscience, New York, **1988**, pp. 955-979.

2. Szabadvary, F., in "*Handbook on the Physics and Chemistry of Rare Earths*", (K.A. Gschneidner and L. Eryring, eds.),Chapter 73, Elsevier, Amsterdam, **1988**.

3. Marks, T.J.; Ernst, R.D., in "*Comprenhensive Organometallic Chemistry*", (G. Wilkinson, F.G.A. Stone, and E.W. Abel, eds.) Chapter 21, Pergamon Press, Oxford, **1982**.

4. Bradley, D.C; Ghotra, J.S.; Hart, F.A. *J. Chem. Soc., Dalton Trans*, **1973**, 1021.

5. Berg, D.J., Ph.D Thesis, University of California, Berkley, **1987**.

6. Kagan, H.B.; Namy, J.L., in "*Handbook on the Physics and Chemistry of Rare Earths*", (K.A. Gschneidner and L. Eryring, eds.), Chapter 50, Elsevier, Amsterdam, **1984**.

7. Molander, G.A. *Chem. Rev.* **1992**, *92*, 29.

8. Johnson, D.A., "*Some Thermodynamic Aspects of Inorganic Chemistry*", 2nd Ed., Cambridge University Press, Cambridge, **1982**, pp. 158-168.

9. Aldrich Catalogue, 1997.

10. Schavarien, C.J. *Adv. in Organomet. Chem.* **1994**, *36*, 283.

11. Schumann, H.; Genthe, W., in "*Handbook on the Physics and Chemistry of Rare Earths*", (K.A. Gschneidner and L. Eryring, eds.), Chapter 53, Elsevier, Amsterdam, **1984**.

12. (a) Gysling, H; Tsutsui, M. *Adv. in Organomet. Chem.* **1970**, *9*, 361. (b) Evans, W.J. *J. Organomet. Chem.*, **1983**, *250*, 217. (c) Evans, W.J. *Adv. in Organomet.Chem.* **1985**, *24*, 131. (d) Evans, W.J. *Polyhedron* **1987**, *6*, 803.

13. Schriver, D.F.; Drezdzon, M.A., "*The Manipulation of Air-Sensitive Compounds*", 2nd ed, John Wiley and Sons, NewYork, **1986**.

14. McCausland, M.A.H; Mackenzie, I.S., "*Nuclear Magnetic Resonance in Rare Earth Metals*", Taylor and Francis Ltd., London, **1980**.

15. Stout, G.H.; Jensen, L.H.,"*X-ray Structure Determination : a Practical Guide*", Macmillian Publishing Co., New York, **1968**.

16. Wilkinson, G.; Birmingham, J.M. *J. Am. Chem. Soc.* **1954**, *76*, 6210.

17. Magin, R.E.; Manastyrskyj, S.; Dubeck, M. *J. Am. Chem. Soc.* **1963**, *85*, 672.

18. (a) Coutts, R.S.P.; Wailes, P.C. *J. Organomet. Chem.* **1970**, *25*, 115. (b) Kalsotra, B.L.; Multani, R.K.; Jain, B.D. *J. Inorg. Nucl. Chem.* **1973**, *35*, 311. (c) Ely, N.M.; Tsutsui, M. *Inorg. Chem.* **1975**, *14*, 2680. (d) Manzer, L.E. *J. Organomet. Chem.* **1977**, *135*, C6

19. Evans, W.J.; Wayda, A.L.; Hunter, W.E.; Atwood, J.L. *J. Chem. Soc., Chem. Commun.* **1981**, 706.

20. (a) Evans, W.J.; Meadows, J.H.; Wayda, A.L.; Atwood, J.L. *J. Am. Chem. Soc.* **1982**, *104*, 2008. (b) Evans, W.J.; Meadows, J.H.; Wayda, A.L.; Hunter, W.E.; Atwood, J.L. *J. Am. Chem. Soc.* **1982**, *104*, 2013.

21. (a) Bercaw, J.E.; Marvich, R.H.; Bell, L.G.; Brintzinger, H.H. *J. Am. Chem. Soc.* **1972**, *94*, 1219. (b) Bercaw, J.E. *J. Am. Chem. Soc.* **1974**, *96*, 5087. (c) Manriquez, J.M.; Fagan, P.J.; Marks, T.J. *J. Am. Chem. Soc.* **1978**, *100*, 3939. (d) Wayda, A.L.; Evans, W.J.; *Inorg. Chem.* **1980**, *19*, 2190. (e) Watson, P.L.; Whitney. J.F.; Harlow, P.L. *Inorg. Chem.* **1981**, *20*, 3271. (f) Schumann, H.; Meese-Marktscheffel, J.A.; Esser, L. *Chem. Rev.* **1995**, *95*, 865.

22. Ballard, D.G.H.; Courtis, A.; Holton, J.; McMeeking, J.; Pearce, R. *J. Chem. Soc., Chem. Commun.* **1978**, 994.

23. (a) Watson, P.L. *J. Am. Chem. Soc.* **1982**, *104*, 337. (b) Watson, P.L.; Roe, D.C. *J. Am. Chem. Soc.* **1982**, *104*, 6471. (c) Watson, P.L.; Parshall, G.W. *Acc. Chem. Res.* **1985**, *18*, 51.

24. Zinnen, H.; Pluth, J.J.; Evans, W.J. *J. Chem. Soc., Chem. Commun.* **1980**, 810.

25. (a) Fagan, P.J.; Manriquez, J.M.; Marks. T.J.; Day, V.W.; Vollmer, S.H.; Day, C.S. *J. Am. Chem. Soc.* **1980**, *102*, 8091. (b) Jeske, G.; Lauke, H.; Mauermann, H.; Sweptson, P.N.; Schumann, H.; Marks, T.J. *J. Am. Chem. Soc.* **1985**, *107*, 8091.

26. den Hann, K.H.; de Boer, J.L.; Teuben, J.H. *Organometallics* **1986**, *5*, 1726.

27. (a) Burns, C.J., Ph.D Thesis, University of California, Berkley, **1987** and references therein. (b) Burns, C.J.; Andersen, R.A. *J. Am. Chem. Soc.* **1987**, *109*, 941.

28. (a) Davidson, P.J.; Lappert, M.F.; Pearce, R. Chem Rev. **1976**, *76*, 219. (b) Elschenbroich, C.; Salzer, A.,"*Organometallics*", 2nd ed., VCH Verlagsgesellschaft mbH, Weinheim, **1992**, pp. 197.

29. Watson, P.L. J. Chem. Soc., Chem. Commun. **1983**, 276.

30. Heeres, H.J.; Heeres, A.; Teuben, J.H. *Organometallics* **1991**, *10*, 1980..

31. Heeres, H.J.; Heeres, A.; Teuben, J.H. *Organometallics* **1990**, *9*, 1508.

32. Hart, F.A.; Massey, A.G.; Saran, M.S. *J. Organomet. Chem.* **1970**, *21*, 147.

33. Edelmann, F.T., in "*Comprenhensive Organometallic Chemistry II* ", (G. Wilkinson, F.G.A. Stone, and E.W. Abel, eds.) Chapter 2, Elsevier Science, Oxford, **1995**.

34. Lappert, M.F.; Pearce, R. *J. Chem. Soc., Chem. Commun.***1973**, 126.

35. Schumann, H.; Muller, J. *J. Organomet. Chem.* **1979**, *169*, C1.

36. Barker, G.K.; Lappert, M.F. *J. Organomet. Chem.* **1974**, *76*, C45.

37. Atwood, J.L.; Hunter, W.E.; Rogers, R.D.; Holton, J.; Mcmeeking, J.; Pearce, R.; Lappert, M.F. *J.Chem.Soc., Chem. Commun.*, **1978**, 140.

38. Schumann, H.; Muller, J.; Bruncks, N.; Lauke, H.; Pickardt, J.; Schwarz, H.; Eckart, K. *Organometallics*, **1984**, *3*, 69.

39. Schumann, H.; Pickardt, J.; Bruncks, N. Angew. Chem., Int. Ed. Engl. **1981**, *20*, 120.

40. Hitchcock, P.B.; Lappert, M.F.; Smith, R.G. *Inorg. Chim.Acta* **1987**, *139*, 183.

41. Hitchcook, B.; Lappert, M.F.; Smith, R.G.; Bartlett, R.A.; Power, P.P. *J. Chem. Soc., Chem. Commun.* **1988**, 1007.

42. Buchler, J.W.; De Cian, A.; Fischer, J.; Kihn-Botulinkski, M.; Paulus, H.; Weiss, R. *J. Am. Chem. Soc.* **1986**, *108*, 3652.

43. Wong, C.P. *Inorg. Synth.* **1983**, *22*, 156.

44. (a) Arnold, J.; Hoffman, C.G. *J. Am. Chem. Soc.* **1990**, *112*, 8620. (b) Arnold, J. *J. Chem. Soc., Chem. Commun.* **1990**, 976. (c) Arnold, J.; Hoffmann, C.G.;

Dawson, Y.; Hollander, F.J. *Organometallics* **1993**, *12*, 3645. (d) Schavarien, C.J.; Orpen, A.G. *Inorg.Chem*, **1991**, *30*, 4968. (e) Schavarien, C.J. *J. Chem. Soc., Chem. Commun.* **1991**, 458.

45. Sewchock, M.G.; Haushalter, R.C.; Merola. J.S. *Inorg.Chim.Acta* **1988**, *144*, 47.

46. Schavarien, C.J.; Meijboom, N.; Orpen, G.; *J. Chem. Soc., Chem. Commun.* **1992**, 124.

47. (a) Fryzuk, M.D.; Haddad, T.S. *J. Chem. Soc., Chem. Commun.* **1990**, 1088. (b) Fryzuk, M.D.; Haddad, T.S. *Organometallics* **1991**, *10*, 2026. (c) Fryzuk, M.D.; Haddad, T.S.; Rettig, S.J. *Organometallics* **1992**, *11*, 2967.

48. Hasinoff, L.; Takats, J.; Zhang, X.W.; Bond, A.H.; Rogers, R.D. *J. Am. Chem. Soc.* **1994**, *116*, 8833.

49. (a) Welder, M.; Noltemeyer, M.; Pieper, U.; Schmidt, H.-G.; Stalke, D.; Edelmann, F.T. *Angew. Chem., Int. Ed. Engl.* **1990**, *28*, 894. (b) Welder, M.; Knösel, F.; Pieper, U.; Schmidt, H.-G.; Stalke, D.; Edelmann, F.T.; Amberger, H.-D. *Chem. Ber.* **1992**, *125*, 217. (c) Duchateau, R.; van Wee, C.T.; Meetsma, A.; Teuben, J.H. *J. Am. Chem. Soc.* **1993**, *114*, 4931. (d)) Duchateau, R.; van Wee, C.T.; Meetsma, A.; van Duijnen, P.T.; Teuben, J.H. *Organometallics* **1996**, *12*, 2279.

50. Shao, P.; Berg, D.J.; Bushnell, G.W. *Inorg. Chem.* **1994**, *33*, 6334.

51. Jordan, R.F. *Adv. in Organomet. Chem.* **1991**, *32*, 324.

52. Bochmann, M. *J. Chem. Soc., Dalton Trans.* **1996**, 255.

53. Pederson, C.J. *J. Am. Chem. Soc.* **1967**, *89*, 7017.

54. (a) Christensen, J.J.; Eatough, D.J; Izatt, R.M. *Chem. Rev.* **1974**, *74*, 351. (b) Johnson, M.R.; Jones, N.F.; Sutherland, I.O. *J.Chem.Soc., Perkin Trans. I*, **1985**, 1637. (c) Krakowiak, K.E.; Bradshaw, J.S.; Zamercka-Kravkowiak, D.J. *Chem. Rev.* **1989**, *89*, 929.

55. (a) Lehn, D.J.M.; Sauvage, J.P.; Blanzat.J. *Tetrahedron*, **1973**, *29*, 1629. (b) Izatt, R.M.; Bradshaw, J.S.; Nielsen, S.A.; Lamb, J.D.; Christensen, J.J. *Chem. Rev.* **1985**, *85*, 27. (c) Sutherland, I.O. *Chem Soc. Rev.* **1986**, *15*, 63.

56. Hart, F.A., in "Comprehensive Coordination Chemistry", (G. Wilkinson, R.D. Gillard, J.A. McCleverty, eds.) Chapter 39, Pergamon Press, Oxford, 1987.

57. (a) Bünzli, J.-C.G.; Wessner, D. *Coord. Chem.Rev.* **1984**, *10*, 191. (b) Bünzli, J.-C,G. in "*Handbook on the Physics and Chemistry of Rare Earths*", (K.A. Gschneidner and L. Eryring, eds.), chapter 60, Elsevier, Amsterdam, **1987**. (c) Adachi, G.; Hirashima, Y. in "*Cation Binding by Macrocycles; Complexation of Cationic Species by Crown Ehters*", (Y. Inoue and G.W. Gokel, eds.), chapter 18, Marcel Dekker, Inc., New York,**1990**.

58. (a) Robinson, G.H.; Rae, A.D.; Campana, C.F.; Byram, S.K. *Organometallics* **1987**, *6*, 1227. (b) Robinson, G.H.; Sangokoya, S.A.*Organometallics* **1988**, *7*, 1453. (c) Robinson, G.H.; Appel, E.S.; Sangokoya, S.A.; Zhang, H.; Atwood, J.L. *J. Chem. Coord. Chem.* **1988**, *17*, 373. (d) Sangokoya, S.A.; Moise, F.; Pennington, W.T.; Self, M.F.; Robinson, G.H. *Organometallics* **1989**, *8*, 2584. (e) Sangokaya, S.A.; Pennington, W.T. *J. Am. Chem. Soc.* **1989**, *111*, 1520. (f) Self, M.F.; Pennington, W.T.; Laske, J.A.; Robinson, G.H. *Organometallics* **1991**, *10*, 36.

59. Gokel, G.W.; Garcia, B.J. *Tetrahedron Lett.* **1977**, 317. (b) Pajerski, A.D.; Cleary, T.P.; Parvarez, M.; Gokel, G.W.; Richey, H.G., Jr. *Organometallics* **1992**, *11*, 1400.

60. Kulstad, S.; Malmsted, L.A. *Acta Chem. Scan. B* **1979**, *33B*, 469.

61. Gatto, V.J.; Arnold, K.A.; Viscariello, A.M.; Miller, S.R.; Morgan, C.R.; Gokel, G.W. *J.Org.Chem.* **1986**, *51*, 5373.

62. (a) Deacon, G.B.; Koplick, A.; Raverty, W.D., Vince, D.G. *J. Organomet. Chem.* **1972**, *182*, 121. (b) Schumann, H.; Jeske, G. *Angew. Chem., Int. Ed. Engl.* **1985**, *24*, 255. (c) Deacon, G.B.; Wilkinson, D.L. *Inorg. Chim. Acta* **1988**, *142*, 155.

63. (a) Bradley, D.C.; Ghotra, J.S.; Hart, F.A.; Hursthouse, M.B.; Raithby, P.R. *J. Chem. Soc.,Dalton Trans.* **1977**, 1166. (b) Aspinall, H.C.; Bradley, D.C.; Hursthouse, M.B.; Sales, K.D.; Walker, N.P.C. *J. Chem. Soc., Dalton Trans.* **1985**, 1585. (c) Heeres, H.J.; Meetsma, A.; Teuben, J.H.; Rogers, R.D. *Organometallics* **1989**, *8*, 2637. (d) Aspinall, H.C.; Moore, S.R.; Smith, A.K. *J. Chem. Soc., Dalton Trans.* **1992**, 153. (e) Allen, M.; Aspinall, H.C.; Moore, S.R.; Hursthouse, M.B.; Karvalov, A.I. *Polyhedron* **1992**, *11*, 409.

64. Shannon, R.D. *Acta Crystallogr.* 1976, A32, 751.

65. Tilley, T.D.; Boncella, J.M.; Berg, D.J.; Burns, C.J.; Andersen, R.A. *Inorg. Synth.* **1990**, *27*, 146.

66. Evans, W.J.; Drummond, D.K.; Zhang, H.; Atwood, J.L. *Inorg. Chem.* **1988**, *27*, 575.

67. Evans, W.J.; Hanusa, T.P.; Levan, K.R. *Inorg. Chim. Acta* **1985**, *110*, 191.

68. Schavarien, C.J. *Organometallics*. **1994**, *13*, 69.

69. Shao, P. Ph.D Thesis, University of Victoria, Victoria, **1997**

70. Coan, P.S.; Hubert-Pfalzgraf, L.G.; Caulton, K.G. *Inorg. Chem*. **1992**, *31*, 1262.

71. Bradley, D.C.; Chudzynska, H.; Hursthouse, M.B.; Motevalli, M. *Polyhedron* **1991**, *10*, 1049.

72. Evans, W.J.; Meadows, J.H.; Kostka, A.G.; Closs, G.L. *Organometallics* **1985**, *4*, 324.

73. van der Heijden, H.; Pasman, P.; de Boer, E.J.M.; Schavarien, C.J. *Organometallics* **1989**, *8*, 1459.

74. Hitchcock, P.B.; Howard, J.A.K.; Lappert, M.F.; Leung, W-P.; Mason, S.A. J. Chem. Soc., Chem. Commun., **1990**, 847.

75. van der Heijden, Schavarien, C.J. *Organometallics* **1989**, *8*, 255.

76. (a) Bergman, R.G. *Science* **1984**, *223*, 902. (b) Crabtree, R.H. *Chem. Rev.* **1985**, *85*, 245. (c) Halpern, *J. Inorg Chim. Acta* **1985**, *100*, 41.

77. Fessenden, R.J.; Fessenden, J.S., "*Organic Chemistry*", 3rd Ed., Brooks/Cole Publishing Co., California, **1986**, pp.596.

78. Atkins, P.W. "*Physical Chemistry*", 3rd Ed., W.H. Freeman and Company, New York, **1986**, pp. 707.

79. "*Model 303 Static Mercury Drop Electrode Operating and Service Manual*"; EG+G Princeton Applied Reseach: Princeton, NJ, **1984**.

80. Heeres, H.J.; Nijhoff, J.; Teuben, J.H. *Organometallics* **1993**, *12*, 2609.

81. (a) Atwood, J.L.; Hunter, W.E.; Wanda, A.L.; Evans, W.J. *Inorg, Chem*. **1981**, *20*, 4115. (b) Evans, W,H.; Bloom, I.; Hunter, W.E.; Atwood, J.L. *Organometallics* **1983**, *2*, 709. (c) Evans, W.J.; Keyer , R.A.; Ziller, J.W. *Organometallics* **1990**, *9*, 2828. (d) Evans, J.W.; Keyer, R.A.; Ziller, J.W. *Organometallics* **1993**, *12*, 2618.

82. Forsyth, C.M.; Nolarn, S.P.; Stern, C.L.; Marks, T.J.; Rheingold, A.L. *Organometallics* **1993**, *12*, 3618.

83. March, J., "*Advance Organic Chemistry: Reactions, Mechanisms and Structures*", 4th Ed., John Wiley and Sons, New York, 1992, pp. 280.

84. Shen, Q.; Zheng, D.; Lin, L.; Lin, Y. *J. Organomet. Chem.*, **1990**, *391*, 307.

85. Duchateau, R.; van Wee, C.T.; Meetsma, A.; Teuben, J.H. *J.Am. Chem. Soc.* **1993**, *115*, 4931.

86. Cox, P.A.; Ewart, I.C.; Stigliani, W.M. *J. Chem. Soc., Faraday Trans 2*, **1975**, 504.

87. Akita, M.; Yasuda, H.; Nakamura, A. *Bull. Chem.Soc.Jpn.* **1984**, *57*, 480.

88. Macbride, J.A.; Wade, K. *Synthetic Comm.* **1996**, *26*, 2309.

89. Gavens, P.D.; Bottrill, M.; Kelland, J.W.; McMeeking, J. in "*Comprenhensive Organometallic Chemistry*", (G. Wilkinson, F.G.A. Stone, and E.W. Abel, eds.) chapter 22.5, Pergamon Press, Oxford, **1982**.

90. Britzinger, H.H.; Fischer, D.; Mülhaupt, R.; Rieger, B.; Waymouth, R.M. *Angew. Chem., Int. Ed. Engl.*, **1995**, *34*, 1143.

91. (a) Jordan, R.F.; Bajgur, C.S.; Dasher, W.E. *Organometallics* **1987**, *6*, 1041. (b) Jordan, R.F.; LaPointe, R.E.; Bradley, P.K.; Baenzinger, N. *Organometallics* **1989**, *8*, 2892. (c) Guram, A.S.; Swenson, D.C.; Jordan, R.F. *J.Am. Chem. Soc.* **1992**, *114*, 8991.

92. (a) Bochmann, M; Wilson, L.M. *J. Chem. Soc., Chem. Commun.* **1986**, 1610. (b) Chien, J.C.W.; Tsai, W.; Rausch, M.D. *J.Am. Chem. Soc.* **1991**, *113*, 8750. (c) Yang, X.; Stern, C.L.; Marks, T.J. *J.Am. Chem. Soc.* **1994**, *116*,10015. (d) Linden, A.; Schavarien, C.J.; Meijboom, N.; Ganter, C.; Orpen, A.G. *J.Am. Chem. Soc.* **1995**, *117*, 3008.

93. Jordan, R.F. *J.Chem.Educ.* **1988**, *65*, 285

94. (a) DeAngelis, S.; Solari, E.; Gallo, E.; Chiesi-Villa, A.; Floriani, C.; Rizzoli, C. *Inorg. Chem.* **1992**, *31*, 2520. (b) Uhrhammer, R.; Black, D. G.; Gardner, T. G.; Olsen, J. D.; Jordan, R. F. *J. Am. Chem. Soc.* **1993**, *115*, 8493. (c) Jacoby, D.; Floriani, C.; Chiesi-Villa, A.Rizzoli, C. *J. Am. Chem. Soc.* **1993**, *115*, 3595.

95. (a) Brand, H.; Arnold, J. *Organometallics* **1993**, *12*, 3655. (b) Brand H.; Arnold, *J. Angew. Chem., Int. Ed. Engl.*, **1994**, *33*, 95.

96. Tjaden, E. B, Swenson, D.C.; Jordan, R.F. *Organometallics* **1995**, *14*, 371.

97. Zucchini, U.; Albizatti, E.; Giannnini, U. *J. Organomet. Chem.* **1971**, *26*, 357.

98. Sandstrom, J. "*Dynamic NMR Spectroscopy*", Pergamon, London, **1982**, pp. 77- 91

99. Zsolnai, L. ZORTEP, University of Heidelberg, Heidelberg, Germany, **1995**.

100. (a) Mintz, E.A.; Moloy, K.G.; Marks, T.J.; Day, V.W.*J.Am. Chem. Soc.* **1982**, *104*, 4692. (b) Edward, P.G.; Andersen, R.A.; Zalkin, A. *Organometallics* **1984**, *3*, 293. (c) Latesky, S.L.; McMullen, A.K.; Niccolai, G.P.; Rothwell, I.P.; Huffman, J.C. *Organometallics* **1985**, *4*, 902. (d) Jordan, R.F.; Lapointe, R.E.; Baenzinger, N.; Hinch, G.D *Organometallics* **1990**, *9*, 1539.

101. Wengrovius, J.H.; Schrock, R.R.*J. Organomet. Chem.* **1981**, *205*,319.

102. Pellecchia, C.; Immirzi, A.; Grassi, A.; Zambelli, A *Organometallics* **1993**, *12*, 4473.

103. (a) Horton, A.D.; de With, J.; van der Linden, A.; van de Weg, H. *Organometallics* **1996**, *15*, 2672. (b) Horton, A.D.*J. Chem. Soc., Chem. Commun.*, **1992**, 185.

104. Thiele, K.H.; Bohme, U.; Sieler,. *A.Z.Anorg. Allg. Chem.* **1993**, *619*, 1951.

105. (a) Heeres, H.J.; Meetsma, A.; Teuben, J.H. *J.Chem.Soc., Chem Commun.* **1988**, 962. (b) Heeres, H.J.; Meetsma, A.; Teuben, J.H. *Organometallics* **1989**, *8*, 2637.

106. Maeda, H.; Furuyoshi, S.; Nakatsuji, Y.; Okahara, M. *Bull. Chem.Soc. Jpn.* **1983**, *56*, 212.

107. Manriquez, J.M.; Fagan, P.J.; Marks, T.J.; Day, C.S.; Day, V.W. *J.Am. Chem. Soc.* **1978**, *100*, 7112.

108. Sonnenberger, D.C.; Mintz, E.A.; Marks, T.J. *J.Am. Chem. Soc.* **1984**, *106*, 3483.

109. Schvarien, C.J. *Organometallics* **1992**, *11*, 3476.

110. Huheey, J. E. "*Inorganic Chemistry: Principles of Structure and Reactivity*", Harper and Row, New York, **1972**, pp. 246- 247.

111. Aspinall, H.C.; Bradley, D.C.; Hursthouse, M.B.; Sales, K.D.; Walker, N.P.C.; Hussain, B. *J. Chem. Soc., Dalton Trans.* **1989**, 623.

112. (a) Fachinetti, G.; Floriani, C.; Marchetti, F.; Mellini, M.*J. Chem. Soc., Dalton Trans*, **1978**, 1398. (b) Shur, V.B.; Berkovich, E.G.; Volpin, M.E.; Lorenz, B.; Wahren, M. *J.*

Organomet. Chem., **1982**, *228*, C36. (c) Vaughan, G.A.; Sofield, C.D.; Hillhouse, G.L. *J.Am. Chem. Soc.* **1989**, *111*, 5491. (d) Alt, H.G.; Herrmann, G.S. *J. Organomet. Chem.* **1990**, *390*, 159. (e) Bhide, V.V.; Farona, M.F. *Organometallics* **1990**, *9*, 1766.

113. (a) Buchwald, S.L.; Lum, R.T.; Dewan, J.C. *J.Am. Chem. Soc.* **1986**, *111*, 7441. (b) Buchwald, S.L.; Nielsen, R.B. *Chem. Rev.* **1988**, *88*, 1047. (c) Vaughan, G.A.; Hillhouse, G.L.; Lum, R.T.; Buchwald, S.L.; Rheingold, A.L. *J.Am. Chem. Soc.* **1988**, *110*, 7215. (d) Buchwald, S.L.; Lum, R.T.; Fisher, R.A.; Davis, W.M. *J.Am. Chem. Soc.* **1989**, *111*, 9113. (e) Buchwald, S.L.; Nielsen, R.B. *J.Am. Chem. Soc.* **1989**, *111*, 2870.

114. Bottrill, M. Gavens, P.D.; Kelland, J.W.; McMeeking, J. in "*Comprenhensive Organometallic Chemistry*", (G. Wilkinson, F.G.A. Stone, and E.W. Abel, eds.) chapter 22.3, Pergamon Press, Oxford, **1982**, pp. 422.

115. Shur, V.B.; Berkovich, E.G.; Volpin, M.E.; Lorenz, B.; Wahren, M. *J. Organomet. Chem.*, **1988**, *347*, 77.

116. Girard, P.; Namy, J.L.; Kagan, H.B. *J.Am.Chem.Soc.* **1980**, *102*, 2693.

117. Hudson, H.R.*J Chem.,Soc (B)*, 1966, 664.

118. Tessier-Youngs, C.; Beachley, O.T. *Inorg. Synth.***1986**, *24*, 95.

119. Jacobs, T, L., in "Organic Reactions", (R. Adams, W.E. Bachmann, A.H. Blatt, L.E. Fieser, J.R.Johnson eds.), Chapter 1, Volume 5, John Wiley and Sons, New York, **1949**.

120. Allen, A.D.; Cook, C.D. *Can.J.Chem.* **1963**, *41*, 1084.

121. MacBride, J.A.H.; Wade, K. *Synth Commun.* **1996**, *26*, 2309.

122. Bianchini,C.; Frediani, P.; Masi, D.; Peruzzini, M.; Zanobini, F. *Organometallics* **1994**, *13*, 4616.

123. C.K. Johnson, ORTEPII, OakRidge National Laboratory: Oak Ridge, TN, **1976**.